

INFORMATION TO USERS

This manuscript has been reproduced from the microfilm master. UMI films the text directly from the original or copy submitted. Thus, some thesis and dissertation copies are in typewriter face, while others may be from any type of computer printer.

The quality of this reproduction is dependent upon the quality of the copy submitted. Broken or indistinct print, colored or poor quality illustrations and photographs, print bleedthrough, substandard margins, and improper alignment can adversely affect reproduction.

In the unlikely event that the author did not send UMI a complete manuscript and there are missing pages, these will be noted. Also, if unauthorized copyright material had to be removed, a note will indicate the deletion.

Oversize materials (e.g., maps, drawings, charts) are reproduced by sectioning the original, beginning at the upper left-hand corner and continuing from left to right in equal sections with small overlaps. Each original is also photographed in one exposure and is included in reduced form at the back of the book.

Photographs included in the original manuscript have been reproduced xerographically in this copy. Higher quality 6" x 9" black and white photographic prints are available for any photographs or illustrations appearing in this copy for an additional charge. Contact UMI directly to order.

UMI

A Bell & Howell Information Company
300 North Zeeb Road, Ann Arbor MI 48106-1346 USA
313/761-4700 800/521-0600

UNIVERSITY OF OKLAHOMA
GRADUATE COLLEGE

RECENT INTERDECADAL VARIATIONS IN THE TROPICAL
ATMOSPHERE: EVIDENCE AND IDEALIZED GCM SIMULATIONS

A Dissertation
SUBMITTED TO THE GRADUATE FACULTY
in partial fulfillment of the requirements for the degree of
Doctor of Philosophy

By
XIAOFENG GONG
Norman, Oklahoma
1998

UMI Number: 9914417

UMI Microform 9914417
Copyright 1999, by UMI Company. All rights reserved.

**This microform edition is protected against unauthorized
copying under Title 17, United States Code.**

UMI
300 North Zeeb Road
Ann Arbor, MI 48103

© Copyright by XIAOFENG GONG 1998

All Right Reserved.

RECENT INTERDECADAL VARIATIONS IN THE TROPICAL ATMOSPHERE:
EVIDENCE AND IDEALIZED GCM SIMULATIONS

A Dissertation APPROVED FOR
THE SCHOOL OF METEOROLOGY

BY











ACKNOWLEDGEMENT

I would like to sincerely thank my major advisor, Dr. Michael Richman, for his advice, support and encouragement during the course of this study. Mike and I have been good friends and colleagues for nearly 10 years, starting from the 'old' time at the Illinois State Water Survey. From working with him during these years, I have gained much insight into the nature of scientific research. He has been always there whenever I needed help, for anything. I also extend my gratitude to Dr. Peter Lamb who has been a special and important person to me. He interested me in the meteorology program at OU, provided me with the opportunity to work on my advanced education, and guided me to success. Without his generous help and strong support professionally and financially during the past 10 years, I would certainly not have been where I am today. Three other members of my committee, Dr. Claude Duchon, Dr. Frederick Carr and Dr. S. Lakshmivarahan, deserve special thanks, not only for their helpful comments and suggestions on this dissertation, but also for the knowledge and enjoyment which I have derived from attending their classes in meteorology and computer sciences over the past six years.

I am deeply indebted to Drs. Neil Ward and Antonio Navarra for their assistance in the early stage of this research. Antonio and his colleagues helped me starting with the ECHAM4 and allowed me to shares their computing resource and data from the ECHAM4 GCM climatological integration performed at the Istituto Per Lo Studio Delle Metodologie Geofisiche Ambientali (IMGA) during my visit to the

IMGA, Italy, in 1997. Discussions with Neil on the research topic have had a large impact in my dissertation. I am also grateful to Dave Montroy for sharing his knowledge and wisdom in ECHAM model and SST dataset with me, which made my work easier.

Finally, my heart goes to all members of my family, my wife Aiping Xing, daughter Haopu, my mother and sister back in China. Without their love, support, encouragement, patience and sacrifice during the course of my graduate study at OU, this work would not have been possible.

This research is supported by NOAA Cooperative Agreement NA67RJ0150 and the Cooperative Institute for Mesoscale Meteorological Studies at the University of Oklahoma.

TABLE OF CONTENTS

LIST OF TABLE	ix
LIST OF ILLUSTRATIONS	x
ABSTRACT	xv
Chapter 1. Introduction	1
1.1 Interdecadal climate variations and the research problem	1
1.2 Review of past studies of interdecadal variability	4
1.2.1 Interdecadal climate variations in the tropics	4
1.2.2 Interdecadal climate changes in the extratropics	9
1.2.3 Modeling studies of interdecadal variability and its possible mechanisms	12
1.3 The motivations and objectives of the present research	19
Chapter 2. Tropical SST interannual and interdecadal variabilities.....	23
2.1 Sea surface temperature dataset	24
2.2 Analysis procedures and methods.....	25
2.2.1 Filtering.....	25
2.2.2 Principal component analysis	27
2.3 Sea surface temperature interannual variations	30
2.4 SST interdecadal variability.....	32
Chapter 3. Atmospheric interdecadal variations over the tropics	37
3.1 Data and analysis procedures.....	38
3.1.1 Height and wind data from the NCEP/NCAR reanalysis	38
3.1.2 Height and wind data from the ECHAM4 GCM climatological run data	39
3.1.3 Analysis procedures	40
3.2 Tropical wide interdecadal atmospheric variability in the reanalysis data	41
3.2.1 Temporal and spatial structures of the geopotential height changes.....	41
3.2.2 Difference maps of the tropical atmospheric height between the two periods before and after the 1976/77 winter	45

3.2.3	Tropical wind circulation changes	47
3.3	Model simulated tropical-wide interdecadal atmospheric variability	50
3.3.1	Temporal and spatial structures of the simulated atmospheric height variations.....	50
3.3.2	Model simulated tropical atmospheric height difference maps	54
3.3.3	Tropical wind circulation changes in the ECHAM4 GCM simulation.....	56
3.4	Relationship between the interdecadal variations in the tropical atmosphere and ocean	58
3.5	A hypothesis for the tropospheric height increase in the tropical Pacific.....	60
Chapter 4.	Tropical atmospheric responses to the interdecadal SST variation in an idealized GCM simulation for boreal winter	63
4.1	The ECHAM4 general circulation model	63
4.1.1	Model general description	63
4.1.2	The model governing continuous equations	64
4.1.3	Brief overview of the major physics	66
4.2	Experimental design.....	68
4.2.1	Basic idea of the simulations and anomalous surface forcing	68
4.2.2	Model experiments : control run and two specified forcing runs	71
4.3	Atmospheric responses to the idealized anomalous SST forcings over the tropical Pacific	73
4.3.1	Changes in the tropospheric height fields over the tropics	74
4.3.2	Tropical general circulation changes	78
4.3.3	Changes in atmospheric heating due to the anomalous surface forcing	89
Chapter 5.	Investigations of the mechanisms for the tropical atmospheric interdecadal variations using the GCM simulations	93
5.1	General description and physical basis for the analyses	94
5.1.1	Thermodynamical balance in atmosphere	94
5.1.2	Model experiments for the physical analyses	96
5.2	Effects of the equatorial central Pacific anomalous SST forcing	99
5.2.1	Tropical atmospheric responses to the SST perturbation over the equatorial central Pacific	100

5.2.2	Changes in atmospheric diabatic heating processes	109
5.3	Effects of the equatorial eastern Pacific anomalous SST forcing	115
5.3.1	Tropical atmospheric responses to the SST perturbation over the eastern Pacific	115
5.3.2	Changes in atmospheric diabatic heating.....	126
5.4	Effects of the anomalous SST over the tropical central and eastern Pacific	132
5.4.1	Atmospheric responses to the specified SST perturbation pattern	133
5.4.2	Changes in atmospheric diabatic heating.....	143
5.5	Tropical Atmospheric heat transport and its impact on the height change pattern over the tropics.....	151
5.5.1	Importance of horizontal heat transport and its general structures in the modeled atmosphere.....	151
5.5.2	Heat transport changes in the forcing runs and their effects on the tropical-wide height change patterns	162
Chapter 6.	Further discussions on the results from the analysis and model simulations.....	187
6.1	Tropical atmospheric interdecadal variability and the idealized simulations	187
6.2	Extratropical atmospheric responses to the tropical SST changes.....	192
6.2.1	Northern Hemisphere height changes.....	193
6.2.2	Wind circulation changes over the North Pacific	198
Chapter 7.	Summary and conclusions	204
7.1	Interdecadal variations over the tropical oceans and atmosphere.....	206
7.2	Idealized model simulations of the atmospheric interdecadal variation	208
7.3	The physical and dynamical mechanisms of the tropical height changes	210
7.4	Concluding remarks	213
References	215

LIST OF TABLES

Table 3.1 Correlation between the time series of the leading PC from SST anomaly data (SSTA) and reanalysis and IMGAs climatological run data	59
---	----

LIST OF ILLUSTRATIONS

Figure 2.1 Lanczos filter response functions. The solid curve is low-pass filter and the dash curve represents the high-pass filter.	26
Figure 2.2 Leading PC loading pattern (top) and its time coefficient (bottom) for high-pass filtered SST anomaly over the domain. The variance explained is given in the upper right-corner of the bottom panel.....	31
Figure 2.3 Leading PC loading pattern (top) and its time coefficient (bottom) for low-pass filtered SST anomaly over the domain. The variance explained is given in the upper right-corner of the bottom panel.....	34
Figure 2.4 Low-pass filtered winter monthly mean SST difference field (Period 2 - Period 1). Unit: °C.	35
Figure 3.1 Time series of leading PC scores for the geopotential height fields at 200, 500, 700, and 1000 hPa using the NCEP/NCAR reanalysis data.....	43
Figure 3.2 Leading PC loading patterns for the geopotential heights at 200, 500, 700, and 1000 hPa using the NCEP/NCAR reanalysis. The number at the upper right of each panel represents the percentage of the variance explained by the PC mode.....	44
Figure 3.3 Difference maps of the winter low-pass filtered monthly mean geopotential height fields between Period 2 and Period 1 at 200, 500, 700, and 1000 hPa using the NCEP/NCAR reanalysis (Period 2 - Period 1). Unit: gpm...	46
Figure 3.4 Difference maps of the winter low-pass filtered monthly mean horizontal wind fields between Period 2 and Period 1 at (a). 200 and (b). 850 hPa using the NCEP/NCAR reanalysis (Period 2 - Period 1). Unit: ms ⁻¹	49
Figure 3.5 Same as Figure 3.1, except using the IMG A climatological run data.	52
Figure 3.6 Same as Figure 3.2, except using the IMG A climatological run data.	53
Figure 3.7 Same as Figure 3.3, except using the IMG A climatological run data.	55
Figure 3.8 Same as Figure 3.4, except using the IMG A climatological run data.	57
Figure 4.1 January mean SST field. Contour interval is 2°C.....	69
Figure 4.2 Idealized SST patterns for the model simulations. a. SST perturbation pattern with a maximum of 1°C (darkest area), the contour interval is 0.2°C; b.	

prescribed SST field for the PACP1 run, and c. SST field for the PACN1 run, the contour interval is 2°C.....	70
Figure 4.3 Difference maps of the monthly mean geopotential height fields between the PACP1 and PACN1 runs at 200, 500, 700 , and 1000 hPa (PACP1 - PACN1). Unit: gpm.	75
Figure 4.4 Simulated January monthly mean wind fields from the CNTR run for a. 200, and b. 850 hPa, unit: ms ⁻¹ ; c. vertical-zonal cross section of vertical motion along the equator, contour interval 0.025 Pas ⁻¹	79
Figure 4.5 Difference maps of the monthly mean wind fields between the PACP1 and PACN1 runs (PACP1 - PACN1) for a. 200, and b. 850 hPa, unit: ms ⁻¹	81
Figure 4.6 Vertical-zonal cross sections of the monthly mean vertical motion difference fields between the PACP1 and PACN1 runs (PACP1 - PACN1) along three selected latitudes. Contour interval is 0.025 Pas ⁻¹	84
Figure 4.7 Vertical-meridional cross sections of the monthly mean vertical motion difference fields between the PACP1 and PACN1 runs (PACP1 - PACN1) along three selected longitudes. Contour interval is 0.02 Pas ⁻¹	85
Figure 4.8 Difference maps of the monthly mean diabatic heating fields between the PACP1 and PACN1 runs (PACP1 - PACN1) for a. 700, b. 500 and c. 200 hPa. Contour interval is 2°Kday ⁻¹	90
Figure 5.1 Idealized SST patterns for the CPACP2 run. a. equatorial central Pacific SST perturbation pattern with a maximum of 2°C (darkest area), contour interval is 0.4°C. b. prescribed SST field for the CPACP2 run, contour interval is 2°C.	97
Figure 5.2 Same as Figure 5.1, except for the EPACP2 forcing run.	98
Figure 5.3 Same as Figure 5.1, except for the PACP2 forcing run.....	98
Figure 5.4 Difference maps of the monthly mean geopotential height fields between the CPACP2 and CNTR runs at 200, 500, 700, and 1000 hPa (CPACP2 - CNTR run). Unit: gpm.	101
Figure 5.5 Difference maps of the monthly mean wind fields between the PACP2 and CNTR runs (PACP2 - CNTR) for a. 200, and b. 850 hPa, unit: ms ⁻¹	105
Figure 5.6 Vertical-meridional cross section of the monthly mean vertical motion difference fields between the CPACP2 and CNTR runs (CPACP2 - CNTR) along 180°. Contour interval is 0.025 Pas ⁻¹	105

Figure 5.7 Difference maps of the flow (stream line) and its magnitude (shaded area) between the CPACP2 and CNTR runs (CPACP2 - CNTR) for a. vertical-meridional cross section along 180°, and b. vertical-zonal cross section along the equator. Shade unit: ms^{-1}	106
Figure 5.8 Difference maps of the monthly mean diabatic heating fields between the CPACP2 and CNTR runs (CPACP2 - CNTR) for a. 700, b. 500 and c. 200 hPa. The contour interval is 2°Kday^{-1}	110
Figure 5.9 Vertical distributions of the differences in the diabatic heating processes between the CPACP2 and CNTR runs (CPACP2 - CNTR) at six locations in the tropics. The unit is Kday^{-1} . The closed circle line is the cumulus convection heating; the open circle line is the large scale precipitation heating; the crossed line is the radiative heating; and the solid line is the total diabatic heating.	114
Figure 5.10 Same as Figure 5.4, except for the EPACP2 run.....	118
Figure 5.11 Same as Figure 5.5, except for the EPACP2 run.....	122
Figure 5.12 Vertical-meridional cross sections of the monthly mean vertical motion differences between the EPACP2 and CNTR runs (EPACP2 - CNTR) along three selected longitudes. Unit: Pas^{-1}	123
Figure 5.13 Vertical-zonal cross sections of the differences for the flow (stream line) and its magnitude (shaded area) between the EPACP2 and CNTR runs (EPACP2 - CNTR) along three selected latitudes. Shade unit: ms^{-1}	124
Figure 5.14 Same as Figure 5.8, except for the EPACP2 run.....	127
Figure 5.15 Same as Figure 5.9, except for the EPACP2 run.....	131
Figure 5.16 Same as Figure 5.4, except for the PACP2 run.	134
Figure 5.17 Same as Figure 5.5, except for the PACP2 run.	138
Figure 5.18 Vertical-meridional cross sections of the monthly mean vertical motion differences between the PACP2 and CNTR runs (PACP2 - CNTR) along three selected longitudes. Unit: Pas^{-1}	139
Figure 5.19 Same as Figure 5.13, except for the PACP2 run.	142
Figure 5.20 Same as Figure 5.8, except for the PACP2 run.	145
Figure 5.21 Same as Figure 5.9, except for the PACP2 run.	149

Figure 5.22 Mean heat flux in the CNTR run for a. zonal mean, b. meridional mean over the 15°S - 15°N region. Unit: Kms^{-1} .	154
Figure 5.23 Vertical mean zonal (a). heat flux in Kms^{-1} and (b) its divergence in Kday^{-1} over the 15°S - 15°N region in the CNTR run. The thick line represents the vertical mean in the 200 - 1000 hPa layer. The thin solid line and dash line are the vertical mean in the 200 - 500 hPa and 600 - 1000 hPa layers, respectively.	156
Figure 5.24 Vertical mean zonal heat fluxes for the six longitudinal zones in the CNTR run, unit: Kms^{-1} . The thick line represents the vertical mean in the 200 - 1000 hPa layer. The thin solid line and dash line are the vertical mean in the 200 - 500 hPa and 600 - 1000 hPa layers, respectively.	159
Figure 5.25 Vertical mean zonal heat flux divergences for the six longitudinal zones in the CNTR run, unit: Kday^{-1} . The thick line represents the vertical mean in the 200 - 1000 hPa layer. The thin solid line and dash line are the vertical mean in the 200 - 500 hPa and 600 - 1000 hPa layers, respectively.	160
Figure 5.26 Differences of the vertical means of the zonal heat flux (top) and zonal heat flux divergence (bottom) between the CPACP2 and CNTR runs (CPACP2 - CNTR). The thick line represents the vertical mean in the 200 - 1000 hPa layer. The thin solid line and dash line are the vertical mean in the 200 - 500 hPa and 600 - 1000 hPa layers, respectively. The unit is Kms^{-1} for the heat flux and Kday^{-1} for the heat flux divergence.	163
Figure 5.27 Differences of the vertical means of the meridional heat flux between the CPACP2 and CNTR runs (CPACP2 - CNTR) for the the six longitudinal zones, unit: Kms^{-1} . The thick line represents the vertical mean in the 200 - 1000 hPa layer. The thin solid line and dash lines are the vertical mean in the 200 - 500 hPa and 600 - 1000 hPa layers, respectively.	165
Figure 5.28 Differences of the vertical means of the meridional heat flux divergences between the CPACP2 and CNTR runs (CPACP2 - CNTR) for the the six longitudinal zones, unit: Kms^{-1} . The thick line represents the vertical mean in the 200 - 1000 hPa layer. The thin solid line and dash line are the vertical mean in the 200 - 500 hPa and 600 - 1000 hPa layers, respectively.	166
Figure 5.29 Same as Figure 5.26, except for the EPACP2 run.	169
Figure 5.30 Same as Figure 5.27, except for the EPACP2 run.	171
Figure 5.31 Same as Figure 5.28, except for the EPACP2 run.	172

Figure 5.32 Same as Figure 5.26, except for the PACP2 run.	175
Figure 5.33 Same as Figure 5.27, except for the PACP2 run.	178
Figure 5.34 Same as Figure 5.28, except for the PACP2 run.	179
Figure 5.35 Profiles of the vertical heat flux divergence differences between the PACP2 and CNTR runs (PACP2 - CNTR) at the six locations in the tropics. Unit: Kday^{-1}	182
Figure 5.36 Mean heat flux divergence difference between the PACP2 and CNTR runs over (a) northern and (b) southern low latitudes. The thick line represents the vertical mean in the 200 - 1000 hPa layer. The thin solid line and dash line are the vertical mean in the 200 - 500 hPa and 600 - 1000 hPa layers, respectively. Unit: Kday^{-1}	184
Figure 6.1 Northern Hemisphere 500 hPa height difference fields between a. the PACP1 and PACN1 runs, b. the PACP2 and CNTR runs, c. the CPACP2 and CNTR runs, and d. the EPACP2 and CNTR runs. Contour interval is 10 gpm. .	195
Figure 6.2 1000 hPa horizontal wind vector difference fields between a. the PACP1 and PACN1 runs, b. the PACP2 and CNTR runs, c. the CPACP2 and CNTR runs, and d. the EPACP2 and CNTR runs. Unit: ms^{-1}	201
Figure 6.3 Same as Figure 6.2, except for 500 hPa.....	202

ABSTRACT

Previous studies have indicated that, in addition to ENSO-cycle changes, the tropical SST records and Northern Hemisphere winter climate experienced an interdecadal scale change in the past several decades, with a marked “regime shift” in the mid-1970s. In this research, the interdecadal atmosphere-ocean variability is further investigated from a different perspective, with an eye toward shedding light on the tropical Pacific. The reconstructed Reynold’s SST data, NCEP/NCAR reanalysis and ECHAM4 GCM climatological run data are used to extract temporal and spatial features in the climate system. The ECHAM4 GCM is utilized to investigate the effects of ocean surface forcing and reveal physical and dynamical processes and mechanisms involved in the tropical atmospheric changes.

A large spatial boreal winter SST anomaly structure is found over the central and eastern Pacific on the decadal time scale. The temporal variation of such signature exhibits a notable interdecadal change, with an evident basic state jump from negative to positive anomaly about the long-term mean in the 1976/77 winter. Associated with this SST variation, the tropical height and circulation also experiences a similar interdecadal variation. In the spatial patterns of the leading geopotential height PC modes from the NCEP/NCAR reanalysis data, the dominant feature is a tropical-wide height change structure through the entire troposphere, with the most significant change in the upper tropospheric layer. The temporal fluctuation of this height mode shows a strikingly consistent trend and sudden jump in the 1976/77

winter with the SST interdecadal trend. Prior to the 1976/77 winter, the tropical height field is in negative anomalous time period and it reverses after the 1976/77 winter. Such an atmospheric variation in the mid-1970s over the tropics is supported by the results from analyses using the data from the ECHAM4 GCM climatological integration with the observed monthly mean SST fields.

A series of model integrations, forced with different SST perturbations over the tropical central and eastern Pacific, has been performed using the ECHAM4 GCM in an attempt to simulate the spatial patterns in tropical atmospheric interdecadal variability and investigate the physical processes and mechanisms responsible for the formation and maintenance of these spatial changes. The resultant height changes from the idealized simulations show large similarities to the patterns found in the reanalysis. The primary features, such as the increase of the tropical-wide height and weakening of the Walker circulation, can be modeled reasonably well. The SST change over the equatorial central Pacific appears to be more dominant in the atmospheric variation structures. Cumulus convection and atmospheric heat transport are found to be the two key physical processes which are largely responsible for the tropical-wide height increase, especially in the upper tropospheric layer. Due to the anomalous SST increase over the central Pacific and eastern Pacific, more latent heat is released from cumulus convection, warming the local atmosphere. Part of the heat energy is transported away by the enhanced local Hadley cell and westerly subtropical jets, leading to the height changes in non-forcing regions. Such transport mechanisms are largely responsible for the upper level height changes over the tropical eastern Pacific and Atlantic regions. In addition, the anomalous sinking motion also plays a

role in the height increase over the tropical Atlantic Ocean in the upper troposphere. The low level height increase over the tropical Indian and western Pacific regions can be largely attributed to the dynamic effects of anomalous sinking motions there.

Chapter 1

Introduction

1.1 Interdecadal climate variations and the research problem

Observed atmospheric and oceanic records exhibit considerable variability on a broad range of time scales. The variabilities of the climate system, in certain ranges of the frequency spectrum, are associated with the corresponding climatic features. Among the characteristic atmospheric time scales, which have been extensively studied, are periods of: several days (synoptic scale weather); about 10-day to a season (intraseasonal variability); several years (interannual variability) and interdecadal and beyond (Lau 1992). Studies of atmospheric variability in both observations and numerical simulations have traditionally focused on the time scales from several days to several years. Research on interdecadal variability in the climate system can be hampered by the scarcity of long and reliable observational records, the lack of insights into the physical processes pertinent to these time scales, as well as the availability of computing and data storage resources for long-term numerical integrations. Before 1989, the research on interdecadal-scale climate variations mainly concentrated on the global warming issues by analyzing the global surface air temperature trend (Folland et al. 1984; Jones et al. 1986). However, more recent studies by Nitta and Yamada (1989) and Trenberth (1990) indicate that there exists an interdecadal-scale change in sea surface temperature in the tropical Pacific and Indian

Oceans, which couple with the changes of the Northern Hemisphere atmospheric circulation and North Pacific Ocean condition, with an abrupt state change in the mid-1970s. Interestingly, the spatial structures of such interdecadal scale atmosphere-ocean interaction are similar to those found during El Niño and Southern Oscillation (ENSO) episodes (Trenberth 1990). Since then, such ENSO-like interdecadal climate variability in atmosphere-ocean coupled system has been the subject for many subsequent studies (cf. Yamagata and Masumoto 1992; Tanimoto et al. 1993; Wallace et al. 1993; Miller et al. 1994; Graham, 1994; Latif and Barnnet 1994; Kawamura 1994; Lau and Nath 1994; Zhang et al. 1997; Kachi and Nitta 1997; Gu and Philander 1997; Nakamura et al. 1997). A common thread these studies report is that, in boreal winter season, the equatorial central and eastern Pacific sea surface temperature (SST) have increased since the 1976/77 winter. At the same time, associated with this tropical SST change, SST in the central North Pacific has dropped substantially, whereas a large surface temperature increase was found in Alaska and along the west coast of North America. During this period, the Aleutian low intensifies, and North Pacific storm track shifts southward. A number of ecological changes related to the interdecadal climate variations in the Pacific have been noted (Mantua et al. 1997). For instances, rapid changes in the production levels of major Alaskan fish stocks have been tied to the interdecadal climate variability in northeast Pacific, and some marine and terrestrial ecological parameters in western North America were found to experience a dramatic shift which is coincided with the physical environment changes in the late 1970s.

In a broad sense, a framework can be placed on interdecadal variability where external and internal forcing are the two causal mechanisms. External forcing includes variation in incident solar radiation, volcanic activity and greenhouse gas increases in the atmosphere. Conversely, internal forcing refers to interactions between different components in climate system. The recent interdecadal variation noted in aforementioned studies has been posited to be a consequence of interactions within the system (Latif 1997).

In this research, the ENSO-like interdecadal atmosphere-ocean variations will be further investigated from a different perspective from previous studies. To do so, one must begin with the assumption that the elucidation of the origin and nature of the atmospheric variability on such a time scale is essential to understand the behavior of the climate system. This research will focus on a domain which includes the tropical and lower latitude belt between 35°S and 35°N in the globe, with an eye toward shedding light on the tropical Pacific. Analyses of the tropical atmospheric circulation and geopotential height field changes and their association with the underlying SST change at the interdecadal scale will be extended from surface to upper troposphere, to reveal the three dimensional spatial structures in the atmosphere associated with this interdecadal variability. Such variability, as seen in the tropical geopotential height field and corresponding atmospheric circulation, has not been investigated previously based on a review of refereed literature. In addition to the investigation into the tropical atmospheric height and circulation changes, this study will diagnose the physical mechanisms which result in the observed change and their maintenance in the atmosphere given the underlying SST change field. Such physical

analyses are crucial to begin to in both observations and numerical simulations fully understand the interdecadal variability in the climate system.

1.2 Review of past studies of interdecadal variability

1.2.1 Interdecadal climate variations in the tropics

During past decade, while studies on atmospheric intraseasonal and interannual variabilities have drawn much of the attention, the interdecadal climate variation problem has also become another common research topic in the climate research community. Many investigators have reported that, based on the observational records, significant climate variations on a decadal time scale occurred in the tropical Oceans, North Pacific and Atlantic Oceans as well as in the Northern Hemisphere atmospheric circulation. The most remarkable change has been the “regime shift” during the winter of 1976/77 which appears to be the most striking feature in recent climate changes on interdecadal scale (Nitta and Yamada 1989, Trenberth 1990; Richman 1994; Zhang et al. 1997). Although most of the changes occurred in extratropics, such interdecadal variability is thought to be rooted in the tropics, initiated by the finding of a significant SST increasing since the mid-1970s in the tropical Oceans.

The work of Nitta and Yamada (1989) is among the earliest studies to focus on the recent interdecadal variations in the climate system. Their work shows that the mean tropical SST, especially in the central and eastern Pacific and Indian Oceans, has been warming since the mid-1970s and appears to have a decadal-scale variation. The

enhancement of the convective activity, associated with the SST increase, has been theorized to be directly related to the changes in atmospheric circulation. For example, Nitta and Yamada has shown that the strength of the east-west Walker circulation in the tropical Pacific becomes weaker. Also, the 500 hPa difference map between two decades of 1967-76 and 1977-86 indicates that the Pacific-North America (PNA) teleconnection pattern (Wallace and Gutzler 1981) became intensified due to the abnormal tropical forcing. Based on the observed time series of heat content and SST anomalies averaged between 2°N and 10°N along 137°E, Yamagata and Masumoto (1992) show a decadal trend from 1976 through 1988 with basically negative oceanic heat content anomalies and cooling in the tropical western Pacific as opposed to the warming in the central and eastern Pacific during the same period. They indicate that this SST anomaly may strongly affect the atmospheric circulation in the Aleutian low and Asian monsoon over the extratropical areas.

To describe various aspects of the interdecadal scale climate shift during the mid-1970s and examine the idea that the decadal-scale shift in winter circulation over Northern Hemisphere is a response to the changes in the tropical SST field and organized convection, Graham (1994) performs a comprehensive study in which both observational and model data are analyzed for the interdecadal climate changes over both the tropics and extratropics. He investigates the interdecadal variability in an array of climate variables such as SST, 700 hPa height, outgoing longwave radiation (OLR), high reflective cloud, convergence of moisture flux and surface wind fields, and applies a canonical correlation analysis method to study the interaction and relations among the selected fields. The Northern Hemisphere winter circulation

changes are found to relate to the SST and organized convection anomalies in the tropical Pacific. All the changes in the studied variable fields are consistent as a dynamical and physical system. During the winters of 1976/77 – 1981/82, SST is 0.75°C higher than those of 1970/71 – 1975/76 over much of the equatorial central and eastern Pacific ocean. He concludes that the evidence of abrupt, simultaneous and apparently related changes can be found in many fields, and the winter climate shift in the mid-1970s is not an artifact. The variations over the tropical Pacific represent the background mean state change in the coupled atmosphere-ocean system, not formed by the changes in ENSO intensity and frequency as proposed in Trenberth (1990) and Trenberth and Herrell (1994).

In a study of Northern Hemisphere general circulation pattern using a unique confirmatory eigenanalysis technique, Richman (1994) finds a circumtropical and subtropical mode to be the leading eigenmode in both winter and summer, explaining a much larger percentage of variance than next order mode in the data during the time period of the 1970s and 1980s, although traditional modes, such as the PNA and North Atlantic Oscillation (NAO), are identified. Each of these eigenmodes has the strongest signal and amplitude at the 200 hPa level. In addition, a sharp discontinuity around 1976 in the time series of the eigenmodes is apparent, with a noteworthy upward trend over the two decade period. He postulates that a possible tropical general circulation change during the mid-1970s caused these results, though his geopotential height field domain only extends southward to 15°N.

Nitta and Kachi (1994) investigate the interdecadal variability of precipitation over the tropical Pacific and Indian Oceans and the relationships of these changes with

the SST field, using surface and satellite data. Their analyses indicate that the precipitation in the tropical central-eastern Pacific increase during the period from the mid-1970s through the 1980s. These changes are consistent with the findings in Nitta and Yamada (1989) that the tropical central and eastern Pacific warming causes the enhancement of the convective activity in the region. On the other hand, precipitation in the tropical western Pacific is found to decrease slightly due partly to the change of the Walker circulation affected by the enhanced convection in the central and eastern Pacific. They also find that South Indian Ocean precipitation has increased since the mid-1970s, consistent with the SST increase during the same period. However, the precipitation before 1970 is nearly constant despite the SST increase in Indian Ocean. They speculate that this unclear relationship between SST and precipitation may be due to an absolutely cool SST in the South Indian Ocean which could not force strong convection. In a more recent research, Kachi and Nitta (1997) study the structures of the interdecadal variability in the tropical area by using SST, surface level pressure (SLP) and surface wind data. They first extract three dominant time scale in the monthly mean data with periods of several years (interannual variability), 10 to 20 years (decadal variability) and longer than 30 years (including linear a trend). Their analyses focus on the decadal scale variations and they find two significant modes by performing an empirical orthogonal function (EOF) analysis on a dataset *combining* SST, SLP and surface wind fields. The first EOF mode of their analysis is the ENSO-like interdecadal variation with a dramatic positive increasing after 1978 in its temporal coefficient. The leading EOF mode, from the analyses based on the composites of two decades (1968-77 and 1978-87), show that the key changes in the

atmospheric structures agree well with the previous findings of Nitta and Yamada (1989), Trenberth (1990), and Graham (1994). However, a new finding from their analyses on the composites is that the East Asian monsoon for both winter and summer appears to strengthen after 1978. For the longer time scale, i.e. longer than 30-year, it shows a decade linear trend of SST anomaly field in winter season, with positive trends dominating over the tropical central and eastern Pacific, Indian and South Atlantic Oceans and negative trends over the central North Pacific and North Atlantic.

Recently, Zhang et al. (1997) examines the global SST field and a selection of atmospheric fields and indices based on data for the period of 1900-1993. They apply a digital filter to the data to extract interdecadal and interannual variability signals, then utilize EOF analysis to the filtered time series and obtain the spatial signatures of the studied fields by regressing the variables, such as global SST, wind stress, SLP, upon the high-pass and low-pass filtered EOF time coefficients. It is found that the SST spatial structures for an ENSO time scale and interdecadal scale resemble one another over the equatorial and North Pacific. It is a dipole structure with large SST anomalies in the tropical Pacific anomalies of opposite polarity in the central North Pacific. While they confirm the previous findings of the interdecadal change with a shift in 1976-77, they also exhibit a similar decadal-scale change but with an opposite direction in 1940s. Such a finding adds another important clue to the changing feature of the interdecadal climate variability during this century.

1.2.2 Interdecadal climate changes in the extratropics

Most studies of the interdecadal variability in the climate system have emphasized on the changing features in the atmosphere and ocean in the extratropics, particularly in Northern Hemisphere. This is, in a large part, due to the fact that the interdecadal climate variations found in middle and high latitudes involve significant intensification of a Northern Hemisphere atmospheric action center (Aleutian low), winter middle latitude flow and storm track shifts, intensified PNA teleconnection pattern and North Pacific ocean circulation alterations. Such variations have direct impacts on our living climate environment and ecosystems.

Trenberth (1990) first reports the observed interdecadal climate changes in the Northern Hemisphere. During the decade of 1977-1986, North Pacific-basin surface temperature features large anomalies, with warming of larger than 1.5°C in Alaska and cooling of larger than 0.75°C in the central and western North Pacific. It is shown that the winter circulation regime shifts after 1976 from the mean SLP field analysis. The Aleutian low in winter season becomes deeper and shifts eastward in the period of 1977 through 1988. Such a change leads to a warmer and moister air advection into Alaska and along the west coast of North America, and a colder air advection over the North Pacific. These atmospheric changes are associated with the surface temperature and surface wind stress changes over the North Pacific which alter the ocean currents. The North Pacific circulation changes are related through teleconnection to the intensified and more frequent ENSO events at the same period in the tropical Pacific. In later research, Trenberth and Hurrell (1994) define a North Pacific index which is a simple measure of the circulation over the central North Pacific using an area-

weighted mean SLP. They update the previous findings in Trenberth (1990) and reveal the southward shift of the North Pacific storm track and changes in the ocean surface sensible and latent heat fluxes. Again, they stress the effect of the tropical forcing on the Northern Hemisphere circulation decadal-scale change and interactions between tropics and extratropics. The Pacific decadal changes are linked to the changes in ENSO after the mid-1970s.

The work by Tanimoto et al. (1993) is the first one to apply a digital filter to separate the North Pacific SST signal into 3 different time scales, i.e., less than 1-year, between 1 and 4-year and longer than 4-year. Their leading EOF mode of SST and its association with the PNA for the time scale longer than 4 years agree with the results obtained by Nitta and Yamada (1989) and Trenberth (1990). The time coefficient of this leading EOF mode exhibits several persistent anomalous periods at an interdecadal scale, whereas the transition between these persistent periods are generally very short. They also point out that the interdecadal SST variability may influence the structures of variability with short time scales through interactions.

Graham (1994) also obtains the major structures of the atmospheric and oceanic interdecadal changes in the North Pacific with difference maps of SST and 700 hPa for the winter season of the two epochs (1970-76, 1977-82). The canonical correlation analysis (CCA) technique is employed to examine the role of the tropical forcing on the North Pacific decadal scale circulation change proposed by Kashiwabara (1987), Nitta and Yamada (1989) and Trenberth (1990). He finds a significantly statistical relationship between the circulation and decadal scale variability of the tropical SST and organized convection. On the basis of his analyses,

he suggests that the major effect of the tropical forcing on the North Pacific interdecadal variations is the background state SST changes on the tropical Pacific, in contrast to the idea of ENSO intensity and frequency changes proposed by Trenberth (1990) and Trenberth and Hurrell (1994).

Kachi and Nitta (1997) apply the singular value decomposition (SVD) technique to the SST and Northern Hemisphere 500 hPa height fields, and show that, in their first SVD pattern at interdecadal time scale, the strong PNA pattern is associated with positive anomalies in the tropical central and eastern Pacific, suggesting that the tropical ocean condition and Northern Hemisphere circulation are strongly coupled with each other. The second mode of the SVD analysis shows that large amplitudes in the circulation spatial pattern over the North Atlantic, Eurasian continent and North Pacific. The temporal fluctuation of this mode completely differs from the leading mode.

Different results are reported in more recent research by Nakamura et al. (1997). It is discovered that the interdecadal SST variability is concentrated around two major oceanic fronts over the North Pacific area, based on an EOF analysis for a low-pass filtered dataset (signal of longer than 7-year period). The leading EOF mode represents the changes of the subarctic front which does not well correlated with the tropical SST variations. The cooling in this mode around the mid-1970s occurs 2 years in advance of the tropical warming, and can not be attributed to the tropical influences. The second mode in the analysis represents the SST fluctuations along the subtropical front. This mode seemingly matches up the North Pacific SST interdecadal variations found in the previous studies (e.g. Nitta and Yamada 1989;

Zhang et al. 1997; Kachi and Nitta 1997). However, the associated tropospheric circulation anomaly pattern with this mode is a south-north dipolar pattern over the eastern Pacific, not a PNA pattern as suggested in the previous findings. Furthermore, the surface pattern associated with such SST mode is the subtropical high, instead of the Aleutian low. Their results suggest some possible self-maintaining mechanisms of the interdecadal variability in the midlatitude North Pacific climate system.

1.2.3 Modeling studies of interdecadal variability and its possible mechanisms

Recent development of the atmospheric and ocean models make them useful tools for understanding of various changes in our climate system. These models have been applied in a research setting to interdecadal climate variability problems in past few years. While some of the studies concentrate on the analyses of the interdecadal variations in the outputs from the long-run of the atmospheric and ocean GCM (Graham 1994; Weaver and Sarachik 1991; Miller et al. 1994), models have been used to simulate and diagnose the interdecadal variability of the climate system by prescribing different forcing as model's input lower-boundary conditions (Lau and Nath 1994; Miller et al. 1994; Graham et al. 1994). In addition, coupled atmosphere-ocean models have been employed in the investigations of the interactions between atmospheric and oceanic components with an eye toward interdecadal climate variability. Again, these coupled modeling studies include analyses of the model outputs (von Storch 1994; Yukimoto et al. 1996; Chen and Ghil 1996; Manabe and Stouffer 1996), and specific simulations to investigate the physical processes of the

interdecadal variations (Latif and Barnett 1994; Robertson 1996). All these modeling studies have enhanced our knowledge and understanding on the interdecadal variability as revealed by the studies based on the analyses of the observed data in previous section.

To reproduce the decadal-scale climate shift in the mid-1970s over the tropical Pacific, Graham (1994) uses a series of ocean and atmosphere models, including the Cane-Zebiak ocean model, MPI ocean model, Zebiak atmospheric model and ECHAM1 GCM. For the experiments using the ocean models, the only success is for the MPI model, which qualitatively reproduces the observed SST increases in the west-central equatorial Pacific. However, when forced with the observed monthly mean SST field, all of the atmospheric models are able to obtain the major changes as observed both in surface wind field over the tropical Pacific by the Zebiak and ECHAM1 models and Northern Hemisphere general circulation pattern by the ECHAM1. The mid-1970s shift is qualitatively reproduced by these atmospheric models. The simulated changes in Northern Hemisphere atmospheric circulation show a relationship to tropical Pacific SST quite similar to that for the observed height field. These results suggest that basic aspects of the atmospheric response is forced by changes in the tropical SST field and the atmospheric GCMs are capable of capturing the most important aspects of the interdecadal variability.

Lau and Nath (1994) and Graham et al. (1994) perform similar atmospheric GCM simulations for investigating the interannual and interdecadal variabilities, independently. The results from these papers indicate the important effect of the tropical Pacific SST changes on the interdecadal variations of the atmosphere-ocean

system. In the work of Lau and Nath (1994), the GFDL atmospheric GCM is integrated over a period of 1946-1988, forced with three different SST boundary conditions. The three lower-boundary conditions are the observed monthly mean SST field over the near-global ocean between 40°S and 60°N (GOGA), the tropical Pacific between 25°S and 25°N (TOGA), and the North Pacific between 25°N and 55°N (MOGA), respectively; in all the ocean grids outside the region for a given experiment the surface SST is assigned to the local, observed SST climatology. The GOGA run successfully obtains the notable decadal-scale variability in height field as seen in the observations, although the amplitudes of the model atmospheric height anomalies are much smaller than the observed values. By comparing the results of the three experiments, they indicate that the model atmosphere is evidently much more responsive to the prescribed SST variability in the tropical Pacific than that in the North Pacific and also conclude that the SST anomaly over the tropical Pacific accounts for most of the oceanic driving force of the interannual and interdecadal variabilities in the model and real atmospheres at mid-latitude. They propose an *atmospheric bridge* which links the changes in the tropical Pacific forcing and worldwide SST anomalies. Such physical processes involve the variability of the North Pacific SST field and is primarily driven by the local atmospheric circulation, which is, in turn, a remote response to the tropical Pacific SST variability. In a closely related study, Graham et al. (1994) conduct three experiments by integrating the ECHAM2 GCM over a period of 1970-1988, forced with the observed SST field prescribed in the following three regions: *a.* tropical ocean only (between 25°S and 25°N, TOGA), *b.* mid-latitude ocean only (poleward of 31, MOGA) and *c.* global

ocean (GAGO3). Their purpose is to isolate the GCM response to SST forcing from different regions. The results show that the TOGA and GAGO3 runs perform better in showing the temporal signals which are consistent with those seen in the observed atmosphere. The interdecadal shift in the mid-1070s is evident in the simulated atmospheres. In agreement with the main findings in Lau and Nath (1994), the response of the atmospheric circulation to the North Pacific forcing is much smaller and less systematic than the response to the tropical SST. They also suggest that the recurrent patterns of atmospheric variability are the apparent links between the North Pacific SST and winter atmospheric circulation.

Recently, the interdecadal variability in the Pacific is studied by Yukimoto et al. (1996), with a 70-year integration of a coupled atmosphere-ocean GCM developed at Meteorological Research Institute (MRI), Japan. By analyzing the model simulation results, they are able to confirm some key findings in previous work based on both observational data and modeling results. Both interdecadal and interannual variabilities are shown in the power spectra of the Pacific SST. Using the low-pass filtered model data, containing only longer than decadal-scale signals, they show that the interdecadal SST spatial pattern (leading EOF mode) is characterized by a marked negative correlation of the central North Pacific with the tropical SST. The correlation map between the model atmospheric 500 hPa height field and SST interdecadal mode exhibits a PNA-like pattern. It is found that, in mid-latitude, the interdecadal SST variation is larger than the ENSO scale variation, while the interdecadal wind variation is smaller than that of ENSO scale. Alternately, in the tropical regions, SST change in the ENSO scale is larger than that for the interdecadal scale; the wind change for the

two time scales are close in magnitude. On the basis of such comparisons, they argue that if the extratropical atmospheric circulation were controlled by local SST anomaly, the atmospheric response for the interdecadal scale would be large since the local SST anomaly is relatively strong. Therefore, they conclude that the interdecadal variability of atmospheric circulation over the North Pacific is forced by the tropical SST variability since the interdecadal variabilities of both the tropical SST and mid-latitude wind fields are small.

In contrast to the studies of Lau and Nath (1994) and Graham et al. (1994), from a 70-year integration with a coupled atmosphere-ocean GCM (ECHAM3 and Hamburg ocean model), Latif and Barnett (1994) illustrate that about 30% of the low-frequency climate variability over the North Pacific and North America can be attributed to unstable air-sea interactions between the North Pacific subtropical gyre circulation and Aleutian low. The tropical forcing is thought to play a minor role (Latif 1997). The model simulation captures the notable decadal variability over the North Pacific and North American coast in the 70-year simulations. The spatial structure of such decadal variability is dominated by a large-scale positive anomaly extending from the Asian coast across almost the entire Pacific centered along about 35°N. The negative anomaly areas spread over the subtropical central Pacific and along the North American coast. A complex EOF (CEOF) method is used to analyze the low-pass filtered model upper ocean heat content. The leading CEOF pattern exhibits a 20-year period with a clockwise rotation of dipole spatial structure over the North Pacific. The atmospheric response to such an ocean thermal structure with a positive height anomaly at 500 hPa, and a negative wind stress curl anomaly over high

latitudes of the North Pacific. Based on these findings, they propose a coupled mechanism for the interdecadal variability of the system. When the subtropical ocean gyre is strong, Kuroshio current transports the warm water poleward and positive SST anomaly extends into the central and eastern North Pacific. The atmosphere responds with a positive height anomaly and the wind speed is reduced. Such a positive feedback can amplify an initial disturbance. However, the negative wind stress curl anomaly will eventually reduce the subtropical gyre circulation, poleward heat transport and initial positive SST anomaly. Since the ocean can memorize the past state, it adjusts the wind stress with a time lag. Such a transient response of ocean, in a form of planetary wave propagation, may lead to a continuous oscillation of the system from one phase to another. During this oscillation, the tropical forcing plays no role.

Apart from other modeling studies, Gu and Philander (1997) propose an interaction theory between the tropical and extratropical atmosphere-ocean system for the generation of the interdecadal variability by means of a simple ocean box model. A shallow wind-driven meridional circulation is hypothesized to serve as the link between the tropical and subtropical oceans. This water circulation involves a downward motion of water parcel in the subtropical region of the eastern Pacific. Then the water parcel travels southwestward along isopycnals into the equatorial thermocline, where the parcel is upwelled to the surface. The water parcel is transferred poleward through Ekman drift at the ocean surface. Positive feedback of the tropical atmosphere-ocean system may amplify an initial perturbation. When given a positive SST perturbation in the tropical Pacific, the atmosphere will respond

with an intensified PNA pattern (Nitta and Yamada 1989; Lau and Nath 1994; and Zhang et al. 1997; among others). The pressure over the North Pacific drops and westerlies are intensified. Such an atmospheric circulation will induce heat loss from ocean and SST decrease in the North Pacific through evaporation. The negative SST anomaly in the North Pacific travels into the equatorial thermocline in several years through the pathways of the meridional circulation. When upwelled to the ocean surface, the cold water will cool the tropical ocean surface and initiate the cold condition there, and lead the atmosphere-ocean into an opposite phase of the cycle. The extratropical wind will be weakened and cause the North Pacific SST to increase. Such a mechanism can lead to interdecadal oscillations with a broad spectrum of time scales, depending on the time by which the water parcel travels from the extratropics to equatorial thermocline. Their modeling experiment shows that an initial small perturbation can be slowly amplified and eventually become an oscillation with a period of 35 years and an amplitude of about 1°C. The tropics and extratropics are out of phase, which can be applied to the interdecadal variability of the warming in the equatorial central and eastern Pacific and cooling in the North Pacific during the past few decades. The links between the tropics and extratropics may cause continual interdecadal climate fluctuations. However, such hypothesis needs to be proven by the observations and more sophisticated coupled atmosphere-ocean models.

1.3 The motivations and objectives of the present research

As indicated in previous literature review section, in addition to ENSO-cycle changes, the tropical SST records exhibit an interdecadal-scale change in the past several decades, with a marked “regime shift” in the mid-1970s. At the same time, the extratropical atmosphere and ocean have experienced significant changes at the same time scale. Many studies have indicated the importance of the changes of the tropical forcing in relation to the interdecadal climate variability over the North Pacific and parts of North America (Zhang et al. 1997). It has been a common understanding that the tropical forcing plays an important role in the Northern Hemisphere interdecadal variations (Nitta and Yamada 1989; Trenberth 1990; Trenberth and Hurrell 1994; Graham, 1994; Zhang et al. 1997; Nakamura et al. 1997). Given this, one of the questions is: what are the physical processes which establish the links between the tropical SST interdecadal variability and the general circulation anomaly in the extratropics? A satisfactory answer to such a question would not be obtained without, at first, a better understanding of how the tropical atmosphere responds to the tropical forcing at the interdecadal time scale. This is the key motivation of the present research. However, there are a dearth of studies of the tropospheric circulation and geopotential height field changes at the interdecadal time scale. This is probably one of the major reasons why few physical mechanisms for such changes can be found in the refereed literature, and the links between the tropical forcing and extratropical interdecadal variations are, to date, mostly studied by statistical analyses.

It has been nearly a decade since Nitta and Yamada (1989) first discovered the interdecadal-scale changes in the tropical SST field and their association with the

Northern Hemisphere atmospheric circulation and oceanic physical state changes. The study of the tropical geopotential height and circulation variations on an interdecadal scale and their association with the surface forcing changes is an important step to gain a fuller understanding of the interactions between the tropical forcing and extratropical circulation variations in the atmosphere-ocean coupled system. This is particularly important given the consistent and abrupt change of the system in the mid-1970s. Numerical experiments with improved atmospheric general circulation model (GCM) may aid in diagnosing and identifying some of the important physical processes which link the atmospheric changes to the ocean boundary conditions.

The objectives of this research are (1). to study the structures of the interdecadal variations in the tropical geopotential height field and corresponding atmospheric circulation, with an emphasis on the changes over the domain of the tropical Pacific; (2). to link these variations to the changes in the tropical ocean SST field, with an emphasis on the interdecadal variability over the tropical central and eastern Pacific; and (3). to investigate the physical processes and mechanisms which are responsible for the development and maintenance of the spatial structures of the interdecadal variations in the tropical height and circulation patterns, given the changes of the SST field.

To facilitate these research objectives, a selection of the NCEP/NCAR reanalysis fields, a newly released comprehensive analysis dataset (Kalnay et al. 1996), will be used to examine the tropical three-dimensional interdecadal variations in height and circulation fields from surface to upper troposphere (200 hPa), and identify the statistical and physical relationship between these height field changes and

the tropical SST interdecadal variability. Furthermore, the ECHAM4 GCM outputs from a long-term climatological run forced with observed monthly mean SST and sea ice fields (Ward and Navarra 1997) will be used to perform the same analyses as with the reanalysis data to test the hypothesis that the identified interdecadal variations in the atmosphere are a consequence of internal interaction in the climate system. Additionally, consistent results from the GCM and reanalysis system may bolster confidence in applying the GCM to diagnose the physical mechanisms responsible for the interdecadal variability in the atmosphere. Therefore, the ECHAM4 (a state of the science GCM developed at University of Hamburg and Max Plank Institute for Meteorological Studies in Germany) will be employed to perform several numerical simulations with prescribed tropical SST fields to investigate how the atmosphere responds the specified surface forcing patterns. Results from these experiments can be used to identify the physical processes which lead to the structures and features found in the analyses of the reanalysis and model datasets.

Such a physical analysis with the GCM forms the key difference which distinguishes the present work from most of the previous studies in that it adds a new dimension – diagnosis of the detailed physical mechanisms, for the interdecadal climate variability research problem. As mentioned in Nakamura et al. (1997), the causes and mechanisms of the low-frequency climate variability in the North Pacific are not fully understood. One of the major circulation features associated with the interdecadal variation is that the intensification of the PNA pattern has been largely enhanced since the mid-1970s. The most equatorward node of the PNA action centers is located over the North Pacific research domain. By careful parallel analysis of the

NCEP/NCAR reanalysis and ECHAM GCM data, elucidation of physical mechanisms, for the tropospheric geopotential height field interdecadal variations, will hopefully better explain the physical linkages between the tropical forcing and extratropical circulation. This, in turn, will be an important step toward a full understanding of the complete interdecadal variability in our climate system.

Chapter 2

Tropical SST interannual and interdecadal variabilities

Previous studies have indicated that the spatial structure in the tropical SST interdecadal variability is reminiscent of the SST structure occurred during a typical ENSO period (Lau and Nath 1994; Zhang et al. 1997; Yukimoto et al. 1997). The SST variation signals with similar spatial structures but different time scales are mixed in the observations. An atmospheric response to the ENSO-like SST structure described in Rasmusson and Carpenter (1982, their figure 3), e.g. the intensified PNA pattern shown by Lau and Nath (1994) and Graham (1994), can be attributed to different surface forcing sources on several time scales such as ENSO event or the interdecadal SST variations, or even the two forcing mixed together. The relative importance of each of the sources on different time scales needs to be examined. To investigate the interdecadal tropical atmospheric circulation changes and their causes, one must at first understand the forcing source changes. In this chapter, we investigate the tropical sea surface temperature changes which may result in the variations in the atmosphere. Our research concentrates on the SST changes and their effects on the atmosphere on interdecadal scale. However, because of the similarity in the spatial structures of the tropical SST variations on interannual and interdecadal scales, here the SST variations at interannual scale will also be examined in order to better understand the mechanisms of atmospheric interdecadal variability.

2.1 Sea surface temperature dataset

To investigate the interannual and interdecadal variations in the tropical oceans, monthly mean SST dataset, from 1958-1995 for $2^\circ \times 2^\circ$ latitude-longitude grid in the domain of $35^\circ\text{S} - 35^\circ\text{N}$, is used in this study. This dataset is drawn from the reconstructed Reynolds SST data obtained from the Climate Prediction Center (CPC) of the National Oceanic and Atmospheric Administration (NOAA) (Smith et al. 1996). The reconstructed Reynolds SST dataset is to provide physically realistic SST fields without extremes or abnormally stretched gradients that might result from data deficiencies in some areas. The SST reconstruction is performed by first producing the spectral EOFs from the 1982-1993 optimum-interpolation (OI) SST dataset of Reynolds and Smith (1994). Then the leading 24 of those EOF modes (accounting for 89% of the SST anomaly variance) are used as basis functions and are fitted to the $2^\circ \times 2^\circ$ grid-cell SST values in the Comprehensive Ocean-Atmosphere Data Set (COADS) for the period 1950 - 1995 to determine the time dependence of each mode. A global field of SST anomalies are then reconstructed from these spatial and temporal modes. Because of limited in situ data, the reconstructed anomalies are only computed from 45°S to 69°N . The resulting anomaly data are converted to full SST fields by adding the adjusted OI climatology (Smith et al. 1996). Since the reconstruction involves the optimum interpolation and only leading EOFs, the small scale features in the original raw SST input data are over-smoothed.

The 1958-1995 period is chosen so as to be consistent with the data temporal coverage of the reanalysis and GCM model outputs used later in this research. The $35^\circ\text{S} - 35^\circ\text{N}$ spatial domain can present entire spatial signatures of the SST variations over the

tropical and subtropical regions. Overall, the SST dataset includes 36×180 grid points and $12 \times 38 (= 456)$ individual monthly mean values, which forms a 456×6480 data matrix.

2.2 Analysis procedures and methods

Most studies of the tropical SST interannual and interdecadal variations have been performed by principal component analysis (PCA) or EOF analysis (e.g., Nitta and Yamada 1989; Zhang et al. 1997; Montroy 1997). Both these two methods are eigentechniques and will achieve the same patterns when applied to the same data matrix. In this study, PCA method is used to extract the dominant modes of the SST anomaly changes in the studied domain. As the raw SST data contain the signals over the whole spectrum domain, a digital filter is applied to the SST dataset to separate the variabilities on different time scales before applying PCA, as suggested by Tanimoto et al. (1993) and Zhang et al. (1997).

2.2.1 Filtering

To discern the interannual and interdecadal variations in our dataset, high- and low-pass filtering methods are used, respectively. The Lanczos filter (Duchon 1979) is applied to the monthly mean SST fields for the 38-year period at the 6480 grid points between 35°S and 35°N . The response functions of these filters are shown in Fig. 2.1. The number of weights is 73 in both of the filters so that the transition of the response between zero and unit responses is as sharp as possible over the spectrum domain and to

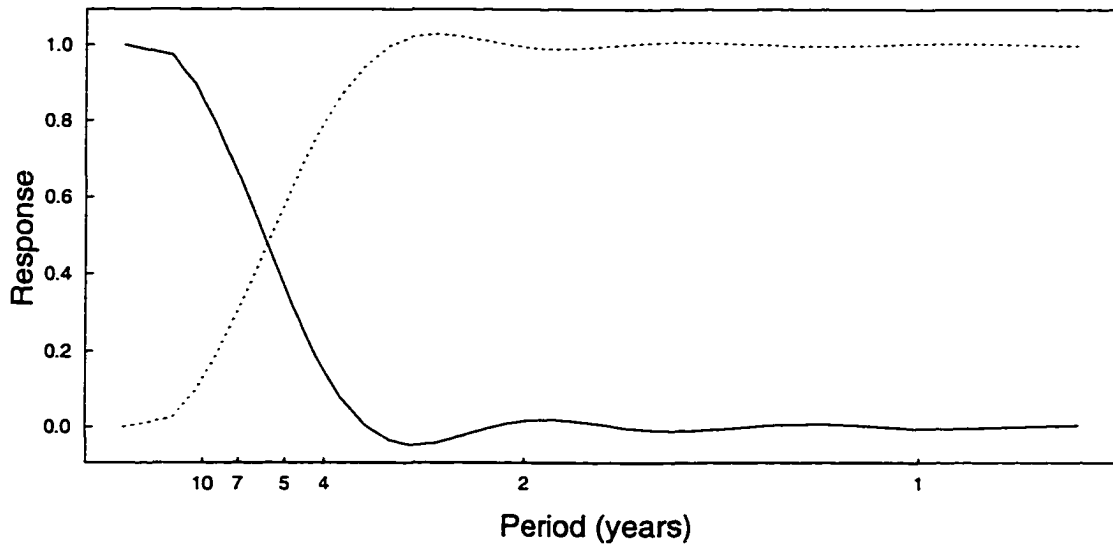


Figure 2.1 Lanczos filter response functions. The solid curve is the low-pass filter and the dash curve represents the high-pass filter.

reduce Gibbs oscillations, at the same time without losing too many individual monthly mean SST values at the beginning and end of the dataset. The Gibbs oscillations, caused by the truncation in the Fourier series, are very small for both high- and low-pass filter responses as seen in Fig. 2.1. For the high-pass filter, a cutoff frequency of 8-year is selected to suppress the information with a period of long than 7 years in the response function. Since only winter months are used in this study, the effects of intraseasonal variability is minimal and the high-pass filtered time series is believed to contain mainly interannual variations of the tropical SST dominated by El Niño and Southern Oscillation (ENSO) signals (Nitta and Yamada, 1989). On the other hand, the cutoff frequency in the low-pass filter is 6-year so that the response of 5-year period is kept

below 0.4, and drops dramatically from 5-year period onto shorter periods. The information from the low-pass filter contains mainly signals with periods longer than decadal time scale as seen in Fig 2.1.

Our SST data times series are weighted by the high- and low-pass filtering weights, respectively to obtain two new datasets. In the filtering processes with 73-weight, the data value at a specific time slot in the filtered dataset is obtained by weighting the data value at that specific time and 36 data values on each side of that specific time in the raw SST dataset. The resultant SST dataset will lose 36 months (3-year data) on each end of the time series. Hence, the new filtered datasets contain the data time series from 1961 to 1992. Since this study will focus on boreal winter season, only filtered December, January and February SST values are used to construct the new data matrices. As a result, two 96 (months) \times 6480 (grids) matrices are formed and subject to further analyses.

2.2.2 *Principal component analysis*

PCA provides a convenient method for analyzing the spatial and temporal variability of long time series of data over large area due to its ability to reduce large data sets into a much smaller dimensionality. In an S-mode analysis (Richman 1986), the PCA approach splits the temporal variance of data into orthogonal spatial pattern called principal component (PC) loading. These PC loading vectors can be arranged in decreasing order based on the variance they explain. Each PC loading pattern is associated with a series of time coefficients, called PC score, which describes the time

evolution of the corresponding spatial mode. The major advantage of the PCA method is that it can provide the most efficient way of compressing geophysical data in both space and time, and the spatial patterns obtained from PCA may be regarded as uncorrelated modes of variability of the studied fields. Mathematically, PCA can reduce a large number of correlated quantities in time and space into a small number of orthogonal functions (PCs) that are linear combinations of the original observations and account for a large percentage of the total variance.

Consider a real-valued geophysical field \mathbf{Z} defined at m positions with n observations, i.e., \mathbf{Z} is an $n \times m$ matrix, the set of the n -row vectors can be represented in an m -dimensional space. For a meteorological variable, there exists large correlation among the n vectors. Thus, the distribution of the n vectors in m -dimensional space will be organized in clusters or along some preferred directions. We want to find a set of orthogonal basis in the vector space ($\mathbf{a}_1, \mathbf{a}_2, \dots, \mathbf{a}_m$) such that each vector \mathbf{a}_i best represents the cluster of the n original vectors. To satisfy such conditions, the basis functions of all the n vectors onto each \mathbf{a}_i is maximized sequentially. The basis vectors are orthogonal each other. Following Richman (1986), the PC model representation of \mathbf{Z} is

$$\mathbf{Z} = \mathbf{F}\mathbf{A}^T \quad (2.1)$$

where the \mathbf{F} is an $n \times r$ PC score matrix; \mathbf{A} is an $m \times r$ PC loading matrix, whose vectors $\{\mathbf{a}_i\}$ form a set of new orthogonal basis in the m -dimensional space. r ($< m$) is the number of PCs we retain (or number of axis). Because large correlation among the n vectors exists, the dimensionality can be greatly reduced.

Toward solving the linear system given in (2.1), we use unit vector, \mathbf{e}_k which is

proportional to vector \mathbf{a}_k , to represents the basis axis direction. The following sum of the squared projections onto the k th axis needs to be maximized

$$\frac{1}{n} \sum_{i=1}^n [\mathbf{z}_i \mathbf{e}_k]^2 = \frac{1}{n} [\mathbf{e}_k \mathbf{Z}^T \mathbf{Z} \mathbf{e}_k] = \mathbf{e}_k \mathbf{R} \mathbf{e}_k^T \quad (2.2)$$

where \mathbf{R} is a symmetric covariance or correlation structure in the data matrix and defined as

$$\mathbf{R} = \frac{1}{n} \mathbf{Z}^T \mathbf{Z} \quad (2.3)$$

The maximizing of $\mathbf{e}_k \mathbf{R} \mathbf{e}_k^T$ subject to the conditions:

$$\mathbf{e}_k^T \mathbf{e}_j = \begin{cases} 1 & k = j \\ 0 & k \neq j \end{cases}$$

leads to an eigenvalue problem of solving the following equation:

$$(\mathbf{R} - \lambda \mathbf{I}) \mathbf{e}_k = 0 \quad (2.4)$$

where λ is the eigenvalue and \mathbf{e}_k is the eigenvector associated with the k th eigenvalue, \mathbf{I} is an $m \times m$ identity matrix.

According to (2.4), eigenvalues λ_k and eigenvector \mathbf{e}_k can be obtained by solving the characteristic equation of \mathbf{R} . The sum of eigenvalues ($\sum_{k=1}^n \lambda_k$) equals to the total variance in the data, and each eigenvalue λ_k gives the variance that the corresponding eigenmode accounts for. When the eigenvalues are arranged in descending order of magnitude, the sequence of the function of the eigenmodes represents the importance of the mode in explaining the fraction of the total variance in the data.

PC loadings \mathbf{a}_k are defined as the eigenvector \mathbf{e}_k rescaled by the square root of its

corresponding eigenvalues, i.e., $\mathbf{a}_k = \mathbf{e}_k \lambda_k^{1/2}$ so that the sum of each squared loading elements becomes the variance explained by that PC mode. Given the PC loading matrix \mathbf{A} , the correspond PC score (time coefficient) matrix \mathbf{F} can be obtained by solving system (2.1).

In this study, the two 96×6480 winter monthly SST anomaly data matrices resulted from high- and low-pass filtering are subjected to the PCA procedures outlined above. The PC modes are obtained from the correlation matrix of the input datasets so that the variance of SST anomalies on each grid point is scaled to unit. The covariance-based PCA is also performed and the resultant modes are consistent with those computed from correlation matrix. Only the most significant mode of these SST anomalies will be examined.

2.3 Sea surface temperature interannual variations

With much of the longer than 7-year period signals filtered out, the monthly mean SST dataset from high-pass filter should mainly contain the variations at interannual time scale which is dominated by the ENSO events in our studied area. Fig. 2.2 shows the spatial loading pattern and score of the first PC mode for the high-pass filtered SST data. This mode accounts for 24% of the total variance in the data. From the spatial pattern (top panel of Fig. 2.2), it can be clearly noted that an extensive area of the positive SST anomaly structure covers the equatorial central and eastern Pacific. Two narrow negative anomaly areas (strips) oriented southwest-northeast and northwest-southeast SST can be found in the North and South Pacific, with less SST anomalous

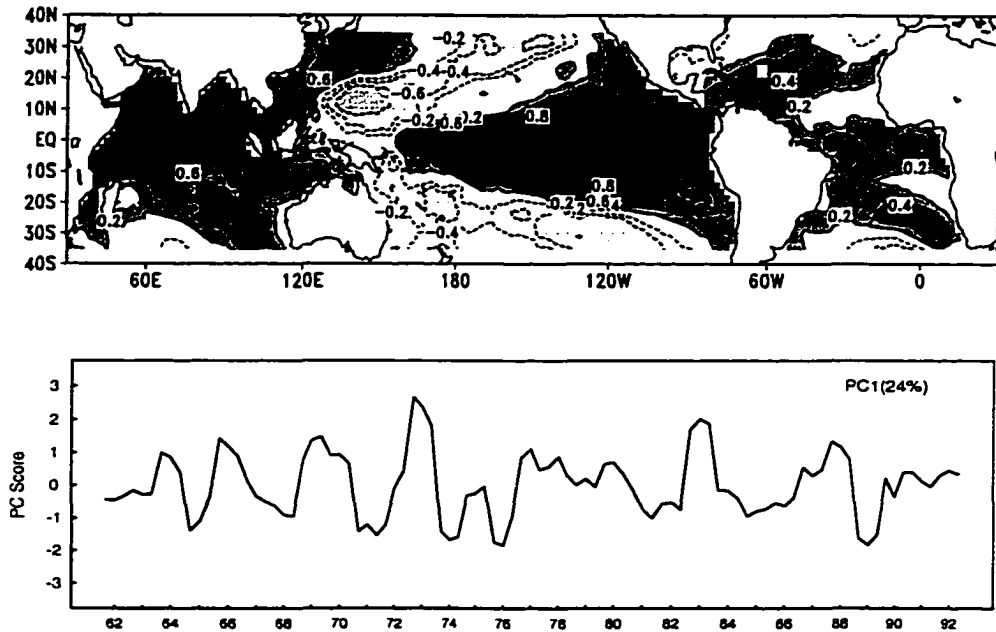


Figure 2.2 Leading PC loading pattern (top) and its time coefficient (bottom) for high-pass filtered SST anomaly over the domain. The variance explained is given in the upper right-corner of the bottom panel

intensities. Positive SST anomalous areas are also present in the equatorial Indian Ocean. Signals over Atlantic ocean are rather noisy. The spatial structure over the Pacific portion of the domain appears to be, to certain extent, symmetric about the equator. This is consistent with the SST PC/EOF patterns found in other studies (Yukimoto et al. 1996; Montroy 1997; and Zhang et al. 1997). Such a spatial SST anomalous structure characterizes the "transition" and "mature" phases of El Niño evolution for the Pacific, as summarized in Rasmusson and Carpenter (1982).

The temporal fluctuation of this ENSO spatial pattern is shown in the lower panel of Fig. 2.2. The El Niño and La Niña events occurred during the 1961 - 1992 period are well captured. The 1963, 1972-73, 1982-83, 1986-87 El Niño events and

1964, 1970-71, 1973, 1975, 1988 La Niña events stand out in the time series. It is difficult to identify any long term trend for the intensity change of the El Niño/La Niña events from the time series in Fig. 2.2. It is interesting and important to notice that after removal of the decadal scale variability, the most famous 1982-83 ENSO event is not the most intensive warm event in our studied time-span. The 1972-73 ENSO appears to be the strongest event. What makes the 1982-83 basin wide warming event so intensive is because of the superimposition of two strong positive phases at both interannual and interdecadal time scale variations over the equatorial central and eastern Pacific as will be seen subsequently.

2.4 SST interdecadal variability

The PC mode shown in Fig. 2.3 is the spatial and temporal structures of the leading mode from the low-pass filtered SST anomaly data, which explains 44% of the total variance, implying the dominance of such a signal in the data. The most pronounced feature in the spatial pattern (top panel of Fig. 2.3) is that there exists a large positive spatial SST anomaly structure over the central and eastern Pacific which is somewhat reminiscent of the dominant SST anomaly signature of ENSO time scale as shown in Fig. 2.2. While the structures in the North and South Pacific are similar to the ENSO pattern, the tropical positive SST PC loading area over the central and eastern Pacific is much more spatially extensive toward the poleward regions, and the overall anomaly is considerably wider in north-south direction than the one found in ENSO event. Strong positive SST anomalous structures occur in the central Pacific area near

the dateline, and eastern Pacific between 145°W - 100°W, which is supported by the finding in Zhang et al. (1997). Since the SST anomalous patterns in the Pacific are qualitatively similar for the variations at both interannual and interdecadal scales and, moreover, the atmospheric changes associated with these SST anomalies are similar as well, as found in Trenberth (1990), Graham (1994), and Lau and Nath (1994), such an interdecadal change in the atmosphere-ocean system is referred as to ENSO-like interdecadal variability (e.g. Zhang et al. 1997).

Large positive SST anomaly areas of the same magnitude as those in the Pacific Ocean are also found over almost the entire Indian Ocean, Atlantic Ocean along the North African coast, and near Gulf of Mexico. The spatial features in the Indian Ocean support the results of Kachi and Nitta (1997) who find the large spatial structure of interdecadal variability over the tropical Indian Ocean.

In the extratropics, the most striking feature is the large negative PC loading area over part of the North Pacific. This is the extratropical portion of the SST interdecadal variation spatial features as indicated in (Yukimoto et al. 1996; Zhang et al. 1997). It is interesting to note that such a feature only occurs in the North Pacific and there is no counterpart over the South Pacific area for this mode.

The temporal variation of the ENSO-like interdecadal signature shown in Fig 2.3 (lower panel) exhibits a notable interdecadal variation, with an evident basic state jump in the 1976/77 winter. The SST anomaly basic state is in the negative phase for all winter months prior to 1977. During winters of 1977-1980, the SST anomalous pattern makes a sharp transition to a state of +1-unit standard deviation of the SST anomaly, and then oscillates in the new background state afterward.

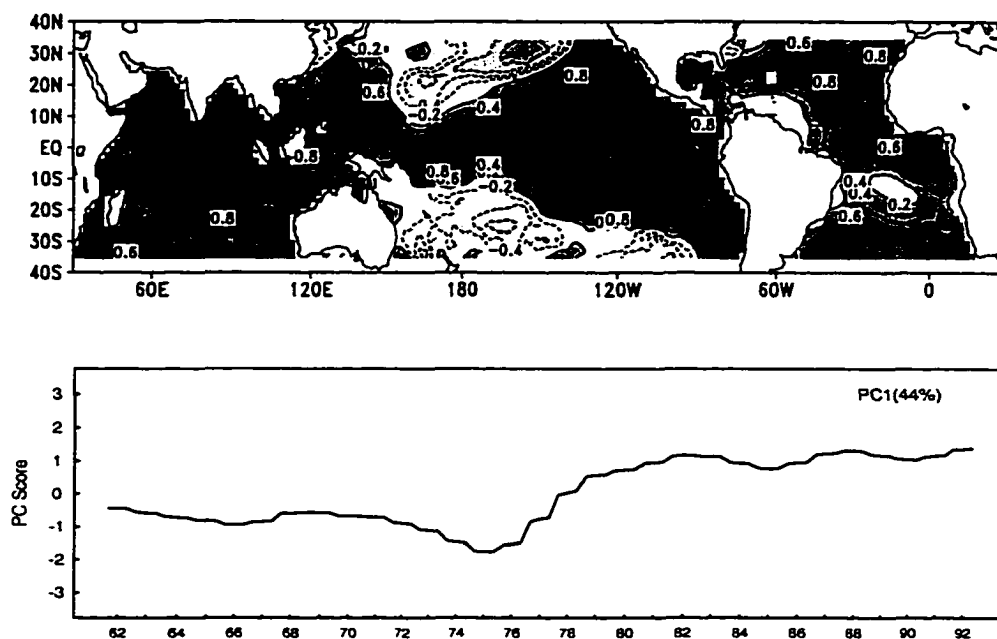


Figure 2.3 Leading PC loading pattern (top) and its time coefficient (bottom) for low-pass filtered SST anomaly over the domain. The variance explained is given in the upper right-corner of the bottom panel.

According to the time series of the most important interdecadal variability mode shown in Fig. 2.3, the studied time-span is broken into two periods. Period 1 (hereafter P1) spans from our starting record to the winter 1975/76 (prior to the jump), during which the interdecadal SST anomalous pattern is in its negative period. Period 2 (hereafter P2) covers the time-span from the 1976/77-winter to the end of our record (after the jump), and during this period, the temporal variation is characterized by an oscillation of time coefficient above zero and the pattern is obviously in the positive period. Fig. 2.4 is the difference map of average values of the low-pass filtered SST field between P1 and P2 ($P2 - P1$). This difference map shows that the average SST difference largely resembles the spatial structure given by the leading PC loading pattern

in Fig. 2.3. Sea surface temperatures increase in the equatorial central Pacific and eastern Pacific in later period, mostly greater than 0.2°C . Regions with a SST increase greater than 0.4°C include a small area in the equatorial central Pacific, a huge area in the eastern Pacific from the equator southward to 20°S , the area near the west coast of North America between 10°N - 30°N . The negative areas (less than -0.2°C) are coincidence with the negative anomalous areas in the subtropical central North and South Pacific oceans. The SSTs in the Indian Ocean also increase by 0.2°C . A large area in the North Atlantic is also found to have a SST increase above 0.2°C . By comparison of the difference map with the spatial SST anomaly PC loading pattern in Fig. 2.3, it is apparent that the leading PC mode mainly extracts the structure of SST difference between the two periods.

Since the first PC mode accounts for a very large percentage (44%) of the interdecadal variability, it can be concluded that the tropical monthly mean background SST state has changed from 1976/77 for boreal winter. As the time fluctuations of the tropical monthly mean SST interannual variability are examined (Fig. 2.2), the results do not support the conclusion that the intensity and occurrence of ENSO events in post

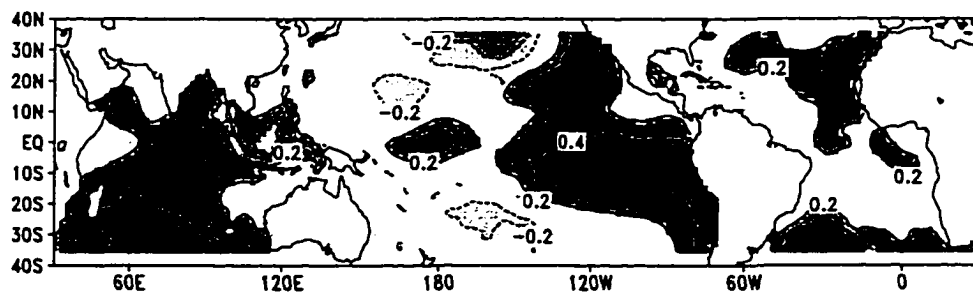


Figure 2.4 Low-pass filtered winter monthly mean SST difference field (Period 2 - Period 1). Unit: $^{\circ}\text{C}$.

1976/77 period are significantly stronger and more frequent than the period before 1976/77 as posited by Trenberth (1990) and Trenberth and Hurrell (1994). An alternate hypothesis is that the tropical SST changes related to the mid-1970 shift found in previous studies can be mostly attributed to the SST climatological background state change. If there exists an interaction between the tropics and extratropics for the decadal changes, such a tropical forcing may not be on the ENSO time scale, but rather driven by the tropical SST interdecadal variability based on our current results.

Chapter 3

Atmospheric interdecadal variations over the tropics

The major interdecadal modes of the NCEP/NCAR reanalysis data and general circulation model (GCM) simulated atmosphere over the tropics are delineated in this chapter. Though a few studies concentrating on the Northern Hemisphere circulation have been performed (e.g. Graham 1994; Lau and Nath 1994; among others), such a study is new to meteorological literature. The structures of the interdecadal variability in the real tropical atmosphere (represented by the atmospheric variable fields in the reanalysis data) will be determined, and furthermore, results on how well the GCM forced with the observed SST fields can simulate such variability on the same time scale will be presented. It has been shown that current GCMs can simulate atmospheric interdecadal variability reasonably well (Graham 1994; Richman 1994; and Lau and Nath 1994). If it can be demonstrated that a GCM is able to produce the interdecadal variation signals in the real atmosphere, it is feasible to use that model to investigate the physical mechanisms underlying the changes in the atmosphere. Such a statement forms the rationale for this research to include the analyses for the interdecadal variability in the atmosphere simulated by the ECHAM4 GCM.

3.1 Data and analysis procedures

3.1.1 Height and wind data from the NCEP/NCAR reanalysis

The data used for investigating the atmospheric changes in this study are from the NCEP/NCAR reanalysis (Kalnay et al. 1996) which is an effort to reanalyze historical data from 1957 through 1996 with a frozen assimilation system. The analysis data from such system may greatly alleviate the spurious signals due to the frequent updates of the operational data assimilation systems. These spurious signals can be easily interpreted as climate anomalies. The core of the NCEP/NCAR reanalysis system is a data assimilation system consisting of the NCEP spectral model, the operational NCEP spectral statistical interpolation and the data and analysis quality control systems (Kalnay et al. 1996). The model employed in the assimilation system is the NCEP Medium Range Forecasting spectral model with T62 spectral truncation (equivalent to a horizontal resolution of about 210 km) and 28 vertical levels in the sigma coordinate. The model parameterizes all major physical processes, including radiation, convection, large-scale precipitation, shallow convection, boundary layer physics, interactive surface hydrology, gravity wave drag and vertical and horizontal diffusion. The whole reanalysis system involves the recovery of land surface, ship, rawinsonde, pibal, aircraft, satellite and other data; quality controlling and assimilating these data (Kalnay et al. 1996).

Basic upper-air meteorological parameters on 17-pressure levels and $2.5^\circ \times 2.5^\circ$ latitude-longitude grid can be obtained from the outputs of the NCEP/NCAR reanalysis. In this work, subsets of geopotential height and wind data are extracted

from the outputs in grided binary (GRIB) format of the reanalysis data. Geopotential height data at 4 pressure levels (1000, 700, 500, 200 hPa) and horizontal wind fields at 2 levels (850, 200 hPa) are used to diagnose the 3-dimensional structure of the interdecadal variability for tropical atmospheric circulation. The height and wind fields used in the analyses are monthly mean data for 1958-1996 period in the domain of 35°S –35°N with 4176 (144 × 29 latitude-longitude) grids. A total of 8 datasets for 3 meteorological variables (height, u- and v-wind fields) at specified pressure levels are constructed. These data will be subjected to further studies.

3.1.2 Height and wind data from the ECHAM4 GCM climatological run data

To investigate the observed interdecadal climate variability using the atmospheric general circulation model (GCM), one needs to validate the ability of the GCMs to simulate the atmospheric variability on the interdecadal time scale. The ECHAM4 GCM is used in the present research. This model is the latest version of the ECHAM model developed at the Max-Planck Institute in Hamburg, Germany. Descriptions of the model is deferred to next chapter. In our analyses, the ECHAM4 atmospheric data are from one of the three long-term climatological runs performed at the Istituto Per Lo Studio Delle Metodologie Geofisiche Ambientali (IMGA), Italy. Hereafter, this dataset will be referred to as "IMGA climatological run". In these experiments, the ECHAM4 GCM are integrated at T30 resolution through the period 1960-1994 forced with the observed sea surface temperature fields compiled by UK Meteorological Office (GISST2.2), starting with three different initial conditions.

Ideally, it would be better to utilize the average of the three simulations to represent model atmosphere as the work of Roeckner et al. (1996) and Moron et al. (1997). However, Moron et al. (1997) show that, for the tropical area, the model's reproducibility is rather high and the model atmospheric variabilities are driven by the external forcing. Since this research focuses on the tropics, only one member of the three simulations is used.

The same type of analysis will be applied to the observed and model atmospheres in this chapter. The data used from the model outputs are the same as those from the reanalysis data, i.e., monthly mean height data at 1000, 700, 500 and 200 hPa and u- and v-wind data at 850 and 200 hPa. The first year (1960) data are not used since that period is the time for model spin-up, so that the time-span of the model data in the study is 1961-1994. The research domain for model data is chosen as the region between 38.97°S – 38.97°N based on the T30 Gaussian grids. Thus, the horizontal grid points for the model data is 2112 (96 longitudes × 22 latitudes).

3.1.3 Analysis procedures

Following the same procedures described in Chapter 2, low-pass filter and PCA are applied to the winter monthly mean geopotential height field data to study 3-dimensional structure of atmospheric height variations on interdecadal scale over the tropics. For the reanalysis data, a 468 (months) × 4176 (grids) data matrix is subjected to low-pass filter and the resultant 96 winter month data forms the input data for PCA analysis for each of the 4 pressure levels. Similarly, each data matrix for model height

data contains 81 individual low-pass filtered winter monthly mean field on 2112 T30 Gaussian horizontal grid points and PCA is performed on the 81×2112 data matrix.

3.2 Tropical wide interdecadal atmospheric variability in the reanalysis data

3.2.1 Temporal and spatial structures of the geopotential height changes

Fig.3.1 shows the temporal variations of the leading PC modes of the low-pass filtered height fields from the NCEP/NCAR reanalysis data at the 4 selected levels. The dominant feature in the time series of the PC score is quite apparent: the sudden jump in the 1976/77 winter for all the levels in the troposphere. The corresponding PC loading patterns are presented in Fig. 3.2. The primary feature is that the whole tropical geopotential height fields between 20°S and 20°N are positively correlated with the time series in Fig. 3.1 above 700 hPa and at most tropical ocean areas at the near surface level (1000 hPa). Accordingly, the whole tropical-wide atmospheric height oscillates in the same phase and the phase changes in the mid-1970s. Prior to the 1976/77 winter, the tropical height field is in negative anomalous period and it reverses after the 1976/77 winter jump. The percentage of the variance explained by the leading PC (see values in the upper right corner of the panels in Fig. 3.2) increases with altitude, with 55% at 1000 hPa and up to 84% in the upper troposphere. Such an increase is not linear, it is larger at the lower levels and very small in the middle and upper troposphere. This implies that the interdecadal variability of the tropical atmosphere is physically and dynamically more consistent in the middle and upper troposphere as certain processes (implied by the leading PC mode) prevail there.

Since the leading PC modes account for large percentage of the total variance in the atmospheric geopotential height field, especially at the upper levels (in agreement with Richman, 1994), the structures of these leading PCs can be regarded as the variations of background state of the tropical atmospheric field.

Further examination of the temporal characteristics of the tropical atmospheric height changes in Fig. 3.1 shows that, in addition to the most noted height jump, there are oscillations in the past three decades. Although the temporal amplitude becomes larger with altitude increasing, the temporal fluctuation structures at different levels are similar, especially in the middle and upper levels. However, the phase differences can also be noted. Changes at the lower levels are leading to those above. During the early 1960s, a decrease trend is found at all the levels, with a slight phase lag and a little large amplitude as altitude increasing. In the mid-1960s, the tropical atmospheric height increases. The increase at the surface leads to the upper levels and starts to increase earlier. Since 1969 the height fields remain almost unchanged until the winter of 1976/77 at the 1000, 700 and 500 hPa levels, but at the upper level (200 hPa) the atmospheric height shows a decrease from later 1960s to the 1976/77. The jump in the mid-1970s actually starts at near surface level earlier. After the mid-1970s, the atmospheric height fields oscillate, with the time coefficients are well above the average (zero).

Several important features of the spatial patterns in Fig. 3.2 can be analyzed. As noted above, the leading geopotential height PC pattern in the tropics exhibits a tropical-wide structure through the entire troposphere. As altitude increases, the zonal structure expands poleward, and the meridional height change gradient becomes

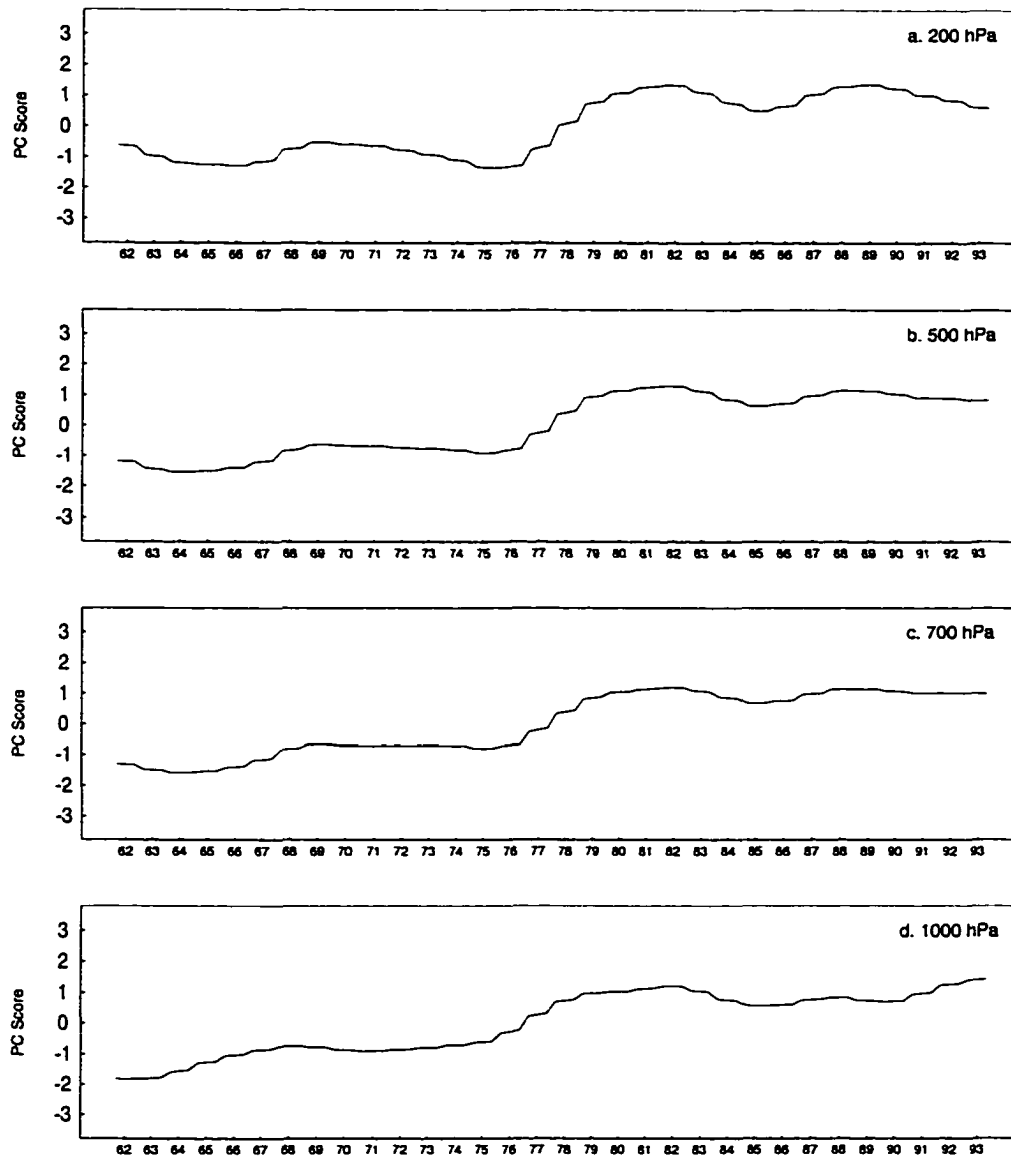


Figure 3.1 Time series of leading PC scores for the geopotential height fields at 200, 500, 700, and 1000 hPa using the NCEP/NCAR reanalysis data.

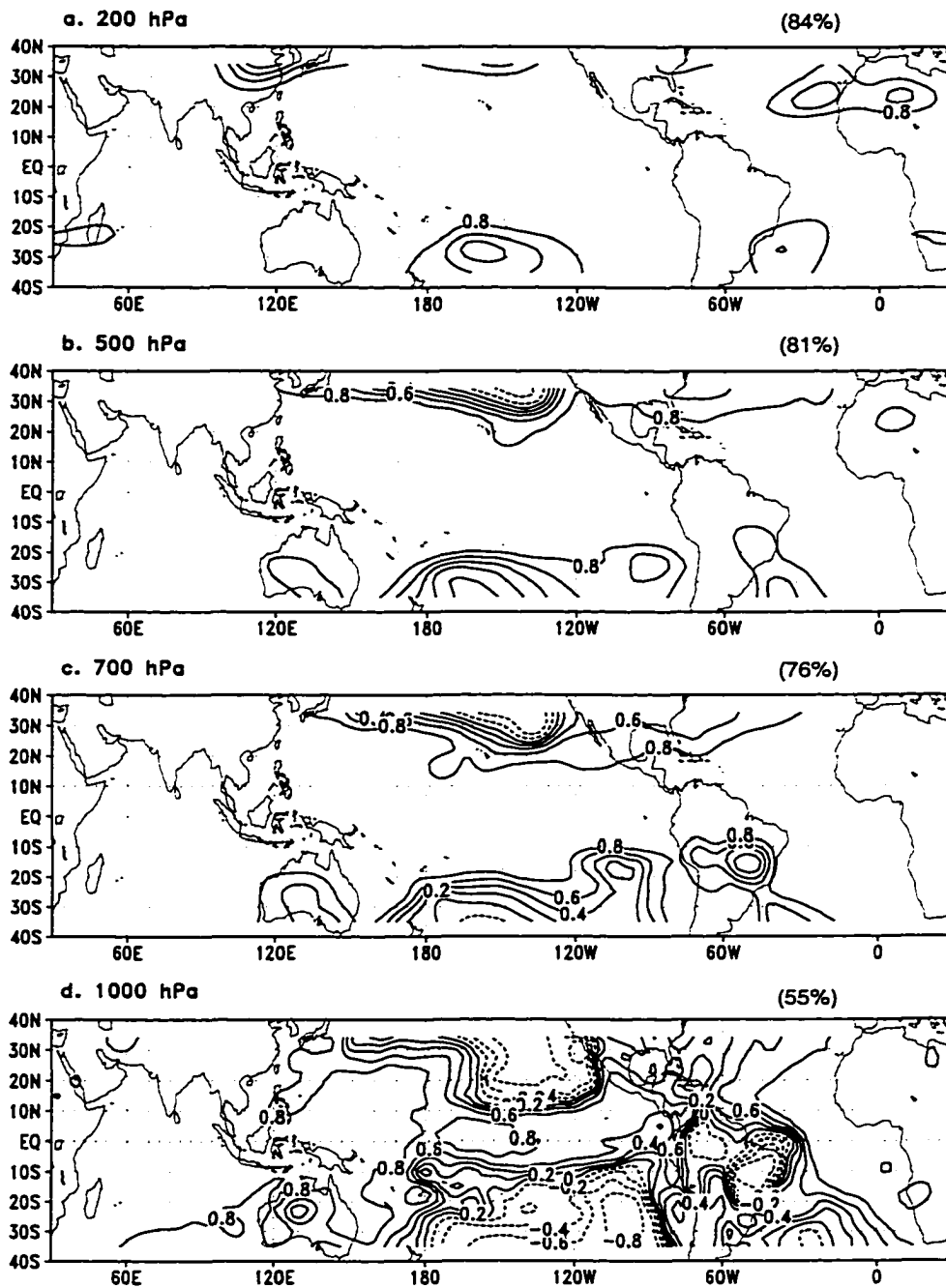


Figure 3.2 Leading PC loading patterns for the geopotential heights at 200, 500, 700, and 1000 hPa using the NCEP/NCAR reanalysis. The number at the upper right of each panel represents the percentage of the variance explained by the PC mode.

stronger in the central and eastern subtropical Pacific. A strong dipole structure can be detected in the North Pacific area, and a similar structure is seen over the South Pacific area at low levels in the atmosphere. The structure in the North Pacific is part of the PNA pattern associated with the interdecadal variability found in some previous studies (Lau and Nath 1994; Graham 1994; Zhang et al. 1997; among others). As this research domain extends from 35°S to 35°N, the finding here reinforces the intensification of the Northern Hemisphere PNA computed by using the geopotential height data poleward of 20°N (see Nitta and Yamada 1989; Zhang et al. 1997). Less detailed structures are found over the Indian and Atlantic Oceans, and the geopotential height field variation amplitudes are larger (PC loading values > 0.9), indicating that *relatively* large positive atmospheric height anomalies after the mid-1970s occurs. However, since the standard deviations of geopotential height are relatively low in these areas (figure not shown), these higher loading areas are not necessarily the higher absolute geopotential height changing areas. This will be clarified in the following analyses.

3.2.2 Difference maps of the tropical atmospheric height between the two periods before and after the 1976/77 winter

Similar to the analyses in Fig. 2.4 for the tropical sea surface temperature, the studied time-span is separated into two periods (as defined in Chapter 2) on the basis of the temporal characteristics shown in Fig. 3.1. Fig. 3.3 shows the mean atmospheric height difference between P1 and P2 (P2 - P1) at the 4-selected levels in the reanalysis data. It can be seen in Fig. 3.3 that the atmospheric height field in the

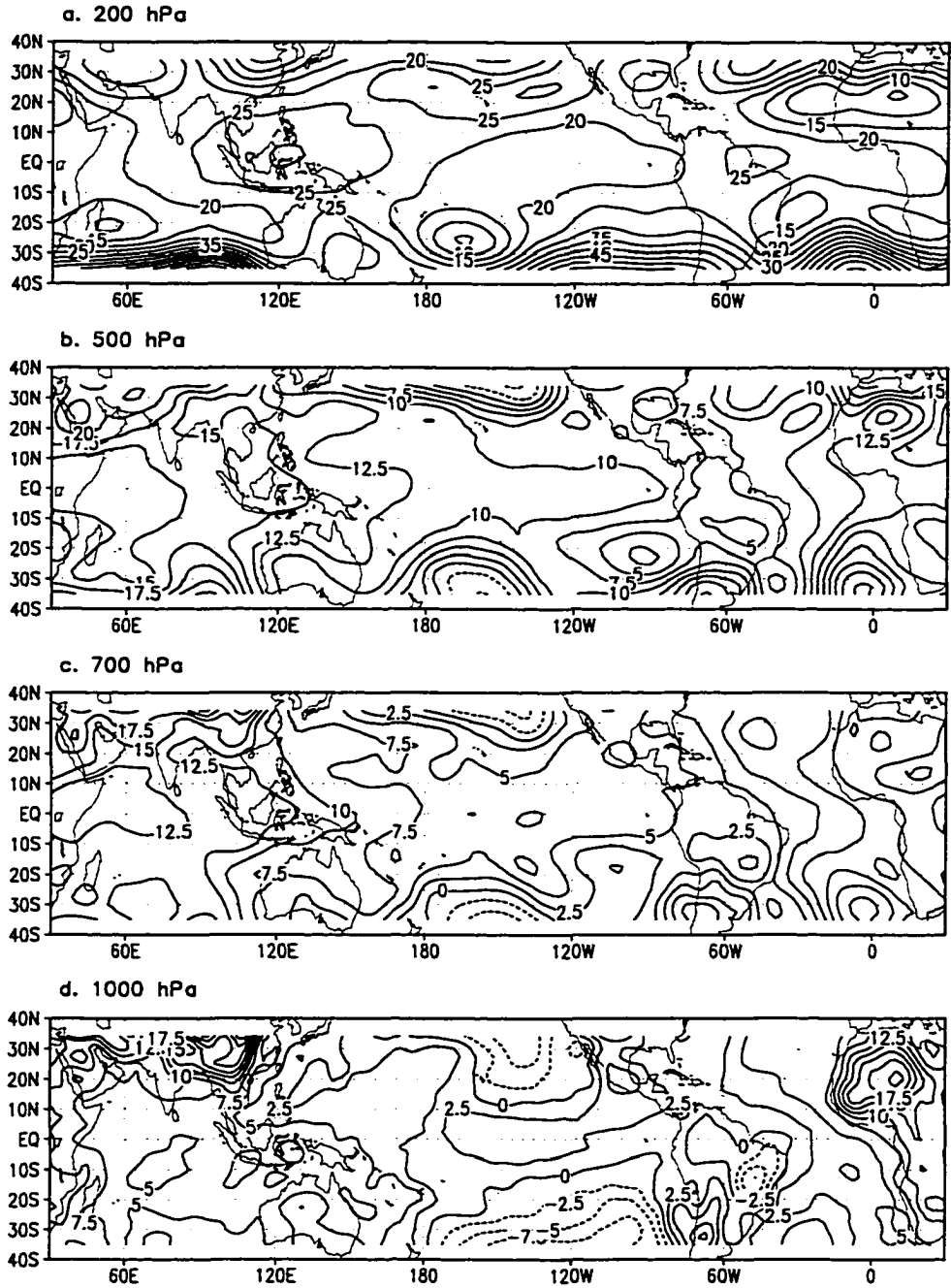


Figure 3.3 Difference maps of the winter low-pass filtered monthly mean geopotential height fields between Period 2 and Period 1 at 200, 500, 700, and 1000 hPa using the NCEP/NCAR reanalysis (Period 2 - Period 1). Unit: gpm.

tropical area (20°S - 20°N) has increased at all the levels. The positive difference increases with altitude because of the accumulated effect of the changes through the entire atmospheric column. Over the equatorial oceans, the Indian Ocean has relatively largest change in the lower and middle troposphere (700 and 500 hPa levels), whereas in the upper troposphere, the atmospheric height increase in P2 appears to be larger over the Indonesia island, extending zonally to parts of the western Pacific and eastern Indian Oceans.

Compared with the spatial patterns in Fig. 3.2, one can notice some similar features, particularly in the Pacific and Atlantic portions of the studied domain, between the geopotential height difference map (see Fig. 3.3) and leading PC loading pattern for a given pressure level. This indicates that the first PC mode depicts the structure before and after the height jump. In other words, the difference of the mean atmospheric height between P1 and P2 accounts for a larger amount of the total variance in the low-pass filtered geopotential data than other low frequency patterns. However, the difference maps in Fig. 3.3 exhibit more detailed structures of the changes and some of these detailed spatial features will be further analyzed and discussed in the subsequent GCM numerical simulations.

3.2.3 Tropical wind circulation changes

Wind field changes associated with the interdecadal variability can be examined to analyze the dynamical consistency in the atmosphere-ocean system and to diagnose the physical mechanisms of the atmospheric height change signatures. The

wind difference between P1 and P2 for both lower and upper troposphere are shown in Fig. 3.4. In the lower troposphere, represented by the 850 hPa level (lower panel in Fig. 3.4), the most notable feature appears to be the westerly changes of about 2 to 3 ms^{-1} over the equatorial central and eastern Pacific. Anomalous low-level convergence is depicted in the eastern Pacific. This is consistent with the findings in the studies of Graham (1994) and Yukimoto et al (1997) using the observed and model surface wind stress data. Over the North Pacific, the wind difference shows a strong cyclonic curvature which is associated with the Northern Hemisphere circulation shift and pressure decrease in that area as found in Trenberth (1990) and Graham (1994). The equatorial Atlantic shows a significant easterly increase. The signals in the equatorial Indian Ocean exhibit discontinuous shift, with westerly increase to the south of the equator and easterly change to the north. The signature in the Pacific sector at the 850 hPa wind difference map show some typical structures of the surface wind anomalies seen during the ENSO period (Rasmusson and Carpenter 1982).

In the upper troposphere (200 hPa, upper panel in Fig. 3.4), an increase in mean easterlies over the eastern Pacific area between the equator and 20°N can be noticed easily. Westerlies increase in the equatorial western Pacific and Indian Oceans. Poleward wind is found in the subtropical central and western North Pacific, which is associated with the intensification of the divergence aloft in those areas. The tropical Atlantic exhibits an increase in westerly wind.

From the wind differences presented in Fig. 3.4, several general remarks can be drawn regarding to the tropical general circulation pattern. First, in boreal winter, the local Hadley circulation is intensified in the central and western Pacific areas for

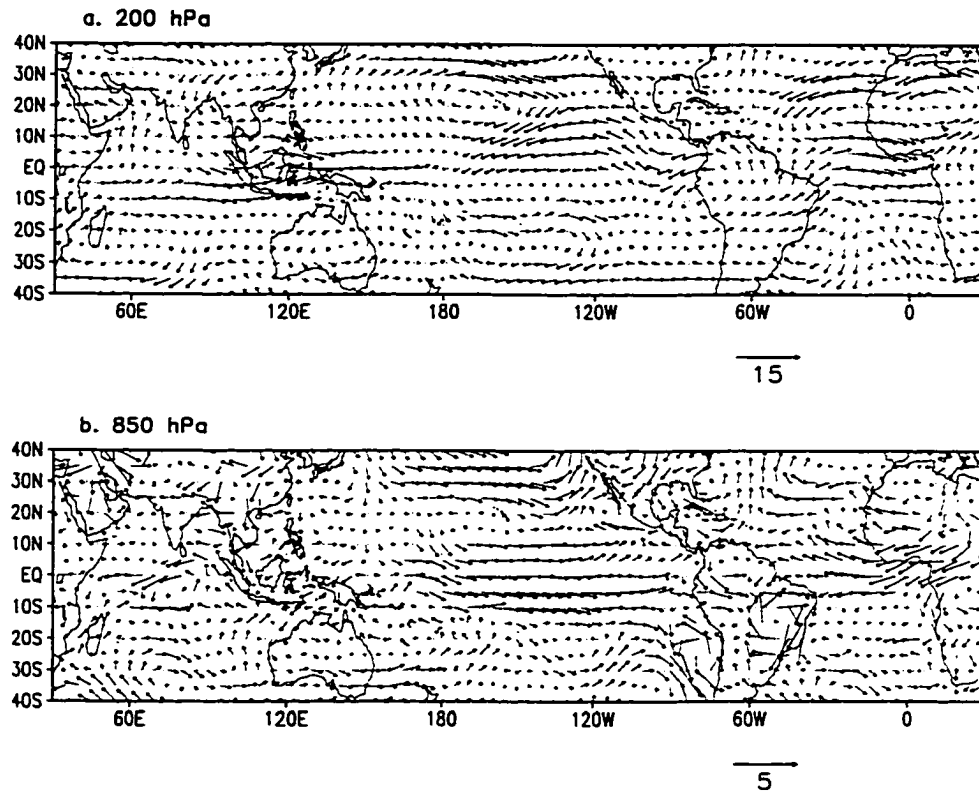


Figure 3.4 Difference maps of the winter low-pass filtered monthly mean horizontal wind fields between Period 2 and Period 1 at (a). 200 and (b). 850 hPa using the NCEP/NCAR reanalysis (Period 2 - Period 1). Unit: ms^{-1} .

the later period (P2) in the present study, due to the equatorward meridional wind difference at the lower level and poleward difference at the upper level over the area between 5°N and 15°N in the central and western Pacific. The Walker circulation in the equatorial plane over the central and eastern Pacific is weakened for the interdecadal variation structure due to the westerly increase at the lower level and westerly decrease aloft. The typical circulation pattern in the equatorial plane in the Atlantic Ocean as classified in Piexoto and Oort (1994, their Fig. 16.5) is strengthened in the structure associated with the tropical interdecadal atmospheric variability.

3.3 Model simulated tropical-wide interdecadal atmospheric variability

3.3.1 Temporal and spatial structures of the simulated atmospheric height variations

The temporal and spatial variations of the leading PC modes computed from the low-pass filtered IMGGA long-term integration geopotential height data at the 4 selected pressure levels are presented in Figs. 3.5 and 3.6. As compared to the results in the reanalysis data, the first PC modes at the 1000, 700, 500 and 200 hPa levels account for 32%, 58%, 66% and 67% of the total variances, respectively. These values are smaller than their counterparts in the reanalysis data results as shown in Fig. 3.2. From Fig. 3.6, a huge zonal pattern with positive PC loading values can be seen in the tropical area between 20°S and 20°N from the lower through upper troposphere. Near the surface (1000 hPa) level, however, the leading PC spatial pattern exhibits an east-west sea-saw structure, with a positive center being in the Indonesia area for the

east part and the other center with negative loading values over the equatorial eastern Pacific. This mode of the model atmosphere at 1000 hPa shows a large difference from the leading mode given in Fig. 3.1d for the atmosphere in the reanalysis data. None of the first 5 PC patterns from the IMGGA climatological run data (not shown) can qualitatively match the spatial structure in the reanalysis at 1000 hPa. The interpretation is that the surface and lower boundary atmospheric processes are far more complicated than what the current ECHAM4 GCM parameterization schemes can handle. When the results are viewed from the surface to the troposphere, the model result matches improve a great deal, becoming closer to the reanalysis atmosphere. The leading PC patterns shown in Fig. 3.6a, b, c exhibit some qualitative similarities to those in Fig. 3.2 for the tropics. In general, the model has successfully simulated the tropical-wide structures of the interdecadal variability found in the atmosphere obtained by the reanalysis data. The PNA appears to be stronger. Compared to Fig. 3.2, the most similar structures given by the leading PC modes are found in the tropical Pacific sector for the 700, 500, and 200 hPa levels. While satisfied with the model interdecadal spatial structures in the equatorial zonal belt, some discrepancies between the corresponding pairs in Figs.3.2 and 3.6 are found. The model patterns given in Fig. 3.6 are much more zonally oriented and exhibit larger meridional gradient at about latitudes 20° north and south. The large gradients over the Indian and Atlantic Oceans seem to be unrealistic.

The characteristics of the time coefficients from the leading PC modes of the ECHAM4 model simulated atmosphere are shown in Fig. 3.5. These agree, quite well, with the features seen in Fig. 3.1 in the reanalysis data, except for 1000 hPa,

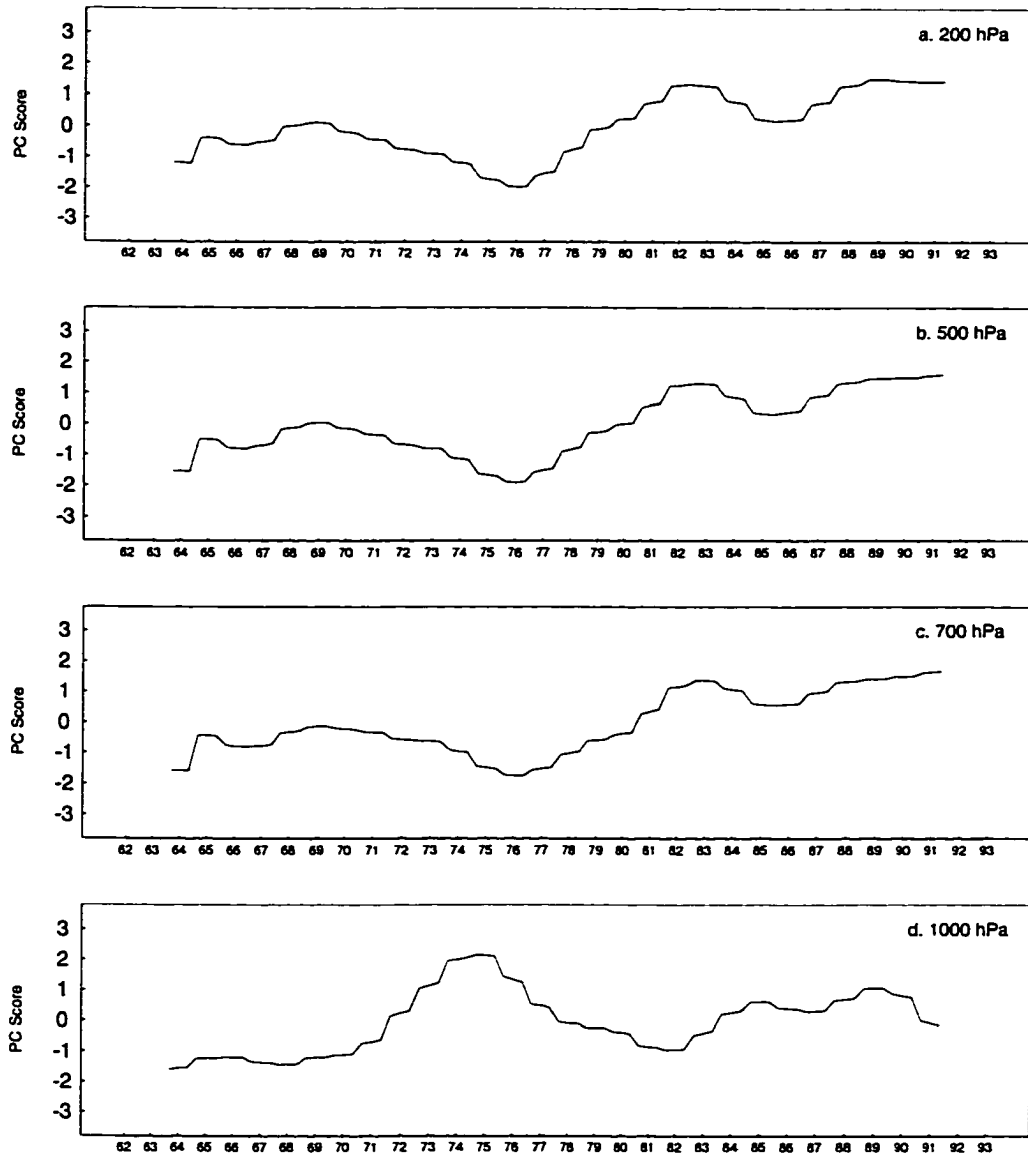


Figure 3.5 Same as Figure 3.1, except using the IMGA climatological run data.

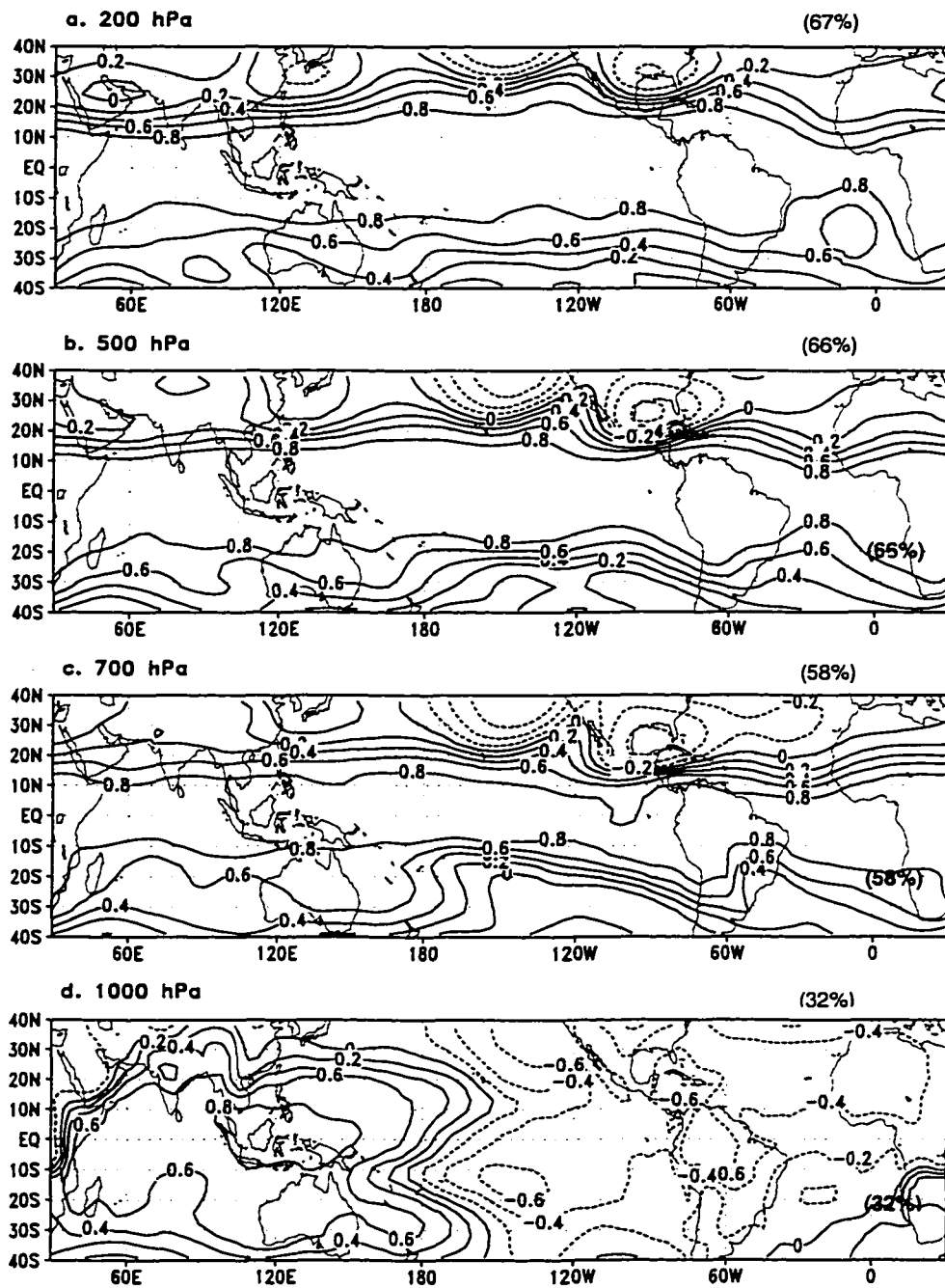


Figure 3.6 Same as Figure 3.2, except using the IMG A climatological run data.

though exhibiting larger amplitudes. The atmospheric height jump in the mid-1970s is seen clearly (Fig. 3.5a, b, c). This large shift matches to such a close degree with the results from the reanalysis data for the tropical atmosphere that it is reasonable to infer that there must be a unique physical mechanism which drives the atmospheric variations. In addition to the mid-1970s shift, the model reproduces the short upward trend in the late 1960s. The oscillations after the mid-1970s jump are also consistent with the features in Fig. 3.1. The model shows a decrease from the late 1960s to the mid-1970s at the 700, 500 and 200 hPa levels. However, in the reanalysis atmosphere, such a decrease only occurs in the upper troposphere as shown in Fig. 3.1. The correlation coefficients between the time series of the leading PC modes for the model data and reanalysis data at 700, 500, 200 hPa are 0.74, 0.77 and 0.87, respectively. This indicates that the temporal variations of the interdecadal modes for both the model simulated and reanalysis atmospheres are likely driven by the same processes and the model can be a useful tool to investigate the interdecadal variability in the real atmosphere, at least, for the tropical area.

3.3.2 Model simulated tropical atmospheric height difference maps

Analyses similar to those shown in section 3.1.2 are performed for the IMGGA run data, and the difference maps between P1 and P2 for the 4 selected levels are given in Fig. 3.7. Again, zonal positive atmospheric height increasing patterns are found to be the major spatial features at the 700, 500, and 200 hPa levels. For each of the 4 levels, the structures are primarily similar to the PC loading patterns in Fig. 3.6.

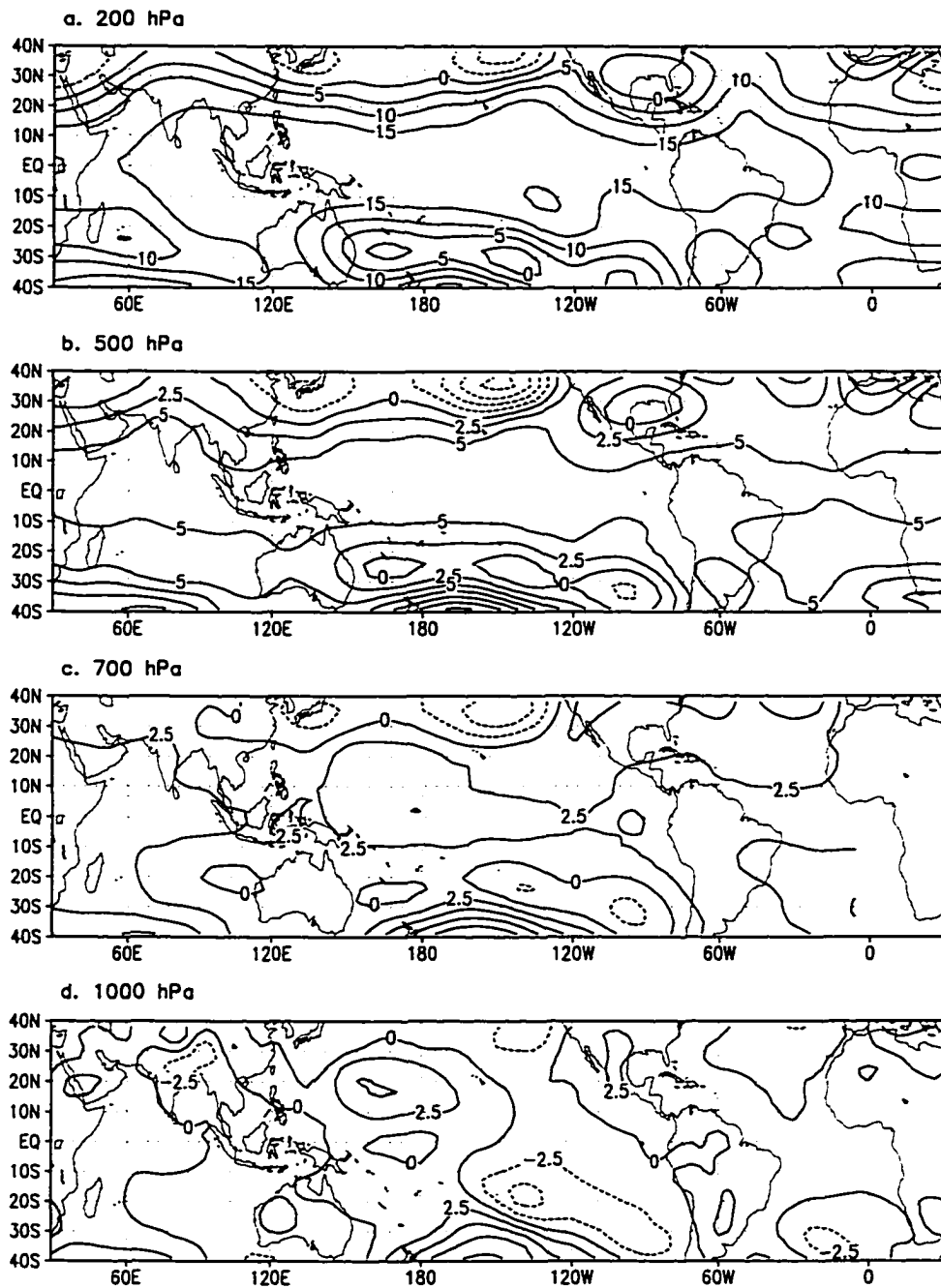


Figure 3.7 Same as Figure 3.3, except using the IMGa climatological run data.

At a given level above the surface (700, 500, 200 hPa), the geopotential height differences between the two specified periods are approximately 5 - 10 gpm smaller than those obtained by the reanalysis data. This is not unexpected because the GCM simulations can not produce appropriate magnitude of atmospheric variability, although the mean state and major atmospheric changes can be simulated reasonably well (Roeckner et al. 1996). It can also be seen from Fig. 3.7 that the structures of the differences obtained by the model geopotential height data are smoother than those shown in the reanalysis data (Fig. 3.3), particularly in the middle and upper troposphere. The ECHAM4 is unable to reproduce the small structures over the equatorial areas in the reanalysis atmosphere. However, the model does produce the tropical-wide atmospheric height increase pattern for the interdecadal time scale, on which the present study will focus.

3.3.3 Tropical wind circulation changes in the ECHAM4 GCM simulation

The wind differences between the two specified periods for the 850 and 200 hPa levels are shown in Fig. 3.8. Although the mean wind fields for both P1 and P2 are qualitatively similar to the mean wind fields in the reanalysis data (figures not shown), the wind changes in both the lower and upper troposphere (Fig. 3.8) exhibit few similarities to those in Fig. 3.4. At 850 hPa, the increase in westerlies over the equatorial eastern Pacific does not prevail as seen in the reanalysis data. Much stronger low level convergence is found in the western Pacific. The most similar part is the strong cyclonic change over the North Pacific which corresponds to the pressure

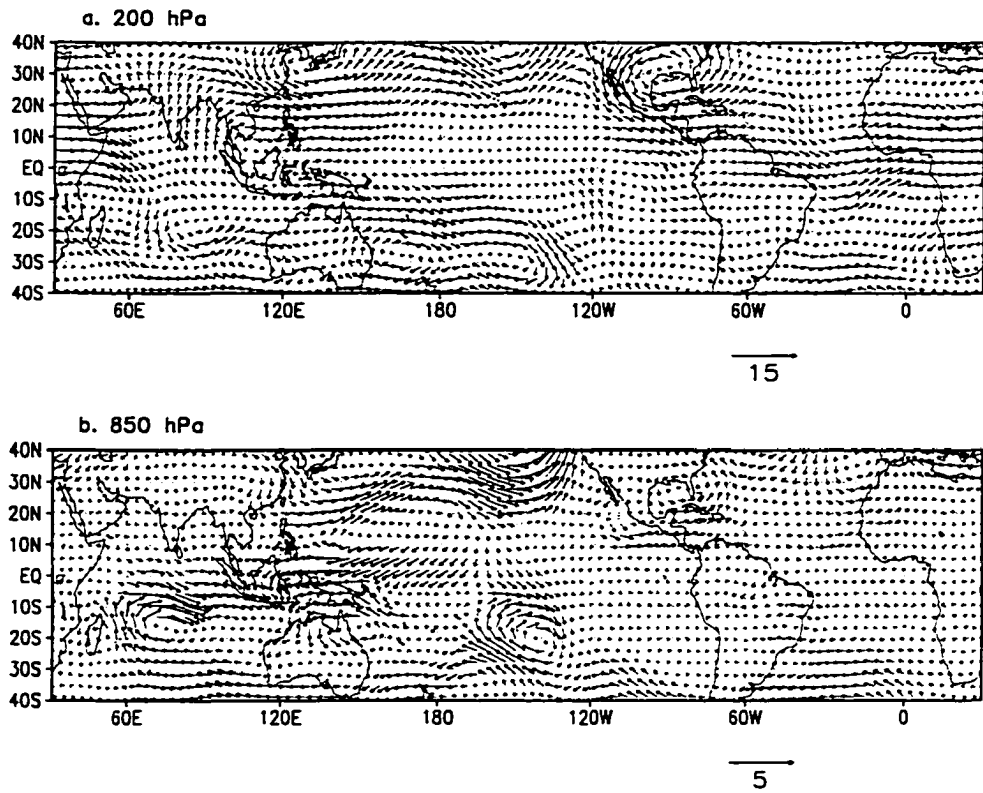


Figure 3.8 Same as Figure 3.4, except using the IMGA climatological run data.

decrease in that area after the mid-1970s shift. The easterly increase over the equatorial Atlantic is far from what has been shown in the reanalysis data. At the 200 hPa level (Fig. 3.8b), the tropical circulation changes in the Atlantic Ocean are simulated reasonably well. However, the change features over other equatorial oceans are generally not in good agreement with the changes found in the reanalysis data. Therefore, some caution should be applied when comparing and interpreting the IMGGA run and reanalysis wind data.

3.4 Relationship between the interdecadal variations in the tropical atmosphere and ocean

It has been a common understanding that the ocean plays a crucial role in our climate system. For the physical processes with shorter than decadal time scale in the climate system, the variations are mainly determined by the interaction of atmosphere and ocean. At a larger time scale, since ocean has a large memory, the oceanic processes become the major forcing in the tropics and the climate variability is primarily dominated by the ocean conditions. Studies such as Graham et al. (1994) and Lau and Nath (1994) have indicated that the tropical SST anomalies are of considerable influence on the interdecadal climate variability on a global scale.

It is not surprising to discover that the interdecadal temporal characters of the leading PC modes for both the reanalysis and IMGGA climatological run data are well matched with the time series of the tropical SST anomaly interdecadal PC mode (Fig. 2.2). Table 3.1 gives the linear correlation coefficients between each of the time series in Fig. 3.1 (reanalysis) and Fig. 3.5 (IMGGA) and the time coefficients of the low-pass

filtered SST anomaly leading PC mode shown in the lower panel of Fig. 2.2. From the numbers in Table 3.1, it can be seen that there exists a quite close relationship between the atmosphere and ocean in the tropics, except for the near surface level in the model atmosphere. The correlation coefficient ranges 0.87 - 0.97 and the changes at the upper level are more correlated with the SST changes.

Table 3.1 Correlation between the time series of the leading PC from SST anomaly data (SSTA) and reanalysis and IMGa climatological run data

	1000 hPa	700 hPa	500 hPa	200 hPa
SSTA vs. Reanalysis	0.88	0.93	0.93	0.97
SSTA vs. IMGa data	-0.11	0.87	0.91	0.91

In fact, the reason why the model atmospheric height PC mode agrees so well with the SST anomaly mode is that the model run is forced with the observed monthly mean SST field. The SST is the only external forcing imposed on the atmospheric model when the long-term integration is performed. The atmospheric variations in this model simulation is even referred as “SST forced variability in the atmosphere” (Moron et al. 1997). On the other hand, the observed SST data are also incorporated in the assimilation model of the NCEP/NCAR reanalysis (Kalnay et al. 1996). Hence, it is reasonable to make such a statement that the interdecadal variability in the reanalysis and IMGa climatological run is the atmospheric response to the surface forcing on that time scale. The present research is in attempting to diagnose the

physical processes responsible for the tropical-wide atmospheric responses to the sea surface forcing.

3.5 A hypothesis for the tropospheric height increase in the tropical Pacific

The major rationale of this research is to investigate the physical mechanisms that are responsible for the tropospheric height increases as shown in Figs. 3.2, 3.3, 3.6 and 3.7, with an emphasis on the Pacific sector of the research domain. To accomplish this, one needs to begin with the most fundamental definition based on first principles and then develop further investigations into the expected processes. In a hydrostatic atmosphere, the geopotential height is given by

$$Z(p) = Z(p_o) + \frac{1}{g} \int_p^{p_o} R_d T_v d \ln(p) \quad (3.1)$$

where T_v is the virtual temperature of the air, and R_d is the gas constant for dry air. At a given location and a specific pressure level, the geopotential height equals the sum of the surface height and the temperature integration from surface to the specified pressure level. The height change is a direct consequence of the temperature change in the atmospheric layer below. In the tropical ocean region, surface height change can be ignored and the geopotential height change is dominated by the temperature in the atmospheric layer.

From Figs. 3.3 and 3.7, it is found that the period increase in the tropical Pacific geopotential height at 200 hPa (500 hPa) is more than twice as much as that at 500 hPa (700 hPa). Furthermore, the spatial structures of the two period atmospheric

height differences over the tropical Pacific exhibit different features for the upper and lower levels. These facts indicate that the geopotential height increase from the middle to the upper troposphere account for more than 50% of the total height increase in an atmospheric column, particularly in the tropical Pacific. Also, the geopotential height (or temperature) changes for the upper and lower troposphere could be attributed to different physical processes.

As indicated in Table 3.1, the tropical atmospheric height changes on the interdecadal time scale is closely related to the variations in the tropical SST field. Such a correlation increases with altitude. In the tropics, the atmospheric convection and associated latent heat release are the major physical processes to heat the troposphere (Newell et al. 1970). Hence, we may propose a hypothetical working theory for explaining the geopotential height increase as followed:

- *The anomalous SST increase over the tropical Pacific region induces more and stronger atmospheric convection and rising motion in the later period (after the 1976/77 winter), leading to more latent heat release into the troposphere and vertical transport, particularly in middle and upper layers;*
- *Part of such heating can be used to warm the local atmosphere and cause height increase in the interdecadal anomalous surface forcing areas;*
- *The thermal structure changes in the atmosphere may modulate the atmospheric circulation; the dynamical effects in the middle and upper levels can be responsible for the transport of the local warm air over the tropical*

area and cause the tropospheric geopotential height increase over a larger area, extending to the subtropical areas in both Hemispheres.

This statement is based on the findings in Newell et al. (1970) and Yanai et al. (1973) that the maximum latent heating occurs in the mid-troposphere. In fact, in the work of Nitta and Yamada (1989) and Graham (1994), convection indices have been used in the investigation of the interdecadal variability. Such a working hypothesis forms a basis for the experiments of the GCM simulations later in this study.

Chapter 4

Tropical atmospheric responses to the interdecadal SST variation in an idealized GCM simulation for boreal winter

4.1 The ECHAM4 general circulation model

4.1.1 Model general description

The numerical experiments in the present study are performed by means of the ECHAM4 GCM at triangular 30 (T30) horizontal resolution. The ECHAM4 is the fourth-generation atmospheric general circulation model of the European Centre for Medium-Range Weather Forecasts (ECMWF)/Max Plank Institute for meteorology (MPI) at Hamburg (European Centre/HAMburg, ECHAM) developed at the MPI (Roeckner et al. 1996). It is the most recent in a series, evolving originally from the spectral weather prediction model of the ECMWF. The ECHAM4 GCM still has many features in common with the current operational ECMWF model, but some of the physical parameterizations have either been replaced or modified for the purposes of climate researches (Roeckner et al. 1996).

The ECHAM4 model is based on the primitive equations. The prognostic variables of the model include vorticity, divergence, temperature, logarithm of surface pressure, water vapor mixing ratio, cloud water and , optionally, a number of trace gases and aerosols. The model equations are solved on 19 vertical levels in a hybrid sigma-pressure coordinate system. Except for the water components and trace gases,

the prognostic variables are represented by truncated series of spherical harmonics with triangular truncation at wavenumber 21, 30, 42 and 106 (T21, T30, T42, T106), respectively. The T42 resolution is the standard version; the T106 is the higher resolution, and the T21 and T30 versions are the low resolution versions of the model. The T30 version is employed in this study, which enables completion of the integrations within a reasonable time without losing much of the physical details in the tropics.

4.1.2 *The model governing continuous equations*

The dynamics and physics of the model simulated atmosphere are governed by the physical laws that are represented by a set of equations, including the momentum, thermodynamic and moisture equations. In order to apply the spectral method, momentum equations are written in vorticity and divergence form. Hence the model prognostic variables are vorticity (ξ), divergence (D), temperature (T), water vapor mixing ratio (q_v) and the cloud water mixing ratio (q_w). The model governing equation set in continuous form are as follows:

$$\frac{\partial \xi}{\partial t} = \frac{1}{a(1-\mu^2)} \frac{\partial}{\partial \lambda} (F_v + P_v) - \frac{1}{a} \frac{\partial}{\partial \mu} (F_u + P_u) + K_\xi \quad (4.1)$$

$$\frac{\partial D}{\partial t} = \frac{1}{a(1-\mu^2)} \frac{\partial}{\partial \lambda} (F_u + P_u) + \frac{1}{a} \frac{\partial}{\partial \mu} (F_v + P_v) - \nabla^2(\phi + E) + K_D \quad (4.2)$$

$$\frac{\partial T}{\partial t} = -\frac{U}{a(1-\mu^2)} \frac{\partial T}{\partial \lambda} - \frac{V}{a} \frac{\partial T}{\partial \mu} - \dot{\eta} \frac{\partial T}{\partial \eta} + \frac{\kappa T_v \omega}{\left(1 + \left(\frac{C_{p_v}}{C_{p_a}} - 1\right) q_v\right) p} + P_T + K_T \quad (4.3)$$

$$\frac{\partial q_v}{\partial t} = -\frac{U}{a(1-\mu^2)} \frac{\partial q_v}{\partial \lambda} - \frac{V}{a} \frac{\partial q_v}{\partial \mu} - \dot{\eta} \frac{\partial q_v}{\partial \eta} + P_{q_v} + K_{q_v} \quad (4.4)$$

$$\frac{\partial q_w}{\partial t} = -\frac{U}{a(1-\mu^2)} \frac{\partial q_w}{\partial \lambda} - \frac{V}{a} \frac{\partial q_w}{\partial \mu} - \dot{\eta} \frac{\partial q_w}{\partial \eta} + P_{q_w} + K_{q_w} \quad (4.5)$$

The continuity equation is

$$\frac{\partial}{\partial \eta} \left(\frac{\partial p}{\partial t} \right) + \nabla \cdot \left(\bar{v}_h \frac{\partial p}{\partial \eta} \right) + \frac{\partial}{\partial \eta} \left(\dot{\eta} \frac{\partial p}{\partial \eta} \right) = 0 \quad (4.6)$$

and the hydrostatic equation takes the form

$$\frac{\partial \phi}{\partial \eta} = -\frac{R_d T_v}{p} \frac{\partial p}{\partial \eta} \quad (4.7)$$

In (4.1) and (4.2), F_U and F_V are given by:

$$F_U = (f + \xi)V - \dot{\eta} \frac{\partial U}{\partial \eta} - \frac{R_d T_v}{a} \frac{\partial}{\partial \lambda} \ln p \quad (4.8)$$

$$F_V = -(f + \xi)U - \dot{\eta} \frac{\partial V}{\partial \eta} - \frac{R_d T_v}{a} (1 - \mu^2) \frac{\partial}{\partial \mu} \ln p \quad (4.9)$$

In the above set of equations, a is the radius of the earth, λ and μ are the longitude and the sine of the latitude, ϕ ; η is the vertical coordinate, which is a monotonic function of pressure, p and depends also on the surface pressure, p_s , in such a way that is zero at the top of the atmosphere and one at the bottom of the atmosphere. ω , T_v , ϕ , R_d , R_v , C_{p_d} , C_{p_v} , and κ have their conventional meanings in meteorology. $\vec{v}_h = (u, v)$ is the horizontal wind vector; $U = u \cos \phi$, and $V = v \cos \phi$.

$E = \frac{1}{2} \frac{u^2 + v^2}{1 - \mu^2}$ is the kinetic energy per unit mass. All the P and K terms in equations

(4.1) through (4.9) are processes which can not be resolved by model grid and require parameterization. P_U , P_V , P_T , P_{q_v} and P_{q_w} represent the rate of changes of the subscript variables due to parameterized physical processes such as radiation, convection, vertical turbulent mixing and phase transition by using a physical model of sub-grid scale processes. Terms K_U , K_V , K_T , K_{q_v} and K_{q_w} represent the influence of the unresolved horizontal scales. Their treatment during the integration only involves scale selective diffusion of a magnitude determined empirically to ensure a realistic behavior of the resolved scales.

4.1.3 *Brief overview of the major physics*

Physical processes, such as radiation, cumulus convection, stratiform precipitation, diffusion, friction, sensible heat flux and evaporation, play important roles in the development of the large-scale atmospheric flow. These processes are related to spatially small or, even, molecular phenomena, so that it is not possible to

explicitly include these processes in numerical models which only resolve scale larger than the truncated wave number in spectral models. The detailed model physics can be found in Roeckner et al. (1992, 1996) and here only major parameterization physical processes are briefly described.

The radiation scheme in the model is based on a two-stream approximation of the radiative transfer equations with 6 spectral intervals in the infrared and 4 in solar spectrum. Gaseous absorption due to water vapor, carbon dioxide and ozone is taken into account as well as scattering and absorption due to aerosols and clouds. The cloud optical properties are parameterized in terms of the cloud liquid water and cloud cover. The parameterization of cumulus convection, composed of the effect of shallow, mid-level and deep convection, follows the bulk mass flux concept of Tiedtke (1989). Cumulus clouds are represented by a bulk model including the effect of entrainment and detrainment on the updraft and downdraft of convective mass fluxes. An adjustment-type closure (Nordeng 1996) is used for deep convection, based on the fact that the organized entrainment is related to buoyancy and organized detrainment can be computed for a spectrum of clouds detraining at different heights. Stratiform clouds are predicted from the respective water budget equation including sources and sinks due to phase changes and precipitation formation. The convective cloud water detrained at the top of cumulus clouds is used as the source term in the stratiform cloud water equation.

4.2 Experimental design

In the numerical experiments presented in this chapter, the ECHAM4 GCM is used to investigate how the tropical atmospheric height and wind circulation respond to the tropical SST changes characterized as the spatial pattern seen in the interdecadal mode (Fig. 2.4). The aim is to provide evidence demonstrating that the model simulations can be used to diagnose the processes and mechanisms which can lead to the development and maintenance of the tropospheric height change pattern over the tropics shown in the reanalysis and IMGGA long-term climatological run results.

4.2.1 *Basic idea of the simulations and anomalous surface forcing*

Surface forcing and solar radiation are the only two external forcings for the atmospheric general circulation model during the integrations. When the solar radiation at the top of atmosphere remains unchanged, the surface boundary condition plays a key role in the development of the atmospheric flow over the tropics where the cumulus convection, latent heat release and heat transport are the major processes in the atmosphere.

The experiments are designed in an attempt to simulate the characteristic structures exhibited in the interdecadal variability of the tropical SST and atmospheric geopotential height. Two different surface conditions are generated for the model runs to investigate the effect of interdecadal anomalous surface forcing pattern as seen in Figs 2.3 and 2.4. First, the January SST climatology in GISST (version 2.2) is chosen as the sea surface boundary condition to represent the normal forcing condition. The

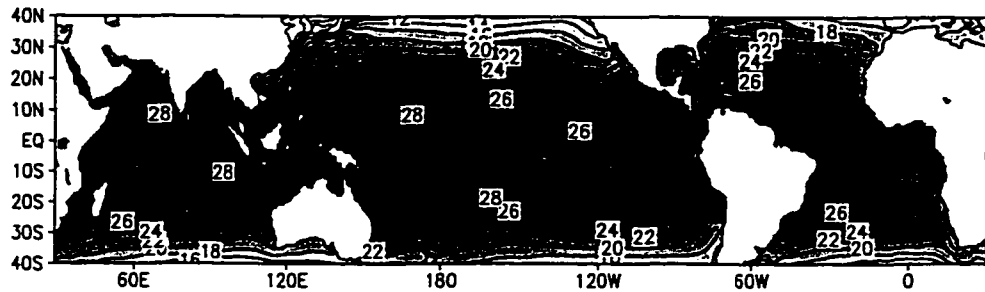


Figure 4.1 January mean SST field. Contour interval is 2°C.

GISST is a grided extension of the UK Meteorological Office Historical Sea Surface Temperature dataset that includes COADS data (Parker et al. 1995a, 1995b). The January climatological SST field is shown between 40°S and 40°N in Fig. 4.1. The surface temperature over the land area is internally generated by the soil model in the ECHAM4 based on the time and day of the year.

To simulate the effect of the SST anomaly pattern over the tropical Pacific in the interdecadal SST variation (Fig. 2.3, top panel), an idealized SST perturbation field is created as shown in Fig 4.2a. This anomalous SST field consists of two patches, with one in the equatorial central Pacific and the other one over large area of the eastern Pacific. The SST perturbation is specified at 1°C in the central area of the patches and decreases to 0°C at the edge of the patches. This ensures that the model atmosphere can react to such a change. The 1°C perturbation areas correspond to the high SST PC loading areas (>0.6) over the tropical Pacific identified in Fig. 2.3 computed by the leading PC of the low-pass filtered SST data. Furthermore, such a

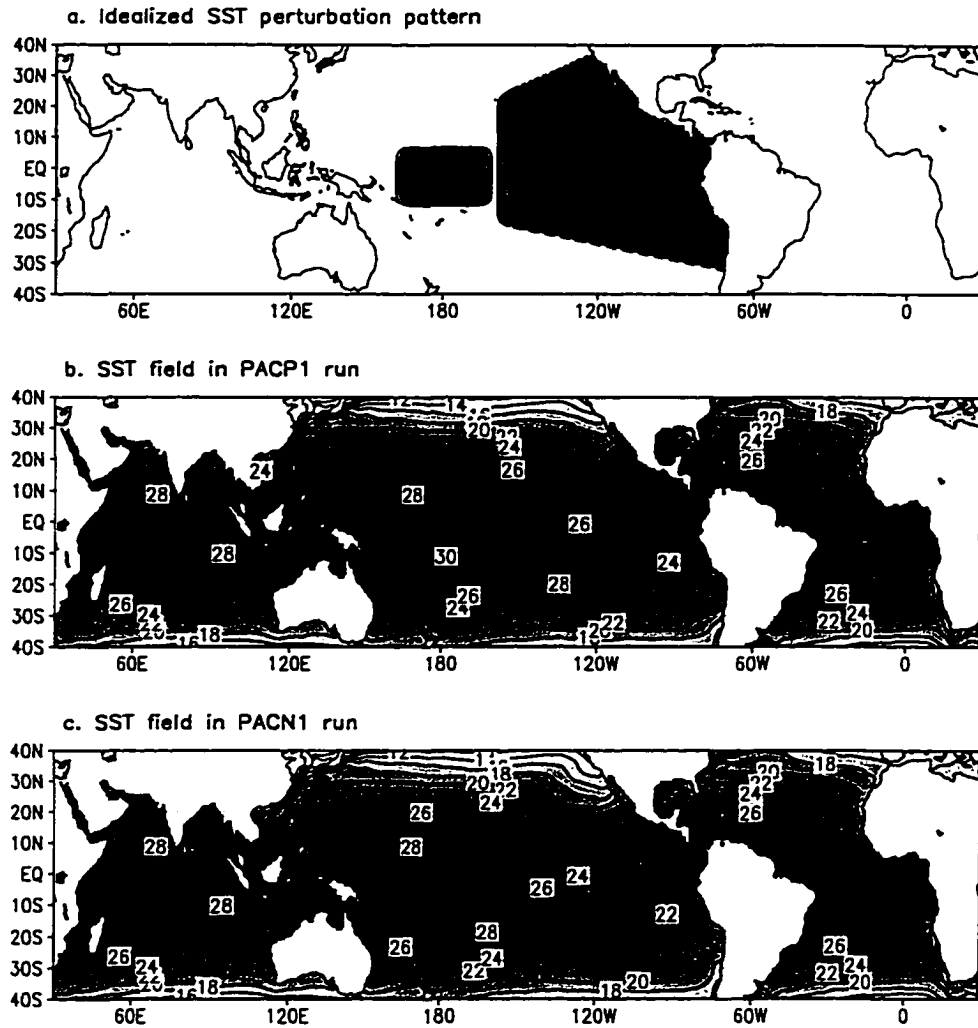


Figure 4.2 Idealized SST patterns for the model simulations. a. SST perturbation pattern with a maximum of 1°C (darkest area), the contour interval is 0.2°C; b. prescribed SST field for the PACP1 run, and c. SST field for the PACN1 run, the contour interval is 2°C.

spatial change pattern can also be seen in Fig.2.4 which depicts the spatial SST change on decadal scale. The idealized SST perturbation pattern over the equatorial central Pacific area centers at (2.5°S, 180°), with 40° in zonal and a 20° in meridional direction. The anomalous SST pattern over the eastern Pacific starts at 160°W, where it extends approximately from 13.5°S to 20°N in latitude. The latitude zone expands gradually poleward until it reaches the west coast line of American continents.

The two SST boundary forcing fields for the model experiments are generated by addition/subtraction of the idealized SST perturbation field onto/from the January SST climatological field, as shown in Fig. 4.2b and 4.2c. The SST pattern in Fig. 4.2b corresponds to the SST loading pattern shown in the top panel of Fig. 2.3 for the period during which the PC scores are above normal (after the 1976/77 winter), whereas the SST field seen in Fig. 4.2c is used to represent the opposite case when the PC scores are below the normal (before the 1976/77 winter). The resulted difference of the two simulations forced by the two prescribed SST fields is expected to represent the interdecadal atmospheric changes over the tropics. Before the model simulations, the constructed surface forcing fields are interpolated into T30 Gaussian grid, and then incorporated into the model.

4.2.2 Model experiments : control run and two specified forcing runs

The specified surface forcings enable integrations with different surface boundary conditions. The model integration forced with the January SST climatology field (Fig. 4.1) as the input lower boundary condition is referred to as the "control run"

(CNTR). The model integration with the idealized anomalous SST forcing is called the "forcing run". Two specific forcing run experiments are performed for the analyses in this chapter. One experiment uses the SST forcing field in Fig. 4.2b with a positive 1°C anomaly about the normal January SST climatology over the tropical Pacific as the lower boundary condition, referred to as the "Pacific positive 1°C" (PACPI) run. The other experiment, called the "Pacific negative 1°C" (PACNI) run, is the simulation which uses the SST field with a negative 1°C SST anomaly as shown in Fig. 4.2c as the sea surface boundary condition. The key results of interest are the differences between the experimental outputs of the two forcing runs. In the analyses and discussions of this chapter, "difference" is used to specifically represent (PACPI - PACNI) results. These analyses enable diagnosis of the effects of the anomalous surface forcing.

The model runs are carried out in a perpetual January mode; no annual cycle is considered since this study only concentrates on the tropical atmospheric variations in boreal wintertime. The January initial condition file provided by MPI is used in the model simulations. For each of the control and forcing runs, the ECHAM4 is integrated for 24 months. The ECHAM4 is integrated for 24 months with the January climatology SST field (see Fig. 4.1) in CNTR. As for the PACPI and PACNI forcing runs, the model is first integrated with the January climatology SST field for the first 3 months. Then, at the beginning of the 4th month, anomalous SST field is applied and the model is integrated for another 21 months. This also leads to a total integration period of 24 months. The first 4 months are considered as the model spin-up period for all the experimental (CNTR, PACPI and PACNI) runs. Therefore, only the

outputs of the last 20 month integrations are analyzed. During the model integration, the outputs are written every 6-hour.

4.3 Atmospheric responses to the idealized anomalous SST forcings over the tropical Pacific

The mean atmospheric fields (e.g. geopotential height) generated from the control run exhibit structures that resemble the January mean patterns in the IMGA long-term climatological run data (figure not shown), since the external forcings (lower boundary conditions and incoming solar radiation) are fixed with January means in the control run. Alternately, the PACP1 and PACN1 runs are forced by specified anomalous SST fields over the tropical central and eastern Pacific, which ideally represent the spatial features in the tropical SST interdecadal variability. Thus, the differences between the atmospheres resulting from the PACP1 and PACN1 runs illustrate the effects of the idealized anomalous surface forcing. Analyses of the differences between the two runs for the selected atmospheric variables may provide the details of the atmospheric responses to the idealized surface forcing anomaly and, in turn, assist in better understanding the development and formation of the spatial features of the tropical interdecadal variability. Monthly mean fields for a given atmospheric variable are used to represent the state of the variable for both the two forcing runs. A representative state of a variable field is obtained by averaging over the 20 monthly means of the variable at a specific pressure level.

4.3.1 Changes in the tropospheric height fields over the tropics

Fig. 4.3 gives the geopotential height difference fields of the two forcing runs at the 4 selected pressure levels. It can be seen that a geopotential height increases over nearly the entire tropical region (e. g. 20°S - 20°N) in the troposphere, except for the near surface level (1000 hPa). The positive height change increases with altitude, with the most notable changes in the upper troposphere (200 hPa level, Fig. 4.3a). At the near surface level, the structures of the differences are essentially different from those found at the upper levels.

At the 200 hPa level (Fig. 4.3a), the most pronounced feature is the height increase greater than 20-gpm over the whole tropical belt. The largest geopotential height increase region is found in the central and eastern Pacific area between the dateline and 50°W within the deep tropical belt, where the height increase is larger than 60 gpm everywhere. Over the lower latitude portion of the eastern Pacific region, the geopotential height difference pattern appears rather symmetric about the equator, with two relatively large height change areas (greater than 100 gpm) located on each side of the equator. The area to the north side of the equator shows a similarity to the height increase structure in the interdecadal variability in Fig. 3.3a, although latter is found a little further north. Moreover, a notable geopotential height decrease area is found poleward of 30°N over the central and eastern Pacific, which forms a dipole structure combined with the height increasing area equatorward. Such a dipole of the geopotential height change in the tropical and extratropical portions of the central and eastern Pacific is reminiscent of the dipole in the interdecadal height variation for the

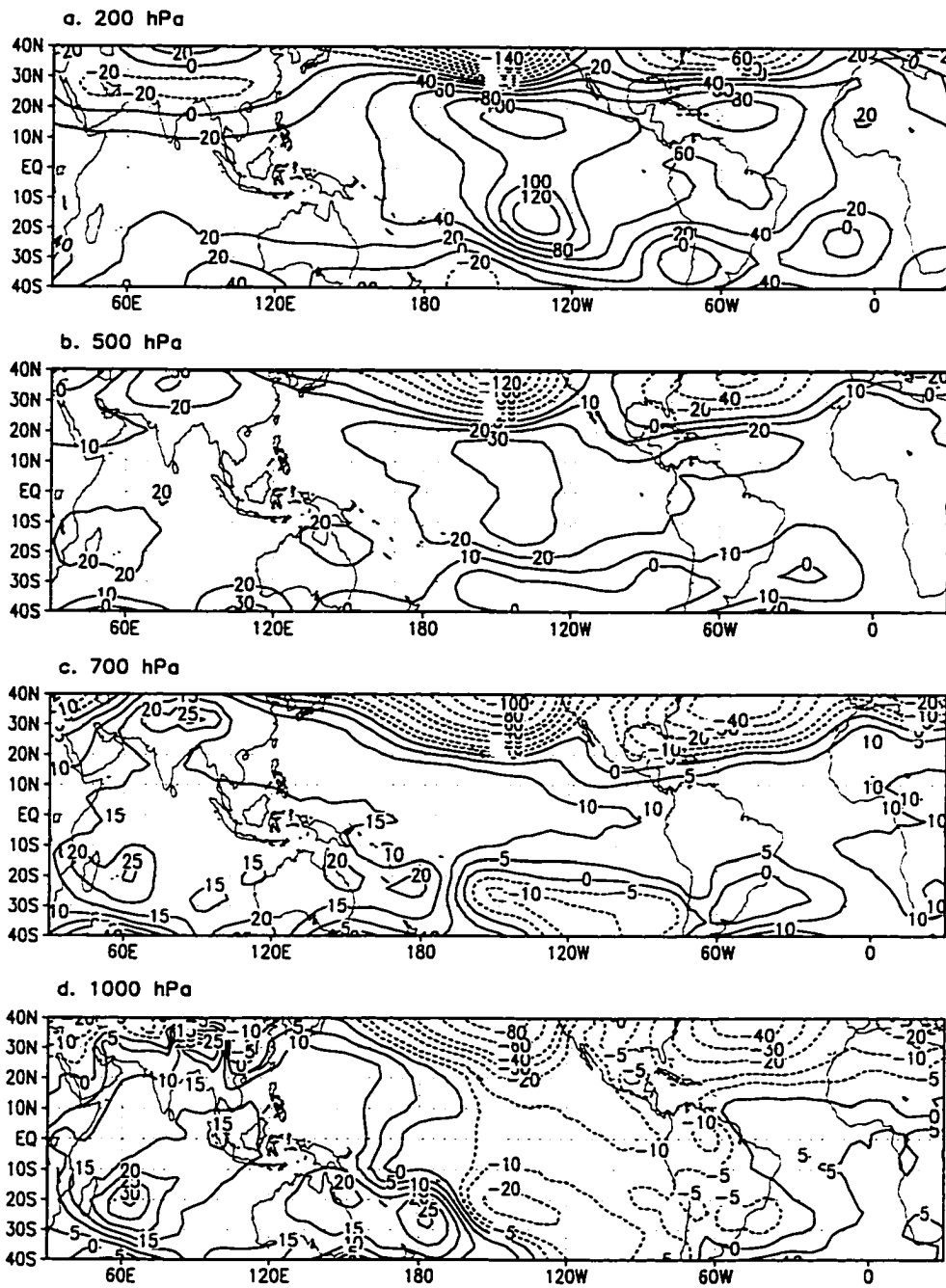


Figure 4.3 Difference maps of the monthly mean geopotential height fields between the PACP1 and PACN1 runs at 200, 500, 700 , and 1000 hPa (PACP1 - PACN1). Unit: gpm.

same geographical region found in the IMGGA climatological run data (Figs. 3.6a and 3.7a).

The tropical-wide geopotential height increase feature is also seen in the middle troposphere as given in the height difference structure at 500 hPa (Fig. 4.3b). Unlike the structure at the upper level, at this level, the geopotential height change is relatively uniform across the tropical belt. The zonal gradient of the height difference field is small and the height increase ranges 10 - 30 gpm mostly. The dipole structure in the central and eastern Pacific still exists on the north side of the equator. In the lower troposphere (700 hPa, Fig. 4.3c), the general structure is somewhat similar to the one at the 500 hPa level over the tropical oceans. The range of the change is about 5 - 15 gpm over the Pacific and Atlantic and 15 - 20 gpm over the Indian Ocean. The dipole in the Pacific has been changed to a strong anomalous low height center in the north as the height increase in the equatorial central and eastern Pacific is rather small. At the near surface level (Fig. 4.3d), while the geopotential height increase over the Indian Ocean and western Pacific appears to be the same as the one at 700 hPa, the height changes over the central and eastern Pacific become negative. Such a height difference between the two forcing runs is consistent with the patterns found in Figs. 3.6d and 3.7d at the 1000 hPa level. When the SST increases over the equatorial central and eastern Pacific, anomalous flow convergence occurs over these regions at surface level in response to the warm anomalous SST. In addition to the pressure decrease center in the northern Pacific, another anomalous surface low pressure appears in the southern portion of eastern Pacific, indicating an intensification of the

Southern Pacific Convergence Zone (SPCZ) due to the interdecadal SST change pattern.

Overall, the atmospheric height responses to the anomalous surface exhibit different features both vertically and horizontally. The geopotential height increases do not show substantial differences in magnitude from the near surface level to the middle troposphere. However, the magnitude of the atmospheric height change increases dramatically from the middle to the upper troposphere over the central and eastern Pacific as well as Atlantic regions. The most likely cause of this is that strong latent heat difference for the two model runs is found around the mid-troposphere, which is transported upward, resulting in such a height difference structure in the vertical. For the Atlantic Ocean, the magnitude of the height difference at 200 hPa ranges from 20 - 60 gpm and is close to double those values at the lower levels. Furthermore, the magnitude (ranging from 40 - 120 gpm) at the 200 hPa level in the tropical central and eastern Pacific appears to be 2 - 4 times as large as those found at 500 hPa. In the equatorial Indian Ocean and western Pacific, the magnitudes of height differences for the lower and upper levels do not differ substantially, suggesting that the major height change occurs near the surface level. For the changes over the tropical Pacific, the anomalous surface forcing is believed to be the source for the strong diabatic heating process in the middle troposphere. Such idealized simulation results support the hypothesis proposed in section 3.5 that the heating process is the key to the height increase in the atmosphere.

The dipole structure over the equatorial and northern middle latitude Pacific region in Fig. 4.3 indicates an intensification, at least in the Pacific portion, of the

PNA pattern when the tropical central and eastern Pacific SST is positively anomalous. Such a finding supports the aforementioned results that the PNA pattern appears stronger in the interdecadal variability (Nitta and Yamada 1989; Lau and Nath 1994; Zhang et al. 1997). Hence, it is reasonable to conclude that the intensification of the PNA pattern over the Pacific on the interdecadal scale after the mid-1970s may be at least partly attributed to the anomalous SST increase in the tropical central and eastern Pacific based on these ECHAM4 GCM simulation results. Another important feature is the height decrease area in the southeastern Pacific. From the difference maps at 1000 hPa (Fig. 4.3d), one may notice that the SPCZ tends to shift eastward and intensify as a result of the idealized anomalous surface forcing in the experiments, and the height decrease is a substantial part of the SPCZ change in the South Pacific. Such a SPCZ displacement has also been found in the interdecadal variability study of Lau and Nath (1994) using GFDL GCM simulations.

4.3.2 Tropical general circulation changes

a. Atmospheric circulation over the tropical region

To assist the analyses and understanding for the atmospheric circulation differences in the two forcing experiments, the wintertime tropical general circulation climatology simulated in the control run is presented in Fig. 4.4. It can be seen that at the upper level (Fig. 4.4a), westerly wind prevails over the tropical eastern Pacific and Atlantic, and strong subtropical jet streams exist over subtropical regions in both Hemispheres. Easterly airflow prevails at the lower troposphere (Fig. 4.4b) over the

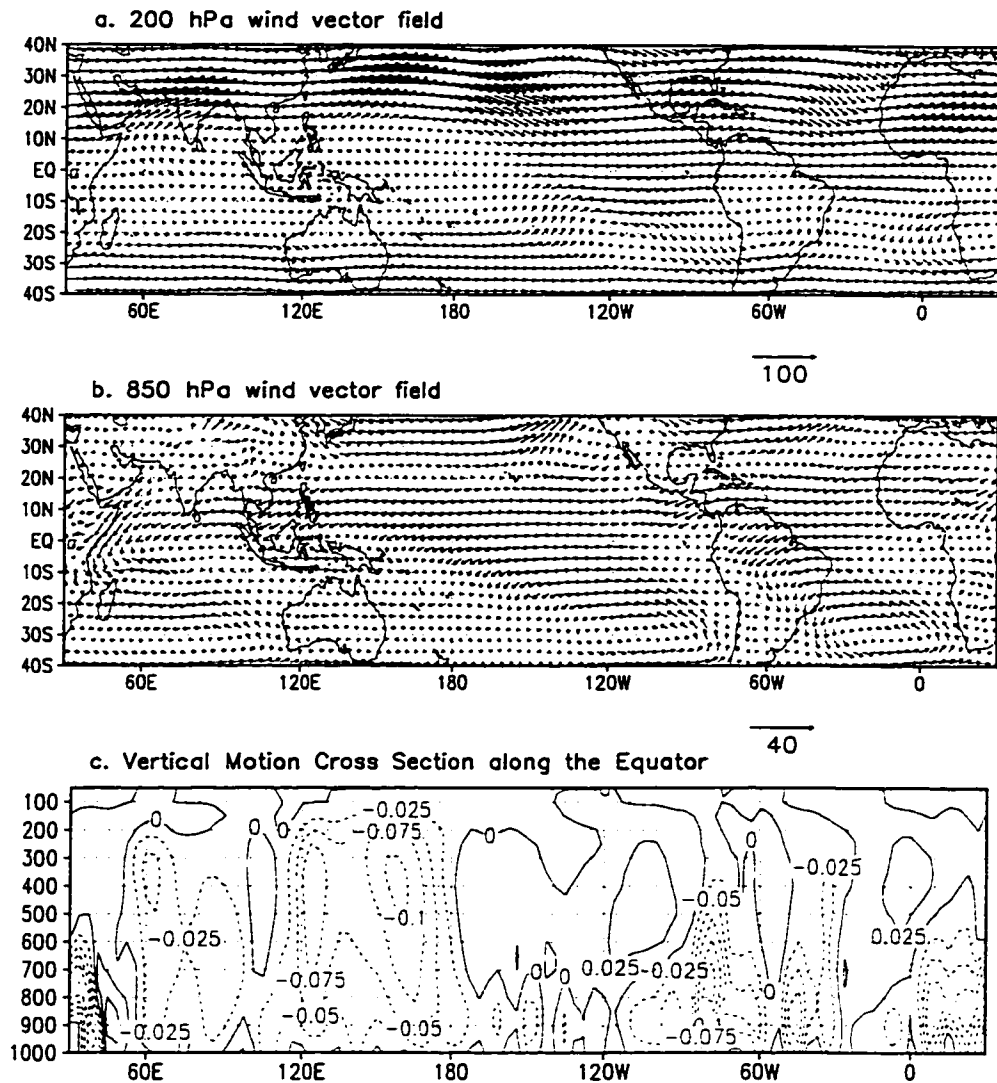


Figure 4.4 Simulated January monthly mean wind fields from the CNTR run for a. 200, and b. 850 hPa, unit: ms^{-1} ; c. vertical-zonal cross section of vertical motion along the equator, contour interval 0.025 Pas^{-1} .

entire tropical Oceans. The vertical - longitudinal structure of vertical motion across the equatorial plane (Fig. 4.4c) qualitatively shows a similar structure in the vertical circulation schematic diagram as given by Peixoto and Oort (1992, their Fig. 16.5). The atmospheric flow structure over the tropical Pacific region is characterized as an east-west Walker circulation.

b. Horizontal wind field difference in the forcing runs

The horizontal wind vector difference maps between the PACP1 and PACN1 runs at 200 and 850 hPa are presented in Fig. 4.5. Since the anomalous SST forcing in the experiments only occurs over the tropical central and eastern Pacific, the local and downstream wind responses are the interest when they are qualitatively compared to the wind changes in the reanalysis and IMGa climatological run data. In the upper troposphere (Fig. 4.5a), large poleward changes in the meridional wind, over both the north and south subtropics, within the central Pacific longitudinal forcing zone can be clearly seen, indicating a strong upper tropospheric divergence in the anomalous surface forcing area. Another strong poleward wind difference area can be found in southern subtropical area of the eastern Pacific region, in response to the effect of the specified SST difference over the eastern Pacific. Concomitantly, strong anomalous easterlies ($10 - 20 \text{ ms}^{-1}$) are evident over the equatorial central and eastern Pacific. The poleward wind difference over the Pacific is deflected toward the east by the Coriolis force in both the north and south subtropical Pacific, which intensifies the subtropical westerly jets of the two Hemispheres. Between the dateline and 120°W , the forcing run difference generates a large anomalous anticyclonic flow centered at

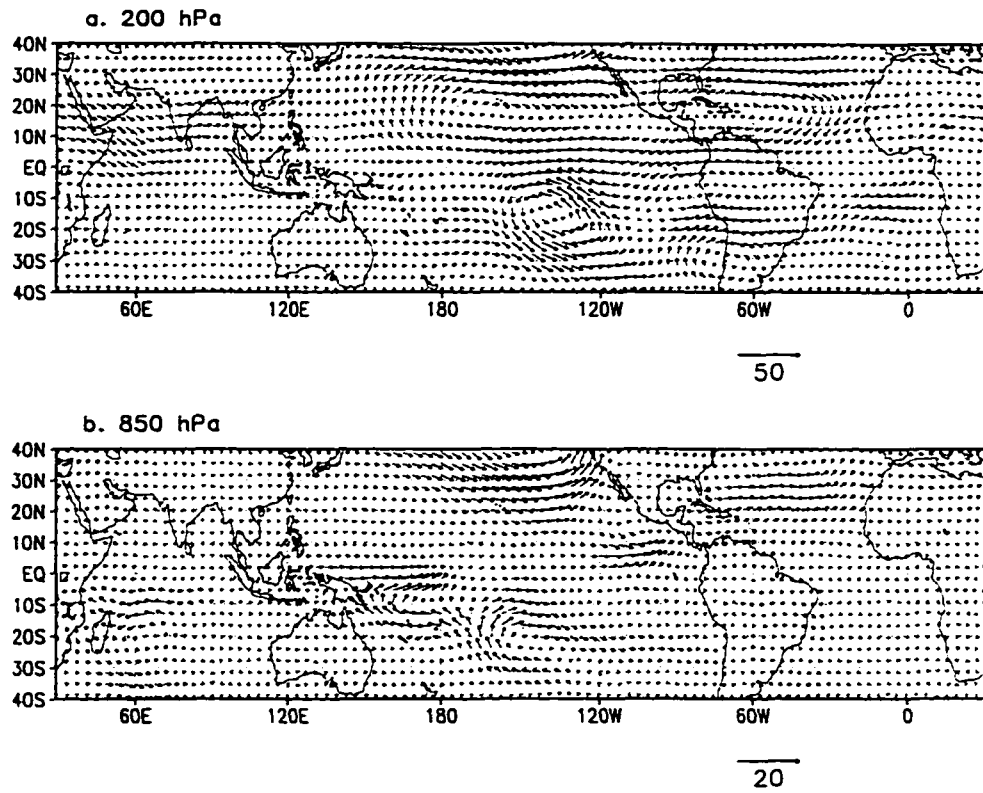


Figure 4.5 Difference maps of the monthly mean wind fields between the PACP1 and PACN1 runs (PACP1 - PACN1) for a. 200, and b. 850 hPa, unit: ms^{-1} .

about 15°N, corresponding to the tropospheric geopotential increase at 200 hPa (Fig. 4.3a) in that area. Simultaneously, there is another anticyclonic flow difference in the area immediately to the south of the tropical eastern Pacific, which corresponds to a circulation change associated with the large positive height change maximum at the 200 hPa level in the same geographical area (Fig. 4.3a).

Some quantitative similarities can be drawn for the 200 hPa horizontal wind difference fields in the current simulation (Fig. 4.5a) and in the reanalysis data (Fig. 3.4a) over the tropical regions. These include the westerly changes over the equatorial Indian Ocean and the anomalous easterlies over the central and eastern Pacific. The westerly wind difference over the north subtropical eastern Pacific region also matches well with the two period wind difference in the reanalysis data. However, the change features over the southern extratropical region can not be matched well with the reanalysis wind difference. Furthermore, the wind differences are quite large in magnitude in the simulation compared to the results of the reanalysis.

At the 850 hPa level (Fig. 4.5b), several notable features exist. As expected, lower level easterly wind decreases over the tropical Pacific. Strong low-level wind difference convergence exists in the equatorial central Pacific, and north side of the equator between 120°W and 90°W and immediately to the east of dateline between 10°S and 20°S over the eastern Pacific areas. A strong cyclonic structure in wind difference is found in the southern subtropical eastern Pacific, associated with the geopotential height decrease at the near surface level (Fig. 4.3c, d), and the eastward shift of the SPCZ shown in Lau and Nath (1994). Over the eastern portion of the North Pacific, another cyclonic wind difference can be seen, and it corresponds to the

anomalous geopotential height low found in the simulation over the North Pacific, exhibiting a dynamical consistency in the lower tropospheric atmosphere for the difference field. Compared to Fig. 3.4b, it is found that some key features, such as the easterly change over the equatorial eastern Pacific and cyclonic wind change over the North Pacific, have been simulated reasonably well. However, the wind change structures over the tropical Indian and Atlantic Oceans show little agreement to those in the reanalysis.

c. Vertical motion changes

Fig. 4.6 presents the vertical-longitudinal cross section of the vertical motion difference (pressure velocity with a unit of Pas^{-1}) in the two forcing runs at three selected latitudes in the tropical Pacific anomalous surface forcing regions. A large upward motion increase induced by the idealized SST forcing difference can be noted over the equatorial central Pacific region (Fig. 4.6a). Such upward motion difference is so large in magnitude that the maximum vertical velocity difference value (greater than 0.125 Pas^{-1}) is even larger than the maximum upward motion (less than 0.125 Pas^{-1} near 160°E) above the central Pacific forcing area in the CNTR run. The increase in the upward motion reaches its maximum in middle troposphere. Such a strong upward motion above the equatorial central Pacific leads to a pronounced upper level divergence as indicated by the poleward wind difference shown in Fig. 4.5a. An enhanced downward motion over the eastern Pacific across the equatorial plane can be found even though positive SST difference is placed in that region. The effect of the eastern Pacific anomalous SST forcing can be noted in zonal-vertical cross sections

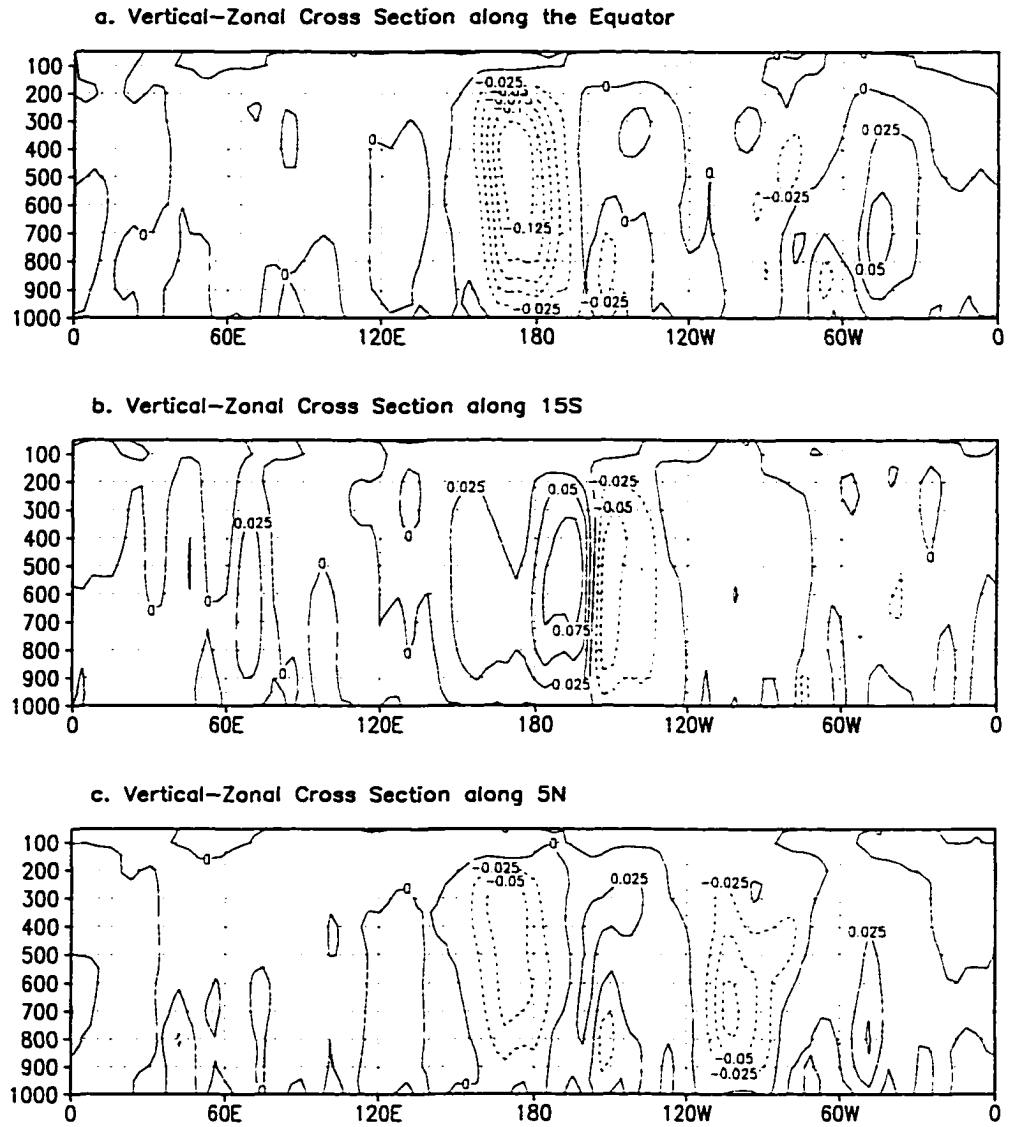


Figure 4.6 Vertical-zonal cross sections of the monthly mean vertical motion difference fields between the PACPI and PACN1 runs (PACPI - PACN1) along three selected latitudes. Contour interval is 0.025 Pas^{-1} .

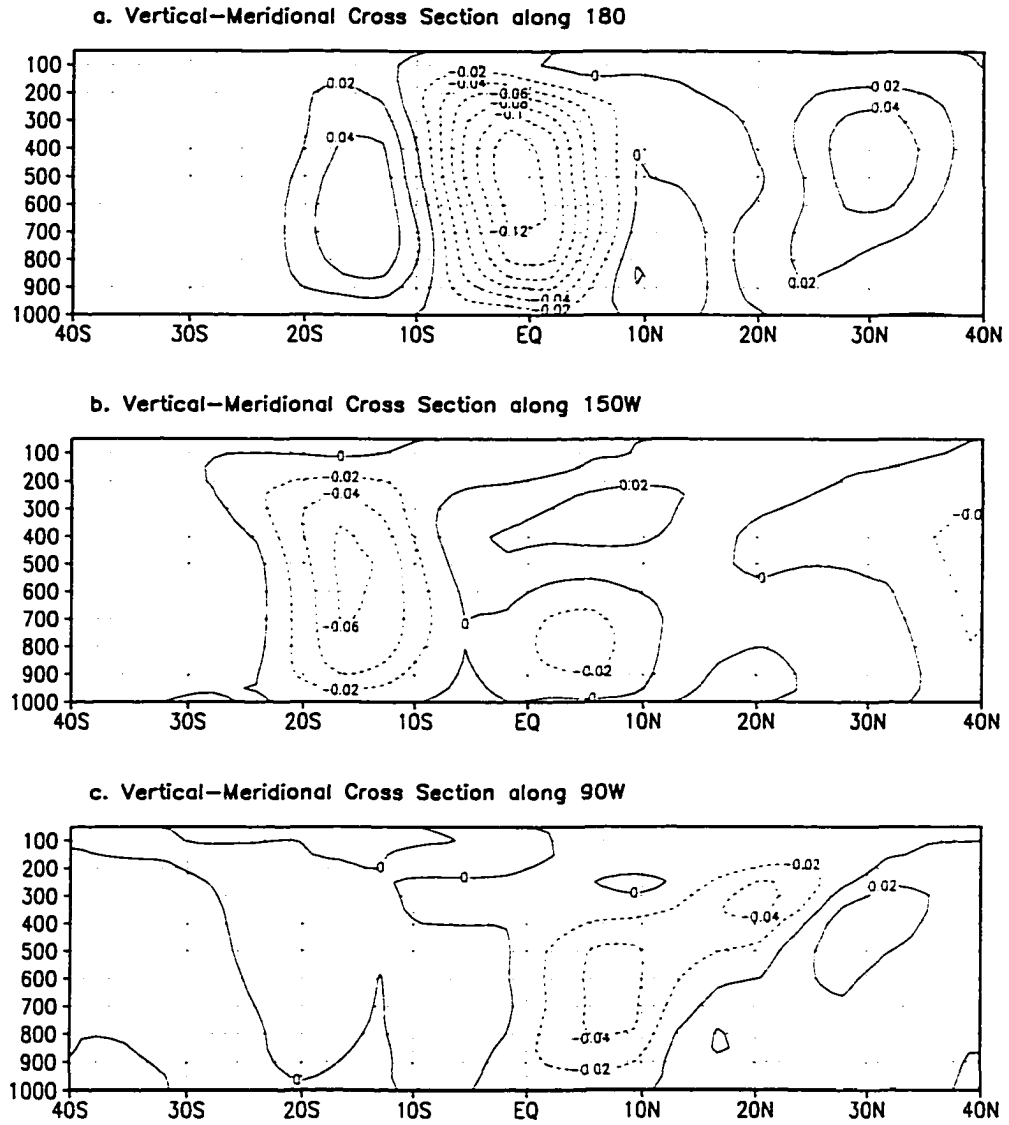


Figure 4.7 Vertical-meridional cross sections of the monthly mean vertical motion difference fields between the PACP1 and PACN1 runs (PACP1 - PACN1) along three selected longitudes. Contour interval is 0.02 Pas^{-1} .

along latitudes 15°S and 5°N as shown in Fig. 4.6b and c. These latitudes are chosen because the differences in atmospheric responses to the surface forcing can be explicitly seen. Previous studies have shown that the tropical convection, large scale vertical motion and SST are closely related (Lau et al. 1997). A 28°C SST is generally suggested to be the critical value for the occurrence of strong deep convection in the tropical region due to the nonlinear relation between water vapor and temperature as well as some other factors (Gadgil et al. 1984; Trenberth 1991; Zhang 1993). It is anticipated that the regions, for instance, along 15°S and 5°N, with an above 28°C SST in PACPI and below 28°C in PACN1 will yield the largest difference in atmospheric response. In the southern portion of the eastern Pacific at 15°S, an upward vertical motion difference is seen at near 150°W region (Fig. 4.6b), whereas in the northward of equator over the eastern Pacific, another upward vertical motion difference can be noticed in the area between 90°W and 120°W (Fig. 4.6c). These positive difference areas of upward motion are dynamically linked to the lower level anomalous wind convergence found in the same regions over the eastern Pacific in Fig. 4.5b. The magnitudes of the maximum upward differences in the vertical motion over the eastern Pacific are less than half of that found over the equatorial central Pacific forcing area. The strong upward motion over the tropical Indian and Atlantic Oceans exhibited in the control run (Fig. 4.4c) has been substantially suppressed by the anomalous forcing in the central and eastern Pacific.

The vertical-meridional cross sections of the vertical motion difference for the two forcing runs over the Pacific are illustrated in Fig. 4.7. It essentially reveals the same circulation difference structures given in Fig. 4.6, with a view from another

direction. As expected, over the central Pacific region (Fig. 4.7a), strong rising motion increase is found near the western equatorial forcing area, and sinking motion changes are seen in the adjacent subtropical areas in both Hemispheres. In the eastern Pacific, upward differences in vertical motion appear to center at 15°S along the 150°W, and 5°N along 90°W (Fig 4.7b, c), respectively. These regions show a greater than 28°C SST in PACP1 and lower than 28°C in PACN1 (see Fig. 4.2b and c). Again, the intensity of the vertical motion change for the two forcing runs over the eastern Pacific region is weaker, compared to the changes in the central Pacific.

A conclusion can be drawn from Figs. 4.6 and 4.7 that the SST forcing difference over the equatorial central Pacific has larger impact on the tropical atmospheric circulation than the forcing difference over the eastern Pacific, although the anomalous surface forcing with 2°C SST difference (PACP1 - PACN1) covers more extensive geographical area over the eastern Pacific than the equatorial central Pacific (see Fig. 4.2). A small increase in SST has larger effect on the atmospheric convection over the areas where the SST is close to 28°C. Hence, the atmospheric convection over the equatorial central Pacific area is more sensitive to the anomalous surface temperature change than that over the eastern Pacific because of its relative high mean absolute SST. The areas with upward vertical motion difference found in Figs. 4.6 and 4.7 consistently corresponds to the areas with above 28°C SST shown in Fig. 4.2b.

d. Atmospheric circulation changes

The strong upward motion in the equatorial central Pacific forcing area is accompanied by an increase in sinking motion in most the subtropical areas. Such an enhancement of local Hadley cell near the dateline can be seen from the vertical-meridional cross section of the vertical motion in Fig 4.7a. The anomalous surface forcing in the equatorial central Pacific leads to a stronger upward and downward motion in the PACP1 run, and a slight northward displacement of the circulation as the stronger southerly wind at the upper level can carry the air parcel further northward before it starts to move downward.

Although the rising branch of the Walker circulation in the west and sinking branch in the east are both enhanced (see Fig. 4.6a), with an eastward displacement of the maximum location of rising branch in the western tropical Pacific toward the dateline due to the surface forcing difference over the equatorial central Pacific, the east-west Walker circulation shows no intensification for the PACP1 run in comparison to the PACN1 run as the horizontal wind difference at both upper and lower levels reduce the wind strength in the zonal direction. In fact, it is weakened when the interdecadal anomalous SST pattern over the central and eastern Pacific regions occurs. Such simulation results are consistent with the findings based on both observation data and model simulations in Nitta and Yamada (1989) and Graham (1994). The strong poleward motion at the upper level caused by the strong vertical rising in the forcing area carries the airflow northward and southward. Dynamically, the circulation around the anomalous forcing in the equatorial central area has to compensate to maintain the mass conservation locally at the upper level. Furthermore,

the warmer SST over the tropical eastern Pacific region may result in the surface pressure decrease, leading to a less east-west pressure gradient in the equatorial zonal plane over the Pacific. As a result, the easterly change in the upper level and westerly change at the lower level in the equatorial eastern Pacific weaken the Walker circulation.

4.3.3 Changes in atmospheric heating due to the anomalous surface forcing

The atmospheric diabatic heating is primarily contributed by radiative, latent and sensible heating (Yanai et al. 1973). The atmospheric heating gradient is the primary driving force of the global atmospheric motion. Latent and sensible heating are considered as the major sources warming the tropospheric atmosphere in the working hypothesis in section 3.5, leading to local tropospheric geopotential height increases over the tropical Pacific. Such a local height change acts as to trigger a large area atmospheric change through dynamical and thermodynamical processes. Before investigating the details of the mechanisms for the interdecadal tropical atmospheric variations, the total atmospheric diabatic heating changes associated with the interdecadal anomalous SST pattern is presented, using the differences between the PACP1 and PACN1 simulation results. Such diabatic heating differences may provide physical evidence for further studies.

One way to obtain the diabatic heating is to compute the residual term in the thermodynamic equation as works done by Yanai (1996) and Ebisuzaki (1995), using the model output variables. The other way is to directly write out the summation of

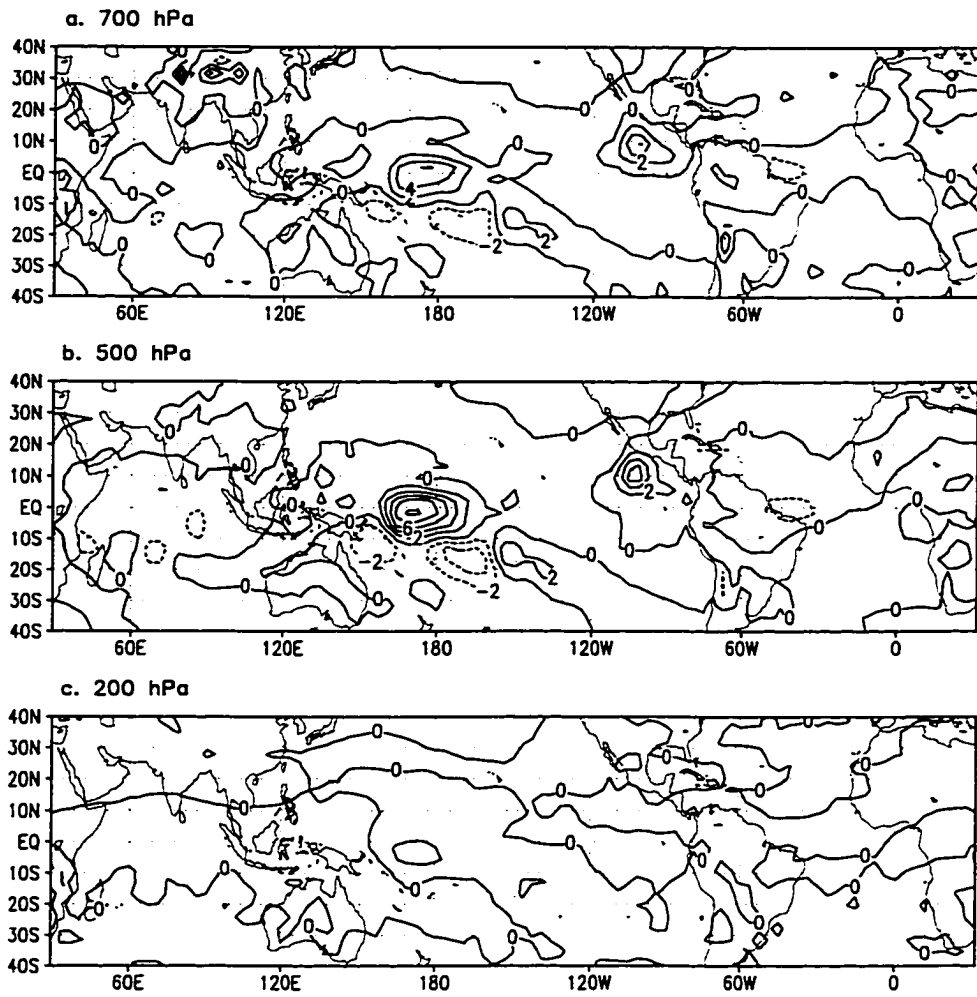


Figure 4.8 Difference maps of the monthly mean diabatic heating fields between the PACP1 and PACN1 runs (PACP1 - PACN1) for a. 700, b. 500 and c. 200 hPa. Contour interval is $2^{\circ}\text{Kday}^{-1}$.

physical parameterization terms when computing the local temperature change during the model integration. Both of the methods are performed herein and the results are similar. Hence, the diabatic heating computed directly from the physical parameterization schemes are presented. Fig. 4.8 illustrates the diabatic heating differences between the PACP1 and PACN1 forcing runs at the 200, 500 and 700 hPa levels.

At the lower troposphere (700 hPa level, Fig. 4.8a), the heating difference explicitly reflects the effects of the idealized anomalous SST forcing over the tropical central and eastern Pacific regions on the atmospheric diabatic heating. Three notable positive heating change areas can be found over the anomalous surface forcing areas. Over the equatorial central Pacific anomalous forcing region, the heating is enhanced strongly in the PACP1 run, with a maximum of greater than 4 Kday^{-1} which is even comparable to diabatic heating resulted from the control run over the western Pacific warming pool (figure not shown). In the zonal mean, the latent heating is dominant above 850 hPa in the tropics, whereas the sensible heating is more important below that level (Newell et al. 1970). Strong rising motion induced by the idealized SST anomaly in the PACP1 run carries the warm and moist air from the surface upward and, heat the atmospheric layer immediately above the anomalous forcing area. One heating increase area over the southern eastern Pacific exhibits a 2 Kday^{-1} local maximum change. This area forms a northwest-southeast oriented narrow zone, indicating a strong SPCZ in the interdecadal atmospheric variability. Another positive diabatic heating difference area over the eastern Pacific is found northward of the equator between 100°W and 80°W . Both of the size and magnitude of this heating

change area are comparable to those over the equatorial central Pacific forcing area. The positive diabatic heating difference areas over the Pacific appear to be consistent with the upward motion difference areas shown in Fig. 4.3, and once again shows the importance of the SST exceeding 28°C over the tropical Pacific. The changes in heating over the tropical Indian and Atlantic Oceans are less significant, with two very small areas exceeding 1 Kday⁻¹ cooling over the eastern Indian Ocean and western Atlantic Ocean because the upward motion in those areas has been largely suppressed.

Increase in diabatic heating reaches its maximum in the middle troposphere as shown in Fig. 4.8b. At 500 hPa level, the overall spatial structures of diabatic heating are nearly the same as those at 700 hPa. It is believed that the latent heat release plays a dominant role in the mid-tropospheric layer heating. Accordingly, the heating increase regions over the equatorial central Pacific and northward of the equatorial eastern Pacific (Fig. 4.8b) are approximately double the maximum magnitudes of the differences at 700 hPa. However, the strength of heating increase over the SPCZ area of the southern eastern Pacific remains unchanged. As altitude increases to 200 hPa in the upper troposphere, the diabatic heating is reduced largely in the PACP1 run because the latent heating has little impact due to the scarcity of the moisture. As a result, the diabatic heating over the forcing area in the equatorial central Pacific is only larger than 1 Kday⁻¹, with a maximum above 2 Kday⁻¹. Over the eastern Pacific region, the size of northern part of the heating increase area has been reduced dramatically, with a maximum of 2 Kday⁻¹, whereas the positive heating difference area found at lower levels over southern eastern Pacific disappears at the upper level.

Chapter 5

Investigations of the mechanisms for the tropical atmospheric interdecadal variations using the GCM simulations

One of the objectives of this study is to investigate the physical processes and mechanisms which are responsible for the initiation and maintenance of the tropical atmospheric interdecadal variability. Based on the NCEP/NCAR reanalysis and IMGa climatological run data analyses, a working hypothesis is proposed in Chapter 3 to link specific physical mechanisms to the atmospheric interdecadal variability over the tropical region. Furthermore, the analyses of the diabatic heating differences simulated by the ECHAM4 GCM experiments forced with idealized anomalous SST patterns in the previous chapter have demonstrated that the atmospheric heating processes in the tropics and low latitude region play an important role in the atmospheric height changes.

In this chapter, the effects of specific atmospheric physical processes, such as cumulus convection, radiative heating and atmospheric heat transport, will be investigated in more detail by means of idealized ECHAM4 GCM simulations. Different model experiments are designed and performed to study the atmospheric responses to SST anomalies in different geographical areas over the tropical Pacific. In doing so, the goal is to develop and improve the understanding of overall tropical

atmospheric processes and some key physical mechanisms which lead to the structures of tropical atmospheric interdecadal variations.

5.1 General description and physical basis for the analyses

5.1.1 Thermodynamical balance in atmosphere

The atmospheric general circulation is primarily driven by the heating differential. In tropical and low latitude regions, the atmosphere is nearly barotropic. Hence, atmospheric motion is dominated by the physical processes in atmospheric heating. The general circulation in these regions is characterized by thermally direct circulation both in zonal and meridional directions, such as the east-west Walker circulation and meridional Hadley cell, which are consequences of the heating difference at the surface and atmosphere at different geographical areas. The atmospheric physical and dynamical processes are in balance as shown in the following thermodynamical equation,

$$\frac{\partial T}{\partial t} + \frac{1}{a \cos \varphi} \frac{\partial}{\partial \lambda} (uT) + \frac{1}{a \cos \varphi} \frac{\partial}{\partial \varphi} (vT \cos \varphi) + \frac{\partial}{\partial p} (\omega T) - \kappa \frac{\omega T}{p} = \frac{Q}{c_p} \quad (5.1)$$

where the residual term Q is the diabatic heating term. a is the radius of the earth, and other symbols in (5.1) represent their conventional meaning in meteorology. (5.1) has been used to diagnose the long-term atmospheric heating climatology and monthly mean diabatic heating (Ebisuzaki 1995).

The thermodynamical equation (5.1) is written in the flux form in order to shed light on the subsequent discussions of atmospheric heat transport. In fact, diabatic heating is primarily balanced by the horizontal and vertical temperature advection terms and air parcel adiabatic motion (dynamical cooling). The terms on the left side of (5.1) can each be evaluated to investigate the relative importance of individual physical process in the spatial distribution of the thermal energy balance. The direct diabatic heating outputs from the ECHAM4 GCM integration are utilized to analyze the atmospheric heating effects. In the ECHAM4, diabatic heating (Q/c_p) term is generated by physical parameterization schemes of several physical processes such as cumulus convection, large scale precipitation, radiative heating, gravity drag and the vertical diffusion processes. Scrutinization of the model outputs reveals that the cumulus convection, large scale precipitation and radiative heating processes in the research domain are the dominant factors in determining the atmospheric diabatic heating in the model simulations. Hence, these three physical processes are chosen as the major targets in the atmospheric physical analyses. It is important to mention that the veracity of these result analyses are strongly limited by the correctness of current ECHAM4 GCM convection and radiation parameterization schemes. As evidence of this, the results from PCA of IMGa climatological run in Chapter 3 have shown the consistent atmospheric change patterns. Moreover, the idealized model experiments in Chapter 4 have also generated physically meaningful and consistent atmospheric responses to the tropical surface forcing. Thus, it is reasonable to interpret results from the model parameterization schemes as providing fundamentally realistic

portrayals of atmospheric processes, although not what precisely occurs in real atmosphere.

The initial results in atmospheric diabatic heating (Chapter 4) have indicated that anomalous surface forcing may induce more heating in the atmosphere. While a large proportion of such energy is used to drive atmospheric motions in accordance with the thermodynamical balance, conceptually it is also useful to consider that the energy is also involved, to certain extent, in heating/cooling the local atmosphere, which may, in turn, lead directly to an atmospheric temperature/geopotential height change.

5.1.2 Model experiments for the physical analyses

The model simulations in this chapter are specifically designed to investigate how the tropical atmosphere responds to the anomalous SST patterns in an attempt to uncover the physical mechanisms and processes through which the interdecadal atmospheric height change patterns are established and maintained. The interdecadal tropical Pacific anomalous SST pattern from the data analyses is shown in Figs. 2.3 and 2.4. The key components in the spatial structure are the two anomalous SST patches over the tropical central and eastern Pacific, as ideally characterized in Fig. 4.2a. The atmospheric response to the anomalous surface forcing condition is sensitive to the geographical areas where the SST anomalies occur because of the effect of the ocean surface thermal state, as indicated in previous studies (Gadgil et al. 1984; Trenberth 1991; Zhang 1996) and the analyses in the PACP1 and PACN1

experiment results. Three model experiments, focused on the effects of anomalous surface forcing at different areas, are performed with the idealized SST fields given in Figs. 5.1 - 5.3. The maximum anomalous SST perturbation in these experiments is prescribed as 2°C. Such a magnitude of SST perturbation doubles the values used in the PACP1 and PACN1 experiments, and seems relatively large for a simulation with a focus of a long term climatological study. However, the purpose of these experiments is to explore the atmospheric physical processes arising from the given anomalous surface conditions. An appropriate SST perturbation magnitude may ensure that the resultant physics in the simulated atmosphere can be identified unambiguously.

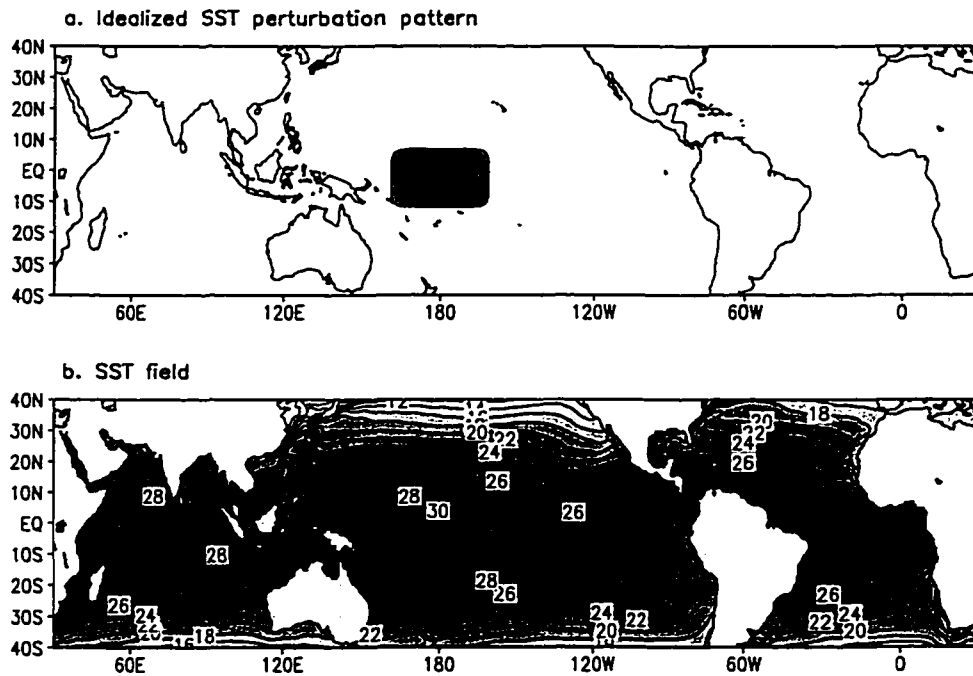


Figure 5.1 Idealized SST patterns for the CPACP2 run. a. equatorial central Pacific SST perturbation pattern with a maximum of 2°C (darkest area), contour interval is 0.4°C. b. prescribed SST field for the CPACP2 run, contour interval is 2°C.

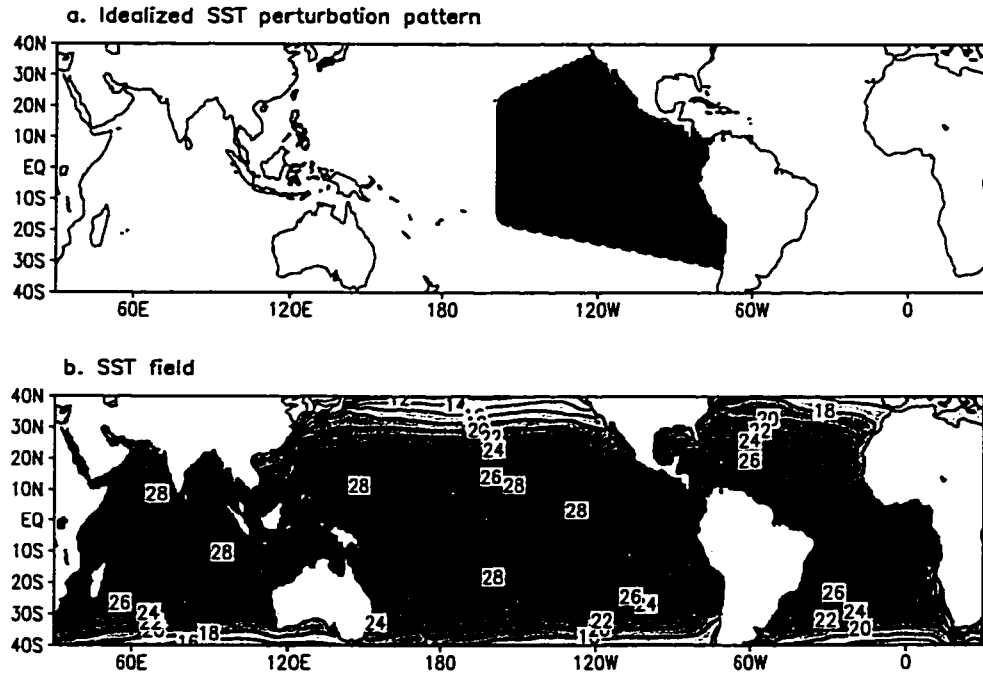


Figure 5.2 Same as Figure 5.1, except for the EPACP2 forcing run.

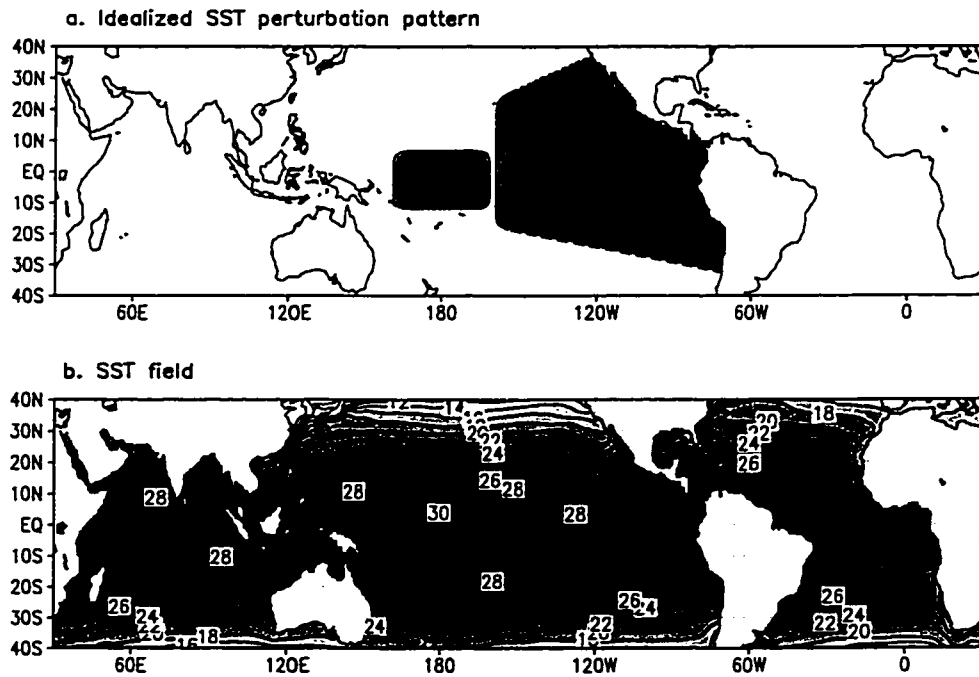


Figure 5.3 Same as Figure 5.1, except for the PACP2 forcing run.

The model integration with the surface boundary condition given in Fig. 5.1b is referred to as “Central Pacific positive 2°C” (CPACP2) run. The motivation behind this experiment is to attempt to isolate the effect of the anomalous equatorial central Pacific surface forcing on the tropical atmospheric changes. The isolated effect of the eastern Pacific anomalous surface forcing is given by the model experiment with the SST field in Fig. 5.2b, called “Eastern Pacific positive 2°C” (EPACP2) run. The experiment, forced with a SST field in Fig. 5.3b, is to simulate the anomalous SST effect over the whole tropical central and eastern Pacific for the interdecadal variability, is referred as to “Pacific positive 2°C” (PACP2) run.

As in the PACP1 and PACN1 runs in the previous chapter, the model experiments are carried out with the same perpetual January mode. Also, the model integration starts with the same January atmospheric initial condition file provided by the MPI. For each of the CPACP2, EPACP2 and PACP2 experiments, the ECHAM4 GCM is first integrated with the January climatology SST field (see Fig. 4.1) for the initial three months. Then the specified SST field is incorporated and the model is integrated for another 21 months, leading to a total integration period of 24 months. As in previous analyses, during the integration, the output variables are written every 6-hours, and only the last 20-month data are utilized in the analyses.

5.2 Effects of the equatorial central Pacific anomalous SST forcing

The model results from CPACP2 are analyzed and compared to the data from the CNTR run. The analyses, presented mostly by the difference field between the

CPACP2 and CNTR runs for an atmospheric variable (CPACP2-CNTR), will explicitly explore the tropical atmospheric changes caused by a single positive SST perturbation pattern over the equatorial central Pacific. Such a simplified and idealized case study will assist in better understanding of the atmospheric physical processes in the more complex interdecadal variation studied.

5.2.1 Tropical atmospheric responses to the SST perturbation over the equatorial central Pacific

a. Tropical atmospheric height changes

The tropical geopotential height difference fields between the CPACP2 forcing run and the CNTR run are presented in Fig. 5.4 at the 4 selected levels. Despite the relatively small area of the idealized anomalous SST forcing located in the tropical central Pacific, the atmospheric response to this anomalous forcing is impressive (Fig. 5.4), indicating a tropospheric geopotential height increasing in an extensive geographical area over the tropics and middle latitudes in Southern Hemisphere. The height changes in the CPACP2 forcing run show different spatial structures as the altitude varies in the troposphere.

As shown in the height difference field for the PACP1 and PACN1 runs (Fig. 4.3), the entire tropical-wide height increase pattern is still the most pronounced spatial feature if the SST perturbation is only placed in the equatorial central Pacific, especially at the upper levels. At the 200 hPa level (Fig. 5.4a), the largest geopotential height increasing region can be found in the tropical central and eastern Pacific, and

Atlantic regions, with a height change value greater than 20 gpm. Furthermore, the height increase in the eastern Pacific and part of the western tropical Atlantic exceeds 40 gpm, with a maximum change above 80 gpm over the eastern Pacific. In the northern low latitude region, the geopotential height decrease dramatically. The area to the north side of the equatorial eastern Pacific shows the largest height decrease. The dipole structure in the eastern Pacific area between the equator and 35°N can also be clearly seen. Such a structure resembles the interdecadal height variation pattern found in the same geographical areas as illustrated in Fig. 4.3. The atmospheric changes at the 200 hPa level over the Indian Ocean and part of the western tropical Pacific are relatively small and less than 20 gpm in general.

In the middle tropospheric level (500 hPa, see Fig. 5.4b), the geopotential height still exhibits an increasing change over the tropical belt. However, the magnitude of the positive change at this level is mostly reduced to only 10 - 20 gpm in the tropical area. Unlike the spatial structure at the upper troposphere, the height difference field is relatively uniform across the tropical belt. The zonal height difference gradient becomes small. The dipole of the height change structure in the eastern Pacific still exists, though it is less well structured due to the smaller positive height difference magnitude in the equatorward node of the structure. It can be noticed in Fig. 5.4b that the height change in the tropical Indian Ocean is of a comparable magnitude to that in the upper level (Fig. 5.4a). In the lower troposphere (700 hPa, Fig. 5.4c), the height increases over the tropical central and eastern Pacific, and a large part of the tropical Atlantic regions become insignificant, mostly ranging at 0 - 5 gpm, with a small height decrease area to the west of the anomalous forcing

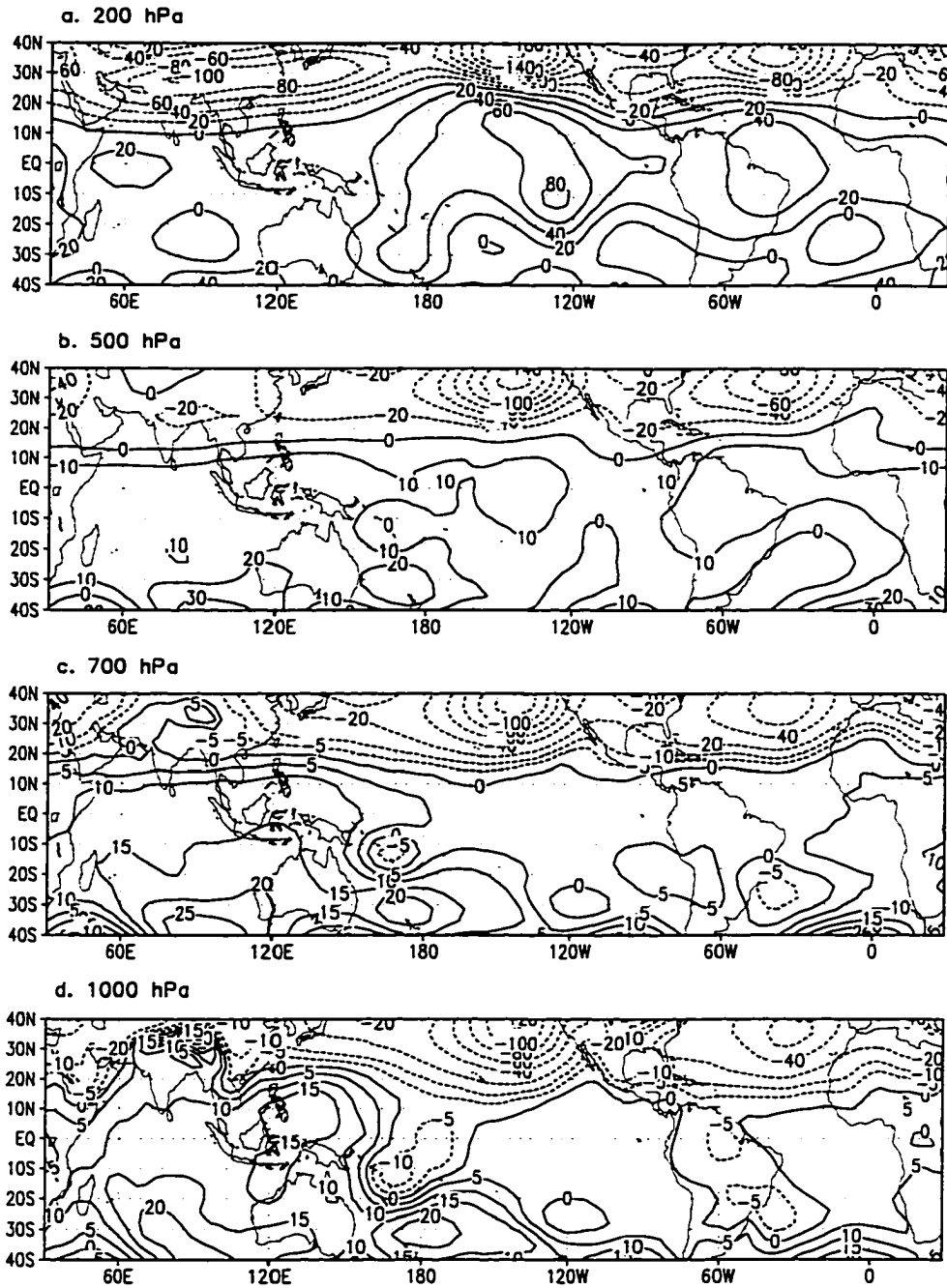


Figure 5.4 Difference maps of the monthly mean geopotential height fields between the CPACP2 and CNTR runs at 200, 500, 700, and 1000 hPa (CPACP2 - CNTR run). Unit: gpm.

SST area. The largest height increase is found in the Indian Ocean region, with a 10 - 20 gpm difference. Near the surface (1000 hPa, Fig. 5.5d), the Indian Ocean still shows the same magnitude in geopotential height increase compared to those at the upper levels. The height increases over the tropical eastern Pacific and Atlantic are negligible. A 5 - 10 gpm height decrease is found in the anomalous forcing area in the equatorial central Pacific, which is a direct consequence of the surface air flow convergence induced by the strong upward motion in the anomalous forcing area.

The height difference fields given in Fig. 5.4 illustrate the isolated effect of the equatorial central Pacific SST perturbation on the tropical tropospheric geopotential height. It can be concluded that the localized positive surface SST anomaly in the tropical central Pacific may lead to a notable tropical-wide height increase above the middle troposphere. The height difference spatial patterns shown in Fig. 5.4 appear to be reminiscent of those patterns in Fig. 4.3 for the simulation of the interdecadal variability in several key aspects. The tropical-wide atmospheric increase, relatively larger height increase above the middle tropospheric level in the tropical central and eastern Pacific, the dipole spatial height change structure in the eastern Pacific sector are all the common features both in Fig. 4.3 and Fig. 5.4. In addition, the insignificant vertical change in the positive height difference over the tropical Indian Ocean can be detected in these two figures as well. All this evidence suggests that the SST anomaly patch located in the equatorial central Pacific sector in the SST interdecadal variability may have a key contribution in the tropical atmospheric interdecadal variations.

b. Wind and circulation changes

The horizontal wind vector difference fields at the 200 and 850 hPa levels, representing the upper and lower troposphere, are given in Fig. 5.5. As expected, strong poleward wind anomaly is found on both sides of the equator near the anomalous surface area at the upper level (Fig. 5.5a), indicating a large anomalous flow divergence aloft. The northward wind difference to the north of the anomalous forcing area appears to be quite vigorous, ranging at $10 - 20 \text{ ms}^{-1}$ in the region between $10^{\circ}\text{N} - 30^{\circ}\text{N}$. Such a large northward wind change is deflected to the east at the northern low latitude regions due to the Coriolis force and angular momentum conservation effect. The deflected westerly anomaly reinforces the upper level subtropical jet stream in those area. A notable anticyclonic wind anomaly can be seen in the eastern Pacific centered at about 10°N (Fig. 5.5a). Moreover, to the southeast of this anticyclonic wind difference, another anticyclonic wind anomaly is found on the south side of the equator in the eastern Pacific area. The two large negative vorticity anomalies dynamically correspond to the height increase centers in the eastern Pacific sector in the upper troposphere (see Fig. 5.4a). Another major feature in the upper level wind change field is the overwhelming westerly anomaly over the northern low latitude regions. Such westerly wind increase can also be found over the tropical eastern and Atlantic Oceans (Fig. 5.5a).

At the lower troposphere (Fig. 5.5b), anomalous air flow convergence occurs near the central Pacific SST perturbation area. The easterly winds in the equatorial belt are greatly weakened and even reversed in the western Pacific. Corresponding to

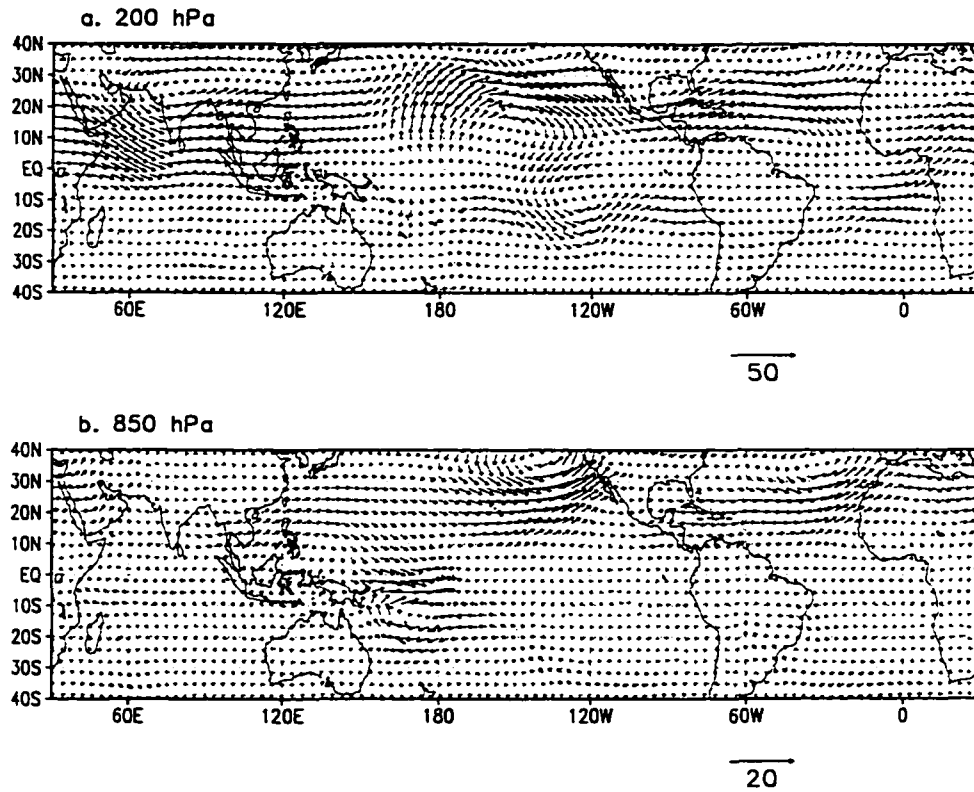


Figure 5.5 Difference maps of the monthly mean wind fields between the PACP2 and CNTR runs (PACP2 - CNTR) for a. 200, and b. 850 hPa, unit: ms^{-1} .

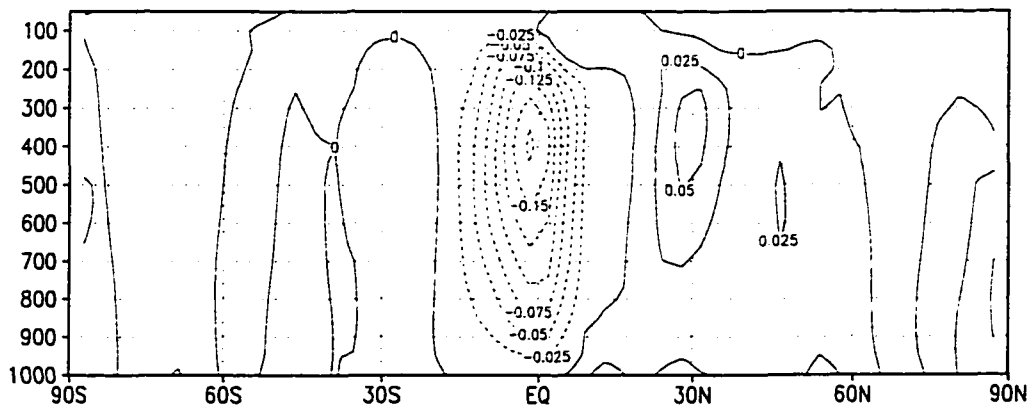


Figure 5.6 Vertical-meridional cross section of the monthly mean vertical motion difference fields between the CPACP2 and CNTR runs (CPACP2 - CNTR) along 180° . Contour interval is 0.025 Pas^{-1}

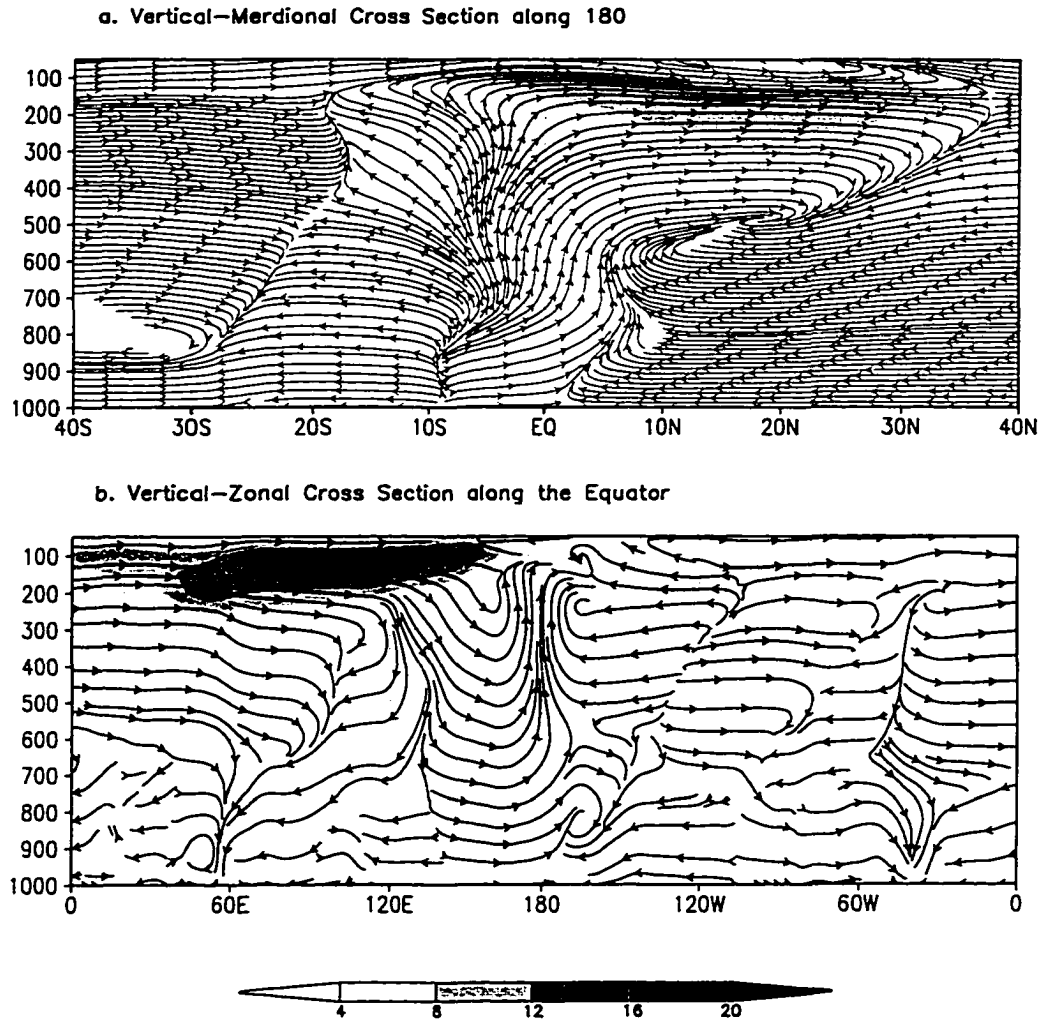


Figure 5.7 Difference maps of the flow (stream line) and its magnitude (shaded area) between the CPACP2 and CNTR runs (CPACP2 - CNTR) for a. vertical-meridional cross section along 180° , and b. vertical-zonal cross section along the equator. Shade unit: ms^{-1} .

the decrease in surface pressure in both north Pacific and north Atlantic regions, cyclonic wind anomaly can be clearly seen in these areas in Fig. 5.5b.

Fig. 5.6 gives the vertical motion changes in vertical-meridional cross section for 180° . As expected, in the forcing area, strong anomalous rising motion change is found due to the warm SST and sinking motion occurs over subtropical regions, especially for the northern Hemisphere. The maximum rising motion change exceeds 0.175 Pas^{-1} at the 400 hPa level over the anomalous surface forcing area, whereas the sinking motion change appears greater than 0.05 Pas^{-1} in the upper levels near 30°N . These rising motion change values are even larger than the original maximum rising (less than 0.1 Pas^{-1}) and sinking (less than 0.05 Pas^{-1}) motions found in the correspondent areas for the CNTR run (figure not shown).

The effects of the anomalous SST in the equatorial central Pacific on the tropical general circulation can be illustrated more explicitly by the cross section of the circulation changes in zonal and meridional directions near the anomalous surface forcing area in Fig. 5.7. The cross section in meridional circulation change along the 180° is given in Fig. 5.7a. It can be clearly seen that significantly large upward circulation occurs in the atmosphere above the anomalous forcing area. This is consistent with the changes shown in Fig. 5.6. At the upper level, a $4 - 16 \text{ ms}^{-1}$ northward wind change is found in the area between the equator and 30°N , whereas a large equatorward wind circulation change occurs in the lower tropospheric layer in the same area. Such changes are already seen in the horizontal wind vector change (Fig. 5.5a). The most pronounced feature in the Fig. 5.7a is the significant

intensification of the local Hadley cell along 180°, induced by the anomalous surface forcing increase in the central Pacific. It is worth mentioning that the zonal mean climatological Hadley cell remains unchanged for the CPACP2 forcing run (figure not shown), suggesting an equatorward wind compensation from other longitudinal areas.

Climatologically, the zonal circulation near the equatorial plane is primarily characterized by three east-west circulation cells with rising air over Indonesia and the western Pacific, eastern equatorial Africa and Amazon area, and sinking motions over the colder waters in the eastern Pacific, western Indian and eastern Atlantic ocean regions (Peixoto and Oort 1992, see their Fig. 16.5). With an anomalous SST perturbation placed over the equatorial central Pacific, the model simulated atmosphere shows a strong upward motion anomaly above the anomalous forcing area (Fig. 5.7b) in the equatorial plane, whereas the strong rising motion near Indonesia and western Pacific (rising branch of the Walker circulation) is largely suppressed. The area with the strongest rising motion over the tropics shifts eastward to the dateline as shown in Fig. 5.7b. Because of the strong poleward wind anomaly in the SST perturbation area (see Fig. 5.5a), the upper level divergence is primarily characterized by a strong poleward air flow. From Fig. 5.7b, upper level zonal wind anomalies converge toward the central Pacific area from both west and east sides. The anomalous westerly to the west side of the SST perturbation area is considerably large, reaching a maximum value of 16 - 20 ms^{-1} . The easterly anomaly to the east side at the upper level weakens the Walker circulation.

5.2.2 *Changes in atmospheric diabatic heating processes*

In the ECHAM4 GCM, the geopotential height at a given point in 3-dimensional space is calculated directly using the temperature integration from the lowest model level to the current pressure level of the point, based on the hydrostatic relation. Therefore, the atmospheric height change is directly related to the vertical temperature profile. Given the thermodynamical relation in (5.1), atmospheric temperature change is determined by the dynamical and physical processes in the atmosphere. The diabatic and adiabatic processes may warm or cool the local atmosphere which, in turn, leads to a change in the atmospheric geopotential height. On the other hand, changes in temperature and geopotential height can also induce a change in the atmospheric dynamical and physical processes through the atmospheric adjustment.

a. Total diabatic heating change in the CPACP2 run

Fig. 5.8 shows the diabatic heating difference fields between the CPACP2 and the CNTR runs at 3 pressure levels. Such a diabatic heating change is considered as the effect exclusively caused by the anomalous SST forcing over the equatorial central Pacific. Diabatic heating increasing in the atmosphere above the positive SST anomaly can be found at all the selected levels (Fig. 5.8).

At the lower level (Fig. 5.8a), the diabatic heating increases at about $1 - 4 \text{ Kday}^{-1}$ in the central Pacific area. A weak cooling area can be noticed in the tropical western and eastern Pacific, and part of the tropical western Atlantic, indicating that SST forcing anomaly in the central Pacific may suppress the rising motion and

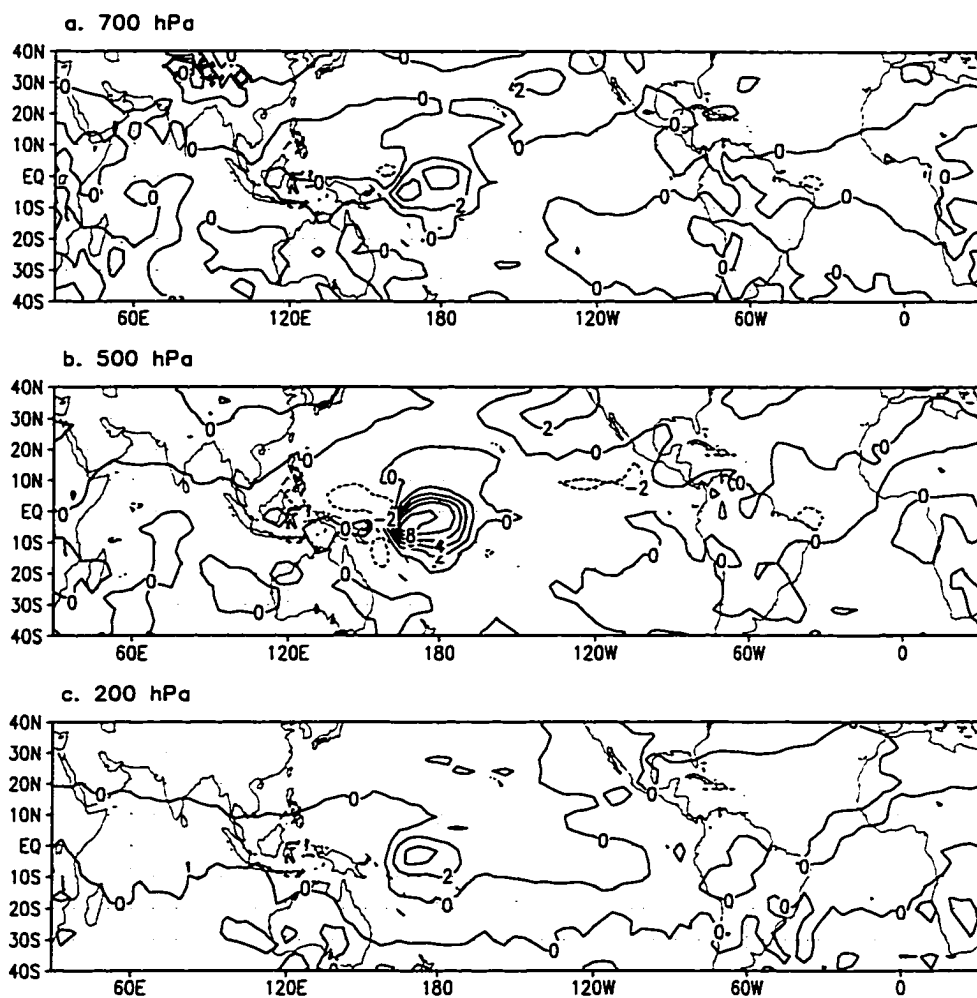


Figure 5.8 Difference maps of the monthly mean diabatic heating fields between the CPACP2 and CNTR runs (CPACP2 - CNTR) for a. 700, b. 500 and c. 200 hPa. The contour interval is $2^{\circ}\text{Kday}^{-1}$.

cumulus convection away from the strong local SST perturbation region (see Fig. 5.5b) and weaken the ITCZ in those areas. The diabatic heating difference field at the 500 hPa level (Fig. 5.8b) exhibits similar spatial structures as seen at the lower level (Fig. 5.8a). However, the magnitude of heating increasing doubles. In the upper troposphere (Fig. 5.8c), strong positive heating change still exists over the equatorial central Pacific, with a heating increase comparable to the one at the 700 hPa level (Fig. 5.8a).

The large diabatic heating increase above the central Pacific anomalous forcing area is consistent with the upward motion changes in the same areas as shown in Figs. 5.4 and 5.5. The increased heating energy is balanced by the strong adiabatic cooling associated with the increased rising motion. However, the tropical-wide geopotential height increase in the CPACP2 run (see Fig. 5.3) indicates that the tropical atmosphere must have been warmed, especially in the middle and upper tropospheric layers. Hence, it can be inferred that certain part of the anomalous diabatic heating energy is used to warm the atmosphere and change the tropospheric geopotential height.

b. Vertical distribution of different diabatic processes

The total diabatic heating in the ECHAM4 is primarily contributed by three physical processes: radiative cooling, cumulus convection and large scale precipitation. Large scale precipitation is generated from stratiform clouds in the model. We now evaluate the effects of these individual processes on the tropical atmospheric heating changes under the specified SST perturbation over the equatorial central Pacific area. In Fig. 5.9, vertical profiles of the three individual portions of the

heating processes and the total diabatic heating at 6 different geographical locations in the tropics are presented. 4 of the 6 locations at the equator are chosen to represent the equatorial central and western Pacific (Fig. 5.9a and b), equatorial Indian and Atlantic Ocean regions (Fig. 5.9e and f). Two locations (Fig. 5.9c and d), selected to represent the tropical eastern Pacific, are located in the areas where approximately the maximum geopotential height increases are found on the north and south sides of the equator in the eastern Pacific (Fig. 5.4). The heating data are results from the model parameterization schemes.

Inside the anomalous surface forcing area (Fig. 5.9a), it is shown that the total diabatic heating change increases with altitude and reaches its maximum at the 500 hPa level. The heating increase between 700 and 200 hPa levels appears to be quite significant as well. Above the 200 hPa level, a thin layer of diabatic cooling change occurs due to a radiative cooling effect in that layer. The large cumulus convection due to the strong surface forcing is the dominant diabatic process for the vertical distribution of the atmospheric heating below 300 hPa level in Fig. 5.9a. For the layer between 300 and 200 hPa levels, heating induced by large scale precipitation and radiation surpasses the heat generated by the cumulus convection latent heat release, although the magnitudes of heating changes are within $0.5 - 2.5 \text{ Kday}^{-1}$. In the anomalous forcing area, below the middle troposphere, the large scale precipitation latent heat release is slightly (approximately 0.5 Kday^{-1} , see Fig. 5.9a) less than the normal surface forcing condition. The radiative process shows a less cooling effect in the atmospheric layer below 200 hPa (Fig. 5.9a), especially in the area between 200 - 300 hPa levels. Such a warming effect of radiative process could be simply explained

as: the more convective and thick clouds, the more long wave radiation is re-emit back to the surface at lower level and the more long wave radiation energy is absorbed by the thick clouds at the upper layer, and the less long wave radiation is radiated to space from the higher top of the thick deep convective clouds. This induces a lower amount of cooling due to the radiative process in the CPACP2 forcing run.

The locations selected at the equatorial western and Indian Ocean regions (Fig. 5.9b,e) show diabatic cooling in the whole tropospheric layer. As seen in the zonal cross section circulation change (Fig. 5.7), the vertical rising motions normally in the tropical western Pacific and Indian ocean warm waters are, to certain extent, suppressed due to the eastward shift of the maximum rising motion to the anomalous surface forcing area. This leads to a reduced strength in cumulus convection and the latent heat release in middle and lower tropospheric layers. In the tropical Atlantic (see Fig. 5.9f), the total diabatic heating is reduced by about 0.7 Kday^{-1} in the mid-troposphere because of a decrease in all the three diabatic processes. In the north side location of the eastern Pacific (Fig. 5.9c), the heating change is about -2 Kday^{-1} mostly due to less cumulus convection latent heat release below 400 hPa. On the south side (Fig. 5.9d), the heating change seems negligible. One common feature in all these vertical profiles is that in the middle and lower troposphere (below about the 300 hPa level), the dominant process in diabatic heating is the cumulus convection in the tropical area, whereas in the upper troposphere, radiation and large scale precipitation processes play a major role in the heating difference.

If the interdecadal SST forcing is indeed limited to the central Pacific, the results and analyses in Figs. 5.8 and 5.9 have indicated that the tropical-wide

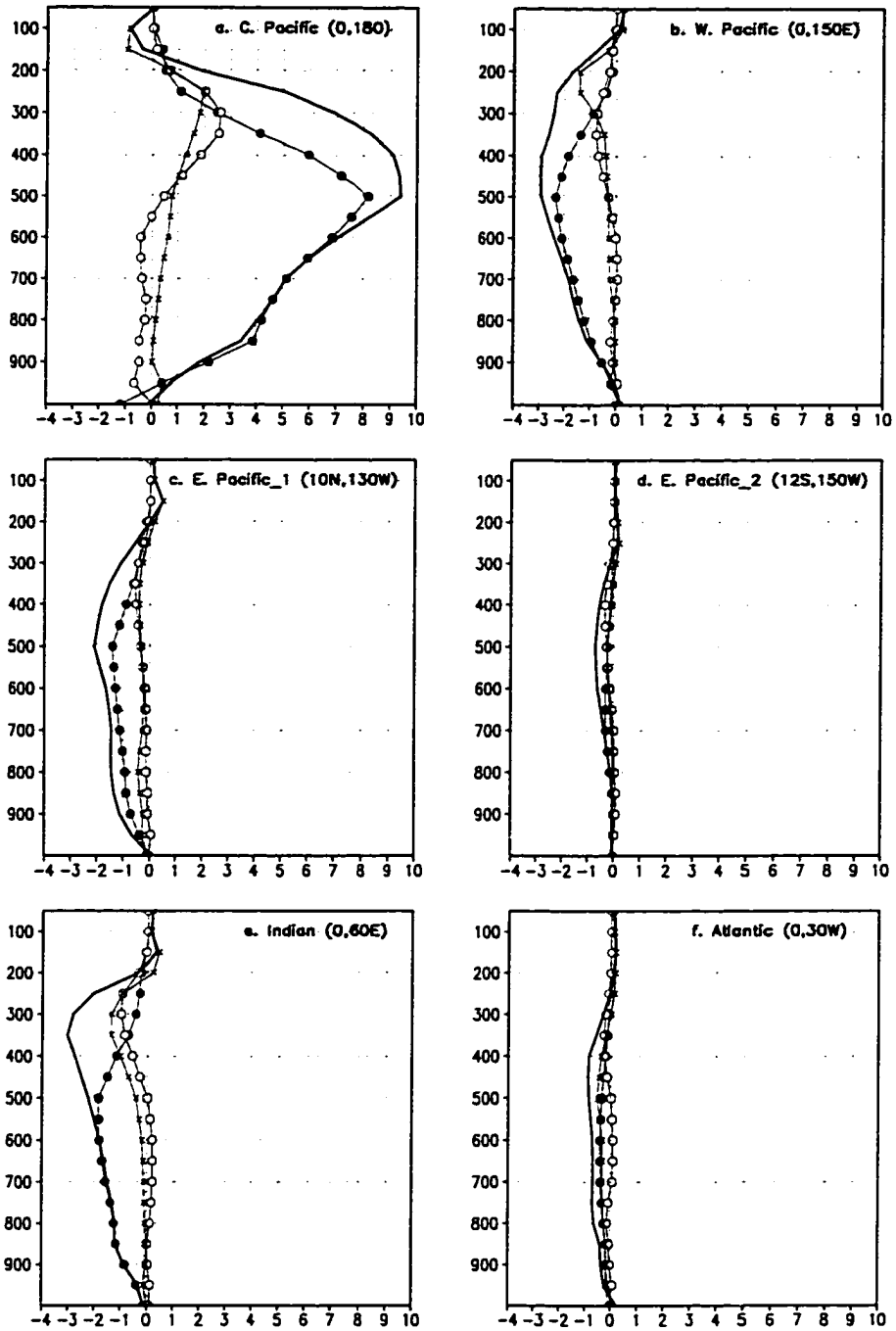


Figure 5.9 Vertical distributions of the differences in the diabatic heating processes between the CPACP2 and CNTR runs (CPACP2 - CNTR) at six locations in the tropics. The unit is K day^{-1} . The closed circle line is the cumulus convection heating; the open circle line is the large scale precipitation heating; the crossed line is the radiative heating; and the solid line is the total diabatic heating.

geopotential height increase shown in Fig. 5.4, due to the anomalous surface warming in the equatorial central Pacific area, is definitely not a simple local heating and warming effect everywhere in the tropical oceans. The tropical central Pacific is the only region where the surplus heat energy could exist due to a large amount of cumulus convection heating increasing, with a maximum value of about 8 Kday^{-1} . At all other regions of the tropics, the atmospheric heating process exhibits a slightly cooling or at least remains unchanged. Hence, the warm temperature associated with the tropical-wide height increasing pattern must be induced by the atmospheric dynamical responses or by certain energy transport mechanisms which redistribute the local heating energy over the entire tropics.

5.3 Effects of the equatorial eastern Pacific anomalous SST forcing

The experimental results from the EPACP2 forcing run are analyzed and discussed in this section. As in the previous section, the difference fields of the atmospheric variables between the EPACP2 and CNTR runs are presented. Hence, the analyses and results represent the isolated effect of the SST anomaly over the eastern Pacific as seen in Fig. 5.2a on the model simulated tropical atmosphere.

5.3.1 Tropical atmospheric responses to the SST perturbation over the eastern Pacific

a. Tropical atmospheric height change

Fig. 5.10 illustrates the tropical geopotential height difference between the EPACP2 and CNTR runs at the 4 selected levels. Interestingly, an overall

geopotential height increase is still found over the entire tropical region, except for the near surface level. At the 200 hPa level (Fig. 5.10a), the most pronounced spatial feature is, again, the tropical-wide geopotential height increasing. The magnitude of the height increase appears to be greater than 20 gpm, except for the tropical Indian Ocean area. The largest height increase at the upper level occurs over the eastern Pacific sector, with a positive change well above 60 gpm. The two greater than 120 gpm height change centers are symmetric about the equator in the eastern Pacific region. Large height decrease area exceeding -20 gpm can be seen in the North Pacific and Northern America, constructing a dipole to the north of the equator between 180° and 80°W. The height increases over the tropical western Pacific and Atlantic region are 20 - 40 gpm, whereas over the tropical Indian Ocean area, the height increase is less than 20 gpm. The anomalous SST over the eastern Pacific area exhibits a quite strong height increasing effect on the height change in the Indian Ocean and the western Pacific area north of 20°N, as opposed to the CPACP2 run in which the geopotential height change in that area is highly negative (Fig. 5.4a). It is also noted that the tropical-wide height increase at 200 hPa in the EPACP2 run extends more poleward than that seen in the CPACP2 run (Fig. 5.4a).

In the middle level (Fig. 5.10b), the height difference field over the eastern Pacific still exhibits the largest change. However, the magnitude of the increase is reduced to only 20 - 40 gpm, which is approximately one third of the height increase seen in the same geographical area at the 200 hPa level (Fig. 5.10a). A maximum height increase area greater than 40 gpm exists on the north side of the equator in the eastern Pacific. The height increase in the rest of the tropical region is about 10 - 20

gpm. The zonal gradient of the tropical height change is much more uniform than that found in the upper level. The negative height changes over the North Pacific and North America remain roughly the same intensity.

At the 700 hPa level (Fig. 5.10c), the geopotential height change in the tropical area is 10 - 20 gpm. The largest change area appears to be in the tropical central and western Pacific and Indian Ocean regions (15 - 20 gpm). At the near surface level (1000 hPa, Fig. 5.10d), while the rest of the tropical region still shows some geopotential height increasing with a change of 5 - 20 gpm, an extensive region over the eastern Pacific is found to have relatively pronounced height decrease. This feature should be an expected atmospheric response to the anomalous SST pattern in the EPACP2 run (Fig. 5.2b), since the anomalous SST will lift the air upward and lead to an anomalous surface air convergence and reduce the surface pressure in the eastern Pacific. A northwest - southeast oriented area with a decrease in surface pressure (less than -10 gpm) is located between 10°S - 30°S in the eastern Pacific (Fig. 5.10d), indicating an enhancement of the SPCZ in the EPACP2 forcing run. Near the central American coast, another area of less than -10 gpm pressure change can be seen between 5°N - 20°N.

The height change in vertical direction shows some different features at various geographical region in the tropics (Fig. 5.10). In the eastern Pacific anomalous SST forcing area, the height change increases dramatically with altitude, especially from the middle to the upper troposphere, suggesting a strong convection anomaly leading to a considerable height increasing in the upper layer. Over the

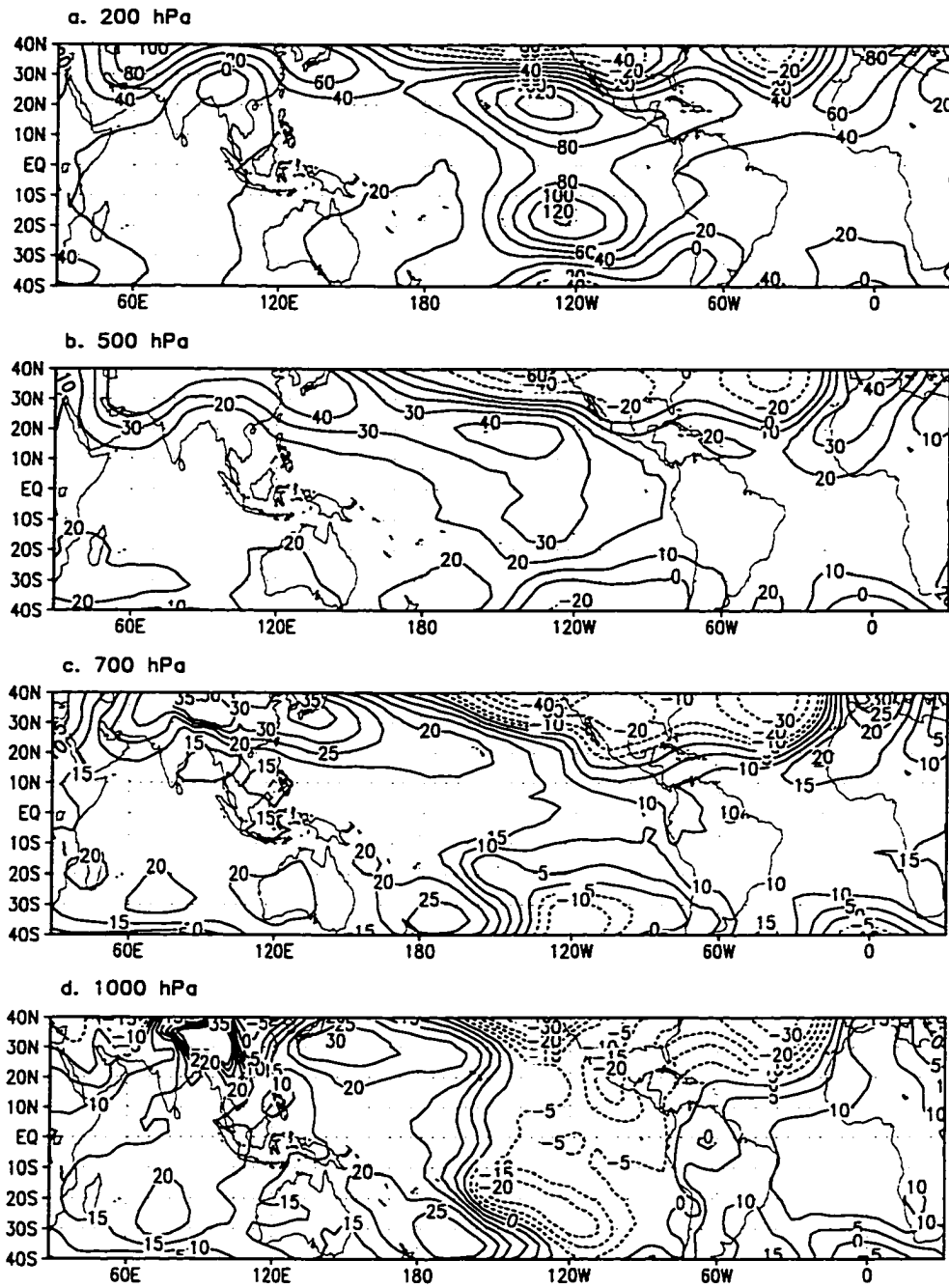


Figure 5.10 Same as Figure 5.4, except for the EPACP2 run.

tropical western and central Pacific and Atlantic regions, the height difference values vary with altitude slowly, from about 10 - 20 gpm at the 1000 hPa to 20 - 40 gpm at the 200 hPa level. Again, for the tropical Indian area, the geopotential height increase seems less variable in the vertical.

Though the spatial pattern in Fig. 5.10 is exclusively generated by the anomalous SST over the eastern Pacific region, some key spatial structures in the tropospheric height changes, such as the tropical-wide increase at the upper layer, the eastern Pacific maximum height increase, show similarities to the geopotential height change patterns in the central Pacific anomalous SST forcing run (Fig. 5.4). Such a similarity in the tropical height change implies a common effect of the anomalous SST forcing on the atmosphere over the central and eastern Pacific near the equator. Spatial height change feature, such as the dipole structure over the eastern Pacific sector, has been documented in the NCEP/NCAR reanalysis and IMG A climatological run data analyses (Figs. 3.3 and 3.7), and in the CPACP2 run (Fig. 5.4).

b. Wind and circulation changes

Fig. 5.11 presents the wind vector difference fields between the EPACP2 and CNTR runs at the 200 and 850 hPa levels. The most pronounced features in the horizontal wind changes at the upper level (Fig. 5.11a) are found over a large area of the eastern Pacific. Strong upper level easterly wind anomaly with a wind speed of mostly $4 - 16 \text{ ms}^{-1}$ appears in the equatorial eastern Pacific region. Two large anticyclonic wind change structures situated in the subtropical regions of the eastern Pacific can be found. The anticyclonic couplet shifts slightly eastward in response to

the anomalous surface forcing change, compared to the one in Fig. 5.5a. These two upper level negative vorticity anomaly areas correspond dynamically to the anomalous height increasing centers in the same geographical areas (Fig. 5.10a). Large poleward anomalous wind can be seen in the subtropics of both hemispheres along the 150°W, exhibiting a strong upper level divergence in the tropical eastern Pacific near the 150°W area. The upper level subtropical westerly jet in the north Pacific sector is intensified due to the anomalous SST forcing placed in the eastern Pacific (see Fig. 5.11a). In the tropical Atlantic area, quite large easterly wind anomaly can be noted north to the equator. The wind changes at the 200 hPa level over the tropical western and central Pacific and Indian Ocean regions are less significant. At the lower tropospheric layer (Fig. 5.11b), westerly anomaly prevails over the tropical eastern Pacific and largely reduces the climatological easterly wind in the region, except for the portion east of 120°W and south of the equator. Such a wind change implies anomalous surface flow convergence area over a large portion of the eastern Pacific, with centers situated in the area of the southward of the equator between 160°W and 130°W and another area near the central American coast (Fig. 5.11b). These regions are the largest surface pressure decrease locations shown in Fig. 5.10d.

Atmospheric response to the change in surface conditions is largely determined by the absolute SST value, instead of the net change. A 28°C SST is considered as a crucial magnitude for atmospheric deep convection and vertical motion. The SST forcing field for the EPACP2 shows a more complex spatial feature in terms of greater than 28°C area in Fig. 5.1c, compared to that in the CPACP2 run (Fig. 5.1b). In order to fully describe the 3-dimensional tropical circulation change structures in zonal and

meridional planes induced by the idealized anomalous SST pattern over the eastern Pacific, vertical motion changes along three longitudes are first presented in Fig. 5.12. In the meridional plane along 150°W shown in Fig. 5.12a, the anomalous rising motion occurs over the tropical belt, with two maximum change centers on each side of the equator. The anomalous upward motion area on the south side, associated with an above 30°C SST region (see Fig. 5.1c) and the largest surface pressure decrease (see Fig. 5.10d), centers at about 10°S with a maximum change above 0.125 Pas⁻¹, whereas the north center locates at 5°N and has a maximum upward motion change of above 0.1 Pas⁻¹. Along 120°W, the change in the tropical area is characterized by a slight sinking motion anomaly, with an exception of some very small negative values between 0° and 10°N at the lower tropospheric layer (Fig. 5.12b). Strong upward motion change with a maximum greater than 0.1 Pas⁻¹, centered at about 10°N area, can be seen along the 90°W meridional plane (Fig. 5.12c). Such a strong vertical motion change is dynamically associated with the surface anomalous convergence and pressure decrease area near the central American coast (see Figs. 5.11b and 5.10d).

Zonal circulation change cross sections at three latitudes, representing the structures over the deep tropics (15°S - 15°N), are shown in Fig. 5.13. In the equatorial plane (Fig. 5.13a), large easterly increase occurs over the eastern Pacific and Atlantic regions at the upper troposphere. The only upward vertical motion change is found over the western Pacific and it reinforces the strong convection there (Fig. 5.13a). Westerly wind anomaly appears at the lower level over the eastern Pacific. Over the Indian ocean, somewhat low level zonal flow divergence change can

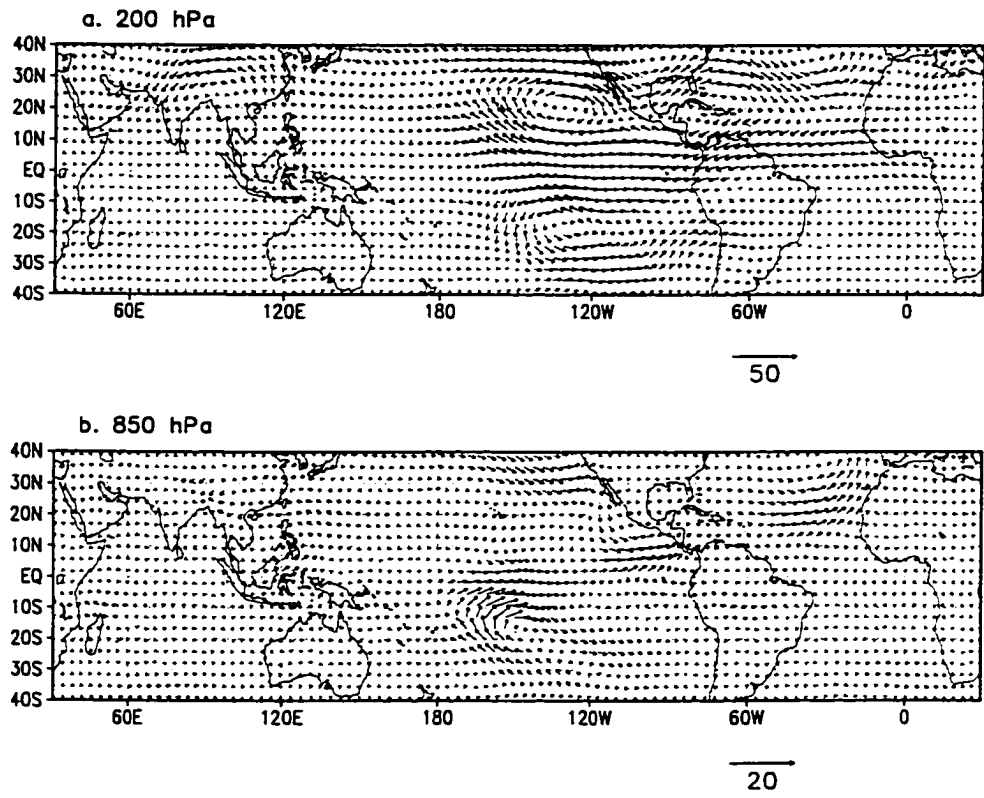


Figure 5.11 Same as Figure 5.5, except for the EPACP2 run.

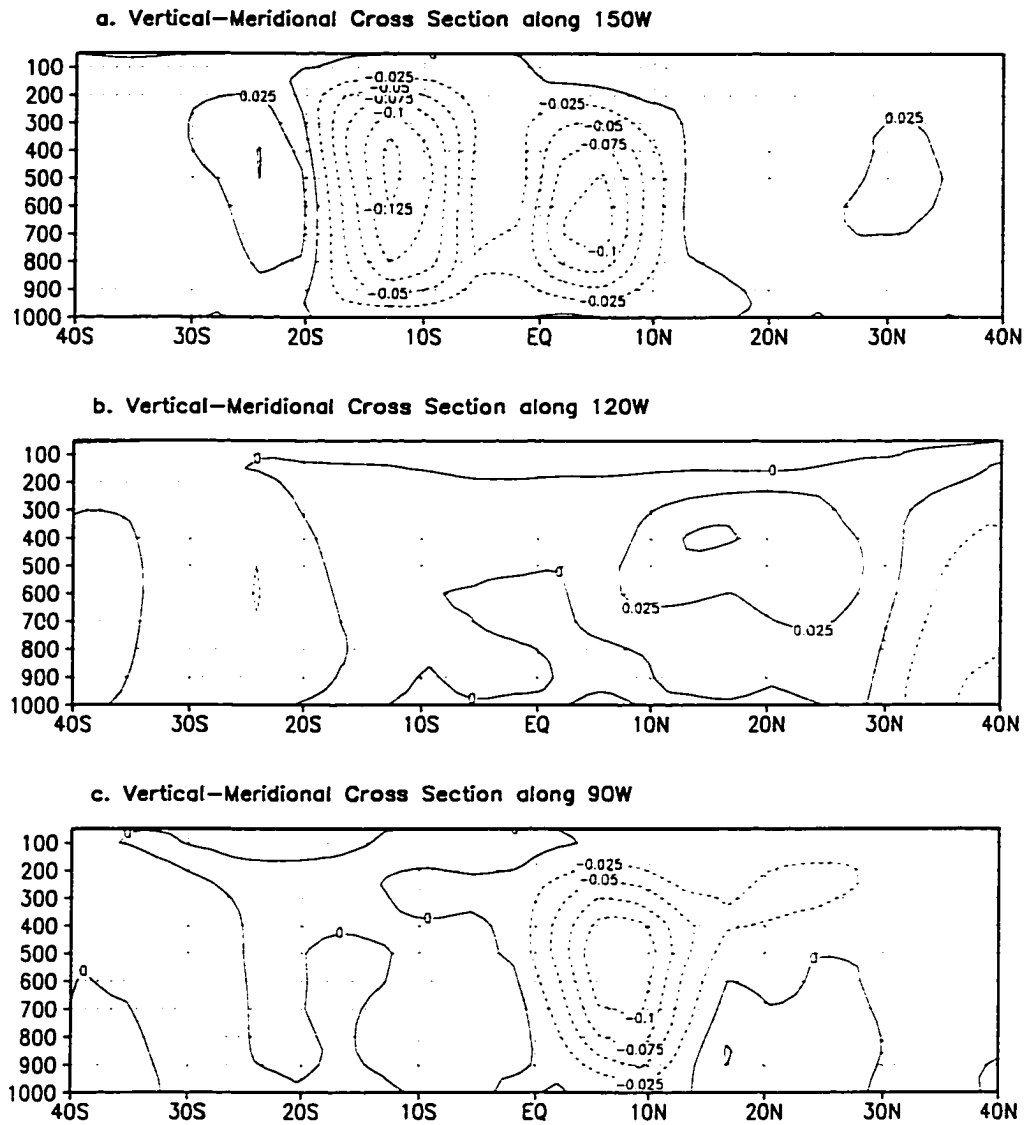


Figure 5.12 Vertical-meridional cross sections of the monthly mean vertical motion differences between the EPACP2 and CNTR runs (EPACP2 - CNTR) along three selected longitudes. Unit: Pas^{-1} .

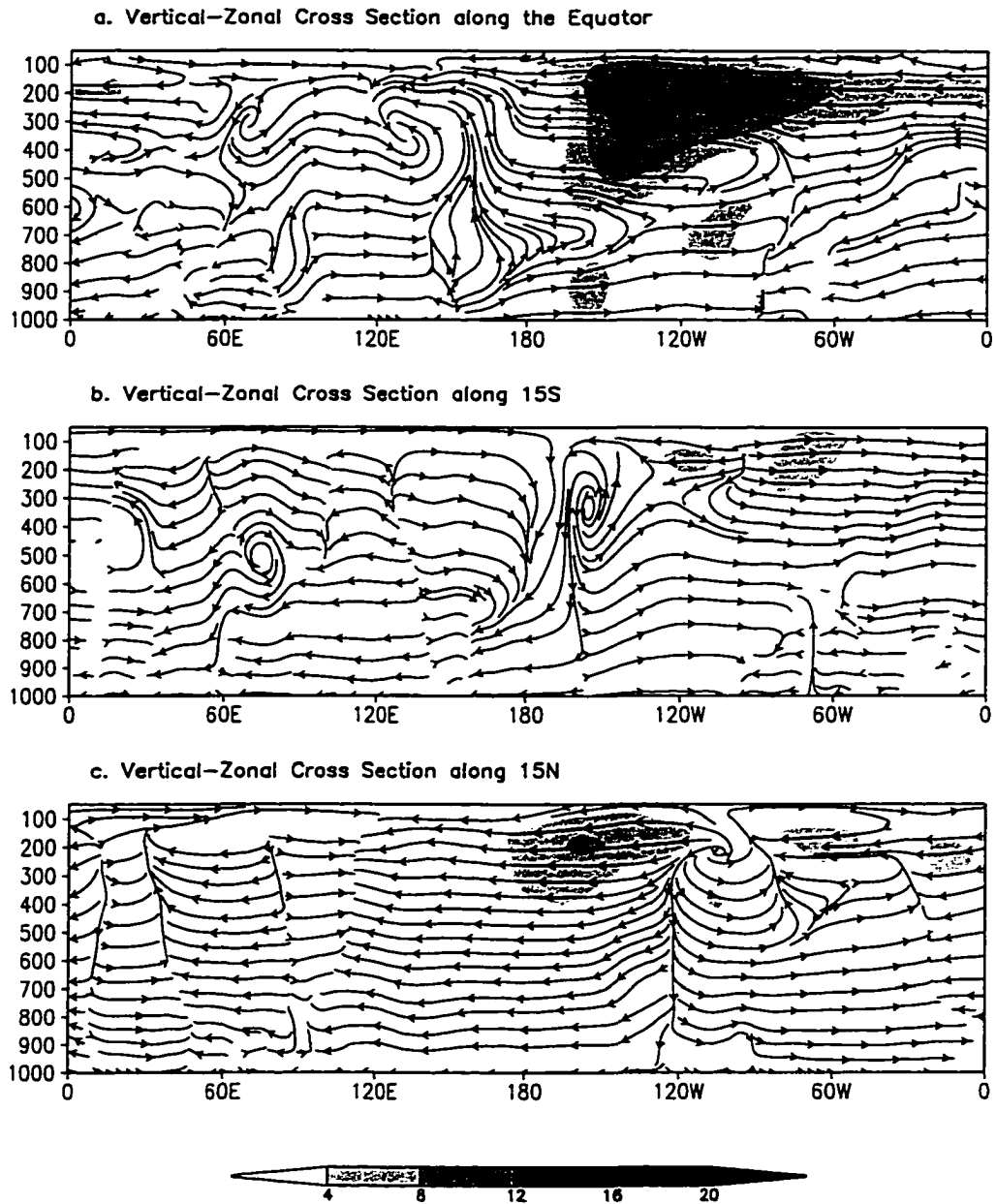


Figure 5.13 Vertical-zonal cross sections of the differences for the flow (stream line) and its magnitude (shaded area) between the EPACP2 and CNTR runs (EPACP2 - CNTR) along three selected latitudes. Shade unit: ms^{-1} .

be noticed. Along the 15°S plane as shown in Fig. 5.13b, westerly anomaly at the low level and anomalous rising motion change at the upper layer can be seen near the 150°W area. Sinking motion change can be noticed over the central Pacific (160°E - 160°W) and Indian Ocean (near 60°E) regions throughout the entire tropospheric layer. To the north of the equator along the 15°N latitude, the circulation change in zonal plane is rather simple and dominated by the horizontal wind change mostly (Fig. 5.13c). Easterly wind anomaly occurs nearly over the entire circumference in the upper level, except small portions over the western Pacific (90°E - 110°E) and eastern Pacific (120°W - 90°W). Also, a large area west to 120°W over the Pacific is under easterly wind change, whereas in the Pacific region east to the 120°W and Atlantic region, westerly wind anomalies prevail at the lower tropospheric layer. A sinking motion change at 15°N latitude exists near the 120°W, whereas upward vertical motion change is seen in the upper level near the 90°W (Fig. 5.13c). Overall, the zonal circulation change in the tropical region shows a feature of weakening the normal east-west circulation structures.

It can be determined, by comparing the tropical circulation changes in the CPACP2 and EPACP2 runs, that the equatorial central Pacific SST anomaly is a more effective means to enhance the local Hadley circulation. Conversely, the idealized eastern Pacific anomalous SST pattern appears to be more responsible for the significant reduction of the Walker circulation strength.

5.3.2 *Changes in atmospheric diabatic heating*

It has been indicated that diabatic heating change plays an important role in the spatial structure formation and maintenance of the atmospheric height and circulation changes due to the surface forcing changes over the tropics in the CPACP2 run. The simulated atmospheric diabatic heating responses to different anomalous surface forcing patterns may provide certain key clues in understanding the physics in the real atmospheric interdecadal variability by means of comparing atmospheric heating differences.

a. Diabatic heating changes in the EPACP2 experiment

Spatial structures of the tropical atmospheric diabatic heating changes induced by the anomalous surface forcing over the eastern Pacific is illustrated in Fig. 5.14. Compared with the heating changes in the central Pacific anomalous forcing run (see Fig. 5.8), a large heating change can be found over all the tropical Pacific region in the EPACP2 run, and the intensification of the ITCZ and SPCZ appears to be the most dominant feature in Fig. 5.14. However, the magnitudes of the model atmospheric diabatic heating changes in the EPACP2 run are overall smaller than those in the CPACP2 run.

At 700 hPa (Fig. 5.14a), the three considerable heating increase areas can be seen in the tropical eastern Pacific region, with a maximum increase value of above 3 - 4 Kday^{-1} . Two of these three areas locate in the poleward sides of the equator along 150°W , and the other one is near the central American coast area between 0° and 10°N . These spatial patterns should be expected as they are all in the strong

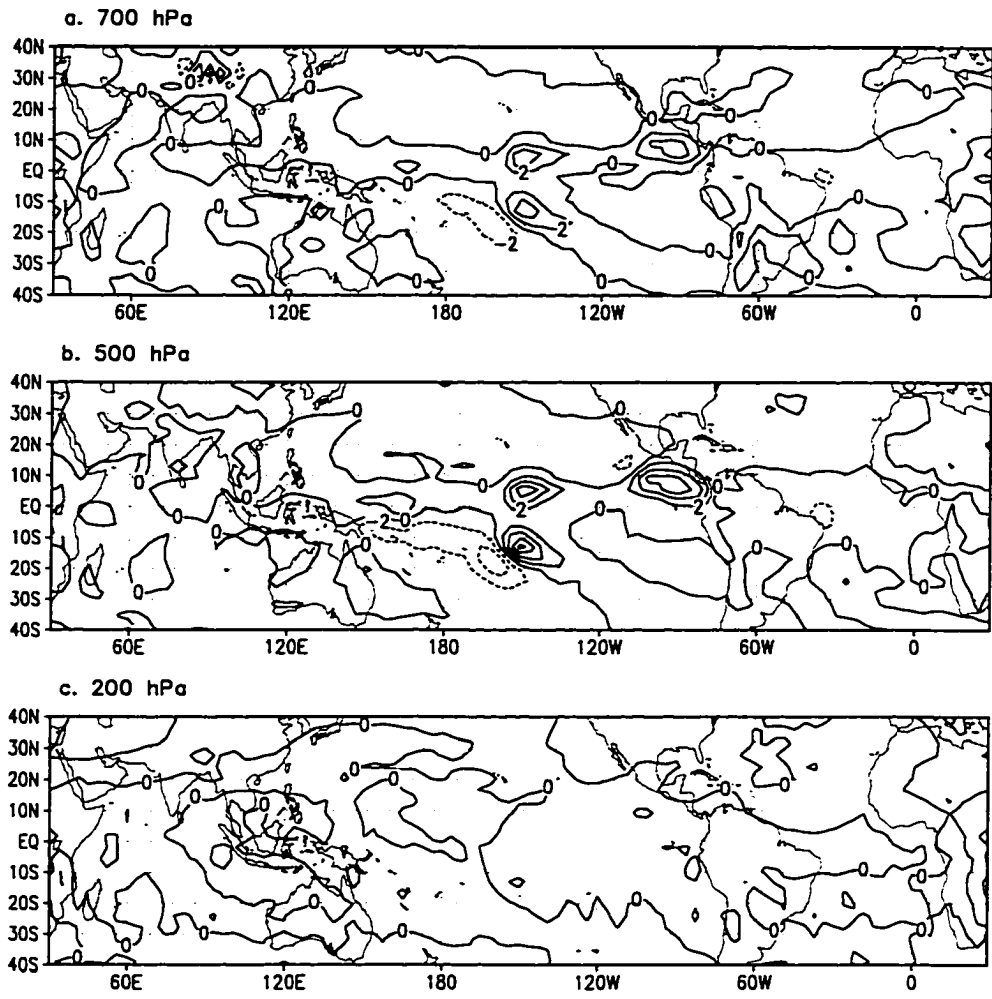


Figure 5.14 Same as Figure 5.8, except for the EPACP2 run.

anomalous rising motion areas found in Figs. 5.12 and 5.13. In the equatorial western Pacific, another heating increasing area is found, with a maximum change above 2 Kday^{-1} , consistent with the upward vertical circulation change in that area as shown in Fig. 5.12a. The three heating increasing patterns within $0^\circ - 10^\circ\text{N}$ form a zonal belt of diabatic heating enhancement, indicating an overall ITCZ intensification due to the eastern Pacific anomalous surface forcing (Fig. 5.14a). To the west of the heating increase area on the south side of the equator near 150°W , a rather large area of diabatic heating less than -1 Kday^{-1} exists, with a northwest-southeast orientation extending from the western Pacific at about 5°S to the eastern Pacific at a latitude of 25°S . Combining such negative heating change area with the strong heating increase pattern over the eastern Pacific in $5^\circ\text{S} - 25^\circ\text{S}$, an effect of eastward shift and intensification of the SPCZ due to the eastern Pacific anomalous surface forcing is quite apparent (Fig. 5.14a). Such a change feature has been also noticed by some previous observational and modeling studies (Lau and Nath 1994; Graham 1994). In the mid-troposphere (Fig. 5.14b), the pattern shows nearly the same spatial structures as those at 700 hPa. However, the magnitudes of the diabatic heating changes increase with a maximum value $6 - 8 \text{ Kday}^{-1}$ over the eastern Pacific and 3 Kday^{-1} for the pattern over the tropical western Pacific. The maximum heating change magnitude at this level appears to be smaller than the one seen in Fig. 5.7 for the CPACP2 run. In the upper troposphere, the diabatic heating change becomes less significant compared to the change at the low levels, and only two small positive increase areas with maximum change exceeding 2 Kday^{-1} can be noted in the central American coast area and the eastern Pacific area between $10^\circ\text{S} - 20^\circ\text{S}$ (see Fig. 5.14c). It is interesting

to notice the similarity of the diabatic heating increase spatial pattern in Fig. 5.14 to the shape of greater than 28°C area (Fig. 5.3b) in the eastern Pacific region. The horizontal diabatic heating changes found in the EPACP2 run (Fig. 5.14) shows some more complex spatial features than those in the CPACP2 run in Fig. 5.8, especially in the eastern Pacific region.

b. Vertical profiles of heating changes for individual physical processes

The vertical distributions of the changes in cumulus convection, large scale precipitation, radiative heating and total diabatic heating at the 6 selected tropical locations are displayed in Fig. 5.15 for the EPACP2 experiment. These 6 locations are the same as those seen in Fig. 5.9 for the CPACP2 run, so that the effects of different anomalous SST patterns on atmospheric heating processes at these fixed tropical locations can be compared and analyzed. The profiles in Fig. 5.15 are presented in terms of the difference between the EPACP2 and CNTR runs.

In the eastern Pacific SST perturbation area, cumulus convection is still the dominant heating process in the total atmospheric diabatic heating changes as shown in Fig. 5.15c and d. Little change in diabatic heating is seen at the location to the north of the equator over the eastern Pacific (Fig. 5.15c), although large change in geopotential height is found there. This location is not in the positive heating increase region as shown in Fig. 5.14, indicating that diabatic heating is only *one* of the processes leading to a local atmospheric temperature increase even within the anomalous forcing area. At the location in the south portion of the eastern Pacific (Fig. 5.15d), the diabatic heating increase is almost identical to the vertical profile of

the cumulus convection heating change below 500 hPa where a 5 Kday^{-1} change is seen, implying little effect of radiative and large precipitation processes. Above the middle troposphere, the profiles of the radiative and large scale precipitation processes are almost identical and maximized at 300 hPa with a change value of 1 Kday^{-1} as seen in Fig. 5.15d. In the layer of 200 - 300 hPa, all the three physical processes contribute almost equally to the atmospheric diabatic heating increase (Fig. 5.15d).

The equatorial western Pacific experiences a moderate diabatic heating increase due to the anomalous SST forcing over the eastern Pacific as shown in Fig. 5.15b, with a maximum increasing of 2.5 Kday^{-1} at the 500 hPa. This can be attributed primarily to the increased cumulus convection heating below 500 hPa, and a combined effect of the latent heat release increase in cumulus convection and large scale precipitation processes in the upper layer (Fig. 5.15b). Such a latent heat release increase is consistent with the rising motion enhancement over the western Pacific shown in Fig. 5.13a. The effect of the rising motion change at the low level in the central Pacific (Fig. 5.13a) can be seen in the slight diabatic heating increase there (Fig. 5.15a). The maximum diabatic heating change of about 1.5 Kday^{-1} is found at the lower level (about 800 hPa), which is an effect of heating increase due to both large scale precipitation and cumulus convection processes. Above the middle troposphere, cumulus convection process dominates the diabatic heating increase which is less than the change at lower level (Fig. 5.15a). The diabatic heating over the tropical Indian and Atlantic Oceans is slightly decreased, due primarily to the suppression of the cumulus convection process (Fig. 5.15e and f). The overall heating changes in these areas are relatively small.

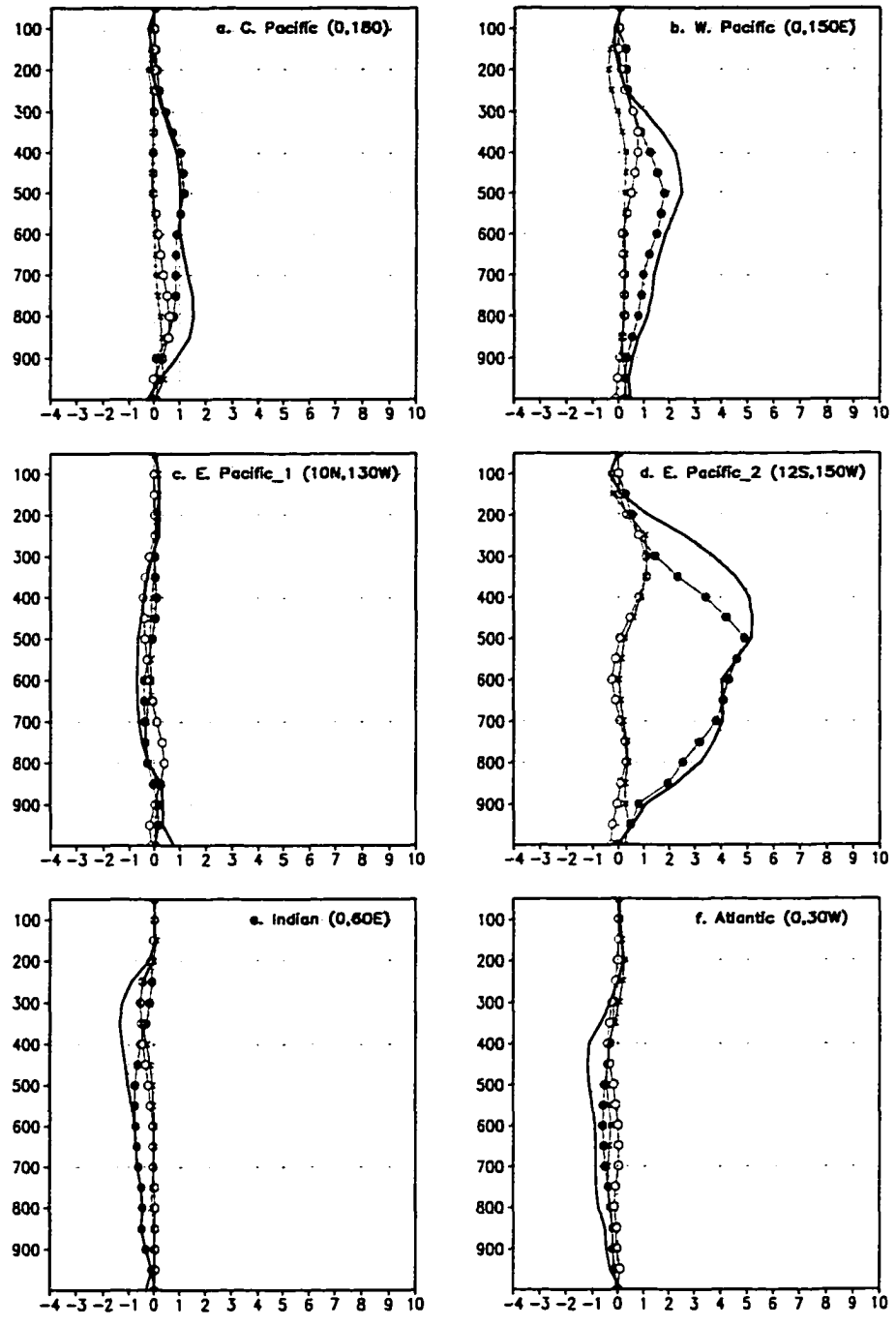


Figure 5.15 Same as Figure 5.9, except for the EPACP2 run.

The substantial diabatic heating increase in the atmosphere over the eastern Pacific region is primarily responsible for the local height increase in that region (Fig. 5.15d). The height increase over the wide tropical area is the atmospheric response to the eastern Pacific anomalous SST field. It, however, can not be attributed to local thermal processes. The widely spread tropical height increase over the areas other than the eastern Pacific are caused by other mechanisms such as the atmospheric dynamical responses to the eastern Pacific SST perturbation pattern and the atmospheric heat transport processes.

5.4 Effects of the anomalous SST over the tropical central and eastern Pacific

The investigations into the effects of the SST perturbations at different portions of the Pacific using the ECHAM4 model have considerably enhanced the understanding of how the tropical atmosphere responds to surface forcing changes at different geographical areas and some key processes involved in the atmospheric changes. However, the main thrust of this research is to study the influence of the interdecadal anomalous SST variation, seen in Figs. 2.3 and 2.4, on the tropical atmospheric interdecadal variability. Having isolated the impacts of anomalous SST over the tropical central and eastern Pacific, the comprehensive effect of the superposition of the two regional SST anomalous patterns (see Fig. 5.3a) is investigated in this section. Such a SST perturbation pattern over the tropical Pacific is used to ideally represent the spatial SST change structure found in the ENSO-like SST interdecadal variability. A model simulation with such a SST change pattern may

provide some insights into the physical processes involved in the atmospheric interdecadal variation.

5.4.1 Atmospheric responses to the specified SST perturbation pattern

a. Tropical atmospheric height changes

The tropical geopotential height changes, due to the combined effect of the tropical Pacific SST anomalous pattern in the PACP2 run, is shown in Fig. 5.16 for 4 selected levels. These height change structures are generated using the geopotential height difference fields between the PACP2 and CNTR runs. It can be easily noticed in Fig. 5.16 that the dominant height change feature in the upper levels is the height increasing over the entire global tropical belt, with the largest increase regions over the eastern Pacific. It appears that both the central and eastern Pacific SST perturbations impact the total atmospheric height changes as there are some key features similar to those found in the CPACP2 and EPACP2 runs (Figs. 5.4 and 5.10).

At the 200 hPa level (Fig. 5.16a), the entire tropics shows a height increase greater than 20 gpm. For large portions of the eastern Pacific, the height increase exceeds 80 gpm, with two maximum height change centers above 160 and 180 gpm on the north and south sides of the equator (Fig. 5.16a). A height increase larger than 80 gpm can be detected over the tropical Atlantic region. Height rises over the tropical Indian and western Pacific regions are relatively modest, approximately 20 - 60 gpm, so that a large zonal gradient in the height increase occurs near the equatorial central Pacific area at the 200 hPa level. Large height decrease regions are found at least 60

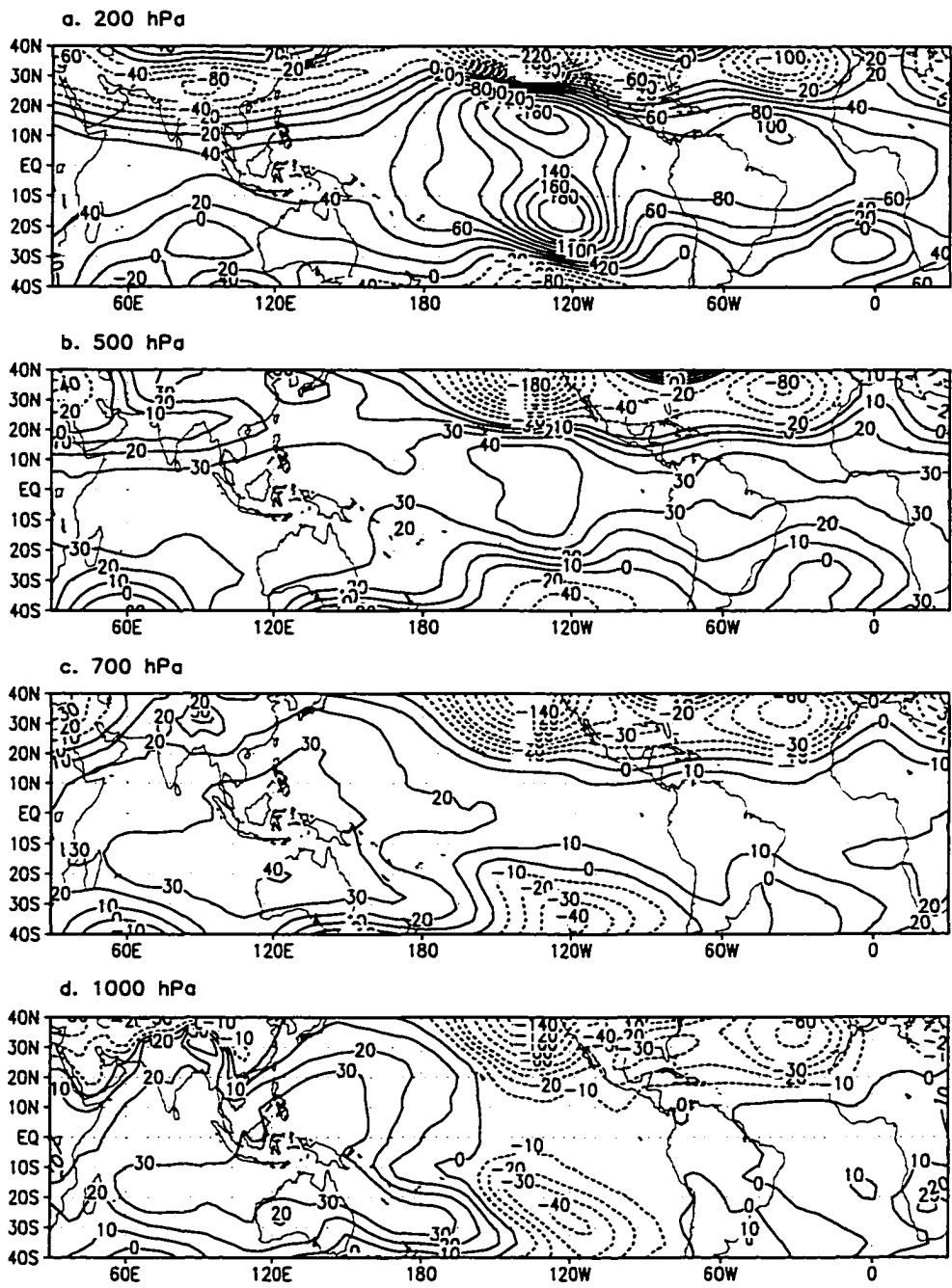


Figure 5.16 Same as Figure 5.4, except for the PACP2 run.

gpm and centered at the southern Eurasian continent, North Pacific and North Atlantic regions (Fig. 5.16a).

The spatial height change structures at 500 hPa (Fig. 5.16b) becomes less complicated. The height increase over the tropical belt is still above 20 gpm. A single center of greater than 40 gpm occurs over the eastern Pacific, whereas the rest of the tropical region height change is between 20 - 40 gpm. It is noteworthy that the height changes over the eastern Pacific and Atlantic regions drop dramatically. The maximum height change drops from approximately 180 gpm at the 200 hPa down to less than 50 gpm at the 500 hPa level over the eastern Pacific and from above 100 gpm to about 40 gpm over the Atlantic region. Height change drops from the 200 hPa to the 500 hPa levels over the western Pacific and Indian Ocean regions are rather small (only approximately 10 gpm). At least a 10 gpm height increase is found in the tropics at 700 hPa as shown in Fig. 5.16c. In contrast to the height increase pattern at the higher levels, the maximum height increase area appears over the western Pacific and Indian regions where height change is mostly larger than 25 gpm, with a maximum increase of above 35 gpm. Compared to those in CPAP2 and EPACP2 runs (Figs. 5.4b and 5.10b), the anomalous height difference lows over the northern Pacific and Atlantic regions dramatically deepen and shift equatorward (Fig. 5.16c). Height decreases occur over the eastern Pacific at the lowest level (1000 hPa, Fig. 5.16d) as a result of the anomalous surface convergence induced by the increased SST. A large height decrease is found over the SPCZ area of the southern eastern Pacific, with maximum decrease larger than 40 gpm. Simultaneously, the 1000 hPa level height

increase over the western Pacific and Indian Ocean regions becomes even larger on the poleward sides of the equator (Fig. 5.16d).

The spatial structures of the height changes at the lower levels (700 and 1000 hPa, Fig. 5.16c and d) appear to be more impacted by the effect of the eastern Pacific anomalous SST changes since the height change structures look more like those arising from the EPACP2 run (as shown in Fig. 5.10b and c). The dynamical responses to the anomalous SST forcing seems more responsible for the low level height change patterns. At the upper levels (Fig. 5.16a and b), the height change structures are closer to the changes caused by the central Pacific anomalous SST forcing (Fig. 5.4a), except for the structures over the eastern Pacific which are the combination of the two isolated forcing effects. It appears that the upper level height changes are primarily triggered by the diabatic heating changes and the central Pacific anomalous surface forcing is more effective according to the height change patterns in the middle and upper troposphere.

b. Wind and circulation changes

Fig. 5.17 shows the horizontal wind difference fields between the PACP2 and CNTR runs at the 200 and 850 hPa levels. As the atmospheric height changes, the tropical horizontal wind changes also exhibit the common features seen in either the CPACP2 (Fig. 5.5) or the EPACP2 (Fig. 5.11) experiments. However, the strength of the anomalous wind vector changes is enhanced, as shown by, for instance, the intensification of the upper level anticyclonic couplet. Furthermore, the low level surface flow convergence anomaly in the central and eastern Pacific, and upper level

poleward wind changes over the central Pacific, appear to be more pronounced shown in the PACP2 run (Fig. 5.17).

In the upper level (200 hPa, Fig. 5.17a), strong poleward wind changes with a largest change of about 20 - 30 ms^{-1} can be found over the central Pacific northward of the equator. Strong anomalous easterlies dominate the wind change pattern over the equatorial eastern Pacific, while large westerly wind changes occur over the subtropical regions of the eastern Pacific, implying a large enhancement of the upper level subtropical westerly jet. The two anticyclonic wind changes over the eastern Pacific become more pronounced (Fig. 5.17a). The tropical Indian Ocean and western Pacific regions show westerly anomalous change. The wind change over the equatorial Atlantic Ocean exhibits rather small easterly, although significant westerly wind changes exist poleward of 10° on both sides of the equator (Fig. 5.17a). The most pronounced wind change feature at the lower level (Fig. 5.17b) is the large westerly and anomalous flow convergence over the tropical central Pacific and westward of 120°W over the eastern Pacific regions, with a center near $10^\circ\text{S} - 20^\circ\text{S}$. Large cyclonic anomalous wind changes can be seen in Fig. 5.17b over the North and South Pacific, corresponding the lower level pressure decrease areas in Fig. 5.16d.

The upper level horizontal wind change structures in the PACP2 run are dominated by the main features shown in the upper level wind changes in the CPACP2 run (Fig. 5.5a), except for the eastern Pacific where the change structure is primarily a combination of the two wind change fields in the CPACP2 (Fig. 5.5a) and EPACP2 (Fig. 5.11a) runs. This indicates that the effects of the equatorial central Pacific SST forcing on the upper level flow change are dominant over the most of the

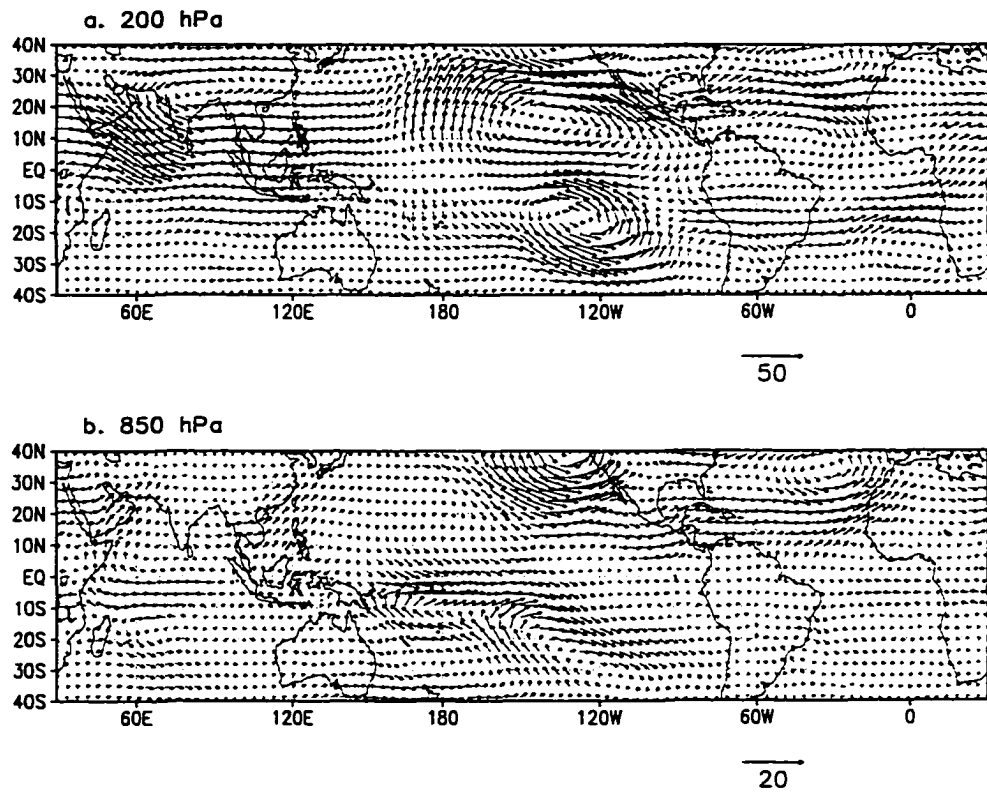


Figure 5.17 Same as Figure 5.5, except for the PACP2 run.

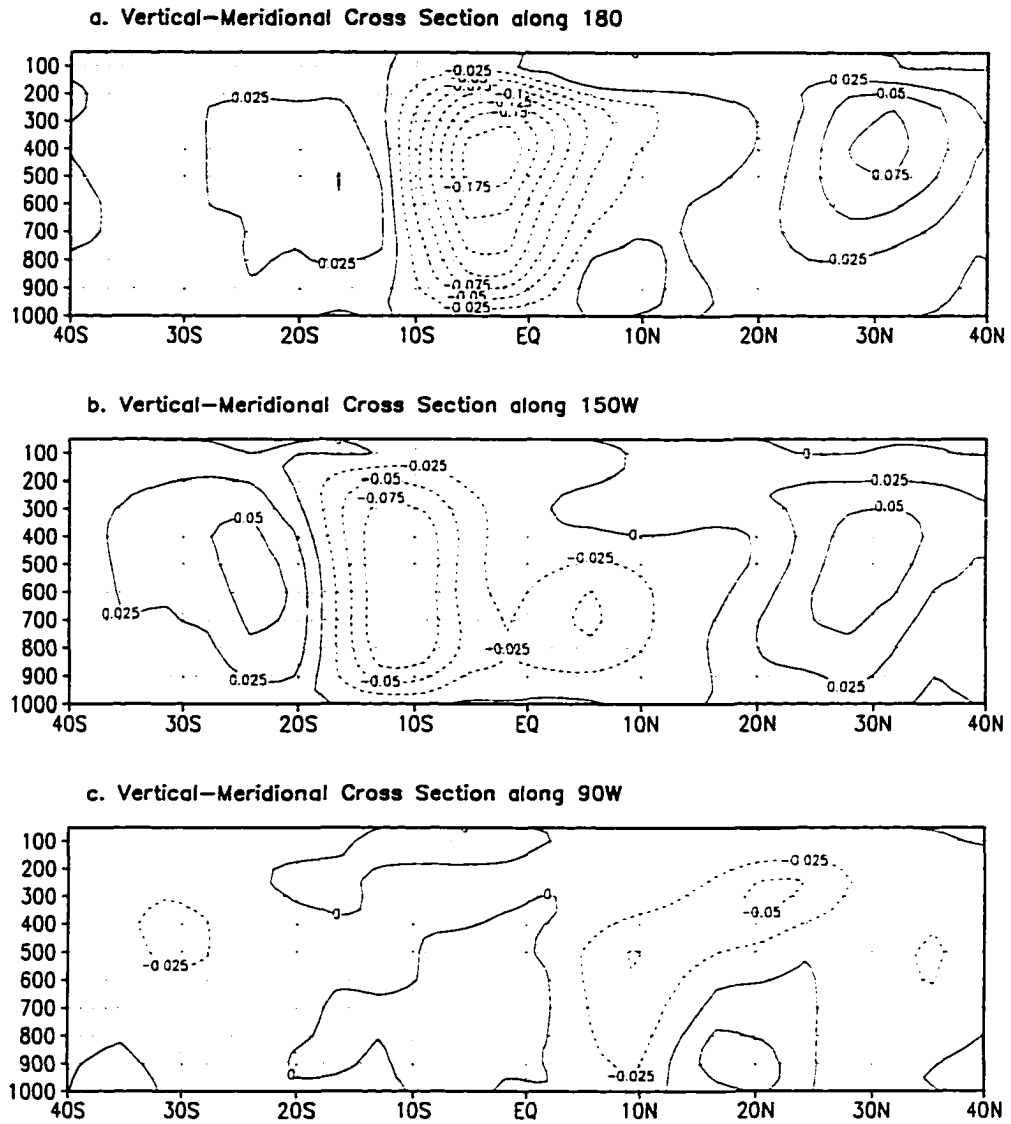


Figure 5.18 Vertical-meridional cross sections of the monthly mean vertical motion differences between the PACP2 and CNTR runs (PACP2 - CNTR) along three selected longitudes. Unit: Pas^{-1} .

tropical region, while the effects of the eastern Pacific anomalous SST forcing on the upper level flow change appear to be more local. The lower level wind change structures in Fig. 5.17b appear to be a combination effect of the two SST perturbations.

The cross sections of the vertical motion difference fields along three longitudes over the Pacific anomalous SST forcing region are given in Fig. 5.18. In the tropical central Pacific region (Fig. 5.18a), strong increase in upward motion occurs in the forcing area, whereas large sinking motion anomalies occur over the subtropics, especially near 30°N, implying a large enhancement of the local Hadley cell. The value of maximum vertical motion change exceeds 0.175 Pas^{-1} in the rising area, and 0.075 Pas^{-1} over the northern sinking center (Fig. 5.18a). These changes are approximately 0.02 Pas^{-1} larger than those in the CPACP2 run in which the eastern Pacific SST perturbation is absent (Fig. 5.12a), indicating that the anomalous SST over the eastern Pacific may reinforce the effect of SST forcing in the central Pacific. This is supported by the lower level anomalous flow convergence over both the central and eastern Pacific shown in Fig. 5.17b. Interestingly, the upward vertical motion changes along 150°W in the eastern Pacific anomalous SST forcing area (Fig. 5.18b) shows an increasing value of less than 0.1 and 0.075 Pas^{-1} , respectively for the two rising motion anomaly centers immediately poleward of the equator. However, these upward changes are, at least 0.05 Pas^{-1} , less than their counterparts (Fig. 5.12a) in the EPACP2 run. Moreover, the sinking motion changes over the subtropical regions appear approximately 0.025 Pas^{-1} greater than the ones found in the experiment without the central Pacific anomalous SST forcing (Fig. 12a). This demonstrates

dominant effect of the central Pacific SST anomaly whose existence diminishes the rising motion effect of the eastern Pacific SST perturbation, and enhances the sinking motion effect. The main reason is that since the central Pacific is the warmest place in the global ocean surface (where the largest upward motion is found), near surface air tends to converge to that area. Due to the compensation effect, it will suppress the rising motion in its neighbor regions. Along 90°W (Fig. 5.18c), the upward change is found to the north of the equator. The effect of the eastern Pacific anomalous SST forcing, however, is diminished as the magnitude of the upward motion change is much smaller than the change value found in the EPACP2 run (Fig. 5.12c).

The zonal circulation change in the PACP2 experiment is given in Fig. 5.19 at three latitude cross sections. As expected, rising motion change occurs in the central Pacific forcing region in the equatorial plane (Fig. 19a). In the eastern Pacific sector, a weakening of the Walker circulation is seen. Evidently, sinking motion changes are found in the western Pacific, Indian and Atlantic Ocean regions. The zonal circulation change pattern in Fig. 5.19a shows quite similar structures as seen in the CPACP2 run (Fig. 5.7b), except for the eastern Pacific region. The sinking motion anomaly at the lower level over the tropical western Pacific and Indian Ocean appear even stronger in the areas slightly off the equator (5°S and 5°N areas, figures not shown). In the 15°S zonal plane (Fig. 5.19b), strong sinking motion anomaly, over the central and western Pacific and Indian Ocean, is the major feature. Westerly flow change dominates in the upper level along this latitude. In the lower level, wind change is also mostly westerly over the eastern Pacific and Atlantic regions. The circulation change in the 15°N

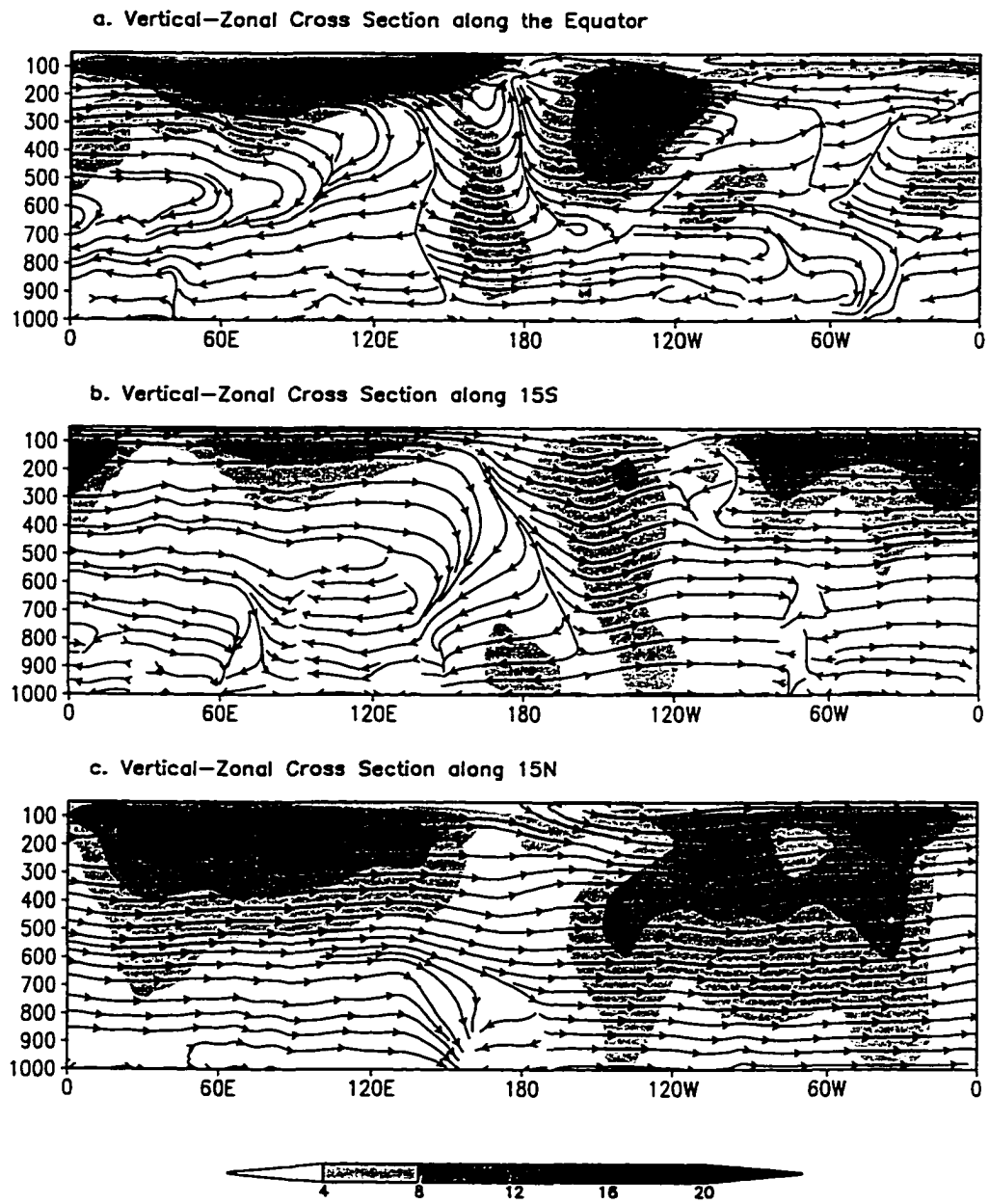


Figure 5.19 Same as Figure 5.13, except for the PACP2 run.

zonal plane shown in Fig. 5.19c is mostly westerly, with exceptions such as the lower level sinking motion at the western Pacific.

Overall, the wind circulation changes in the PACP2 and their comparisons to those generated by the CPACP2 and EPACP2 runs demonstrate the dominant effects of the central Pacific forcing anomaly. However, the circulation changes in the tropical eastern Pacific region are still largely dominated by the anomalous surface forcing in that local region.

It is noteworthy to point out that the lower level westerly anomaly between 120°W and 80°W over the equatorial and south eastern Pacific (Fig. 5.19a and b) may have a significant impact on the South American coast. This implies that, if the central and eastern Pacific SST is positively anomalous, the surface southeasterly trade winds are weakened and the water upwelling off the South American coast will be suppressed. This will, in turn, enhance the local surface warming off the South American coast.

5.4.2 Changes in atmospheric diabatic heating

The changes in the diabatic heating processes have exhibited some rather different characteristics in the experiments for isolating the effect of the anomalous SST over the tropical central and eastern Pacific regions (Figs. 5.8, 5.9, 5.14 and 5.15). The positive heating change is solely found in the anomalous forcing area in the CPACP2 run (Figs. 5.8 and 5.9), whereas in the EPACP2 run (Figs. 5.14 and 5.15), the remote tropical western Pacific area experiences a larger than normal

cumulus convection heating, in addition to the local heating increase, due to the eastern Pacific SST perturbation. Based on the findings in the circulation changes, it is believed that, in the PACP2 experiment, the tropical physical processes should be dominated by the structures arising from the central Pacific SST anomaly effect.

a. Total diabatic heating changes

Fig. 5.20 gives the spatial distribution of the diabatic heating changes at three levels in the PACP2 experiment. A large heating increase occurs in the tropical central Pacific area through nearly the entire troposphere, with a largest increase at the 500 hPa level where the maximum heating increase is stronger than the increase seen in CPACP2 run (Fig. 5.8b) and exceeds 12 Kday^{-1} as shown in Fig. 5.20b. Diabatic cooling seems to be the major features over the equatorial western Pacific and Indian Ocean regions, especially at the higher levels (Fig. 5.20). The positive diabatic heating changes (approximately $1 - 3 \text{ Kday}^{-1}$ at the 500 hPa level) over the western Pacific region, due to the enhanced surface flow convergence in the EPACP2 run, disappear in the PACP2 run (Fig. 5.20).

There exists a heating increase area characterized as a northwest - southeast oriented band over about $160^{\circ}\text{W} - 120^{\circ}\text{W}$ to the south of the equator in the eastern Pacific, with an increase change mostly $2 - 5 \text{ Kday}^{-1}$ at the middle level (Fig. 5.20b). This represents the intensification and eastward shift of the SPCZ under the specified SST anomaly patterns. However, the strength of the heating increase has been slightly weakened, in comparison to the heating changes in the EPACP2 run (Fig. 5.14), by 1 Kday^{-1} in general, except at the 700 hPa level at which the intensity remains roughly

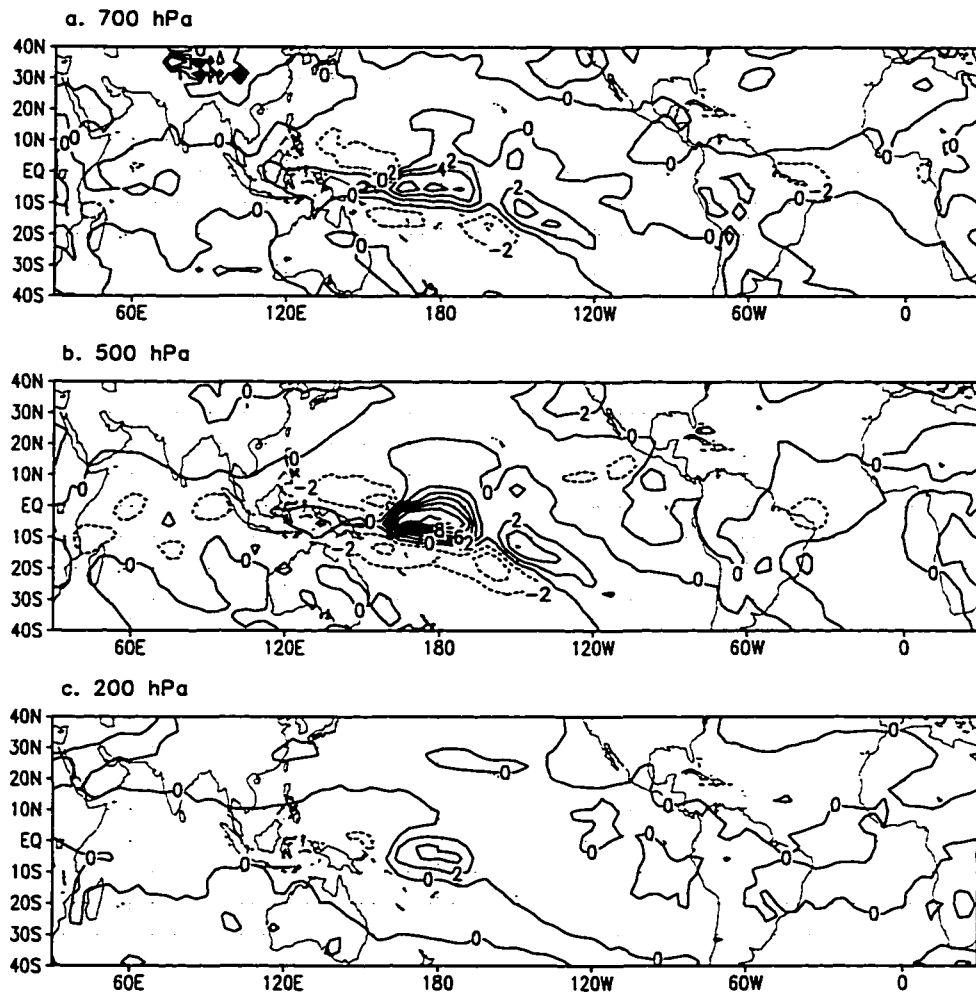


Figure 5.20 Same as Figure 5.8, except for the PACP2 run.

unchanged. The atmospheric cooling processes occur in a large region to the south of the heating increase area in the central Pacific and the west of the eastern Pacific northwest - southeast oriented heating increase band (Fig. 5.20), suggesting an eastward shift of the SPCZ. The cooling is mostly 2 - 4 Kday⁻¹ at 500 hPa (Fig. 5.20b), and is slightly stronger than the corresponding cooling effect resulting from the eastern Pacific SST perturbation (Fig. 5.14b). The cooling is of a similar magnitude to that seen in the EPACP2 run (Fig. 5.14a and c) at the 700 and 500 hPa levels, mostly above 1 and 0.5 Kday⁻¹, respectively. The diabatic heating change at the 200 hPa level primarily shows a local heating increase over the equatorial central Pacific (Fig. 5.20c), with a maximum above 4 Kday⁻¹.

In the areas of immediately north to the equator at 150°W and near the central American coast, anomalously large diabatic heating increasing (larger than 6 Kday⁻¹ at the 500 hPa) is found due solely to the forcing effect of the eastern Pacific SST perturbation as shown in Fig. 5.14. Because of the existence of the central Pacific anomalous SST forcing, the eastern Pacific SST perturbation heating effect has been substantially diminished in these areas, and these large changes can hardly be noticed at the 500 hPa level (Fig. 5.20b), although a very weak effect (less than 1 - 2 Kday⁻¹) is still discernable at the lower level (Fig. 5.20a). In addition, the intensification of the SPCZ in the PACP2 run (Fig. 5.20a and b) is less strong than that in the EPACP2 run in which only eastern Pacific SST is anomalous. It can be summarized that the spatial heating change in Fig. 5.20 is composed of the features in both the CPACP2 and EPACP2 runs. However, the central Pacific anomalous forcing is swamping some of the features only occurring when the eastern Pacific SST perturbation is prescribed.

Hence, the main features resulting from the eastern Pacific SST anomaly, such as the heating increases in the SPCZ and near the central America coast areas, appear to be weaker than their strengths when the central Pacific SST anomalous forcing is not present. These results, again, demonstrate the important role of the equatorial central Pacific SST anomaly in the tropical atmospheric processes for the ENSO-like interdecadal atmospheric variations.

b. Vertical profiles of the individual physical heating processes

Vertical profiles of the diabatic heating changes resulted from different processes for the 6 selected tropical locations in the PACP2 run are given in Fig. 5.21. In the central Pacific forcing region (Fig. 5.21a), the cumulus convection increase dominates the total diabatic heating change in the lower and middle tropospheric layers, reaching its maximum of about 6 Kday^{-1} at 500 hPa. The vertical distributions of the large scale precipitation and radiative cooling are almost identical to those resulted from the experiment with only the presence of the equatorial central Pacific anomalous SST forcing (Fig. 5.9a) since the eastern Pacific SST perturbation has little effect on these processes in the central Pacific location (0° , 180°) chosen, except a tiny increase for the two processes shown in Fig. 5.15a. The contributions of these two processes to the total diabatic heating become equal to and larger than that of cumulus convection at approximately 350 hPa. The total diabatic heating change maximizes at the 400 hPa level (a change from 500 hPa in Fig. 5.9a), with a heating value exceeding 7.5 Kday^{-1} (Fig. 5.21a). Such an evidence can be used to partly explain why the maximum atmospheric height/temperature change occurs in the upper level. It is

interesting to note that the maximum diabatic heating increasing becomes smaller than the one (larger than 9 Kday^{-1}) in the CPACP2 run (Fig. 5.9a). This does not necessarily mean that the tropical atmospheric diabatic heating response to the anomalous SST pattern in PACP2 is weaker than that in CPACP2. It has been shown from the height and circulation changes that the atmospheric response becomes more vigorous in the PACP2 run. The problem is that the location ($0^\circ, 180^\circ$) for the display is not the center of the forcing perturbation and 2.5° north to the local SST perturbation center. It can be clearly seen that the atmospheric diabatic heating response to the forcing in the PACP2 experiment in Fig. 5.20b is stronger than that in the Fig. 5.8b) for the CPACP2 run, though the center over the central Pacific moves slightly southward, and the heating change near the center area has a sharper north-south gradient from its center to the north.

In the equatorial western Pacific and Indian Ocean regions, a maximum of 3 - 4 Kday^{-1} diabatic cooling occurs (as shown in Fig. 5.21b and e). For the tropical western Pacific (Fig. 5.21b), the maximum cooling reaches nearly 4 Kday^{-1} at 500 hPa. Such a change is 1 Kday^{-1} larger than that in the CPACP2 run (Fig. 5.8b). The cooling effect of all the three individual physical processes is enhanced in the middle and upper troposphere due to the presence of the eastern Pacific SST anomaly in the PACP2 experiment. As previously discussed, the presence of the eastern Pacific SST perturbation reinforces the upward motion and surface flow convergence in the equatorial central Pacific, and reduces the convective activities over the tropical western Pacific. This leads to a less cumulus convection, large scale precipitation which, in turn, enhances the radiative cooling process at the upper level of the

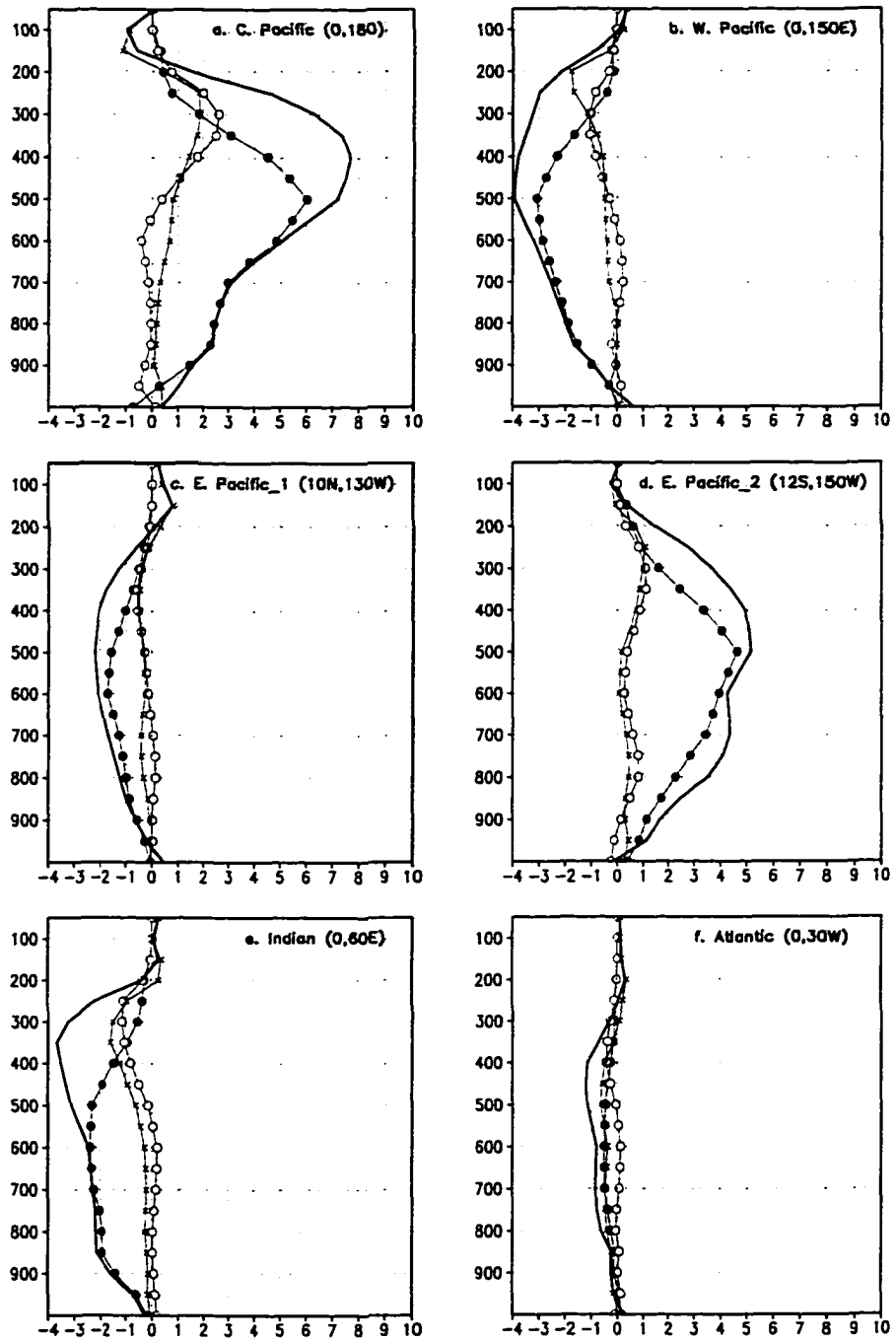


Figure 5.21 Same as Figure 5.9, except for the PACP2 run.

troposphere. The vertical distribution of the diabatic cooling changes over the tropical Indian Ocean (Fig. 5.21e) exhibit a similar structure to that of the CPACP2 run in Fig. 5.8e. But, the cooling is enhanced in the PACP2 run, especially below the 500 hPa level (Fig. 5.21e). The total diabatic cooling there reaches its maximum of above 3.5 Kday^{-1} near the 350 hPa level. The largest changes due to the presence of the eastern Pacific SST perturbation occur below 600 hPa where the cumulus convection activity is largely suppressed by the intensified central Pacific forcing.

The vertical profile of the diabatic heating change at the location to the south of the equator in the eastern Pacific (Fig. 5.21d) shows a similar bimodal distribution to the one in the EPACP2 run (Fig. 5.15d). The large scale precipitation and radiative processes remain unaffected by the anomalous SST over the central Pacific, whereas the cumulus convection appears to be weakened slightly at the lower level (Figs. 5.21d and 5.14d). However, the selected location at the north portion of the tropical eastern Pacific in Fig. 5.21c exhibits a cooling effect in total diabatic heating, which, again, shows a considerable suppressing effect of the central Pacific forcing on the atmospheric response over the eastern Pacific. The anomalous SST forcing at that location is insignificant, compared to the positive forcing anomaly at the central Pacific. Little change in the three diabatic heating processes is noted over the equatorial Atlantic region (Fig. 5.21f). However, the total diabatic heating contributed by all the three processes still shows approximately 1 Kday^{-1} cooling in the middle troposphere.

Overall, the vertical structures of the diabatic heating processes over the tropical central and western Pacific, and Indian Ocean exhibit the primary features

seen in the CPAP2 runs, indicating a dominant effect of the equatorial central Pacific anomalous SST pattern. However, the atmospheric cooling in the tropical western Pacific and Indian Ocean has been enhanced due to the effect of the eastern Pacific SST perturbation. The locations over the eastern Pacific show a decrease in heating structure caused mainly by the eastern Pacific anomalous SST change because of the suppression effect of the central Pacific SST change. The SST forcing perturbations over the Pacific have little impact on the local atmospheric heating processes over the tropical Atlantic region.

5.5 Tropical Atmospheric heat transport and its impact on the height change pattern over the tropics

Heat transport is a key component in the formation and maintenance of the global climate and general circulation. It is well known that heat is transported poleward by means of atmospheric flow and ocean currents due to the heat surplus in the tropical and low latitude areas and deficit in the high latitude and polar regions (Peixoto and Oort 1992). The tropospheric heat transport mechanisms and their influences on the tropospheric height change pattern in the tropics will be examined in this section.

5.5.1 Importance of horizontal heat transport and its general structures in the modeled atmosphere

In the present study, it has been shown that when an anomalous heat source is placed to a specified region in the tropics, the atmosphere, due primarily to enhanced

cumulus convection, responds with a height increase nearly everywhere in the tropical belt within the troposphere, particularly in the middle and upper tropospheric layers, although such height change is not zonally uniform. Other than near the anomalous forcing area (e.g. over the tropical Atlantic region), the atmospheric diabatic heating remains unchanged in the prescribed forcing runs. If, at least, part of such a wide spread geopotential height change is assumed to be a thermal effect (atmospheric temperature increase), certain transport mechanisms must exist to carry the heat energy away from the local source area and redistribute this heat over the remainder of the tropics.

a. Representation and computation of horizontal heat transport

Horizontal heat/temperature flux (uT , vT) is used to describe general heat transport structures in the climate system (Peixoto and Oort 1992). The heat flux itself does not affect the local atmospheric temperature. As shown in (5.1), it is the heat flux divergence term which balances the diabatic heating and adiabatic cooling terms in the thermodynamical equation. Hence, the atmospheric heat transport can be described more clearly using heat flux divergence/convergence term. The zonal and meridional heat fluxes (uT , vT) are first calculated using the 6-hourly model outputs, and then the divergence of the horizontal heat fluxes is calculated using the expressions as the second and third terms in (5.1). The monthly mean results of these heat flux and divergence terms over the 20-month integration period are reported and discussed.

b. General structures of horizontal atmospheric heat flux in the tropics

To aid in a better understanding of relative importance of various transport mechanisms, cross sections of the zonal mean meridional heat flux (vT) and zonal heat flux (uT) in the deep tropical region ($15^{\circ}\text{S} - 15^{\circ}\text{N}$), generated in the CNTR run, are at first given in Fig. 5.22. It presumably represents a model heat flux climatology for the January simulated atmosphere over the tropics. The meridional mean heat flux exhibits a structure characterized by the Hadley cell (Fig. 5.22a). A large northward heat flux area exists above mid-troposphere induced by the upper branch of the zonal mean Hadley cell, with an area of greater than 200 Kms^{-1} in $5^{\circ}\text{S} - 20^{\circ}\text{N}$ centered at 250 hPa. At the lower level, a strong southward flux can be seen below 700 hPa at the $0^{\circ} - 20^{\circ}\text{N}$ region where the maximum northerly zonal mean wind ($2 - 4 \text{ ms}^{-1}$) is found. The magnitude of such a southward flux is rather large with a local maximum greater than 1000 Kms^{-1} at 10°N . In the southern subtropics ($20^{\circ}\text{S} - 30^{\circ}\text{S}$), a weak equatorward flux also exists.

The effect of zonal heat transport over the tropical region may not be as important as that of the meridional heat transport in the global climate system and general circulation maintenance, since the solar radiative energy in this region varies little zonally and the weak temperature gradient along the circumference is established only by the differentials in local surface and atmospheric processes. However, the overall zonal tropical easterly and westerly wind is far greater than the meridional air flow in magnitude of wind speed. Such a large zonal wind leads to a quite large heat flux in the tropics and lower latitude regions. The zonal gradient of heat flux may play an important role in distributing and transporting heat in the zonal direction. As will

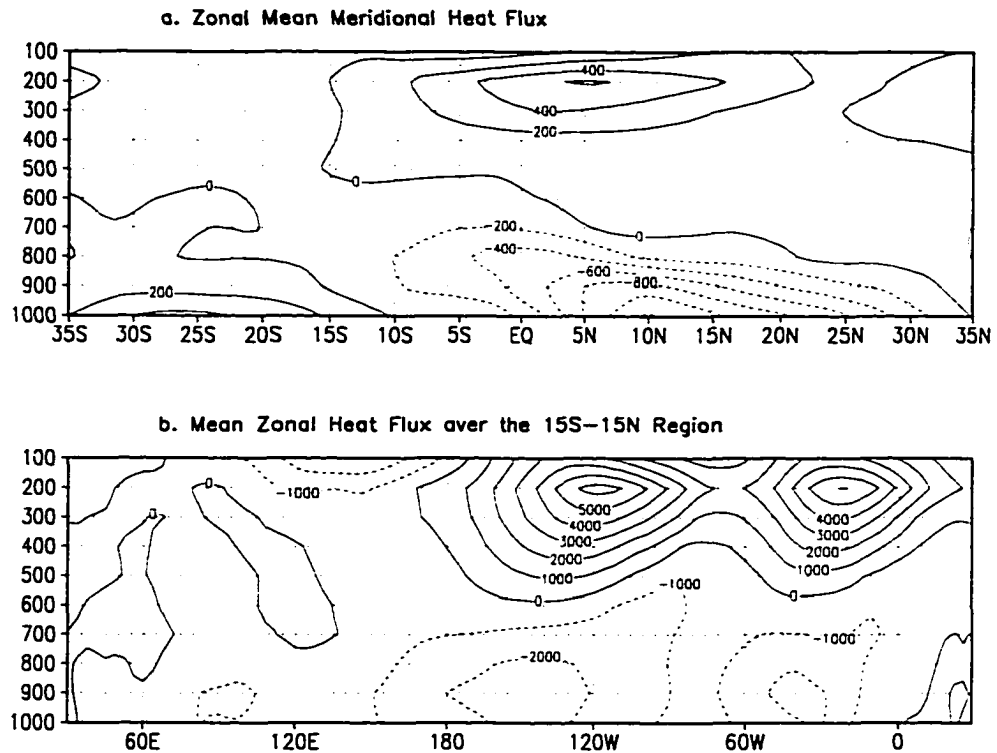


Figure 5.22 Mean heat flux in the CNTR run for a. zonal mean, b. meridional mean over the 15°S - 15°N region. Unit: Kms^{-1} .

be shown, the zonal heat flux appears to be one of the mechanisms which carry the warm air away from the localized heating source region and redistribute part of the anomalous heat energy within the tropical and lower latitude regions.

To illustrate the zonal heat transport in the deep tropics, the mean zonal heat flux over the 15°S - 15°N belt is used, and its cross section from the CNTR run modeled atmosphere is shown in Fig. 5.22b. The dominant feature is the overwhelmingly large flux magnitude in the upper troposphere. Overall, large westerly heat flux is seen to the east of dateline in the middle and upper troposphere, whereas in the lower troposphere, the flux appears to be mostly negative due to the easterly wind transport (see Fig. 4.4). Two considerable local flux maximum areas,

with maximum flux magnitudes above 6000 Kms^{-1} can be noticed in the upper troposphere over the eastern Pacific and Atlantic regions. In the western Pacific and Indian Ocean regions, the upper level heat flux is mostly westward and relatively small in magnitude (below 2000 Kms^{-1}). In the lower troposphere, easterly heat flux occurs almost in the entire tropics, mostly greater than 1000 Kms^{-1} except for the western Pacific and Indian Ocean regions. It is noteworthy that the heat flux structure northward of 10°N exhibits a prevailing eastward heat flux above 700 hPa level and westward flux in the near surface layer over the entire tropics (figure not shown). This region is close to the upper level subtropical jet and the large westerly heat flux in the upper level may become convergent downstream, leading to a positive heat transport into those areas.

c. Vertical mean structures of zonal and meridional heat flux and its divergence

Vertical mean values are employed to simplify the study of the horizontal heat transport at various geographical regions. Such a vertical mean flux in zonal and meridional directions represents an average value of the heat flux across a unit area in the vertical over the atmospheric levels examined.

The vertical mean heat transport is evaluated in three layers, which are the upper layer (500 - 200 hPa), lower layer (1000 - 600 hPa) and total layer (1000 - 200 hPa). Fig. 5.23 gives the vertical mean of zonal heat fluxes and its divergence over the tropical belt of $15^\circ\text{S} - 15^\circ\text{N}$. The two peak regions of the vertical zonal heat flux in the upper layer can be clearly noted in the eastern Pacific and Atlantic areas as shown in Fig. 5.23a, with a maximum above 3500 Kms^{-1} immediately west to the 120°W . To

the east of the central Pacific, an easterly heat flux occurs in the lower layer, whereas, the zonal heat flux in the total layer is dominated by weak westerly flux, indicating the dominant influence of the upper level westerly wind. Over the western Pacific and Indian Ocean regions, the vertical mean of the zonal heat flux is rather small in all layers.

The heat sources and sinks of atmospheric heat energy become evident when the divergence/convergence of the heat flux is displayed in Fig. 5.23b. In the upper layer, heat sources in zonal direction are located at approximately 160°E - 130°W

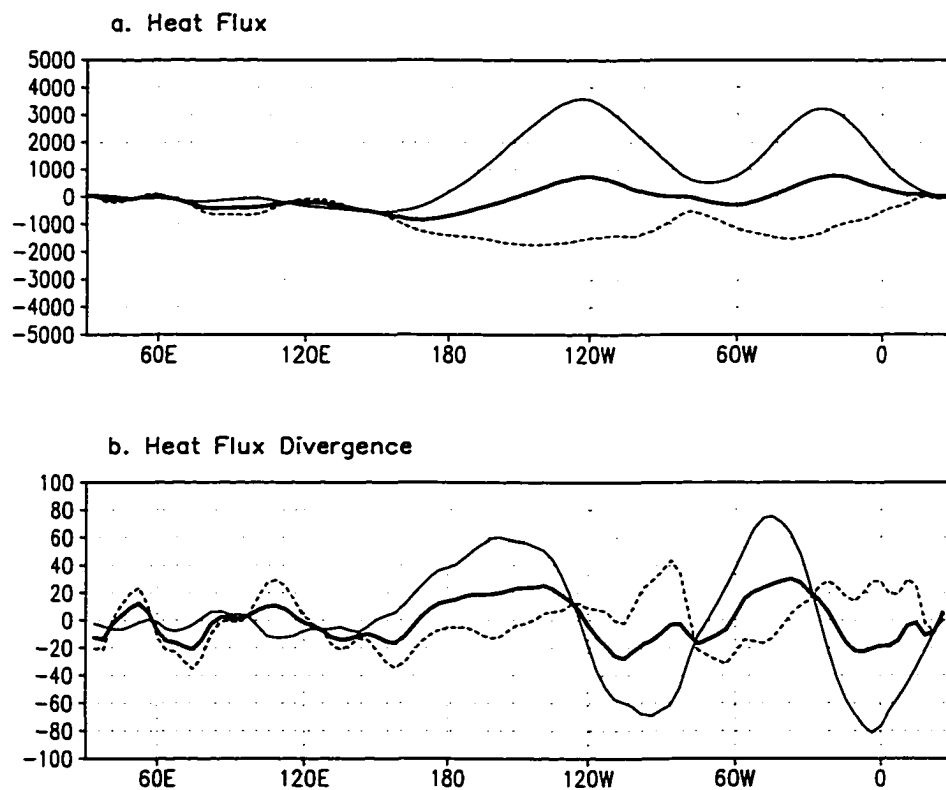


Figure 5.23 Vertical mean zonal (a). heat flux in Kms^{-1} and (b) its divergence in $Kday^{-1}$ over the $15^{\circ}S - 15^{\circ}N$ region in the CNTR run. The thick line represents the vertical mean in the 200 - 1000 hPa layer. The thin solid line and dash line are the vertical mean in the 200 - 500 hPa and 600 - 1000 hPa layers, respectively.

portion of the Pacific and the eastern tropical Atlantic regions where large heat flux divergence is found. Heat convergence exists in the lower layer of these regions. The total atmospheric layer has a net heat loss over these areas in the zonal direction (Fig. 5.23b). Heat sinks are found over the eastern portions of the tropical eastern Pacific and Atlantic. The overall heat flux divergence in the tropical Indian and western Pacific regions is relatively small, indicating little heat loss in the east-west direction in the areas with these higher surface temperature.

Detailed analyses of horizontal heat transports will reveal the relative importance of the zonal and meridional transports at different regions over the tropics. In turn, this enables an identification of the physical processes and mechanisms responsible for the tropical geopotential height change patterns. As seen in Fig. 5.24, the vertical mean of the meridional heat flux is locally computed for six representative longitudinal zones which are determined simply by the geography for the convenience of the subsequent analyses and discussions. These regions cover the tropical Indian Ocean, the western and central Pacific, eastern and western portions of the eastern Pacific, and a large part of the tropical Atlantic region. In the Indian and western Pacific regions (Fig. 5.24a, b), upper level northward flux is found in the area north to 10°S , whereas the flux at the lower level is southward. This indicates a strong surface forcing near 10°S for boreal winter season. The net heat flux in the total layer is rather small between 15°S - 15°N . Relatively large northward upper level heat fluxes can be seen in the central Pacific, the 160°W - 120°W area of the eastern Pacific and the Atlantic (Fig. 5.24c, d and f). Maximum upper level northward flux is found south of the equator, especially for the eastern Pacific and Atlantic (upto 1000 Kms^{-1}),

implying a relative weak tropical surface forcing in these areas. In addition, strong southward heat flux is found near 20°N latitude for these areas. The zonal mean of the meridional heat flux in the 120°W - 60°W portion of the eastern Pacific exhibits a quite different structure than other regions (Fig. 5.24e). In the upper level, a southward flux to the south of the equator is generated by the northwesterly wind there, whereas large northward heat flux is found over the northern subtropics. The flux for the total layer is small in general over the tropics (Fig. 5.24e).

The divergence structure of the vertical mean meridional heat flux for the same six geographical areas is given Fig. 5.25. Within the upper tropospheric layer, heat sources are found in the area immediately south to the equator over the Indian Ocean (Fig. 5.25a), a lower level heat sink can be seen in this region. In the western Pacific warming pool region, upper level heat divergence is found in a large area from 10°S to 25°N (Fig. 5.25b). In the central Pacific, heat diverges in the 8°S - 16°S area and converges in 0° - 20°N area in the upper layer. This indicates a relative heat gain in the meridional direction for the 0° - 20°N area in the upper level. The western portion of the equatorial eastern Pacific region (15°S - 15°N) is a large heat sink (Fig. 5.25d). Such net heat comes from the sources on both poleward sides because the upper level meridional wind converges to the tropical zone. The maximum convergence area for the total tropospheric layer is to the north of the equator due to the heat flux convergence both at the upper and lower layers (Fig. 5.25d). Similar meridional structure is also seen in the Atlantic region, with an exception of the upper level convergence found slightly northward (Fig. 5.25f). Due to the upper level poleward

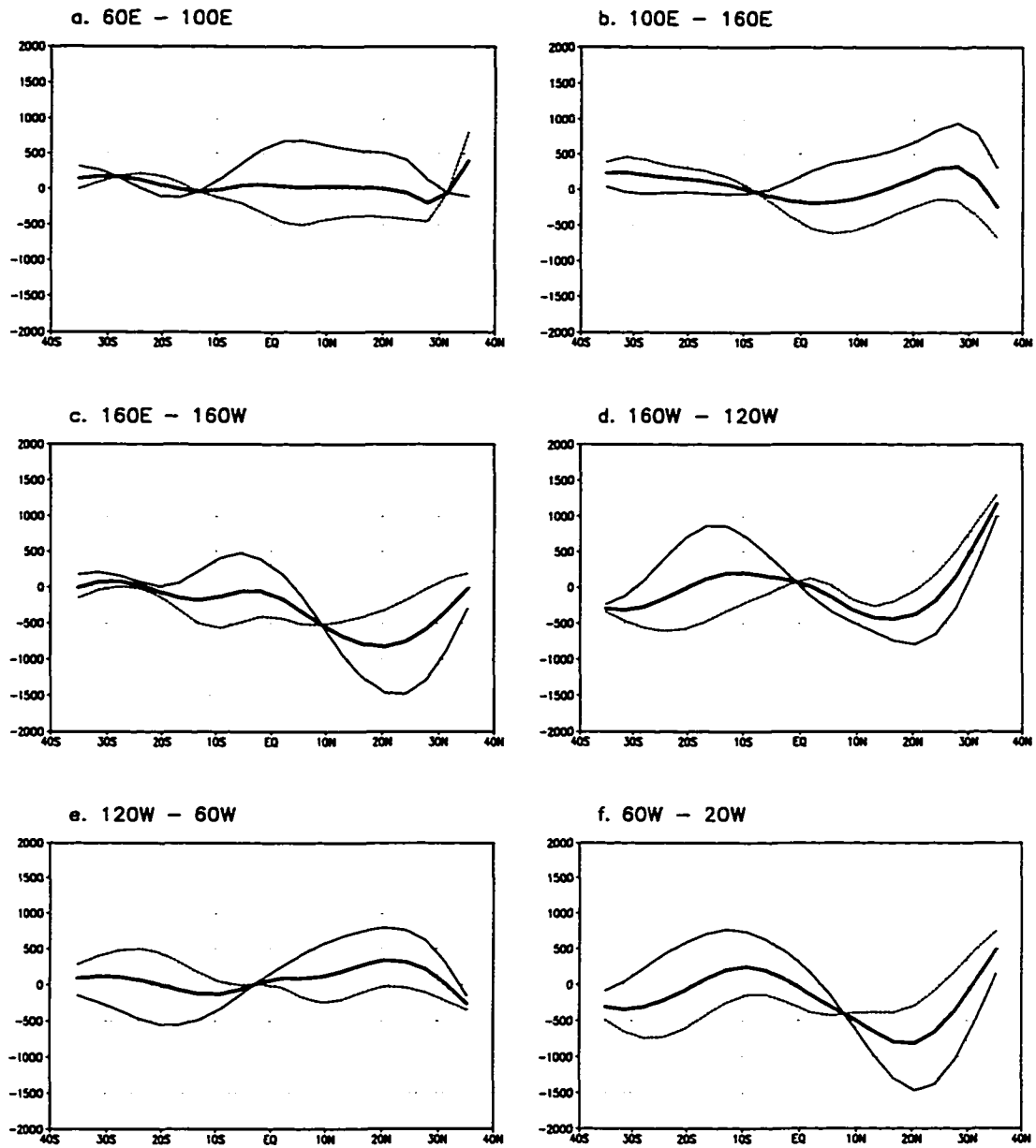


Figure 5.24 Vertical mean zonal heat fluxes for the six longitudinal zones in the CNTR run, unit: Kms^{-1} . The thick line represents the vertical mean in the 200 - 1000 hPa layer. The thin solid line and dash line are the vertical mean in the 200 - 500 hPa and 600 - 1000 hPa layers, respectively.

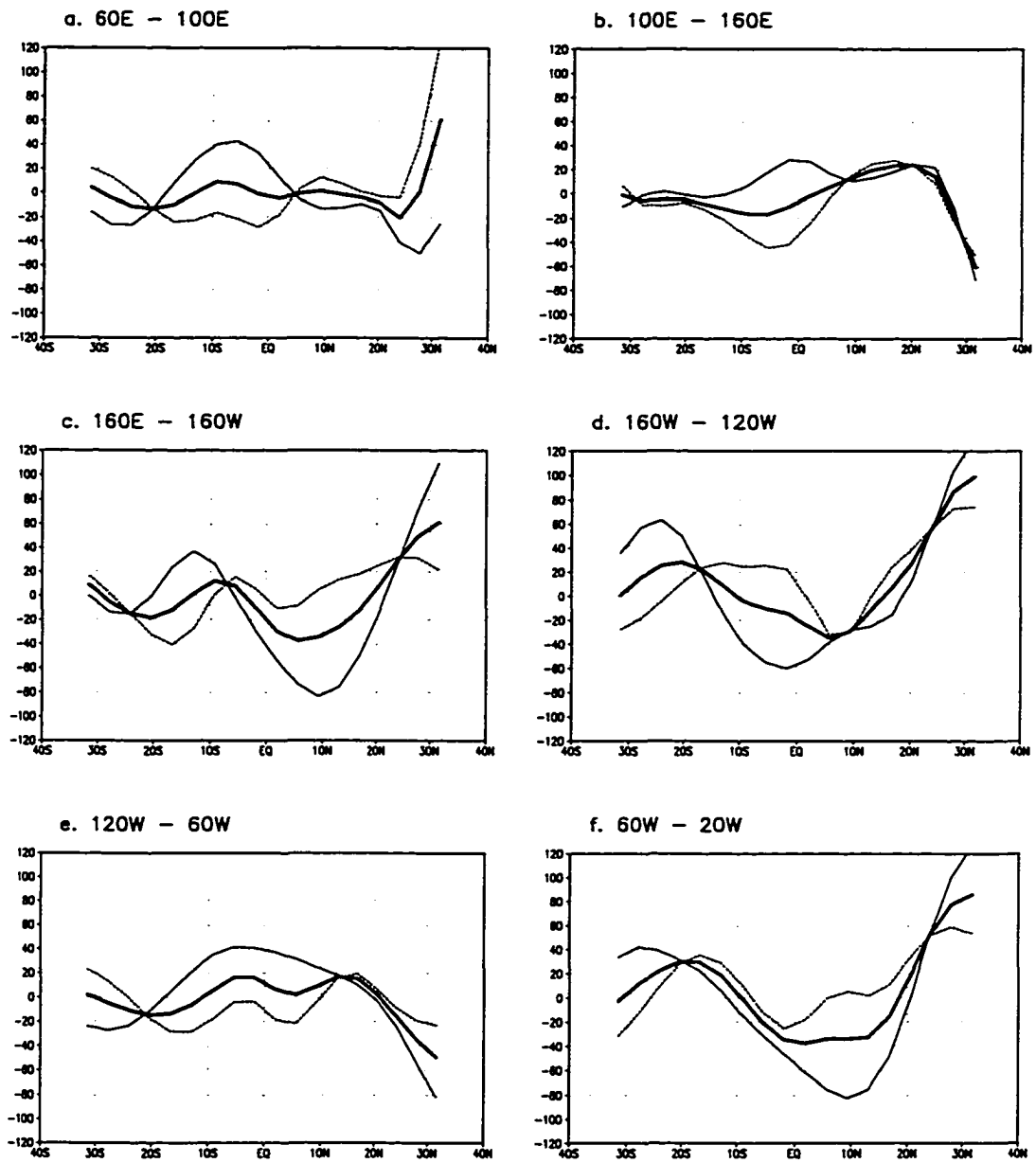


Figure 5.25 Vertical mean zonal heat flux divergences for the six longitudinal zones in the CNTR run, unit: Kday^{-1} . The thick line represents the vertical mean in the 200 - 1000 hPa layer. The thin solid line and dash line are the vertical mean in the 200 - 500 hPa and 600 - 1000 hPa layers, respectively.

wind in the subtropical areas of both Hemispheres in $120^{\circ}\text{W} - 60^{\circ}\text{W}$ region (mostly eastern portion of the eastern Pacific), the equatorial area appears to be a large heat source in the upper troposphere as shown in Fig. 5.25e, and the net heat loss in the troposphere is not as large owing to the compensation effect in the lower layer.

Given the horizontal heat flux divergence structures in Figs. 5.23b and 5.25, the heat transport mechanisms in the upper troposphere can be generalized for the winter climatology. In the Indian and western Pacific regions, the zonal transport is the smallest of the entire tropical belt (Fig. 5.23b), the heat energy generated by the convective processes in these regions is transported poleward by upper level northward wind circulation. The heat energy is also generated over the south subtropical area of the central Pacific, $160^{\circ}\text{W} - 120^{\circ}\text{W}$ portion of the eastern Pacific and Atlantic regions. Part of the heat energy is transported northward to the equatorial region (Fig. 5.25). Such heat energy can then be carried eastward by the strong westerly in the regions near 10°N and southward of 20°S . In the deep tropics ($15^{\circ}\text{S} - 15^{\circ}\text{N}$), westerly wind maximum occurs near 120°W and 30°W , leading to a zonal heating gain in the easternmost parts of the tropical eastern Pacific and Atlantic regions, and heating loss in large part of the tropical eastern Pacific and Atlantic regions to the west of the wind maxima (Fig. 5.24b). The equatorward wind convergence, occurring in the eastern Pacific and Atlantic, induces large heat flux convergences (50 and 80 Kday^{-1} , see Fig. 5.25d and f) which are about enough to compensate the heat loss in the zonal direction. The overall zonal heat gain in $120^{\circ}\text{W} - 60^{\circ}\text{W}$ appears somewhat larger than the meridional loss (Fig. 5.25e), suggesting that

the heat transport brings net heat energy horizontally and tends to warm the upper tropospheric air in that area climatologically.

5.5.2 Heat transport changes in the forcing runs and their effects on the tropical-wide height change patterns

Heat transport is the mechanism that redistributes the heat energy generated in the dynamical and physical processes within the atmospheric system. The mean heat transport is one component of the processes in the atmospheric thermal balance. The structures given in Figs 5.24 and 5.25 are partially responsible for the mean thermal state in the troposphere over the tropics. The atmospheric circulation is apparently the primary component in the establishment of these heat transport mean structures. When the tropical atmospheric circulation is modified due to the SST interdecadal variation as discussed in the previous sections, the heat transport will, in turn, be changed. It is believed that the climatological transport mechanisms and their changes are largely responsible for those height change spatial patterns which are remotely located from the local heat source region in the forcing experiments.

a. Horizontal heat transport mechanisms in the CPACP2 forcing run

The tropical tropospheric circulation response to the anomalous SST over the equatorial central Pacific in the CPACP2 run is characterized by a strong anomalous upward vertical motion, the upper level poleward meridional wind and large lower level flow convergence near the forcing region (Figs. 5.5 and 5.6). Fig. 5.26 shows

the differences of the vertical mean of the zonal heat flux and the flux divergence over the 15°S - 15°N belt between the CPACP2 and CNTR runs. In Fig. 5.26a, it is shown that there is an increase in the westerly heat flux over the Indian, eastern Pacific and Atlantic regions associated with the upper level westerly wind anomaly seen in Fig. 5.5a. A large increase in the lower level easterly heat flux (about 1200 Kms⁻¹) is found to the west of the dateline due to the surface flow convergence toward the surface anomalous forcing area. Overall, a moderate westerly heat flux anomaly for

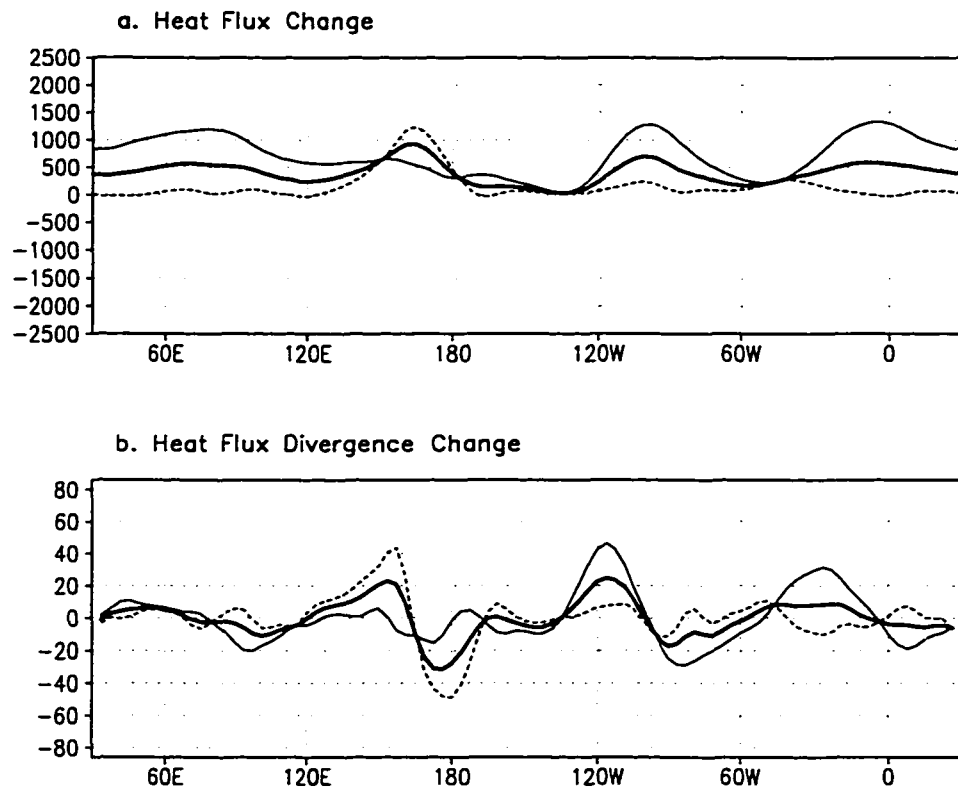


Figure 5.26 Differences of the vertical means of the zonal heat flux (top) and zonal heat flux divergence (bottom) between the CPACP2 and CNTR runs (CPACP2 - CNTR). The thick line represents the vertical mean in the 200 - 1000 hPa layer. The thin solid line and dash line are the vertical mean in the 200 - 500 hPa and 600 - 1000 hPa layers, respectively. The unit is Kms⁻¹ for the heat flux and Kday⁻¹ for the heat flux divergence.

the total layer can be seen over a large part of the tropical region. The changes in the heat flux divergence show that the upper level zonal heat sources in the deep tropics exist in the 120°W eastern Pacific and Atlantic regions as seen in Fig. 5.26b because of the strong anomalous wind divergence in the upper layer over these areas. In the 110°W - 80°W portion of the eastern Pacific, it appears to be an upper level zonal heat sink region. A large lower layer heat sink with a maximum of about 40 Kday⁻¹ is noted over the tropical western Pacific (Fig. 5.26b), whereas the central Pacific appears to be a lower level heat sink due to the lower level wind change structure (see Fig. 5.5b). The zonal heat transport over the deep tropics for the total layer is dominated by the upper level changes over the eastern Pacific and the lower level changes over the central and eastern Pacific regions, respectively.

The meridional transport is a more effective mechanism in atmospheric heat energy distribution. The meridional heat flux changes in the six selected longitudinal regions are illustrated in Fig. 5.27. The flux over the tropical Indian Ocean and the 120°W - 60°W sector of the eastern Pacific exhibit little change shown in Fig. 5.27a and e in the troposphere. A lower level equatorward flux change is found in the western Pacific (Fig. 5.27b), with a maximum less than 200 Kms⁻¹. As expected, an extraordinary northward heat flux increase, with a maximum about 800 Kms⁻¹, is found in Fig. 5.27c at the upper level in the 0° - 30°N region of the central Pacific, associated with strong northward wind anomaly. More interestingly, a large upper level southward flux change of similar magnitude (a maximum approximately 700 Kms⁻¹) is found in the 160°W - 120°W portion of the eastern Pacific at 0° - 25°N, in accordance with the extremely strong southward meridional wind difference in that

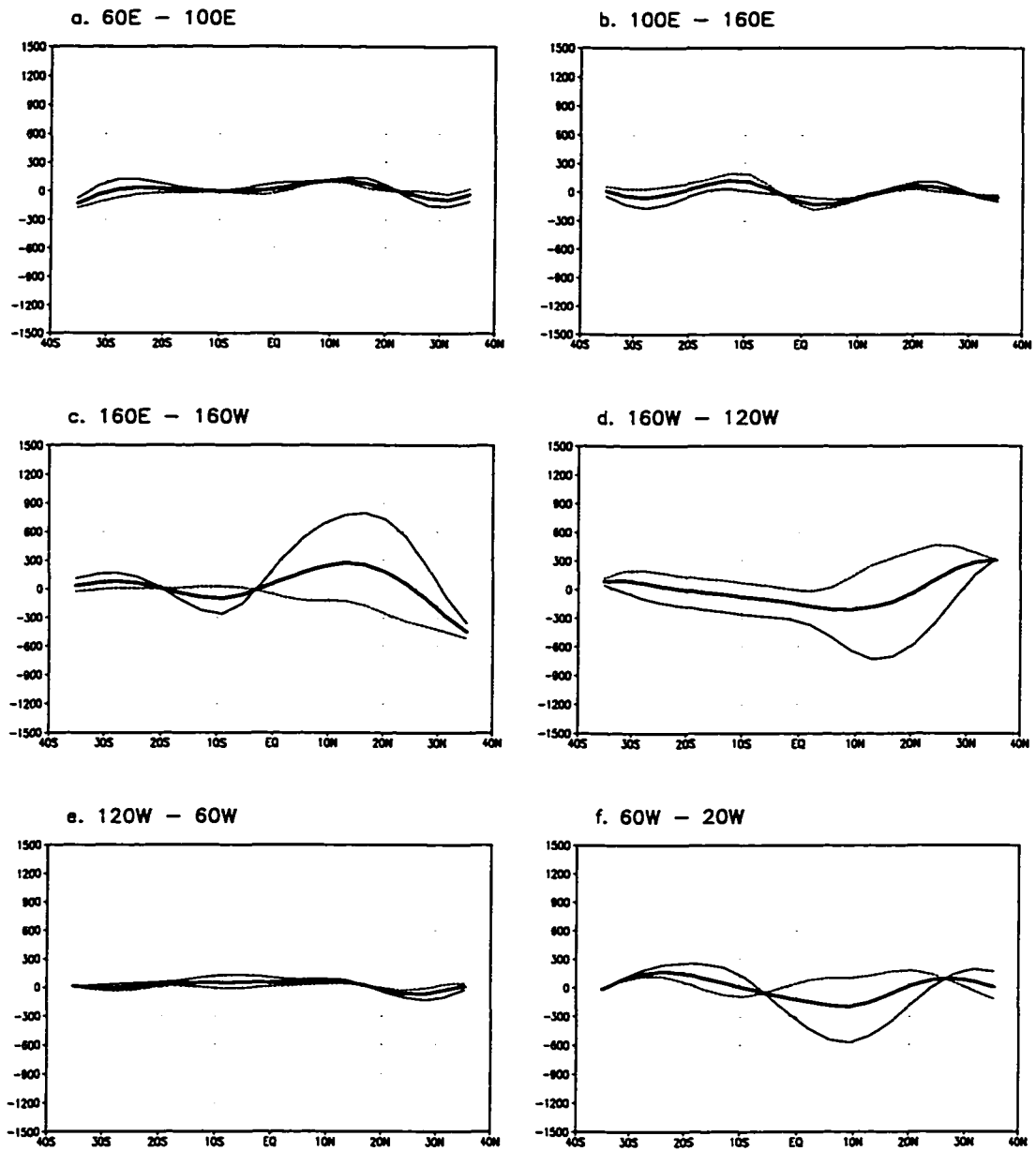


Figure 5.27 Differences of the vertical means of the meridional heat flux between the CPACP2 and CNTR runs (CPACP2 - CNTR) for the the six longitudinal zones, unit: Kms^{-1} . The thick line represents the vertical mean in the 200 - 1000 hPa layer. The thin solid line and dash lines are the vertical mean in the 200 - 500 hPa and 600 - 1000 hPa layers, respectively.

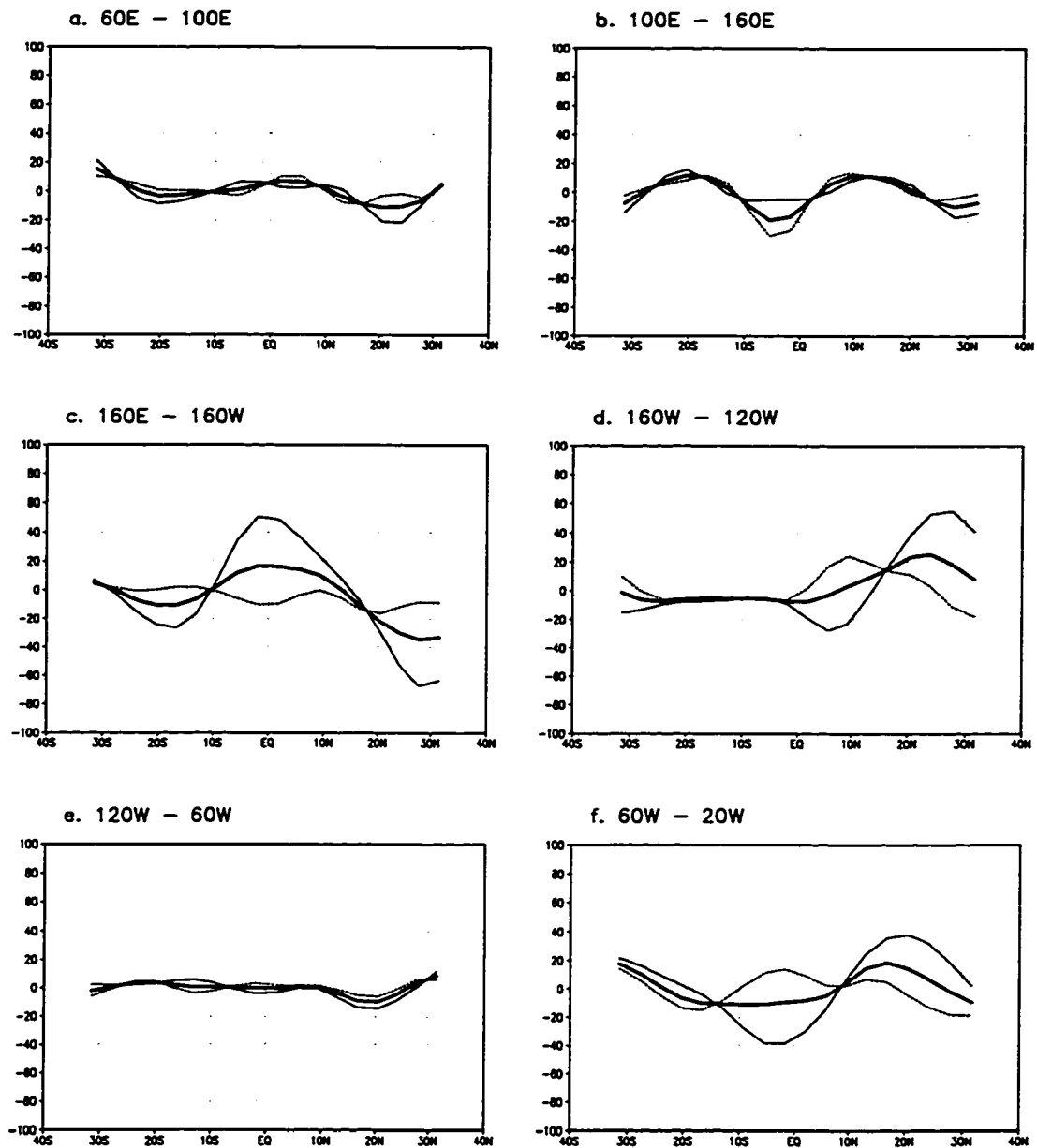


Figure 5.28 Differences of the vertical means of the meridional heat flux divergences between the CPACP2 and CNTR runs (CPACP2 - CNTR) for the the six longitudinal zones, unit: Kms^{-1} . The thick line represents the vertical mean in the 200 - 1000 hPa layer. The thin solid line and dash line are the vertical mean in the 200 - 500 hPa and 600 - 1000 hPa layers, respectively.

area (see Fig. 5.5a). Furthermore, a relatively large upper level southward flux change is seen in the Atlantic region (Fig. 5.27f), with a maximum value of 600 Kms^{-1} at 10°N . In general, the upper level heat flux change dominates the total layer flux change structure in the tropics.

The heat flux divergence change structures shown in Fig. 5.28 are more representative in describing the heat transport changes in the tropical regions. The heat convergence south to the equator seen in Fig. 5.28b over the tropical western Pacific arises from the lower level anomalous equatorward wind change. Over the central Pacific anomalous forcing area, a large anomalous heat loss with a divergence value of about 50 Kday^{-1} at the equator can be seen in Fig. 5.28c for the upper tropospheric layer, much of which is carried northward by the southerly wind change. Both the $160^\circ\text{W} - 120^\circ\text{W}$ eastern Pacific and Atlantic areas (Fig. 5.28d and f) show a relatively large heat sink and heat energy accumulation in the upper layer of the deep tropics. The source of such heat energy is from northward of $10^\circ\text{N} - 15^\circ\text{N}$ as seen in Fig. 5.16d and f. Such heat energy is transported equatorward by the upper level meridional wind anomalies in these areas.

The strong anomalous rising and upper level poleward motion due to the anomalous surface forcing are responsible for the redistribution of the heat generated by the diabatic heating change in the tropical atmosphere. However, the zonal heat transport within the tropical region (Fig. 5.26b) is not an effective mechanism for the heat energy redistribution in the horizontal direction. It will be shown subsequently that the upper level flow in subtropical regions is the key for the zonal heat energy transport. The meridional wind convergence in the eastern Pacific and Atlantic

regions acts to carry heat energy into the equatorial zone from the lower latitudes and warm the atmosphere. Heat transport from the northern low latitudes to the equator is strong in the tropical eastern Pacific and Atlantic regions, leading to a relatively large geopotential height increase shown in Fig. 5.4a. However, the adiabatic sinking effect throughout the entire atmospheric layer below 200 hPa in the equatorial Atlantic Ocean (see Fig. 5.7b) also contributes to the height increase in that region. Certain dynamical mechanisms can be involved for the height change pattern at 500 hPa for the eastern Pacific area. The anomalous downward airflow over the eastern Pacific area (see Fig. 5.7b) may be one of the sources for the height increase in the layer immediately below the 500 hPa. It has been shown that the upper layer heat transport appears to have little change over the Indian and western Pacific Oceans. The height increase in these areas occurs mostly at the lower atmosphere. Because of the anomalous SST forcing in the equatorial central Pacific, the maximum rising motion is shifted toward the central Pacific and the normal strong upward motion in the western Pacific and Indian Ocean is suppressed as shown in Fig. 5.6b, leading to a less surface level air convergence and a positive height change in the near surface atmosphere.

b. Horizontal heat transport mechanisms in the EPACP2 forcing run

The atmospheric circulation change induced by the SST perturbation pattern over the eastern Pacific is significant mostly over the eastern Pacific and Atlantic regions as shown in Fig. 5.11. The heat transport processes driven by such circulation change exhibit different features. Fig. 5.29 gives the changes in the vertical mean of zonal heat flux and its divergence in 15°S - 15°N deep tropical belt in the EPACP2

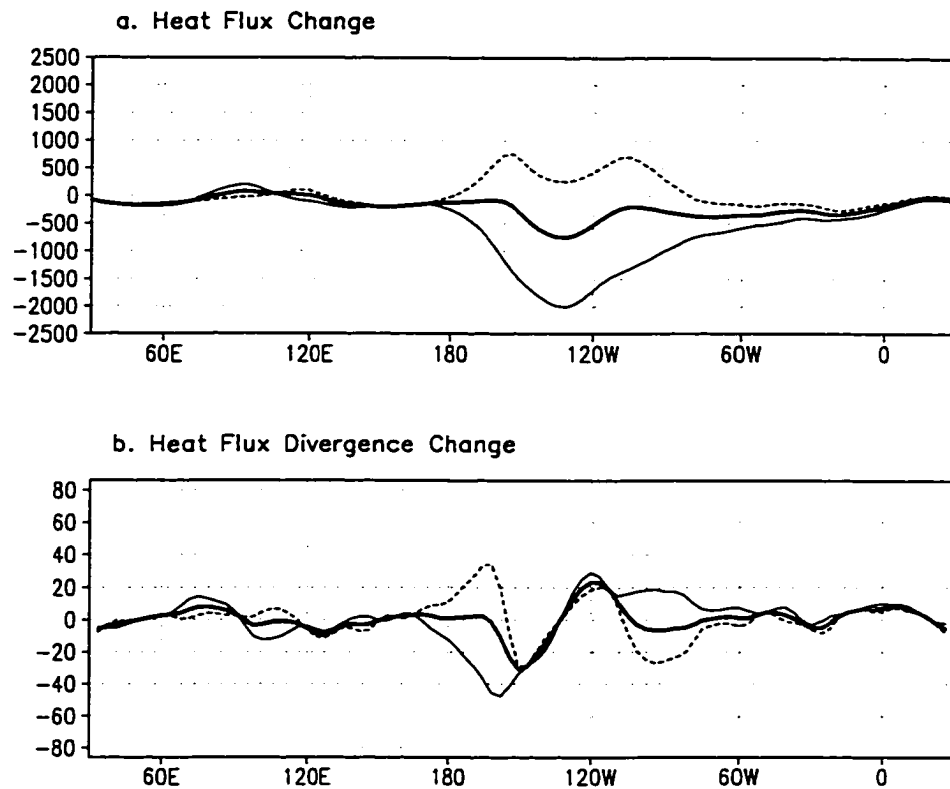


Figure 5.29 Same as Figure 5.26, except for the EPACP2 run.

forcing run. The change in the heat transport is mostly seen over the eastern Pacific, in agreement with the zonal circulation changes caused by the anomalous SST forcing. In the upper layer, the westerly heat flux experiences a large decrease with a maximum exceeding 2000 Kms^{-1} , whereas in the lower atmosphere westerly flux increase occurs in the eastern Pacific region. This clearly results from the large upper level easterly wind and lower level westerly wind changes in that large geographical region (see Fig. 5.11). Although the zonal heat flux change is rather large in the anomalous SST forcing area, the changes in local heat gain or loss appears much less

striking (Fig. 5.29b). Due to the strong upper level easterly wind anomaly to the east of 150°W, an anomalous heat convergence and gain area exists just to the east of the dateline in the upper layer. Most portions of the eastern Pacific appear to be a weak upper level heat source (Fig. 5.29b).

The vertical mean changes of the meridional heat flux for the six longitudinal regions in the EPACP2 forcing run are presented in Fig. 5.30. The meridional heat fluxes in the Indian and western Pacific Oceans are little affected (Fig. 5.30a and b), except an upper level flux change in the subtropical area between 20°N - 30°N. The anomalous upper level southerly flux north of the equator and northerly flux south of the equator in the central Pacific region (Fig. 5.30c) can be largely attributed to the poleward wind anomaly between 160°W - 180° as seen in Fig. 5.11a. Also, the upper level poleward wind anomaly over the eastern Pacific causes a poleward heat flux change in that area (Fig. 5.30d). Positive flux change (above 300 Kms⁻¹) dominates the area of the eastern Pacific near the southern American coast (Fig. 5.30e). Over the Atlantic region, only the portion north to the equator experiences a meridional flux change comprised of a southward change in the upper level and northward change in the lower layer, respectively.

The change in the meridional heat transport given by the heat flux divergence is shown in Fig. 5.31, which indicates relatively large changes over the central and eastern Pacific regions. Over the central Pacific, an anomalous heat source is seen at the upper level, indicating a heat loss there (Fig. 5.31c), whereas in the lower layer, heat converges anomalously to the equator, mostly from southern subtropical area, and warms the atmosphere. As shown in Fig. 5.31d, an anomalous meridional heat source

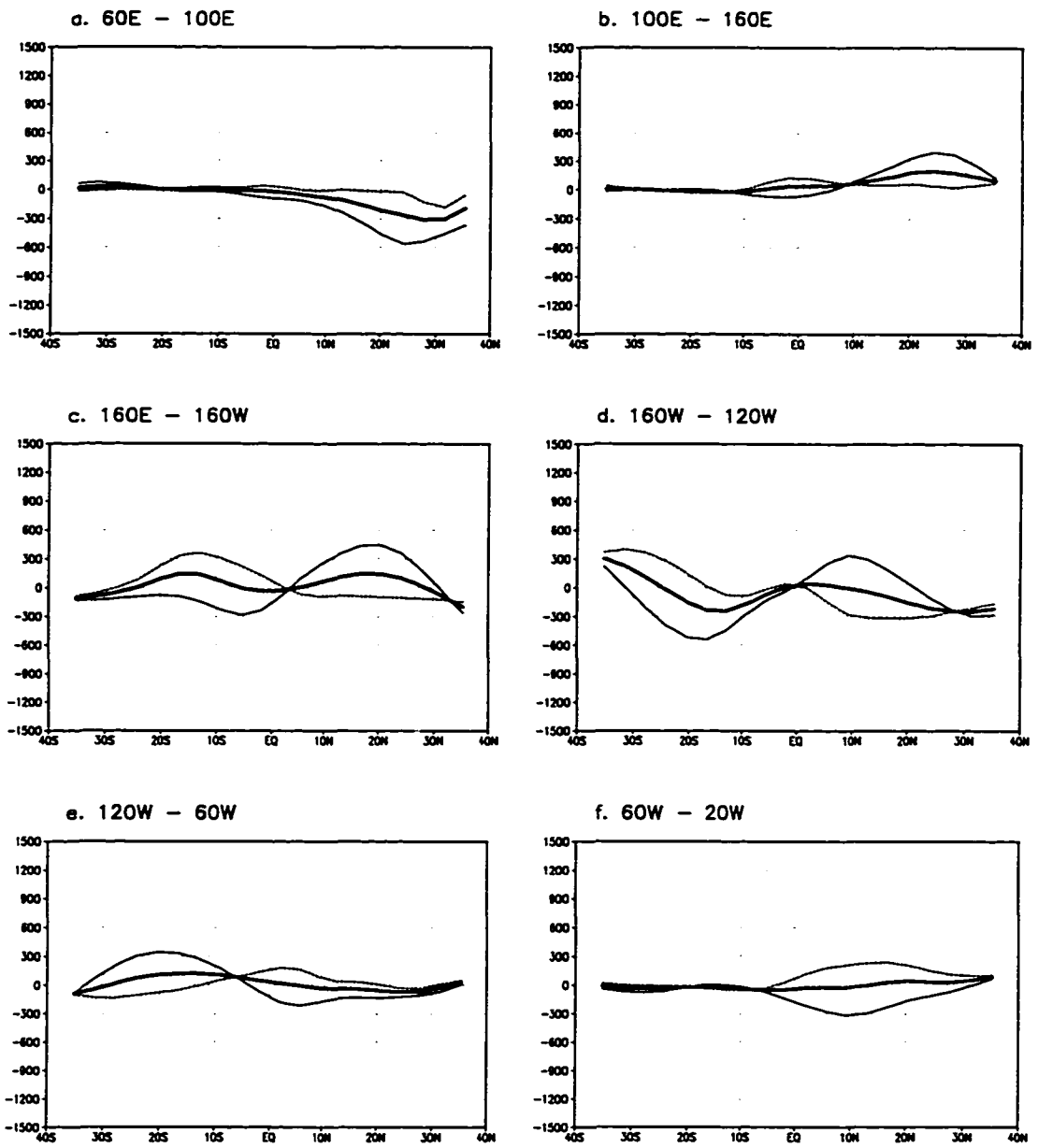


Figure 5.30 Same as Figure 5.27, except for the EPACP2 run.

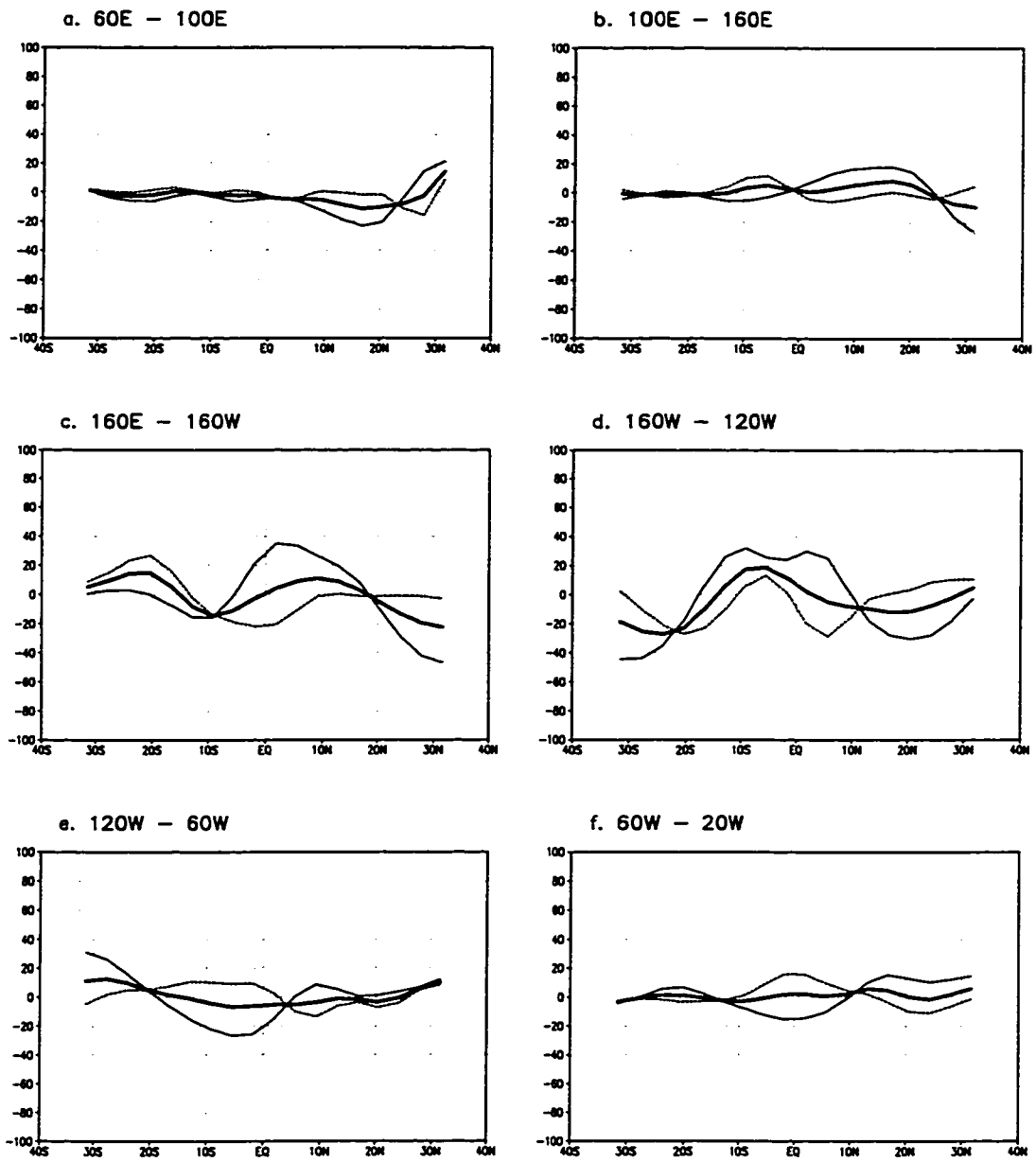


Figure 5.31 Same as Figure 5.28, except for the EPACP2 run.

exists in the 160°W - 120°W portion of the eastern Pacific, centered at 10°S near the highest SST (over 30°C) area in the experiment for the whole troposphere. This heat source diverges to both sides and. On the northern side, the heat converges in the areas between 0° - 10°N at the lower level and 10°N - 30°N at the upper level where the largest height increase is found (Fig. 5.10a). The heat convergence on the south side of the anomalous source is even larger (Fig. 5.31d), with a maximum above 40 Kday⁻¹ between 20°S - 30°S. The upper level of the eastern Pacific (120°W - 60°W) exhibits a heat gain for most of the tropical area (Fig. 5.31e). In the equatorial Atlantic region (see Fig. 5.31f), there is a moderate heat gain in the upper layer from the poleward sides, and also a heat loss there, in the lower layer, to the north. The eastern Pacific anomalous SST forcing shows little impact on the meridional heat fluxes over the Indian and western Pacific regions (see Fig. 5.31a and b).

The effect of horizontal heat transport on the tropical-wide height change pattern, arising from the SST perturbation over the eastern Pacific, is less strong than that in the CPACP2. The most significant height change occurs just above the anomalous surface forcing area, and the diabatic heating increase is largely responsible for the height change in the middle and upper troposphere over the eastern Pacific area. However, the heat transport mechanisms may reinforce the warming effect by transporting heat energy to the positive height change areas. Such processes are realized largely through the meridional heat energy convergence, because the zonal transport shows little change (Fig. 5.29b). Over the eastern Pacific, the upper level poleward wind in the anomalous SST forcing region carries the heat to the south and north. The heat is transported eastward in the areas of about 20° - 30° areas of

both hemispheres (see Fig. 5.11b). Meridional wind convergence redistributes such anomalous heat energy back to 0° - 20°N area between 160°W - 120°W and to 20°S - 0° area of 120°W - 60°W , reinforcing the atmospheric heating contribution to warming the upper troposphere in these regions. The meridional heat gain over the tropical Atlantic region will affect the 500 - 200 hPa height thickness increases (Fig. 5.10). The height thickness between 1000 and 500 hPa in the equatorial Atlantic region shows little change. The likely cause for this is the anomalous lower layer heat energy loss (Fig. 5.31f). Again, the height increase over the tropical Indian and western Pacific region is concentrated in the lower level due to atmospheric dynamics. Little heat energy from either diabatic heating or transport processes can be used to expand the height thickness of 1000 - 200 hPa. The thickness between 700 and 500 hPa in the tropical eastern Pacific is approximately 10 - 30 gpm (Fig. 5.10). Such a magnitude is larger than that in the CPACP run (Fig. 5.4) and proves the importance of the diabatic heating change effect in the atmospheric height change in that forcing area.

c. Horizontal heat transport mechanisms in the PACP2 forcing run

The atmospheric heat transport mechanisms and their impacts on the tropical-wide atmospheric height change in the PACP2 run combine the primary features shown in both of the two isolated SST change structures in the CPACP2 and EPACP2 experiments. Such a property has been exhibited in the atmospheric height and circulation responses to the anomalous SST forcing over the Pacific (see Fig. 5.3b), and been discussed in the previous sections. Because of the similarity of the Pacific

SST perturbation pattern in Fig. 5.3b to the morphology of spatial structures in the SST interdecadal variability in Fig. 2.4, the analyses of the PACP2 run atmospheric heat transport processes may provide some insightful clues to address the issue of how the atmospheric transport mechanisms influence the maintenance of the tropical-wide geopotential height increase in the ENSO-like interdecadal atmospheric variability.

Fig. 5.32 shows the changes in the vertical mean of zonal heat flux and flux divergence in the PACP2 run. For the zonal heat flux change (Fig. 5.32a), it exhibits a westerly flux change in the upper tropospheric layer everywhere except the eastern Pacific where a large easterly flux change (greater than 1500 Kms^{-1}) is found. For the

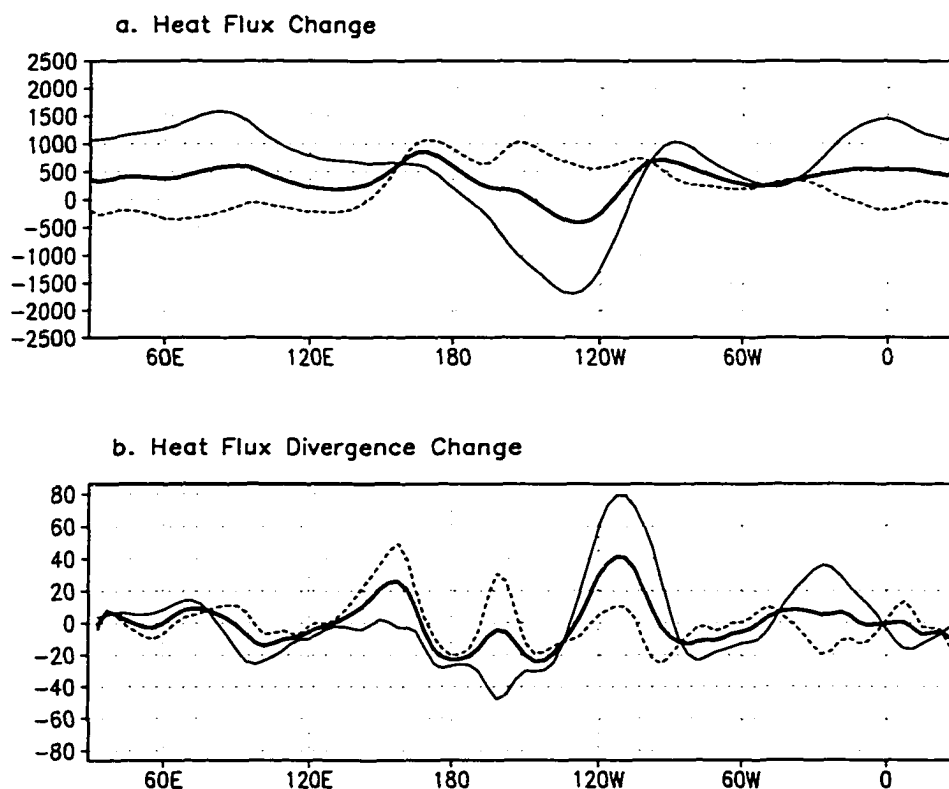


Figure 5.32 Same as Figure 5.26, except for the PACP2 run.

lower layer, a westerly flux change occurs over the central and eastern Pacific regions. The whole tropospheric layer shows a 300 - 600 Kms^{-1} westerly heat flux change, with an exception for the 160°W - 120°W sector in the eastern Pacific which has a 0 - 400 Kms^{-1} easterly heat flux change (Fig. 5.32a). It can be noted that the features in the Indian, Atlantic and the western and central Pacific regions are substantially dominated by the central Pacific SST forcing, whereas the eastern Pacific flux change is more similar to the change features found in the EPACP2 run. This statement appears to be true also for the heat flux divergence changes seen in Fig. 5.32b. However, the existence of the eastern Pacific anomalous SST forcing enhances the positive change in the upper level heat flux divergence near the 120°W area of the eastern Pacific in the CPAPC2 run (see Fig. 5.26b), and the magnitude of the divergence (40 Kday^{-1}) is nearly doubled. This is a consequence of the superposition of the two anomalous SST forcing because a small anomalous upper level divergence peak also exists near 120°W area in the EPACP2 run (Fig. 5.29b). Such a local zonal upper level heat source mainly provides the heat energy for the easternmost part of the eastern Pacific near the South American coast.

The changes in the meridional heat flux and its divergence are given in Figs. 5.33 and 5.34. The visual comparisons of the heat flux changes in Figs. 5.27, 5.30 and 5.33 indicate that the heat flux changes over the Indian Ocean, western and central Pacific and Atlantic regions predominately show the features arising from the central Pacific anomalous SST forcing. Similarly, the change structures in the eastern Pacific are primarily dominated by the local features due to anomalous SST perturbations over the eastern Pacific. However, as seen in the atmospheric circulation changes, the

anomalous eastern Pacific SST forcing amplifies the heat flux change features caused by the sole central Pacific SST perturbation in the CPACP2 run over the central Pacific region, whereas the change features found in the eastern Pacific area in the EPACP2 run are modified due to the appearance of the central Pacific SST perturbation in the PACP2 run. The northward heat flux increase is as large as 1200 Kms^{-1} or higher in the $10^{\circ}\text{N} - 20^{\circ}\text{N}$ part of the central Pacific (Fig. 5.33c), and the southward flux increase reaches 600 Kms^{-1} at 10°S , exhibiting a large amount of heat energy which is carried poleward by the anomalous meridional wind in the central Pacific. The upper level northerly heat flux change found on the north side of the equator over the Atlantic due to the central Pacific anomalous SST forcing (Fig. 5.27f) is amplified to almost 500 Kms^{-1} (Fig. 5.33f). In the eastern Pacific $120^{\circ}\text{W} - 60^{\circ}\text{W}$ area, the upper (lower) level northward (southward) heat flux increase south to 5°S and the upper (lower) level southward (northward) heat flux changes north to 5°S seen in the EPACP2 run (Fig. 5.30e) are enhanced in the PACP2 experiment (see Fig. 5.33e), particularly for the southern part of the area. The modulate effect of the central Pacific SST perturbation on the $160^{\circ}\text{W} - 120^{\circ}\text{W}$ eastern Pacific heat flux change is somewhat confusing as shown by in Fig. 5.30d and Fig. 5.33d. The features south to the 10°S in Fig. 5.30d are simply amplified due to the effect of the central Pacific anomalous SST forcing, whereas those to the north of the equator in the Fig. 5.30d is displaced southward and weakened.

The meridional heat flux divergence change is presented in Fig. 5.34 for the PACP2 run. The heat flux divergence change in the tropical region for the Indian Ocean (Fig. 5.34a) is less significant. The enhanced equatorward wind anomaly

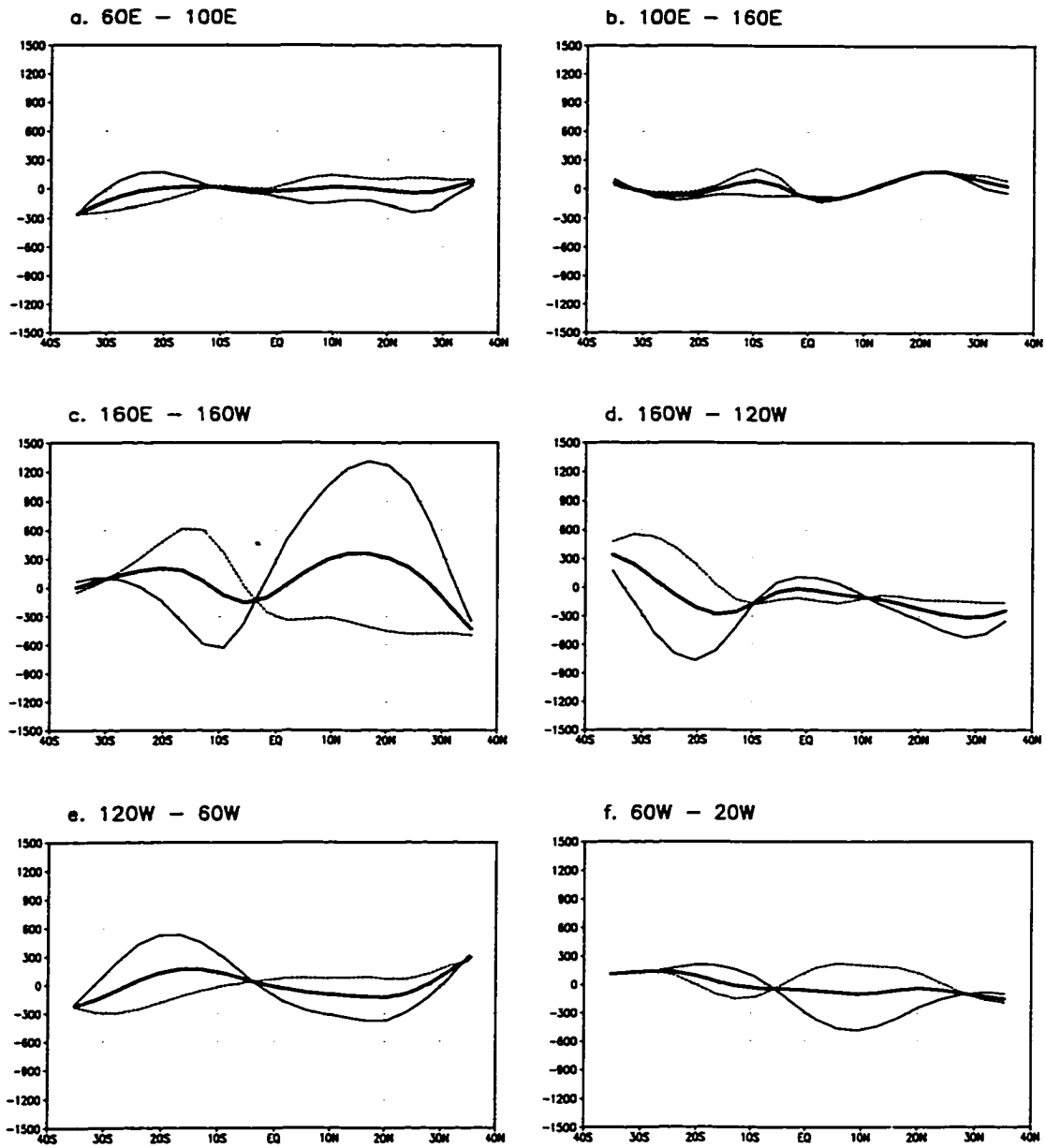


Figure 5.33 Same as Figure 5.27, except for the PACP2 run.

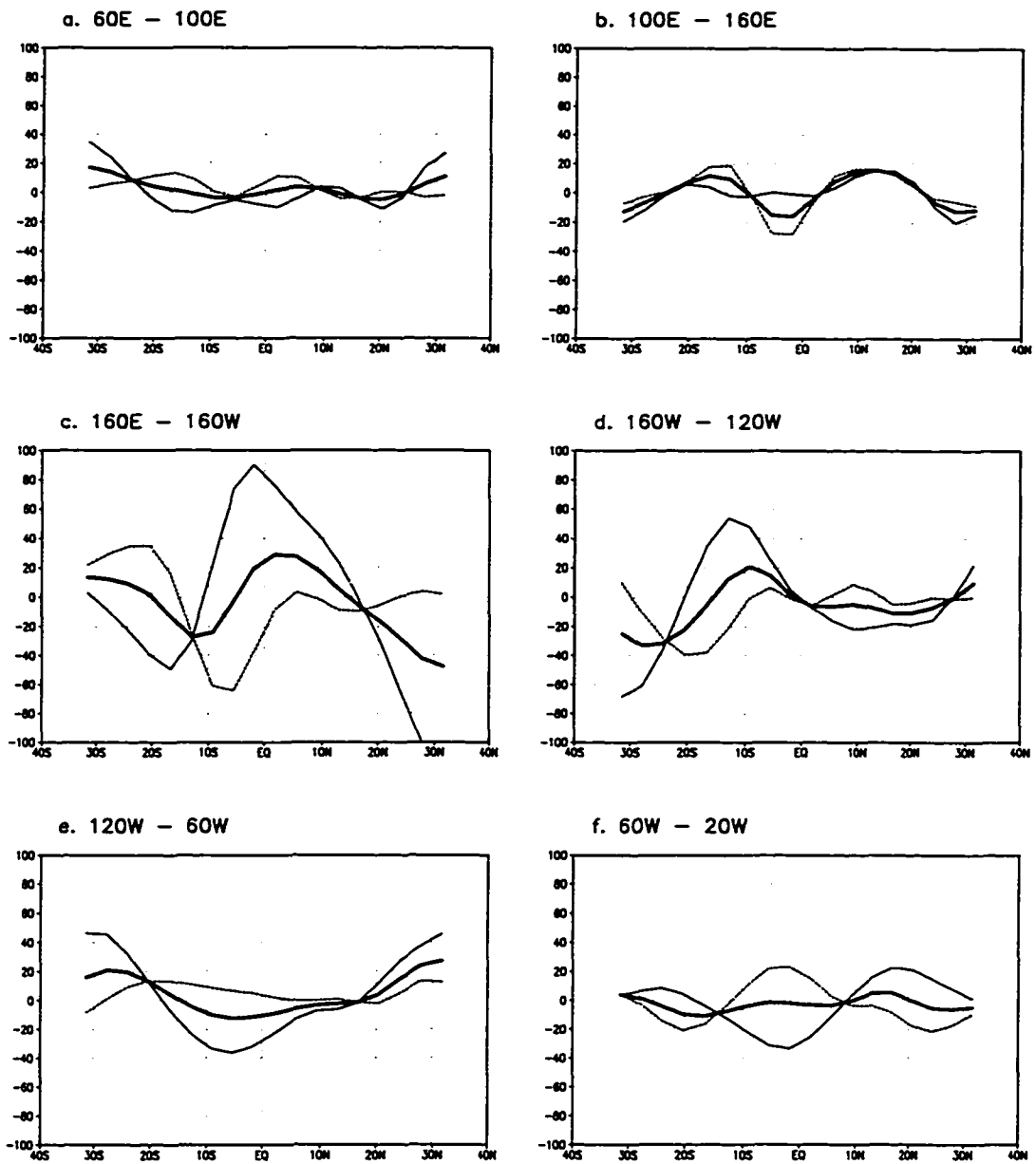


Figure 5.34 Same as Figure 5.28, except for the PACP2 run.

within the lower layer over the western Pacific leads to heat convergence (Fig. 5.34b) and contributes partly to warm the near surface atmosphere and increase the height at the lower levels in that area. In the central Pacific (Fig. 5.34c), the predominant heat flux change feature is a huge upper level anomalous heat divergence peak of about 90 Kday^{-1} in the tropical area. A large amount of heat energy is transported poleward and accumulated in the areas northward of 20°N and south to 15°S (Fig. 5.34c). Such anomalous heat energy sink locations are quite crucial in the transport mechanisms for the maintenance of the upper tropospheric height increase patterns. Over the 160°W - 120°W portion of the eastern Pacific (Fig. 5.34d), an anomalous heat source is seen in the upper layer from the equator to 20°S , whereas an upper layer heat sink with a less strength is situated northward of the equator. The atmosphere in the lower level near 20°S over the eastern Pacific (where a large anomalous surface convergence occurs) appears to receive heat from its north and south through heat transports (Fig. 5.34d). Heat convergence is also found in the 120°W - 60°W tropical eastern Pacific area in the upper layer (see Fig. 5.34e). The equatorial Atlantic is an upper level anomalous heat sink and lower level heat source in meridional direction as shown in Fig. 5.34f.

The key horizontal heat transport mechanisms for the maintenance of the middle and upper tropospheric geopotential height change structures shown in the interdecadal variation have been mostly illustrated and summarized in the discussions on the heat transport effects based on the two isolated ECHAM4 forcing experiments above. The comprehensive effect of superposition of the anomalous SST perturbations over the tropical central and eastern Pacific (see Fig. 5.3b) shows the importance of both SST change areas, and the major heat transport changing features

are the combination of the two anomalous forcing effects. The extent of the heat transport changes are amplified in some areas. The anomalous SST forcing over the equatorial central Pacific appears to have more impact on the height changes in the non-anomalous forcing regions.

d. Vertical heat transport in the PACP2 forcing run

In the previous discussions, it is indicated that the strong anomalous rising motion is responsible for the vertical heat transport from the lower and middle to upper troposphere over the tropical Pacific anomalous SST forcing regions. Fig. 5.35 illustrates the changes in the vertical heat flux (ωT) divergence for the six selected locations over the tropical oceans. The divergence of the vertical heat flux is calculated using the expression as the fourth term in (5.1) for both the CNTR and PACP2 runs. Since the vertical heat flux (ωT) is negative for the upward motion, the resultant vertical heat transport has a negative (positive) sign for the vertical heat flux divergence (convergence) in Fig. 5.35.

It can be clearly seen in Fig. 5.35a that the tropospheric layer above 400 hPa is a large anomalous vertical heat flux sink over the central Pacific area, with a maximum heat flux convergence of approximately 150 Kday^{-1} at 250 hPa. The heat is transported upward by the anomalous rising motion from the heat source in the middle and lower tropospheric layers. Another strong positive heat transport in the upper level is found in the area to the south of the equator over the eastern Pacific (Fig. 5.35d). This is one of the locations where the absolute SST exceeds 30°C (see Fig. 5.3b). Above the 500 hPa level, heat flux is convergent, whereas it is divergent below

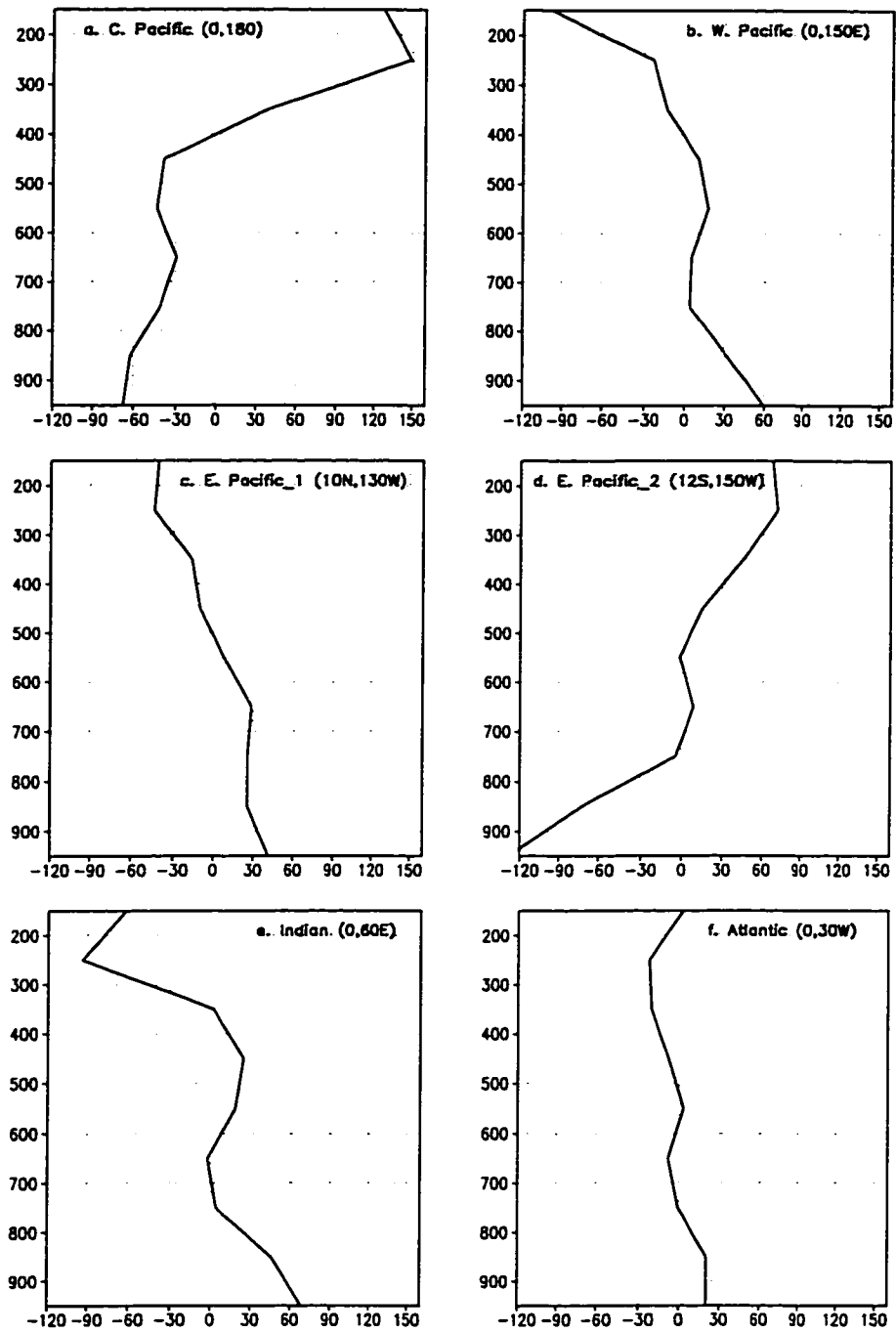


Figure 5.35 Profiles of the vertical heat flux divergence differences between the PACP2 and CNTR runs (PACP2 - CNTR) at the six locations in the tropics. Unit: Kday^{-1} .

700 hPa. In the northward location of the tropical eastern Pacific (Fig. 5.35c), it shows a moderate heat flux divergence and convergence (less about 30 Kday^{-1}) in the upper and lower tropospheric layers, respectively. This, in fact, can be inferred from the small anomalous diabatic cooling effect in the location seen in Fig. 5.21c. The anomalously positive surface forcing is not strong enough to induce an anomalous cumulus convection due to the suppression effect. From Fig. 5.35b and e, tropical western Pacific and Indian Ocean regions show a downward heat transport because of the anomalous sinking motions there. Little change in the vertical heat transport is found over the tropical Atlantic region (Fig. 5.35f).

e. A generalization of heat transport effects in the tropical-wide atmospheric height change

The heat transport mechanisms that are largely responsible for the upper level geopotential height change structures become more apparent when the transport processes over different regions are integrated using the results from the PACP2 run. Part of the anomalous diabatic heating generated in the central and eastern Pacific is carried upward by the strong rising motion (shown in Fig. 5.35), and transported poleward in the upper troposphere. For this boreal winter season case, the northward transport prevails at the upper level (see Fig. 5.17a). Driven by the wind circulation, such heat energy is then redirected eastward by the climatological westerly superpositioned by the westerly wind change in the PACP2 run in the regions of 15°N - 30°N and 15°S - 30°S . Such zonal heat transport mechanisms over the subtropical

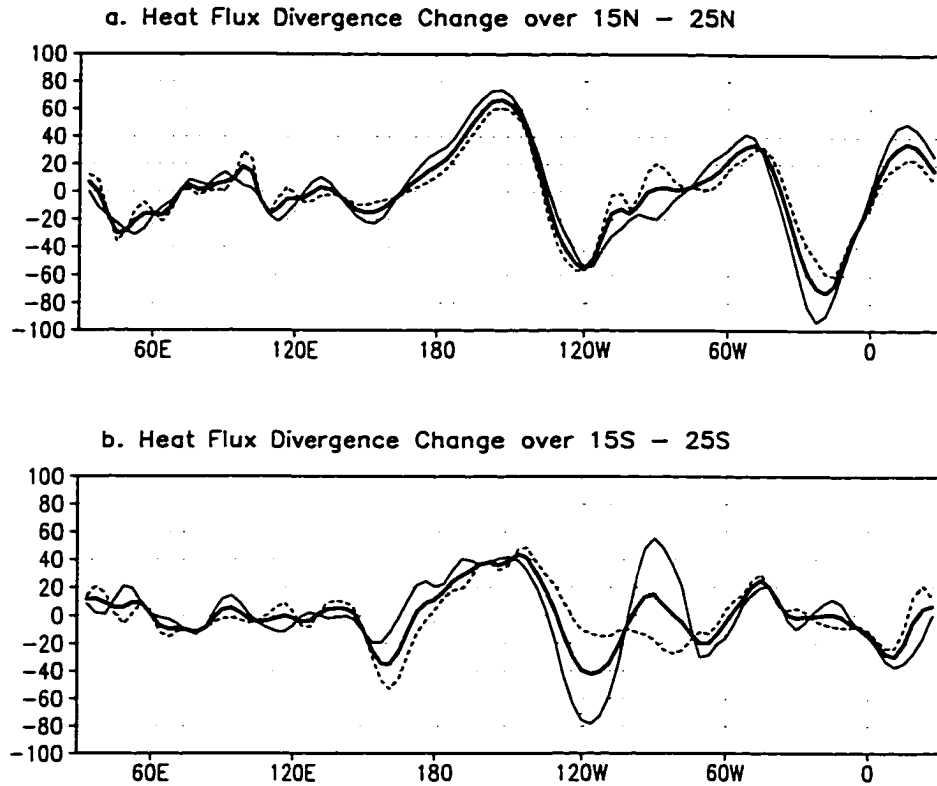


Figure 5.36 Mean heat flux divergence difference between the PACP2 and CNTR runs over (a) northern and (b) southern low latitudes. The thick line represents the vertical mean in the 200 - 1000 hPa layer. The thin solid line and dash line are the vertical mean in the 200 - 500 hPa and 600 - 1000 hPa layers, respectively. Unit: Kday⁻¹.

regions can be seen more clearly from Fig. 5.36 in which the changes in the average zonal heat flux divergences over the 15°N - 25°N and 15°S - 25°S belts are given. For both north and south sides, the central Pacific and 140°W - 160°W part of the eastern Pacific are the heat sources, whereas near the 120°W, zonal heat converges. In addition, the zonal heat energy accumulates in the Atlantic region on the north side (Fig. 5.36a). Such lower latitude zonal heat transport features are dominated by the structures found in the equatorial central Pacific anomalous surface forcing run. The

subtropical zonal heat transport in the EPACP2 run is quite small in general, except for the Atlantic region where a small zonal heat convergence exists on the north side (figures not shown). The meridional wind convergence will redistribute such heat to the deep tropical region in the eastern Pacific and Atlantic regions, and warm the local atmosphere. Furthermore, the extraordinarily strong northerly wind change in the upper level of these regions are found in the PACP2 run (see Fig. 5.17a). This greatly strengthens heat transport from the northern low latitudes to the equator and warms the local air in the tropical eastern Pacific and Atlantic regions, leading to a relatively large geopotential height increase shown in Fig. 5.16a. Hence, it can be concluded that the maximum geopotential height increase over the eastern Pacific is primarily an effect of both local diabatic heating and horizontal heat transport. Additionally, the dynamical consistency for the height and wind changes in the system is shown by the anomalous anticyclonic flow changes (see Fig. 5.17a). The upper level height increase over the tropical Atlantic region can be largely attributed to the heat transport through the mechanisms discussed above. In addition, the adiabatic sinking effect in the equatorial plane (see Fig. 5.13a) is also important to the geopotential height increase in the tropical Atlantic Ocean.

The diabatic heating increase and atmospheric heat transport are largely responsible for the geopotential height increase over the eastern Pacific surface forcing area. However, the height increase in the regions away from the local heating source at the middle level (500 hPa, see Fig. 5.16b) can not be easily explained using the horizontal heat transport in the lower layer. More complex dynamical processes may be involved for the height change pattern at 500 hPa. The height increase over the

Indian and western Pacific Ocean occurs mostly in the lower atmosphere, i.e., the thickness between the 1000 and 200 hPa changes little (Fig. 5.16). The lower level height increase can be largely attributed to the dynamical effect of the anomalous sinking motion. Because of the anomalous SST forcing in the equatorial central Pacific, the maximum rising motion is shifted toward the central Pacific and the normal strong upward motion in the western Pacific and Indian Ocean is suppressed as shown in Fig. 5.6b. This leads to a less surface level air convergence and a positive height change in the near surface atmosphere. The lower level does show a certain amount of heat energy convergence over the tropical western Pacific (Fig. 5.25b) which may affect the lower level height change there.

Chapter 6

Further discussions on the results from the analysis and model simulations

6.1 Tropical atmospheric interdecadal variability and the idealized simulations

The model experimental design in this study arises from the idea that the GCMs are capable of generating the global climatology, given the specific external conditions. For the boreal wintertime, the periods before and after the 1976/77 winter are considered to have two system background states, in agreement with the time fluctuations of the tropical atmospheric geopotential height and sea surface temperature shown in Figs. 2.3, 3.1 and 3.5. On the decadal time scale, it is believed that the tropical ocean change is the trigger for the studied atmospheric interdecadal variation (Lau and Nath 1994). This research aims at investigating the physical mechanisms and processes in the climate system that are responsible for *how* the two background atmospheres differ, instead of attempting to seek the reasons for *why* the ocean surface state experiences a sharp jump in the winter of 1976/77. Hence, comparison of the diagnostic analyses of the modeling simulations may provide some key differences of the physical and dynamical processes in the simulated atmospheres under certain idealized experimental designs which attempt to model what has happened in the real world.

In the previous chapters, it has been shown by visual comparison that the model experiments do simulate the major features of the studied atmospheric variations reasonably well. However, it is necessary and important to point out that the modeled atmospheres are not the real atmosphere. The changes of the ocean boundary conditions in the experiments are exaggerated to force the atmosphere to respond vigorously enough so that the mechanisms of the atmospheric changes can be examined and analyzed. Furthermore, the NCEP/NCAR reanalysis data are also generated by the model. Since the observations over tropical regions are sparse, one needs to exercise caution when interpreting specific features or using them as a validation. Despite this, previous scientific findings (Nitta and Yamada 1989; Graham 1994; Richman 1994; Trenberth and Hurrell 1994) offer strong evidence of the tropical atmospheric interdecadal variation found herein using the reanalysis data.

Further comparison of the tropical atmospheric variations from the NCEP/NCAR reanalysis, IMGa climatological run data and the present idealized experiments may assist evaluation of the key features in the atmospheric changes resulting from the ECHAM4 GCM and the model's capability of simulating the atmospheric variability. As described in the previous chapters, from Figs. 3.3, 3.7 and 4.3, the key feature is a tropical-wide atmospheric height change in the middle and upper troposphere which can be seen in all these results. The interdecadal changes in the NCEP/NCAR reanalysis are more complicated than the model results. The model simulations simplify the spatial changes in the atmosphere. For the 200 hPa level, the reanalysis height change (Fig. 3.3) exhibits the relative maxima over the equatorial western Pacific and the eastern Pacific, whereas the IMGa climatological run gives a

tropical-wide change pattern with a rather smooth zonal gradient (Fig. 3.7). For the idealized simulation (PACP1 - PACN1, Fig. 4.3), the maximum of the tropical height change occurs over the eastern Pacific portion. This is because the effect of the surface changes over the tropical central and eastern Pacific are stressed and exaggerated in the experiments. The maximum height increase north of the equator over the eastern Pacific is in good agreement with that found in the reanalysis data, except the center slightly displacing southward. Under the experimental designs, the simulations are not able to produce the maximum height change over the tropical western Pacific. In the middle tropospheric level, though a tropical-wide height increasing pattern exists, the maximum changes are found over the tropical Indian Ocean and part of the western Pacific regions in the reanalysis (Fig. 3.3b). Such a feature can not be well simulated in either the IMGa climatological run or the idealized experiments (Figs. 3.7 and 4.3). This suggests that there are certain processes acting here other than the anomalous diabatic heating over the Pacific. Moreover, the differences in the physical parameterizations in the NCEP/NCAR reanalysis and the ECHAM4 GCM may be partially accountable for such a different height change pattern at the 500 hPa level. In the lower troposphere (e.g. 700 hPa), the height increasing spatial features in the idealized experiments (Fig. 4.3c) visually match those of the reanalysis (see Fig. 3.3c) over the Pacific and Indian Ocean regions reasonably well. It is believed that effects of the anomalous cumulus convection becomes less dominant at this level, compared to that in the middle and upper tropospheric layers. Hence, the atmospheric heating and warming effects over the Pacific regions are less overwhelming, and the Indian and western Pacific regions

show larger height increase. Both the IMGGA climatological run and the idealized simulations yield a height change pattern at the near surface level (Figs. 3.7d and 4.3d) largely different from that of the reanalysis data over the eastern Pacific. While the atmospheric processes near the surface are more complicated and difficult for any of the GCMs to simulate, the height change pattern at the 1000 hPa level over the eastern Pacific resulting from the ECHAM4 gives the structures which should be expected to occur given the anomalous SST changes in Fig. 4.2.

The idealized model simulations are able to reproduce the major features of the wind vector changes in the studied interdecadal variability as shown in the reanalysis data. The upper level tropical easterly anomalous wind over the eastern Pacific is seen both in the reanalysis and idealized simulations (Figs. 3.4a and 4.5a). Additionally, westerly anomalous wind can be found over the northern lower latitude regions in the Pacific. Since the upper level anomalous poleward wind changes shown in the simulation results are much less strong in the reanalysis data, the pronounced anticyclonic wind change northward of the equatorial eastern Pacific in Fig. 4.5a can be not seen clearly in the reanalysis data, though weak anticyclonic wind change does exist in that geographical area (Fig. 3.4a). At the lower level, the equatorial central and eastern Pacific westerly change appears to be the key feature in both the reanalysis and the idealized simulations (Fig. 3.4b and 4.5b). In general, wind change structures over the North Pacific area for the reanalysis and idealized simulations agree well. However, the IMGGA climatological run is not able to generate the primary features for the wind changes seen in the reanalysis.

Although the model simulations yield certain major patterns and structures of the interdecadal tropospheric variability, some inconsistencies can also be noticed, especially at the lower levels. One of them is the change features in both the height and wind in the eastern Pacific area near 10°S - 30°S produced by the ECHAM4 GCM. The IMGGA climatological run data shows a relatively large surface pressure decrease and cyclonic vorticity change in that region for the two different periods studied (Figs 3.7d and 3.8b), indicating an enhancement of the SPCZ. Such a change is largely due to the eastern Pacific SST changes, and is supported by the results from the idealized ECHAM4 simulations (Figs. 4.4d and 4.5b). It seems that the ECHAM4 GCM is more sensitive at the lower level to the surface temperature over the south eastern Pacific. This leads to the difference of the ECHAM4 near surface height and wind change patterns from those given in the reanalysis data. It is not clear that whether such an inconsistency is attributed to the ECHAM4's over-estimation in the physical parameterization schemes or the inaccuracy of the parameterization schemes in the model used to carry out the NCEP/NCAR reanalysis.

The lower level height and wind change features over the equatorial Indian and Atlantic Oceans yielded in the idealized simulations appear to be less satisfactory. This is because the designs of the experiments emphasize on the impact of the tropical Pacific SST changes and neglect the interdecadal SST changing structures over the tropical Indian and Atlantic regions as shown in see Fig. 2.4.

In general, the ECHAM4 GCM's capability of simulating the general features in the atmospheric changes due to the anomalous surface forcing changes appears to be encouraging. The major change structures shown in the tropical atmospheric

interdecadal variability from the reanalysis data, such as the tropical-wide geopotential height increasing and the weakened east-west Walker circulation, can be largely and reasonably modeled. Therefore, it is possible to encourage further application of the ECHAM4 GCM to perform the experiments which generate different atmospheres representing the climate states for the Period 1 and Period 2, respectively. The diagnostic analyses on the differences in the atmospheric processes for different atmospheres can provide a good deal of physical insight to the studied tropical interdecadal variability.

6.2 Extratropical atmospheric responses to the tropical SST changes

The global climate can be thought of as a closed system and any perturbations therein may cause the changes and responses in the whole system. As indicated from the past literature review, the studied interdecadal variation with a breakpoint in the mid-1970s involves both tropical and extratropical atmospheric changes in the climate system. The major changes over the extratropics reported by some previous researchers (Nitta and Yamada 1989; Trenberth and Hurrell 1994; Graham 1994; among others) include the intensification of the PNA teleconnection pattern, the deepening of the Aleutian low and southward shift of the North Pacific storm track. Based on their GCM experiments forced with different prescribed SST conditions, Lau and Nath (1994) find that the tropical SST is the major driven force for the global circulation and the interdecadal variations of the extratropical atmosphere are due primarily to the anomalous SST over the tropics.

To validate the idealized model simulation designs in this research and further investigate the effects of the tropical Pacific anomalous SST on the extratropical atmosphere, a limited number of detailed analyses discussions based on the ECHAM4 simulation data over the Northern Hemisphere are presented in this section.

6.2.1 Northern Hemisphere height changes

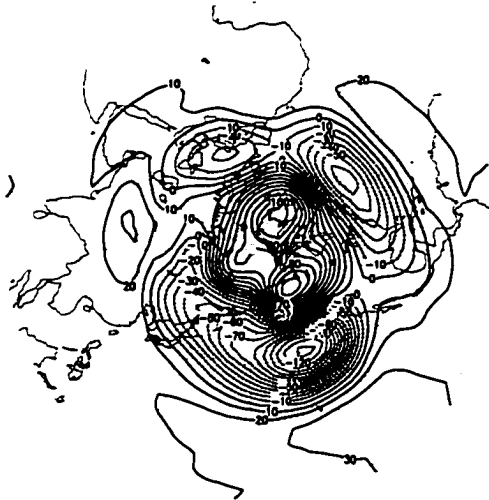
In Nitta and Yamada's (1989) landmark study of the mid-1970s interdecadal climate variability, a Northern Hemisphere tropospheric geopotential height change with a PNA-like structure has been associated with the interdecadal variation. Subsequent researches have confirmed their findings (e.g. Graham 1994; Lau and Nath 1994). This implies that a successful simulation of the studied interdecadal variability should be able to generate an enhancement of the PNA intensity in the Northern Hemisphere geopotential height change pattern. Fig. 6.1 presents the geopotential differences at 500 hPa for the 4 analysis sets from the idealized simulations as used in the previous two chapters.

It can be discerned in Fig. 6.1 that a wave-like pattern in middle and high latitudes is the dominant structure in the geopotential height change. Such a change structure exhibits some similarities to the canonical PNA pattern in Wallace and Gutzler (1981) and the height difference (PNA-like) associated with the mid-1970s interdecadal variability found by several previous investigators (Nitta and Yamada 1989; Lau and Nath 1994; among others), although certain discrepancies can be noted. The difference between PACP1 and PACN1 runs is used to model the interdecadal

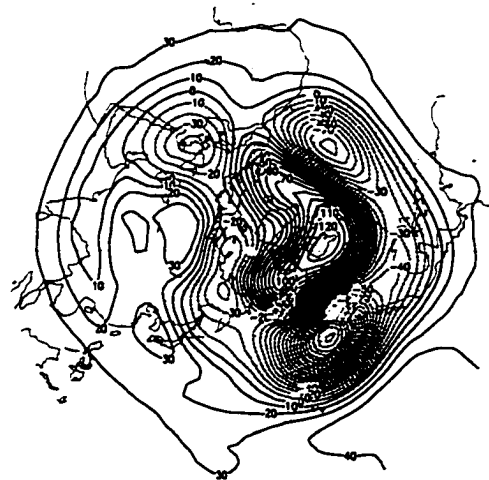
variation for a specific atmospheric variable in Chapter 4. The geopotential height change in these idealized simulations (Fig. 6.1a) shows a spatially extensive Pacific trough centered near 150°W at 40°N, flanked by a tropical/subtropical ridge in the eastern Pacific and a ridge in Canada and northern United States. A trough, centered at the North Atlantic, extends to the southeastern United States. An integration of these structures displays a middle tropospheric height configuration similar to the observed height difference pattern between the 1977-1986 and 1967-1976 winters given by Nitta and Yamada (1989, their Fig. 6) and the model simulated height pattern in Lau and Nath's TOGA model run (1994, their Fig. 8). The pronounced positive height anomaly over the Greenland and a small height increase center over Asia are not the features in the canonical PNA pattern. Such an atmospheric height response pattern indicates that, when the SST anomaly pattern as shown in Fig. 4.2 occurs, the height changes in the action centers in PNA will be intensified. Simultaneously, the anomalous surface forcing can trigger other changes in the global circulation. Fig. 6.1a shows that the northern Pacific center appears to be most prominent in the height change centers, which is actually a typical feature in the PNA pattern (Wallace and Gutzler 1981; Trenberth and Hurrell 1994).

The differences between a specific forcing run and the control run have been utilized in Chapter 5 to diagnose the physical mechanisms and processes in the atmosphere for the interdecadal variability. Such an approach ensures that the atmosphere responds strongly enough to the anomalous forcing so that the physics can be investigated. This can be used to evaluate the relative importance of various SST change patterns over different geographical areas on the Northern Hemisphere

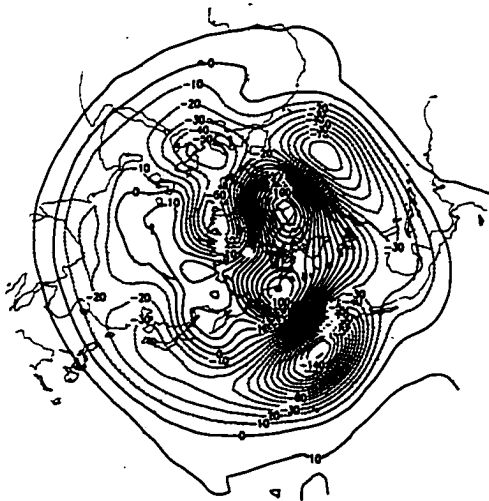
a. 500 hPa height difference (PACP1 - PACN1)



b. 500 hPa height difference (PACP2 - CNTR)



c. 500 hPa height difference (CPACP2 - CNTR)



d. 500 hPa height difference (EPACP2 - CNTR)

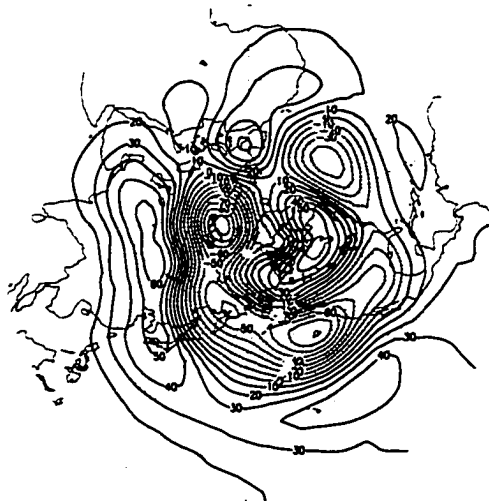


Figure 6.1 Northern Hemisphere 500 hPa height difference fields between a. the PACP1 and PACN1 runs, b. the PACP2 and CNTR runs, c. the CPACP2 and CNTR runs, and d. the EPACP2 and CNTR runs. Contour interval is 10 gpm.

circulation changes. Fig. 6.1b gives the height change for the PACP2 run, and it represents the combination effect of the anomalous SST changes over the tropical central and eastern Pacific. The difference field in Fig. 6.1b exhibits generally the similar spatial structures to those seen in Fig. 6.1a, with certain changes in the intensity and position of the centers. Due to the extraordinarily strong anomalous forcing, every change center's intensity is enhanced, exhibiting a maximum change value greater than 200 gpm in the northern Pacific low pressure action center. The equatorward height increasing node of the PNA-like structure appears to exceed 40 gpm over the eastern Pacific. The high pressure center of action over the northern portion of the North American Continent becomes more pronounced and intensified and shifts slightly southeastward, accompanying by an approximately 20° eastward displacement of the North Atlantic low height center (Fig. 6.1b). In Fig. 6.1c and d, the 500 hPa height difference structures produced by the CPACP2 and EPACP2 forcing runs are displayed. It shows that both the anomalous SST perturbations over the tropical central and eastern Pacific can yield certain types of teleconnection structures, and all the PNA height change centers are present in these difference fields, along with some other non-PNA change structures. However, it is quite evident that most of the height change structures shown in Fig. 6.1a and b are dominated by the features in the CPACP2 and CNTR run difference (Fig. 6.1c), indicating a prominent effect of the equatorial central Pacific SST anomaly on the global atmosphere. The positions and strengths of the PNA action centers shown in Fig. 6.1c are quite comparable to those generated by both the SST anomalies in the central and eastern Pacific (Fig. 6.1a and b), except for the height change center over the

tropical/subtropical eastern Pacific. The eastern Pacific SST anomaly provides much of the changing in the tropical/subtropical region of the eastern Pacific, and is more responsible for the equatorward action center of the eastern Pacific due to the relatively local impact of the anomalous cumulus convection (Fig. 6.1d). In addition to the canonical PNA pattern features, a geographically extensive ridge with a change (greater than 30 gpm) is found over the Eurasia continent and western portion of North Pacific. Also, the strengths of the height changes centers over the extratropics are rather weak as seen in Fig. 6.1d.

One of the physical and dynamical mechanisms which lead to the intensification of the PNA teleconnection pattern can be attributed to the upper level anomalous westerly wind over the northern subtropical Pacific area as shown in both reanalysis data and the GCM experiments (see Figures 3.4, 3.8, 4.5, 5.5, 5.11 and 5.17). Such a westerly wind anomaly is largely induced by the earth rotation effect on the strong upper level poleward wind over the central and eastern Pacific. The increase in the westerly shear with altitude results in an atmospheric temperature decrease over the northern Pacific region based on the thermal wind relation, which contributes to the geopotential height anomaly dipole found in the PNA structure.

The comparisons of the Northern Hemisphere atmospheric height responses to the surface forcing anomalies over different geographical areas in the Pacific indicate the importance of the equatorial central Pacific SST in the global climate system. Even for the dominant mode in the atmospheric circulation changes like the PNA can be triggered by the anomalous SST change over the central Pacific. This can be implied by the fact that the equatorial central Pacific SST anomaly induces stronger

upper level northward wind anomaly and more intensified subtropical westerly increase (see Figures 5.5 and 5.17). For the PNA-like height change structures associated with the mid-1970s interdecadal atmospheric variation found in this and previous studies, the SST changes over the eastern Pacific is of secondary effect. In a comprehensive study using three sets of the GFDL GCM model experiments (their GOGA, TOGA and MOGA runs), Lau and Nath (1994) have shown the dominance of the tropical SST changes in the global circulation. However, the model experiments in this study explicitly demonstrate that much of the tropical ocean SST predominant effect in the interdecadal SST variation arises from the central Pacific.

6.2.2 Wind circulation changes over the North Pacific

The cyclonic surface circulation change over the North Pacific is another significant feature associated with the mid-1970s interdecadal variation in the global climate system (e.g. Trenberth 1990; Lau and Nath 1994; Zhang et al. 1997). Such a wind change structure is quite important in the extratropical air-sea interaction and is believed to be a key process that leads to the North Pacific ocean SST interdecadal variation structure (Trenberth and Hurrell 1994; Lau and Nath 1994). Fig. 6.2 shows the horizontal wind vector difference fields at 1000 hPa over the Pacific computed from the model run results in this study, and agrees largely with the surface wind change structures found previously in both analysis and model simulation results (Lau and Nath 1994; Zhang et al. 1997).

The wind difference field between the PACP1 and PACN1 forcing runs is considered as an idealized simulation to the interdecadal SST variation, and shown in Fig. 6.2a. A quite large cyclonic wind change is found over the North Pacific (Fig. 6.2a), with a northerly wind anomaly in the central and western North Pacific and considerable southerly lower level wind anomaly in the eastern Pacific along the North American coast. The southerly surface wind anomaly advects warmer and moister air along the west coast of North America and Alaska, whereas the northerly anomalous wind carries colder water to the central and western North Pacific. Consequently, there are increases in temperatures and SSTs along the west coast of North America and Alaska but decreases in SSTs over the central North Pacific as documented in Trenberth (1990). To the south of the equator, a wind convergence can be seen near the central Pacific, and a cyclonic surface wind change exists in the eastern Pacific. The main features in Fig. 6.1a exhibit a consistency with the model experiment results in Lau and Nath (1994, their Fig. 15a) and Zhang et al. (1997, their Fig. 11).

Fig. 6.2b shows the wind change caused by the SST perturbation patterns over the central and eastern Pacific (Fig. 5.3). Interestingly, the wind changing features appear to be closer to the Lau and Nath (1994) GCM long-term integration results. Strong northerly wind changes over the central and even part of the eastern North Pacific, and southerly wind anomalies are confined to the narrow area along the west coast of North America. Such a North Pacific wind change pattern can be largely attributed to the strong anomalous SST forcing over the equatorial central Pacific. This isolated effect can be seen by comparing the two wind change fields from the

experiments of SST perturbations over the central and eastern Pacific regions. Fig. 6.2c indicates that the cyclonic surface wind change over the North Pacific is dominated by the equatorial central Pacific SST forcing. The SST perturbation over the eastern Pacific region does not generate the North Pacific surface wind changing features as shown in Fig. 6.2b (see Fig. 6.2d), although it shows a relatively weak cyclonic anomaly. On the other hand, the cyclonic wind change over the south eastern Pacific is totally dominated by the changing structures due to the eastern Pacific SST anomalous change (Fig. 6.2d), indicating the dominance of the eastern Pacific SST change in the intensification of the SPCZ. From these comparisons, it can be confirmed once again that, given the tropical anomalous SST pattern found in the Pacific interdecadal variability, the extratropical atmospheric change features over the North Pacific and North America are dominated by the forcing anomaly over the equatorial central Pacific. The remote effect of the anomalous SST over the eastern Pacific is of secondary importance. However, the local effect of the anomalous SST over the eastern Pacific is a key to the changing features found over the tropical eastern Pacific region.

The wind changes in middle troposphere is given in Fig. 6.3. Cyclonic wind change is seen over the eastern portion of the North Pacific and west coast of North America (Fig. 6.3a, b and c). The strength of westerly wind is enhanced to the south of about 35°N and weakened to the north. Such a circulation change pattern have a large impact on the local climate over the Northern American coast. The inland wind and southerly wind anomalies may lead more precipitation over California and other areas along the coast.

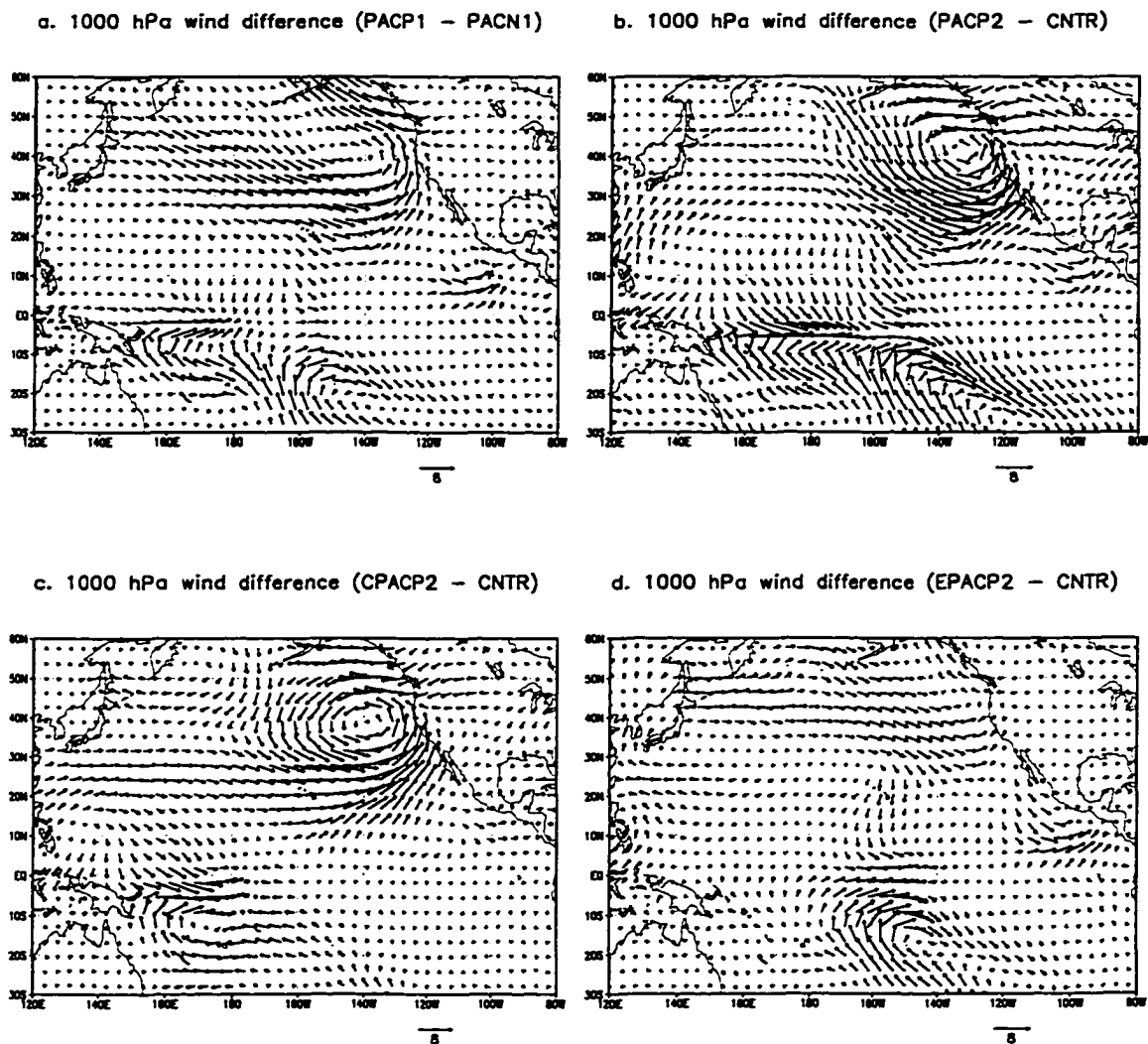
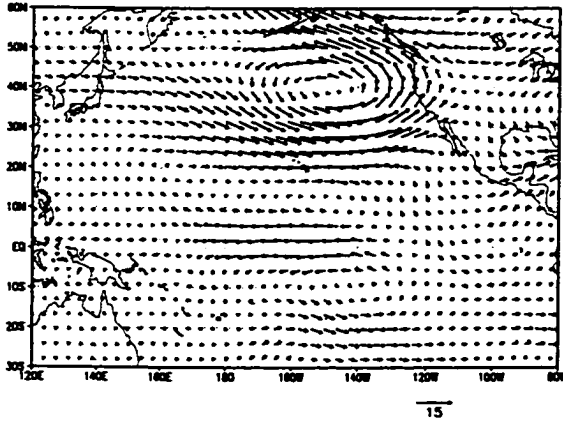
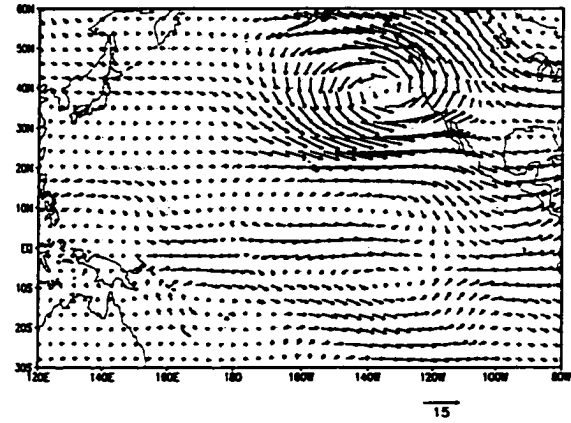


Figure 6.2 1000 hPa horizontal wind vector difference fields between a. the PACP1 and PACN1 runs, b. the PACP2 and CNTR runs, c. the CPACP2 and CNTR runs, and d. the EPACP2 and CNTR runs. Unit: ms^{-1} .

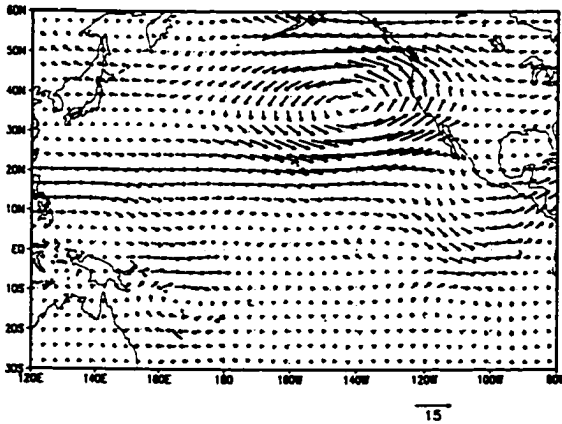
a. 500 hPa wind difference (PACP1 - PACN1)



b. 500 hPa wind difference (PACP2 - CNTR)



c. 500 hPa wind difference (CPACP2 - CNTR)



d. 500 hPa wind difference (EPACP2 - CNTR)

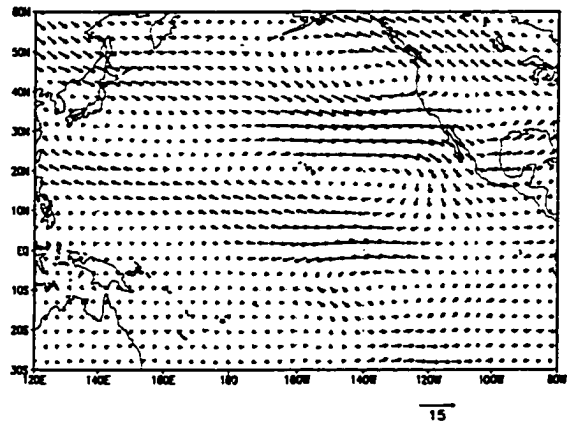


Figure 6.3 Same as Figure 6.2, except for 500 hPa.

The primary configurations in the studied interdecadal atmospheric variability over the tropics and extratropics, documented in the previous observational analyses and model experiments, have been well matched by the results from the ECHAM4 model simulations in the present research. Such a consistency adds confidence about the idealizations in the experiments presented herein. Hence, it is believed that the forcing run simulations are scientifically sound methodology for generating climate states representing the winter atmospheres for the periods before and after the 1976/77 winter respectively, although the magnitudes and spatial structures of the prescribed SST perturbations are exaggerated.

Chapter 7

Summary and conclusions

Previous studies have indicated that the tropical SST records exhibit an interdecadal-scale variation in mid-1970s. Associated with such a change, the extratropical atmosphere and ocean have also experienced significant variations on the same time scale. The objectives of this dissertation are (1) to study the structures of the interdecadal variations in the tropical-wide geopotential height increase and corresponding atmospheric circulation changes; (2) to establish a relationship between the studied tropical atmospheric and oceanic interdecadal variability; and (3) to investigate the physical and dynamical mechanisms which are responsible for the formation and maintenance of the spatial features of the interdecadal variations of the tropical geopotential height field. The present study focuses on the contribution of the tropical Pacific SST change to the atmospheric interdecadal variability. Reconstructed Reynolds's SST data, NCEP/NCAR reanalysis and outputs of an IMGA climatological integration (ECHAM4 GCM) have been used to explore the sudden jump in atmospheric and oceanic mean states in the mid-1970s. Through several idealized model simulations and diagnostic analyses of those experimental outputs, the ECHAM4 GCM serves as the tool for investigating those mechanisms responsible for the atmospheric interdecadal variability.

The results of the present study show that, in addition to the extratropical atmospheric variations reported in the previous studies, the tropical atmosphere also

exhibits an interdecadal variation for boreal winter season, with a pronounced feature of tropical-wide geopotential height increase around the global circle after the mid-1970s, particularly in the upper troposphere. Such a scientific finding expands our knowledge of the global atmospheric interdecadal variation in the mid-1970s. Such tropical atmospheric height changes are found to be dynamically consistent with the change features over the extratropics in previous studies, which indicates that both the extratropical and tropical atmospheric variations in mid-1970s are ingredients of the systematic atmospheric interdecadal variability on the globe, and are closely related to the changes in tropical SST fields.

Another major contribution of this work to the knowledge base of the interdecadal variations in the mid-1970s is the methodical investigation of the mechanisms in the atmospheric changes through detailed GCM simulations. Based on the interdecadal-scale temporal variations in the tropical SST and atmospheric geopotential height fields for boreal winter, the two periods (one prior to and one post mid-1970s) are considered to have different basic background climates. Such a concept forms a fundamental basis for the unique designs of the idealized GCM simulations which, in turn, enable the diagnosis of the physical and dynamical mechanisms leading to the spatial structures in the atmospheric changes. Diabatic and adiabatic processes and heat transports play important roles in the tropical-wide height increase. The synthesis of these processes largely provides the answers to how the atmosphere links to the SST changes and why the atmospheric changes exhibit the structures which are revealed in the data analyses.

7.1 Interdecadal variations over the tropical oceans and atmosphere

The leading PC mode from the low-pass filtered SST anomaly data displays a large positive spatial SST anomaly structure over the central and eastern Pacific. The temporal variation of the spatial pattern exhibits a notable variation on a decadal time scale, with a salient basic state jump in 1976/77 winter. The SST anomaly basic state is below the long-term average for all boreal winter months prior to 1977. During the winters of 1977-1980, the SST anomalous pattern makes a sharp transition to a state of +1-unit standard deviation of the SST anomaly, and then oscillates in the new background state afterward. The SST difference field, which corresponds to the winter from 196/77 onward minus the winters prior to 1976/77, largely resembles the spatial structure given by the leading PC loading pattern. Hence, the tropical monthly mean background SST has changed since 1976/77 for boreal winter. Such a finding agrees with the results from previous studies of Nitta and Yamada (1989), Graham (1994) and Zhang et al. (1997).

One significant finding of this research is that the tropical atmosphere has also shown a similar temporal variation pattern to that in the tropical SST field during the studied time-span. In the spatial patterns of the leading geopotential height PC modes, based on the NCEP/NCAR reanalysis, the dominant spatial feature is a tropical-wide height change structure around the globe through the entire troposphere. As altitude increases, the zonal structure expands poleward, and the meridional height change gradient becomes stronger in the subtropical regions of the central and eastern Pacific. The temporal fluctuation of this tropical-wide height mode exhibits a strikingly consistent trend and sudden jump in the 1976/77 winter with the SST interdecadal

variation for all the levels in the troposphere. Accordingly, the whole tropical-wide atmospheric height oscillates in the same phase and the phase changes in the mid-1970s. Prior to the 1976/77 winter, the tropical height field is in a negatively anomalous time period, and it reverses after the 1976/77 winter jump. The mean height difference fields between the two time periods prior to and post the 1976/77 winter exhibits similar tropical-wide height increase structures for all the levels, but with more small spatial structures. The height increase in the upper troposphere is larger than that at the lower levels. The interdecadal variability of the tropical atmosphere is physically and dynamically more consistent in middle and upper troposphere as certain processes (implied by the leading PC mode) prevail there. Since the leading PC modes account for a large percentage of the total variance in the geopotential height field, especially at the upper levels (in agreement with Richman, 1994), the structures of these leading PCs can be regarded as the variations of background state of the tropical atmospheric field, and apparently the background state of the tropical atmosphere has a shift in the mid-1970s for boreal winter.

The atmospheric height change structure exhibits a strong dipole over the North Pacific area above the 700 hPa level. This research adds to the body of knowledge of the atmospheric interdecadal variability as it ties the tropical variations into the extratropical features (such as the PNA pattern) as reported by previous investigators (Nitta and Yamada 1989; Lau and Nath 1994; Graham 1994; Richman 1994; Zhang et al. 1997; among others). The importance of this is that the changes in the mid-1970s is a systematic one in the global system. The tropical atmospheric

changes found in the present research and the extratropical changes reported in previous studies are a first step in identification of the full atmospheric variability.

The discontinuity in the tropical atmospheric height variation on a decadal scale in mid-1970s is supported by the results from similar analyses using the data from the IMGA climatological integration forced with the observed monthly mean SST fields. Except for the near surface level, there exists a tropical-wide height increase after the mid-1970s for boreal winter season in the model simulated atmosphere. The atmospheric height background shifts in the mid-1970s in both the reanalysis and GCM integration, matching well by visual comparison; therefore, it is reasonable to infer that they are likely driven by the same mechanisms (the ones used to force the GCM). Moreover, there is a high correlation (0.87 - 0.97) between the atmospheric height and the tropical SST interdecadal variations, further suggesting that the tropical ocean is likely to be the driving force of the climate system, and that the interdecadal variability in the reanalysis and those difference fields (used in the analyses) in the model simulated atmospheres are the correct atmospheric response to the surface force variation on an interdecadal time scale.

7.2 Idealized model simulations of the atmospheric interdecadal variation

The GCM experiments are performed in an attempt to simulate the characteristic structures exhibited in the interdecadal variability of the tropical atmospheric height field. Two SST fields, representing the boundary conditions for the two time periods prior to and after the 1976/77 winter, are generated for the model

runs to investigate the effect of the surface change in the mid-1970s. The resulting difference of the two simulated atmospheres is considered to represent the interdecadal atmospheric changes.

The geopotential height difference fields of the two forcing runs show large similarities to the change patterns found in the NECP/NCAR reanalysis and IMGa climatological run data. A height increase structure appears over nearly the entire tropical region in the troposphere, except for the near surface level. The positive height change increases with altitude, with the most notable changes in the upper troposphere (200 hPa). In the middle and upper troposphere, the largest height increase is found over the central and eastern Pacific, and the PNA-like height change structure is quite pronounced. In the lower tropospheric layer, the height increase over the Indian and western Pacific Oceans appears to be most dominant. Idealized prescribed anomalous SST patterns and the diabatic heating increase which arises from those SST changes are believed to be the primary reasons for the stronger height increase in the upper level of the central and eastern Pacific regions. The wind circulation changes show a significant easterly change in the upper layer and westerly change in the lower layer over the tropical Pacific, indicating a weakening of the Walker circulation. Such a tropical zonal circulation change is in agreement with the early finding in Nitta and Yamada (1989). The strongest rising motion area over the tropics shifts to the central Pacific and the local Hadley cell there is enhanced greatly. This circulation change is consistent to the changes found in the reanalysis data.

The idealized GCM experiments presented herein have successfully simulated the primary structures of the tropical atmospheric interdecadal variability, thereby

providing strong evidence of correlation between the tropical atmospheric height variation and the surface forcing. Moreover, it implies that the tropical Pacific forcing change is, at least, one of the key physical factors for the atmospheric variations. Additionally, it enhances confidence in using the GCMs to investigate the physical processes and mechanisms involved in the atmospheric changes by direct interpretation of the model outputs.

The lower level westerly anomaly between 120°W and 80°W over the areas near the equator and to the south of the eastern Pacific may have a large impact on the portions of South America. If the identified atmospheric interdecadal variation is in the positive mode, the surface southeasterly trade winds are weakened and the water upwelling off the South American coast will be suppressed. Such a regional warming may yield a negative impact, similar to what has happened in a strong ENSO event, on the South American regional economy.

7.3 The physical and dynamical mechanisms of the tropical height changes

Based on the interdecadal SST change structures over the tropical central and eastern Pacific, three sets of GCM experiments have been performed to diagnose the physics and dynamics in the simulated atmospheric variations. Two of these forcing runs (CPACP2 and EPACP2) are designed to isolate the effects of the SST perturbation structures over the tropical central and eastern Pacific regions, respectively. The other experiment (PACP2) is designed to emphasize on the SST

change structure over both the tropical central and eastern Pacific simultaneously and diagnose its impacts on the atmosphere.

From these model experiments, cumulus convection, atmospheric heat transport and atmospheric adiabatic sinking are found to be the primary processes which are largely responsible for the formation and maintenance of the tropical-wide height increase pattern. The SST anomaly pattern over the equatorial central Pacific appears to be the dominant forcing for the atmospheric height and circulation change structures over the tropical and extratropical regions, whereas the SST change over the tropical eastern Pacific reinforces the tropical-wide change pattern and its major impact is on the atmospheric changes over the eastern Pacific region.

Anomalous diabatic heating increase, primarily in the form of cumulus convection latent heat release, is generated in the central and eastern Pacific areas. Part of such heating is transported upward by the strong rising motion, and carried poleward (mostly northward) in the upper troposphere. Driven by the upper level (200 hPa) wind circulation, this heat energy is then redirected eastward by the climatological westerlies enhanced by the anomalous westerly wind change in the regions of $15^{\circ}\text{N} - 30^{\circ}\text{N}$ and $15^{\circ}\text{S} - 30^{\circ}\text{S}$. For both the northern and southern sides, the central Pacific and the $130^{\circ}\text{W} - 160^{\circ}\text{W}$ part of the eastern Pacific are the notable heat sources, whereas near the 120°W , zonal heat flux converges. The zonal heat energy accumulates in the Atlantic region to the north of the equator. The meridional wind convergence in the eastern Pacific and Atlantic regions redistributes such heat to the deep tropical regions, thereby warming the local atmosphere. Furthermore, the extraordinarily strong northerly wind changes in the upper level (200 hPa) of the

eastern Pacific and Atlantic regions are found. This strengthens heat transport from the northern low latitudes to the equator and warms the local air in the tropical eastern Pacific and Atlantic regions, leading to a large geopotential height increase. Hence, the maximum geopotential height increase area over the eastern Pacific is a consequence of both local diabatic heating and horizontal heat transport, whereas the upper level height increase over the tropical Atlantic region results from the heat transport and warming effects of the anomalous atmospheric adiabatic sinking motions.

The height increase in the regions away from the local diabatic heating sources in the middle troposphere can not be simply explained using the heat transport mechanisms in the lower layer. The height increase over the Indian and western Pacific Ocean occurs mostly at the lower atmosphere, i.e., the thickness between the 1000 and 200 hPa changes little. The lower level height increase can be largely attributed to the dynamical effect of the anomalous sinking motions in these regions. Because of the anomalous SST forcing in the equatorial central Pacific, the maximum rising motion is shifted toward the central Pacific and the normal strong upward motion in the tropical western Pacific and Indian Ocean is suppressed. This leads to reduced surface level air convergence and a positive height change in the near surface atmosphere.

The findings of the physical and dynamical mechanisms identified herein have advanced the knowledge of the atmospheric responses to interdecadal SST variation and the tropical atmospheric changes which have been detected since the mid-1970s. Moreover, the atmospheric pattern changes over the tropics and extratropics are

dynamically consistent. The northern subtropical westerly jet is enhanced due to the anomalous surface forcing, especially in the Pacific regions. Such a westerly enhancement requires a larger meridional temperature gradient in the subtropical belt, owing to the atmospheric baroclinicity, leading to a positive height anomaly over the equatorial area and negative height anomaly over the middle latitude regions. Hence, this study can serve as a step toward a fuller understanding of the extratropical atmospheric variations given by the previous researchers.

It is vital to point out that mechanisms described herein are drawn from the experiments in this research, which only concentrates on the ENSO-like interdecadal SST variation pattern over the central and eastern Pacific regions. In reality, SST changes over other tropical regions also occurred on the same time scale. The physical mechanisms identified here may not reflect the atmospheric change nature completely when the SST change over all the tropical areas are taken into account in the model experimental design. However, the mid-1970s tropical decadal SST changes are found most pronounced over the central and eastern Pacific (i.e. ENSO-like). Identification of the physical mechanisms involved in the interdecadal atmospheric variability is crucial to a fully understanding of the entire tropical atmospheric change. This research provides such an understanding.

7.4 Concluding remarks

An abrupt change at the winter of 1976/77 for the atmospheric and oceanic system over the tropics has been documented through analyses of a range of data

sources in this research. Such a change is an example of decadal time-scale variability. The primary spatial features of the atmospheric variation are simulated with idealized GCM experiments. The atmospheric processes involved in the formation and maintenance of such change structures have been investigated in this context and diagnosed by analyzing several prescribed model runs representing various climatic scenarios. A unique aspect of this research is the diagnosis of the physical processes and mechanisms responsible for the atmospheric changes. However, it is important to indicate that the model simulations are artificially idealized and the changes in the ocean and atmosphere have been, to certain extent, exaggerated in order to unambiguously trace the atmospheric responses and the physical mechanisms. The atmospheric changes found in the idealized simulations are not the entire atmospheric picture since only the SST changes over the Pacific is emphasized. The SST changes over the rest of the tropical ocean regions may also modify somewhat the structures if considered in the experiments.

Finally, it is also important to explicitly comment that the capability of current atmospheric GCMs in correctly modeling the changes is largely limited by the uncertainties in the model physical parameterization schemes. This can directly affect the validity of the modeling results and conclusions in this research that purely relies on the state of the science in modeling. Hence, while the fidelity of the primary results of this research appears robust, it is also believed that further upgraded model physical parameterization schemes will lead to even better understanding of the atmospheric variations and the related physical mechanisms with less uncertainties.

References

- Chen, F., and M. Ghil, 1996: Interdecadal variability in a hybrid coupled ocean-atmosphere model. *J. Phys. Oceanogr.*, **26**, 1561-1578.
- Duchon, C. E., 1979: Lanczos filtering in one and two dimensions. *J. Appl. Meteor.*, **18**, 1016 -1022.
- Ebisuzaki, W., 1995: Consistency of the diabatic heating in the NMC/NCAR reanalysis, *Proc. 20th Climate Diagnostics Workshop*, Seattle, Washington, Natl. Oceanic Atmos. Admin., 232-234.
- Folland, C. K., D. E. Parker and F. E. Kates, 1984: Worldwide marine temperature fluctuations 1856-1981. *Nature*, **310**, 670-673.
- Gadgil, S., P. V. Joseph, and N. V. Joshi, 1984: Ocean-atmospheric coupling over monsoon regions. *Nature*, **312**, 141-143.
- Graham, N. E., 1994: Decadal-scale climate variability in the 1970s and 1980s: Observations and model results. *Climate Dyn.*, **10**, 135-162.
- Graham, N. E., T. P. Barnett, R. Wilde, M. Ponater, and S. Schubert, 1994: On the roles tropical and midlatitude SSTs in forcing interannual to interdecadal variability in the winter Northern Hemisphere circulation. *J. Climate*, **7**, 1415-1441.
- Gu, D., and S. G. H. Philander, 1997: Internal climate fluctuations that depend on exchanges between the tropics and extratropics. *Science*, **275**, 805-807.

- Jones, P. D., S. C. B. Bradley, H. F. Diaz, P. M. Kelly and T. M. L. Wigley, 1986: Northern Hemisphere surface air temperature variations: 1851-1984. *J. Climate Appl. Meteor.*, **25**, 161-179.
- Kachi, M., and T. Nitta, 1997: Decadal variations of the global atmosphere-ocean system. *J. Meteor. Soc. Japan*, **74**, 657-675.
- Kalnay, E., and Co-authors, 1996: The NCEP/NCAR 40-year reanalysis project. *Bull. Amer. Meteor. Soc.*, **77**, 437-471.
- Kawamura, R., 1994: A rotated EOF analysis of global sea surface temperature variability with interannual and interdecadal scales. *J. Phys. Oceanogr.*, **24**, 707-715.
- Kashiwabara, T., 1987: On the recent winter cooling in the North Pacific (in Japanese). *Tenki*, **34**, 777-781.
- Latif, M., 1997: Dynamics of interdecadal variability in coupled ocean-atmosphere models. *Report No. 239*, Max-Planck Institute for Meteorology, Hamburg, Germany, 75pp.
- Latif, M., and T. P. Barnett, 1994: Causes of decadal climate variability over the North Pacific/North American sector. *Science*, **226**, 634-637.
- Lau, K.-M., H.-T. Wu, and S. Bony, 1997: The role of large-scale atmospheric circulation in the relationship between tropical convection and sea surface temperature. *J. Climate*, **10**, 381-392.
- Lau, N. C., 1992: Climate variability simulated in GCMs. *Climate System Modeling*, K. E. Trenberth (Ed.), Cambridge University Press, 617-642.

- Lau, N. C., and M. J. Nath, 1994: A modeling study of the relative roles of the tropical and extratropical SST anomalies in the variability of the global atmosphere-ocean system. *J. Climate*, **7**, 1184-1207.
- Manabe, S., and R. J. Stouffer, 1996: Low-frequency variability of surface air-temperature in a 1000-year integration of a coupled atmosphere-ocean-land surface model. *J. Climate*, **9**, 376-393.
- Mantua, J. N., S. R. Hare, Y. Zhang, J. M. Wallace, and R. C. Francis, 1997: A Pacific interdecadal climate oscillation with impacts on salmon production. *Bull. Amer. Meteor. Soc.*, **78**, 1069-1080.
- Miller, A. J., D. R. Cayan, T. P. Barnett, N. E. Graham, and J. M. Oberhuber, 1994: Interdecadal variability of the Pacific Ocean: Model response to observed heat flux and wind stress anomalies. *Climate Dyn.*, **9**, 287-302.
- Montroy, D. L., 1997: Linear relation of central and eastern North American precipitation to tropical Pacific sea surface temperature anomalies. *J. Climate*, **10**, 541-558.
- Moron, V., A. Navarra, M. N. Ward, and E. Roeckner, 1997: Skill and reproducibility of seasonal rainfall patterns in the tropics in GCM simulations with prescribed SST. *IMGA Report No. 5*, Consiglio Nazionale Delle Ricerche, Italy, 45pp.
- Nakamura, H., G. Lin, and T. Yamagata, 1997: Decadal climate variability in the North Pacific during the recent decades. *Bull. Amer. Meteor. Soc.*, **78**, 2215-2225.

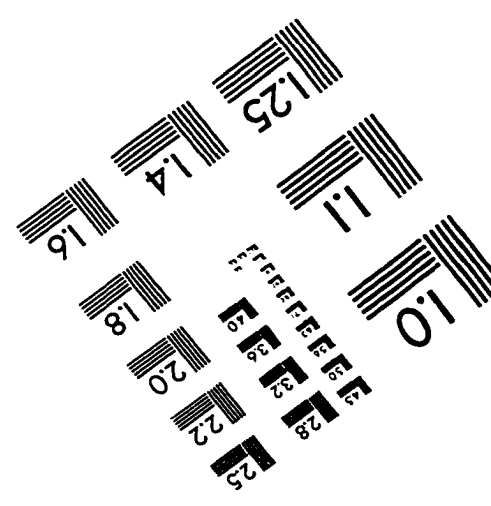
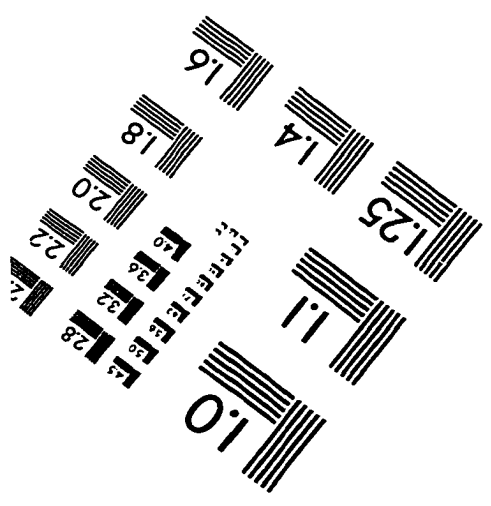
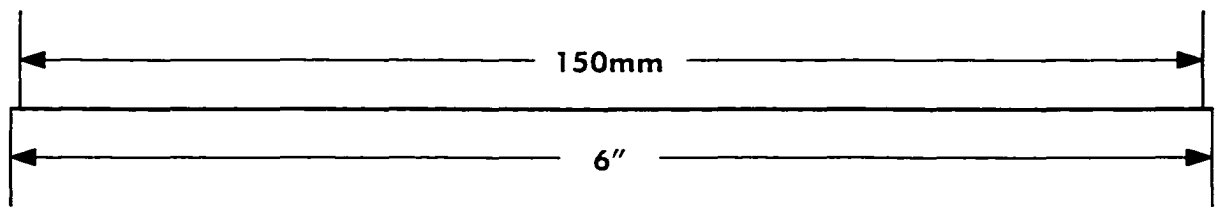
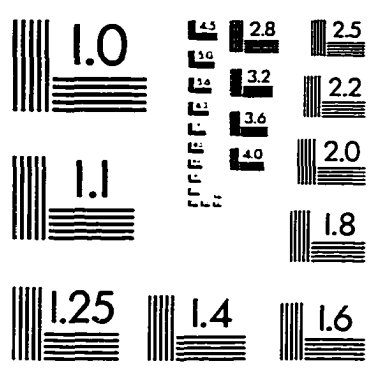
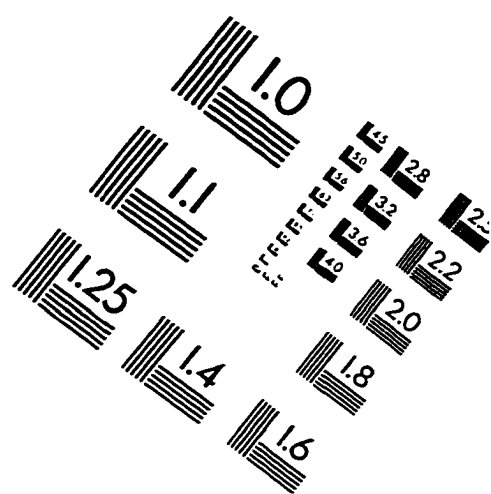
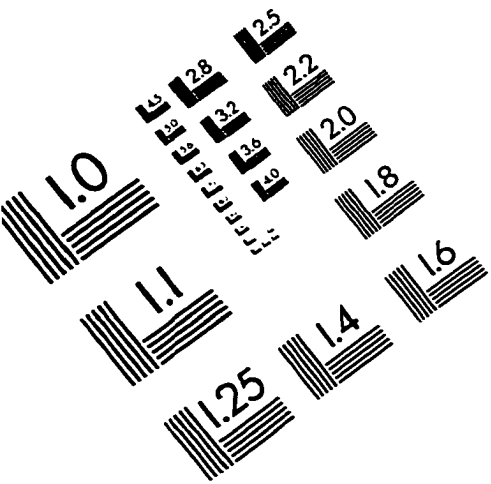
- Newell, R. E., D. G. Vincent, T. G. Dopplick, D. Ferruza, and J. W. Kidson, 1970: The energy balance of the global atmosphere. *The global circulation of atmosphere*, G. A. Corby (ed.), Royal Meteorological Society, London, 42-90.
- Nitta, T., and S. Yamada, 1989: Recent warming of tropical sea surface temperature and its relationship to the Northern Hemisphere circulation. *J. Meteor. Soc. Japan*, **67**, 187-193.
- Nitta, T., and M. Kachi, 1994: Interdecadal variations of precipitation over the tropical Pacific and Indian Oceans. *J. Meteor. Soc. Japan*, **72**, 375-382.
- Nordeng, T. E., 1994: Extended versions of the convective parameterization scheme at ECMWF and their impact on the mean transient activity of the model in the tropics. *Technical Memorandum No. 206*, The European Centre for Medium-Range Weather Forecasts, 41pp.
- Parker, D. E., M. Jackson, and E. B. Horton, 1995a: The GISST2.2 sea surface temperature and sea-ice climatology. *Climate Research Technical Note 63*, Hadley Centre, Meteorological Office, Bracknell, U. K., 35pp.
- Parker, D. E., C. K. Folland, A. Bevan, M. N. Ward, M. Jackson, and K. Maskell, 1995b: Marine surface data for analysis of climate fluctuations on interannual to century time scales. *Natural Climate Variability on Decade-to-Century Time Series*. D. G. Martinson, K. Bryan, M. Ghil, M. M. Hall, T. R. Karl, E. S. Sarachik and L. D. Talley (Eds.). National Academic Press, Washington, DC. 241-250.
- Peixoto, J. P., and A. H. Oort, 1992: *Physics of Climate*, American Institute of Physics, 520pp.

- Rasmusson, E. M., and T. H. Carpenter, 1982: Variations in tropical sea surface temperature and surface wind field associated with the Southern Oscillation/El Niño. *Mon. Wea. Rev.*, **100**, 1103-1113.
- Reynolds, R. W., and T. M. Smith, 1994: Improved global sea surface temperature analyses using optimum interpolation. *J. Climate*, **7**, 929-948.
- Richman, M. B., 1986: Rotation of principal components. *J. Climatol.*, **7**, 929-948.
- Richman, M. B., 1994: On the use of multivariate statistics to validate global climate models. *Ph.D. thesis*, The University of Illinois, 321pp.
- Roeckner, E., K. Arpe, L. Bengtsson, S. Brinkop, L. Dumenil, M. Esch, E. Kirk, F. Lunkeit, M. Ponater, B. Rockel, R. Sausen, U. Schlese, S. Schubert and M. Windelband, 1992: Simulation of the present-day climate with the ECHAM model: Impact of model physics and resolution. *Report No. 93*, Max-Planck Institute for Meteorology, Hamburg, Germany, 171pp.
- Roeckner, E., K. Arpe, L. Bengtsson, M. Christoph, L. Dumenil, M. Esch, M. Giorgetta, U. Schlese, U. Schulzweida, 1996: The atmospheric general circulation model ECHAM-4: Model description and simulation of the present-day climate. *Report No. 218*, Max-Planck Institute for Meteorology, Hamburg, Germany, 90pp.
- Robertson, A. W., 1996: Interdecadal variability over the North Pacific in a multi-century climate simulation. *Climate Dyn.*, **12**, 227-241.
- Smith, T. M., R. W. Reynolds, E. E. Livezey, and D. C. Stokes, 1996: Reconstruction of historical sea surface temperatures using empirical orthogonal functions. *J. Climate*, **9**, 1403-1420.

- Tanimoto, Y., N. Iwasaka, K. Hanawa, and Y. Toba, 1993: Characteristic variations of sea surface with multiple time scales in the North Pacific. *J. Climate*, **6**, 1153-1160.
- Tiedtke, M., 1989: A comprehensive mass flux scheme for cumulus parameterization in large-scale models. *Mon. Wea. Rev.*, **117**, 1779-1800.
- Trenberth, K. E., 1990: Recent observed interdecadal climate changes in the Northern Hemisphere. *Bull. Amer. Meteor. Soc.*, **71**, 988-993.
- Trenberth, K. E., 1991: General characteristics of El Niño-Southern Oscillation. *Teleconnections Linking Worldwide Climate Anomalies: Scientific Basis and Societal Impact*, M. H. Glantz, R. W. Katz, and N. Nicholls (Eds.), Cambridge University Press, 12-41.
- Trenberth, K. E., and J. W. Hurrell, 1994: Decadal atmospheric-ocean variations in the Pacific. *Climate Dyn.*, **9**, 303-309.
- von Storch, J.-S., 1994: Interdecadal variability in a global coupled model. *Tellus*, **46A**, 419-432.
- Wallace, J. M., and D. S. Gutzler, 1981: Teleconnections in the geopotential height field during the Northern Hemisphere winter. *Mon. Wea. Rev.*, **109**, 784-812.
- Wallace, J. M., Y. Zhang, and K. H. Lau: Structure and seasonality of interannual and interdecadal variability of geopotential height and temperature fields in the Northern Hemisphere troposphere. *J. Climate*, **6**, 2063-2082.
- Ward, M. N., and A. Navarra, 1997: Pattern analysis of ensemble GCM simulations with prescribed SST: Boreal summer examples over Europe and the tropical Pacific. *J. Climate*, **10**, 2210-2220.

- Weaver, A. J., and E. S. Sarachik: 1991: Evidence for decadal variability in an ocean general circulation model: An advective mechanism. *Atmos.-Ocean*, **29**, 197-231.
- Yamagata, T., and Y. Masumoto, 1992: Interdecadal natural climate variability in the western Pacific and its implication in global warming. *J. Meteor. Soc. Japan*, **70**, 167-175.
- Yanai, M. S., 1996: Seasonal and interannual variability of atmospheric heat sources. *Workshop on El Niño, Southern Oscillation and Monsoon*, International Center for theoretical physics.
- Yanai, M., S. Esbensen, and J. Chu, 1973: Determination of bulk properties of tropical cloud clusters from large-scale heat and moisture budgets. *J. Atmos. Sci.*, **30**, 611-627.
- Yukimoto, S., M. Endoh, Y. Kitamura, A. Kitoh, T. Motoi, A. Noda, and T. Tokioka, 1996: Interannual and interdecadal variabilities in the Pacific in an MRI coupled GCM. *Climate Dyn.*, **12**, 667-683.
- Zhang, C., 1993: Large-scale variability of atmospheric deep convection in relation to sea surface temperature in the tropics. *J. Climate*, **6**, 1898-1912.
- Zhang, Y., J. M. Wallace, and D. S. Battisti, 1997: ENSO-like interdecadal variability: 1990-93. *J. Climate*, **10**, 1004-1020.

IMAGE EVALUATION TEST TARGET (QA-3)



APPLIED IMAGE, Inc
 1653 East Main Street
 Rochester, NY 14609 USA
 Phone: 716/482-0300
 Fax: 716/288-5989

© 1993, Applied Image, Inc., All Rights Reserved